

INFORMATION TO USERS

This manuscript has been reproduced from the microfilm master. UMI films the text directly from the original or copy submitted. Thus, some thesis and dissertation copies are in typewriter face, while others may be from any type of computer printer.

The quality of this reproduction is dependent upon the quality of the copy submitted. Broken or indistinct print, colored or poor quality illustrations and photographs, print bleedthrough, substandard margins, and improper alignment can adversely affect reproduction.

In the unlikely event that the author did not send UMI a complete manuscript and there are missing pages, these will be noted. Also, if unauthorized copyright material had to be removed, a note will indicate the deletion.

Oversize materials (e.g., maps, drawings, charts) are reproduced by sectioning the original, beginning at the upper left-hand corner and continuing from left to right in equal sections with small overlaps.

ProQuest Information and Learning
300 North Zeeb Road, Ann Arbor, MI 48106-1346 USA
800-521-0600

UMI[®]

**INTER- AND INTRAMOLECULAR PHENOLIC HYDROGEN ATOM
ABSTRACTION BY AROMATIC KETONE TRIPLETS**

By

EDWARD CAMIEL LATHIOOR, B.Sc.

A Thesis

Submitted to the School of Graduate Studies

in Partial Fulfillment of the Requirements

for the Degree

Doctor of Philosophy

McMaster University

© Copyright by Edward Camiel Lathioor, September 2001

PHENOLIC HYDROGEN ABSTRACTION BY AROMATIC KETONE TRIPLETS

DOCTOR OF PHILOSOPHY (2001)
(Chemistry)

McMaster University
Hamilton, Ontario

**TITLE: Inter- and Intramolecular Phenolic Hydrogen Atom Abstraction by Aromatic
Ketone Triplets**

AUTHOR: Edward C. Lathioor, B.Sc. (Simon Fraser University)

SUPERVISOR: Dr. W.J. Leigh

NUMBER OF PAGES: xxi, 263

ABSTRACT

The photochemistry of aromatic compounds containing the ketone chromophore has been studied in the presence of phenols. The research may be divided into two main branches. The first involves a study of bimolecular reactions between photoexcited aromatic ketones and phenols conducted by nanosecond laser flash photolysis techniques. From these experiments, a new mechanism of hydrogen atom abstraction has been proposed. The second branch involves efforts to examine the reaction in compounds where both aromatic ketone and phenol moieties are present in the same chemical structure.

The main result is the emergence of a new mechanism of hydrogen atom abstraction involving initial hydrogen-bonding between the reaction partners, followed by hydrogen transfer as a coupled electron-/proton-transfer. This mechanism rationalised many aspects of phenolic quenching. In the case of bimolecular reactivity, very fast overall quenching rates are observed for both lowest n, π^* and π, π^* triplets, and a large variety of aromatic ketones of varying structure have been examined. The intramolecular reactivity was based upon the triplet lifetimes of various linked phenolic ketones. The triplet lifetimes are found to vary depending on isomerism and, to a lesser extent, chromophore. Studies of the acetophenone, indanone and benzophenone chromophores have been undertaken.

ACKNOWLEDGEMENTS

This thesis is dedicated to my parents, Magda and Romain, and my wife, Betty, whose presence from year one was instrumental to the pursuit of my Ph.D. dreams. Thank you for supporting, inspiring, and pushing me ever onwards.

Dr. William Leigh receives my thanks for his patience as a supervisor and his enthusiasm for chemistry. It is contagious!

I would like to thank my committee, Profs. Joseph Laposa and John Warkentin, for their helpful input over the years.

Other individuals deserve credit for their profound 'chemical' influences on me: Ms. June Wells, Prof. Eberhard Kiehlmann and Prof. Andrew Bennet.

Special thank yous are necessary for a large group of fantastic colleagues, whose daily presence in the lab kept everything on an even keel. It is a long list; it includes Nick Toltl, Bruce Cook, Tracy Morkin, Thomas Owens and Cam Harrington.

Training and technical assistance (and much helpful advice) from Mike Malott, George Timmins, Brian Sayer, Don Hughes and George Zibens is also gratefully acknowledged, as is the administrative magic of Carol Dada.

Financial support for the work came from NSERC, McMaster University and the Canadian pulp and paper industry.

TABLE OF CONTENTS

List of Schemes	x
List of Figures	xii
List of Tables	xviii
 CHAPTER ONE: GENERAL PHOTOCHEMICAL PROCESSES, AROMATIC	
KETONE PHOTOCHEMISTRY, AND PHENOLS AS DONORS	
IN THE HYDROGEN ATOM ABSTRACTION REACTION 1	
1.1.	Introduction to Photochemistry. Light Absorption and Photophysics. 1
1.2.	The Theoretical Basis of Photodynamical Processes. 4
1.3.	Aromatic Ketone Photochemistry. Triplet States and their Configurations. 8
1.3.1.	The formaldehyde model. 8
1.3.2.	Lowest triplet configurations: n, π^*, π, π^* and charge-transfer. 10
1.4.	Photoreduction and Hydrogen Atom Abstraction. 17
1.4.1.	Energetics of hydrogen atom abstraction. 17
1.4.2.	Mechanisms of hydrogen atom abstraction. 21
1.4.3.	Role of the lowest triplet state in hydrogen atom abstraction. 27

1.4.4.	Reactivity of upper triplet levels in radical-like HAA reactions.	29
1.5.	Photochemical Hydrogen Atom Abstraction from Phenols.	33
1.5.1.	Previous studies involving phenols.	35
1.5.2.	The ketone triplet/phenol interaction studied by nanosecond laser flash photolysis.	39
1.5.3.	The photochemistry of para, para'-linked phenolic acetophenone in fluid solution and ordered media. Intramolecular phenolic hydrogen atom abstraction.	40
1.5.4.	Preliminary study of the effects of chromophore and geometry on intramolecular HAA.	44
1.6.	Thesis Goals.	49
CHAPTER TWO: A STUDY OF THE BIMOLECULAR REACTIVITY OF AROMATIC KETONE TRIPLETS WITH PHENOLS		50
2.1.	Quenching of Aromatic Ketone Triplets by <i>para</i> -Cresol.	50
2.1.1.	Introduction. General considerations.	50
2.1.2.	Results. Transient ultraviolet absorption spectra.	55
2.1.3.	Results. Transient decays and absolute quenching rate constants.	59
2.1.4.	Discussion. General observations on the phenolic hydrogen atom abstraction reaction.	70

2.1.5.	Discussion. Benzophenone reactivity.	76
2.1.6.	Discussion. A nucleophilic mechanism.	79
2.1.7.	Discussion. Feasibility of electron transfer in a hydrogen-bonded complex.	92
2.1.8.	Discussion. Generality of the new mechanism.	95
2.1.9.	Conclusions.	105

CHAPTER THREE: INTRAMOLECULAR PHENOLIC HYDROGEN ATOM ABSTRACTION REACTIONS. PART ONE. THE STUDY OF DIFFERENT CHROMOPHORES

3.1.	Bimolecular <i>versus</i> Intramolecular Reactions.	107
3.2.	<i>para, para'</i> -Linked Phenolic Ketones and their Methoxy Analogues.	109
3.2.1.	Introduction. Species of interest.	109
3.2.2.	Results. Preparation of LPKs.	111
3.2.3.	Results. Ultraviolet, infrared and phosphorescence spectra.	113
3.2.4.	Results. Steady-state photochemistry.	119
3.2.5.	Results. Transient spectroscopy of compounds 9 , 11 , and 57 .	123
3.2.6.	Results. Transient lifetimes of compounds 9 , 11 , and 57 .	137
3.2.7.	Results. Biradical lifetimes of compounds 9a , 11a , and 57a .	143
3.2.8.	Results. Kinetic isotope effects.	147

3.2.9.	Discussion. NLFP results.	147
3.2.10.	Discussion. Solvent effect. MeCN <i>versus</i> DCM.	151
3.2.11.	Conclusions.	152

CHAPTER FOUR: INTRAMOLECULAR PHENOLIC HYDROGEN ATOM		
ABSTRACTION REACTIONS. PART TWO. THE EFFECT OF POSITIONAL		
ISOMERISM IN THE INTRAMOLECULAR PHENOLIC HYDROGEN ATOM		
ABSTRACTION REACTION		154
4.1.	Motivation for a Study of Positional Isomerism.	154
4.2.	Photochemistry of LPKs with <i>meta</i> Geometries.	156
4.2.1.	Introduction. Previous work and species of interest.	156
4.2.2.	Results. Preparation of LPKs and their <i>O</i> -methyl ethers.	159
4.2.3.	Results. Spectroscopy and steady state photochemistry.	160
4.2.4.	Results. NLFP of compounds 14b-16b .	170
4.2.5.	Results. NLFP of compounds 14a-16a .	177
4.2.6.	Results. Molecular modeling of compounds 9a and 14a - 16a .	190
4.2.7.	Discussion. LPK triplet lifetimes and the ' <i>meta</i> -acyl' effect.	194
4.2.8.	Discussion. Symmetry restricted electron transfer.	197
4.2.9.	Discussion. Triplet lifetime of the methoxy ketones in dry solvent.	200
4.2.10.	Discussion. The effect of water.	200

4.2.11.	Conclusions on the acetophenone study.	204
4.3.	Positional Isomerism in the Benzophenone and Indanone Chromophores.	206
4.3.1.	Results. NLFP of compounds 58a and 58b .	206
4.3.2.	Results. NLFP of compounds 59a and 59b .	212
4.3.3.	Discussion. Mechanistic assignment.	219
4.3.4.	Discussion. Chromophore effect on the " <i>meta</i> -acyl" effect.	219
4.3.5.	Conclusions.	223
CHAPTER FIVE: EXPERIMENTAL SECTION		224
5.1.	General Instrumentation.	224
5.2.	Photochemistry.	225
5.2.1.	Steady state photolysis.	225
5.2.2.	Nanosecond laser flash photolysis.	226
5.3.	Chemicals.	227
5.3.1.	Solvents.	227
5.3.2.	Ketones and quenchers.	227
5.3.3.	Synthetic reagents	228
5.3.4.	Linked phenolic ketones and their <i>O</i> -methyl ethers.	231
APPENDIX		242
REFERENCES		252

LIST OF SCHEMES

1.1.	Triplet-triplet energy transfer between acetophenone and naphthalene	5
1.2.	Energetics of photoinduced electron transfer.	7
1.3.	Valence bond representations of n, π^* and π, π^* triplet states.	15
1.4.	Comparison of CT triplets to n, π^* and π, π^* triplets.	16
1.5.	The " π -type" exciplex.	26
1.6.	The Norrish-Yang reaction for substituted valerophenones.	31
1.7.	A series of para, para'-oxyethyl-linked phenolic ketones and their <i>O</i> -methyl ethers.	42
1.8.	Intramolecular phenolic hydrogen atom abstraction.	43
2.1.	Bimolecular hydrogen atom abstraction from <i>para</i> -cresol by ketone triplets.	68
2.2.	Two extreme cases of reactivity between triplet benzophenone and phenol.	93
2.3.	Mechanism of triplet quenching <i>via</i> a hydrogen bonding equilibrium.	98
3.1.	Kinetic schemes for inter- and intramolecular reactions.	108
3.2.	Configuration of intramolecular HAA in the alkoxyindanone LPK 57a.	111

3.3.	Preparation of LPKs <i>via</i> silyl-protected hydroxyphenethyl bromides.	111
3.4.	Preparation of LPKs <i>via</i> a ditosylate intermediate.	112
3.5.	The "self-quenching" reaction of triplet LPKs.	146
3.6.	Intramolecular charge transfer deactivation in alkoxyindanone 57b.	150
4.1.	Ground-state parameters for hydrogen atom abstraction reactions in solids.	191
4.2.	Results of Hückel calculation on <i>para</i>- and <i>meta</i>-substituted methoxyacetophenone and cresol molecules.	198
4.3.	A representation of "water-assisted" quenching.	204

LIST OF FIGURES

- | | | |
|--------------|--|----|
| 1.1. | Jablonksi diagram depicting common absorptive, emissive and non-radiative transitions in a molecular system. | 2 |
| 1.2. | Molecular orbital formulation for formaldehyde. | 9 |
| 1.3. | Triplet π, π^* state stabilizations by aromatic substituents modeled on benzonitriles. | 12 |
| 1.4. | Hydrogen atom abstraction by an aromatic ketone triplet leading to various photoreduced products. | 18 |
| 1.5. | A thermochemical cycle to predict the enthalpy of HAA reactions. | 19 |
| 1.6. | The three main classes of hydrogen atom abstraction.
Path A: full electron-transfer. Path B: charge-transfer assisted.
Path C: alkoxyl-radical like abstraction. | 23 |
| 1.7. | Plot of bimolecular reaction rate constants of ketone triplet quenching by <i>para</i> -xylene in acetonitrile as a function of triplet reduction potential. | 25 |
| 1.8. | Plot of benzophenone triplet decay rates in cyclopentane <i>versus</i> total Hammett sigma parameter. | 28 |
| 1.9. | Photochemical reaction of benzophenone with 2,6-disubstituted phenols. | 36 |
| 1.10. | Hammett plots of benzophenone and <i>para</i> -methoxypropiophenone | |

	(MPP) triplet quenching by substituted phenols in benzene.	41
1.11.	Linked phenolic ketones previously studied by MSP.	45
2.1.	List of ketones studied.	51
2.2.	Transient absorption spectra and decays recorded by 337-nm laser flash photolysis of deoxygenated acetonitrile solutions of (a) 0.1 M benzophenone (17), (b) 8×10^{-5} M <i>para</i> -dimethylaminoacetophenone (38) and (c) 4×10^{-4} M xanthone (55) at 23 to 25 °C.	56
2.3.	Transient absorption spectra and decays recorded by 337-nm laser flash photolysis of deoxygenated MeCN solutions of (a) 0.1 M benzophenone (17), (b) 8×10^{-5} M <i>para</i> -dimethylaminoacetophenone (38) and (c) 4×10^{-4} M xanthone (55) at 23 to 25 °C in the presence of ~ 0.01 to 0.02 M <i>para</i> -cresol.	63
2.4.	Transient decays of a 0.03 M deoxygenated acetonitrile solution of <i>para</i> -methoxyacetophenone (42) in the presence of (a) zero, (b) 3×10^{-4} M, and (c) 1.2×10^{-3} M <i>para</i> -cresol.	67
2.5.	Plots of k_{decay} versus <i>para</i> -cresol concentration for 4-methoxybenzophenone in dichloromethane, and <i>para</i> -thiomethylbenzophenone, <i>para</i> -dimethylaminoacetophenone, α, α, α -trifluoroacetophenone, fluorenone and xanthone in MeCN.	74
2.6.	Log rate constant versus sum of Hammett substituent parameter	

	for the <i>para</i> -cresol quenching of substituted benzophenone triplets (17 - 30) in deoxygenated acetonitrile solution at 23 °C.	77
2.7.	Updated plot of bimolecular reaction rate constants of ketone triplet quenching in acetonitrile as a function of triplet reduction potential.	80
2.8.	Two possible pathways of nucleophilic ketone triplet interaction with phenol: acid/base (full protonation) and hydrogen-bonding (partial protonation).	82
2.9.	Plot of pK_{HB} (<i>para</i> -fluorophenol in CCl_4 at 25°C) versus pK_{AH+} for various carbonyl-containing compounds.	89
2.10.	Plot of $\log k_q$ versus sum of Hammett σ for the <i>para</i> -cresol quenching of substituted acetophenone triplets in deoxygenated MeCN at 23 to 27 °C.	96
2.11.	Plot of $\log k_q$ versus E_{RED}^* for the <i>para</i> -cresol quenching of ketone triplets (17 - 56) in deoxygenated MeCN at 23 to 27 °C.	100
2.12.	Plot of $\log k_q$ or k_{et} versus ΔG_{et} for the <i>para</i> -cresol quenching of ketone triplets (17 - 56) in deoxygenated MeCN at 23 to 27 °C.	104
3.1.	Several <i>para</i> , <i>para'</i> -oxyethyl linked acetophenones and their <i>O</i> -methyl ethers.	110
3.2.	Ultraviolet absorption spectra of compounds 11b, 57a and 57b in acetonitrile (MeCN) and 9a, 9b, 11a, 11b, 57a and 57b in	

	dichloromethane (DCM).	114
3.3.	Phosphorescence spectra of compounds (a) 11b , (b) 57a , and (c) 57b , recorded in 4:1 ethanol/methanol mixtures at 77 K with 300-nm excitation and gated detection.	120
3.4.	Transient ultraviolet spectra and decays of $< 10^{-3}$ M ketone solutions of compounds 9a , 9b , 11a , 11b , 57a , and 57b in deoxygenated MeCN at room temperature.	125
3.5.	Transient ultraviolet spectra and decays of 10^{-4} M ketone solutions of compounds 9a , 9b , 11a , and 11b in deoxygenated DCM at room temperature.	132
3.6.	Probe methods for determining triplet lifetimes.	138
3.7.	Fits of the 1-methylnaphthalene probe data to eq. 3.1 at 23 to 25 °C for LPKs 9a and 11a .	140
3.8.	Stern-Volmer plot of the reduction of the initial yield of the transient (<i>top Δ-OD</i>) from 308-nm NLFP of 57a in deoxygenated MeCN by 1,3-cyclohexadiene, monitored at 400-nm.	144
4.1.	The acetophenone LPK series and meta, meta'-attached LPKs for study.	157
4.2.	UV spectra of compounds 14a , 14b , 15a , 15b , 16a and 16b in DCM at room temperature.	161
4.3.	UV spectra of compounds 58a , 58b , 59a , and 59b in MeCN and DCM at room temperature.	163

- 4.4. Phosphorescence spectra of compounds (a) **58a**, (b) **58b**, (c) **59a**, and (d) **59b** in 4:1 EtOH:MeOH glasses at 77K. 168
- 4.5. Transient ultraviolet spectra and decays of 10^{-4} M solutions of compounds **14b**, **15b** and **16b** in deoxygenated MeCN at 23-25 °C. 171
- 4.6. Transient ultraviolet spectra and decays of 10^{-4} M solutions of compounds **14b**, **15b** and **16b** in deoxygenated DCM at 23-25 °C. 173
- 4.7. Transient ultraviolet spectra and decays of 10^{-4} M solutions of compounds **14a**, **15a** and **16a** in deoxygenated MeCN at 23-25 °C. 179
- 4.8. Transient ultraviolet spectra and decays of 10^{-4} M solutions of compounds **14a**, **15a** and **16a** in deoxygenated DCM at 25 °C. 182
- 4.9. Plot of k_{decay} versus ketone concentration from 248-nm laser flash photolysis of deoxygenated, dry ($[H_2O] \leq 10^{-4}$ M) MeCN solutions of compound **16a**. 187
- 4.10. Semi-empirical (PM3) calculated geometries for LPKs **9a** and **14a-16a** and the difference in the calculated heats of formation of the indicated conformers and relaxed all-*trans* geometries. 192
- 4.11. Transient ultraviolet spectra and decays of 10^{-4} M solutions of compounds **58a** and **58b** in deoxygenated MeCN at 23 to 25 °C. 207
- 4.12. Transient ultraviolet spectra and decays of 10^{-4} M solutions of compounds **58a** and **58b** in deoxygenated DCM at 23 to 25 °C. 209
- 4.13. Transient ultraviolet spectra and decays of 10^{-4} M solutions of

	compounds 59a and 59b in deoxygenated MeCN at 23 to 25 °C.	214
4.14.	Transient ultraviolet spectra and decays of 10^{-4} M solutions of compounds 59a and 59b in deoxygenated DCM at 23 to 25 °C.	216

LIST OF TABLES

1.1.	Ring substituent effects on aromatic ketone triplet energies as modeled on benzonitriles.	13
1.2.	$D_{R''-H}$ values for various donors.	20
1.3.	$\Delta H_{R(HAA)}$ values for various ketones and donors.	20
1.4.	Norrish-Yang abstraction rates, per-bond reactivities and reactivity ratios of γ -substituted valerophenones and <i>para</i> -methoxyvalerophenones in benzene.	32
1.5.	Rates constants of quenching of biacetyl phosphorescence by various donors in benzene and acetonitrile, and proposed HAA mechanisms.	37
1.6.	Lowest triplet assignments, kinetic isotope effects, triplet lifetimes of LPKs 9-16, and bimolecular rate constants of quenching of model ketone triplets with the appropriate cresol in deoxygenated MeCN at temperatures ranging from 20 to 27 °C.	47
2.1.	Triplet energies and ground and triplet state reduction potentials of some of the benzophenones studied.	52
2.2.	Triplet energies and ground and triplet state reduction potentials of some of the acetophenones studied.	53
2.3.	Triplet energies and ground and triplet state reduction potentials	

	of some of the indanones and other lowest π, π^* ketones studied.	54
2.4.	Triplet-triplet absorption maxima and triplet lifetimes of the benzophenones studied.	60
2.5.	Triplet-triplet absorption maxima and triplet lifetimes of the acetophenones studied.	61
2.6.	Triplet-triplet absorption maxima and triplet lifetimes of the indanones and other lowest π, π^* ketones studied.	62
2.7.	Absolute rate constants for quenching of benzophenone triplets by <i>para</i> -cresol in deoxygenated acetonitrile at 23 to 25 °C.	71
2.8.	Absolute rate constants for quenching of acetophenone triplets by <i>para</i> -cresol in deoxygenated acetonitrile at 23 to 25 °C.	72
2.9.	Absolute rate constants for quenching of substituted 1-indanones and other lowest π, π^* triplets by <i>para</i> -cresol in deoxygenated acetonitrile at 23 to 25 °C.	73
2.10.	Ground and excited state pK_{AH^+} values for some aromatic ketones.	84
2.11.	K_{HB} values for the formation of 1:1 hydrogen-bonded complexes between carbonyl compounds and <i>para</i> -fluorophenol in CCl_4 at 25 °C.	88
2.12.	Values of pK_{HB} and pK_{AH^+} for Figure 2.9.	90
3.1.	Phosphorescence data for species 9, 11 and 57.	122
3.2.	Triplet lifetimes of compounds 9b, 11b, and 57b in MeCN and	

	DCM, and triplet quenching rates by 1,3-cyclohexadiene (CHD) in MeCN.	131
3.3.	Values of $k_q \tau_T$, triplet quenching rates of model compounds by 1-methylnaphthalene (MN) and derived triplet lifetimes of compounds 9a , and 11a in acetonitrile (MeCN).	141
3.4.	Values of $k_q \tau_T$, triplet quenching rate constants of model compounds by 1-methylnaphthalene (MN), and derived triplet lifetimes of compounds 9a and 11a in dichloromethane (DCM).	142
3.5.	Values of $k_q \tau_T$, the triplet quenching rate constant of compound 50 by 1,3-cyclohexadiene, and the derived triplet lifetimes of LPK 57a in MeCN at 23 to 25 °C.	145
3.6.	Values of $k_q \tau_T$ and triplet lifetimes and kinetic isotope effects for compounds 9a , 11a , and 57a determined in 5% water/MeCN and 5% D ₂ O/MeCN solutions at 23 to 25 °C.	148
4.1.	Triplet lifetimes of compounds 9b , 14b , 15b , and 16b in deoxygenated MeCN, 0.028 M H ₂ O/MeCN and DCM, and triplet quenching rates by 1,3-cyclohexadiene in MeCN.	178
4.2.	Triplet lifetimes of compounds 9a , 14a , 15a , and 16a in deoxygenated MeCN and DCM, rates of 1,3-cyclohexadiene triplet quenching in MeCN, self-quenching rate constants in MeCN, and absolute rate constants of <i>para</i> - or <i>meta</i> -methoxyacetophenone	

	triplet quenching by <i>para</i> - or <i>meta</i> -cresol in MeCN.	185
4.3.	Triplet lifetimes of compounds 9a , 14a , 15a , and 16a in deoxygenated 0.028 M L ₂ O/MeCN solutions, kinetic isotope effects and absolute rate constants of <i>para</i> - or <i>meta</i> -methoxyacetophenone quenching by <i>para</i> - or <i>meta</i> -cresol in 5% aqueous MeCN.	189
4.4.	Triplet lifetimes of compounds 58a and 58b in MeCN and DCM and rate constants for triplet quenching by 1,3-cyclohexadiene(CHD) in MeCN at 23 to 25 °C.	211
4.5.	Triplet lifetimes of compounds 58a and 59a in 0.05% L ₂ O/MeCN and kinetic isotope effects.	213
4.6.	Triplet lifetimes of compounds 59a and 59b in MeCN and DCM and triplet quenching rate constants by 1,3-cyclohexadiene(CHD) in MeCN at 23 to 25 °C.	218
4.7.	Comparison of <i>para</i> , <i>para'</i> -/ <i>meta</i> , <i>meta'</i> -attached LPK pairs 9a and 16a , 11a and 58a , and 57a and 59a in MeCN and DCM.	220

CHAPTER ONE
GENERAL PHOTOCHEMICAL PROCESSES, AROMATIC KETONE
PHOTOCHEMISTRY, AND PHENOLS AS DONORS IN THE HYDROGEN
ATOM ABSTRACTION REACTION

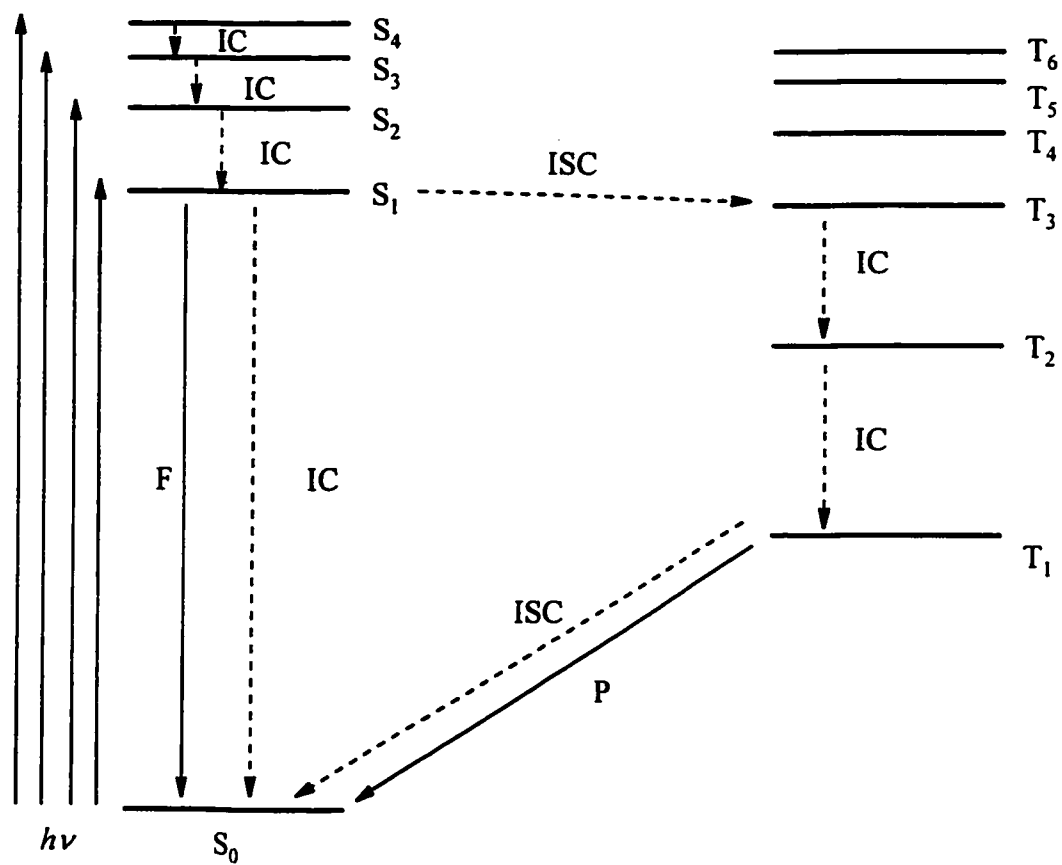
1.1. Introduction to Photochemistry. Light Absorption and Photophysics.

Photochemistry is a branch of the chemical sciences that involves the use of light as a reagent to cause chemical changes.

Molecules absorb light (electromagnetic radiation) due to a quantum mechanical effect known as resonance. In a resonance transition, the electromagnetic radiation matches precisely the energy required for a transition between two states. In the case of light absorption, such a transition is of the energy required to excite valence electrons, usually from the molecule's highest occupied molecular orbital (HOMO) to an upper molecular orbital. Due to the nature of quantum mechanical selection rules, such events are most probable if the electron maintains its original spin. As such, the excited state has the same spin as the ground state; usually in organic molecules all spins are paired and this is called a singlet state.

The effect of light absorption is two fold. First, the excited species is faced with a multitude of photophysical relaxation pathways, which are summarized in the traditional Jablonksi diagram, Figure 1.1.¹ This diagram depicts what can occur after light absorption from the ground electronic state, which is labeled S_0 in the case of ground

Figure 1.1. Jablonski diagram depicting common absorptive, emissive and non-radiative transitions in a molecular system.



state singlets. Several arrows on the left indicate different possible absorption events (labeled $h\nu$) leading to various excited electronic singlet states S_1 , S_2 , *etc.*

Relaxation pathways from the singlet states now arise due to the molecule's sudden great increase in potential energy. Collisions with other molecules allow for vibrational relaxation within an electronic state (not shown) and state relaxation, called internal conversion, IC. Usually, a cascade of IC from upper singlet states to S_1 is very fast, thus the properties of S_1 are usually what determine what happens next. This observation was made in the early years of photochemistry and while there are exceptions, it is known as Kasha's Rule.

Once in S_1 the molecule can undergo radiationless decay to the ground state, or lose energy in the form of a quantum of light (fluorescence). Another photophysical decay channel involves an electronic spin inversion. Such a process produces a spin isomer with two unpaired spins. This is dubbed the triplet state (T) because in an external magnetic field, three energy sublevels arise from this configuration (called the Zeeman splitting) as opposed to only a singlet for S states.

IC from triplet levels is also very fast until T_1 is reached, at which time intersystem crossing or light emission (phosphorescence) can regenerate S_0 .

The second result of light absorption, which competes with the photophysics and thus is not part of the Jablonksi diagram, is the creation of new reaction channels. It is from these that the various photochemical reactions occur.

1.2. The Theoretical Basis of Photodynamical Processes.

Chemical reactions occur when two or more species approach one another and their valence electron shells interact, breaking and reforming bonds to produce products that necessarily arise from an intermediary transition state. All chemical reactions are associated with a Gibbs free energy change, ΔG , which is related to the reaction enthalpy (heat) change ΔH , the entropy change ΔS , and the reaction temperature, T , by the following well-known equation:²

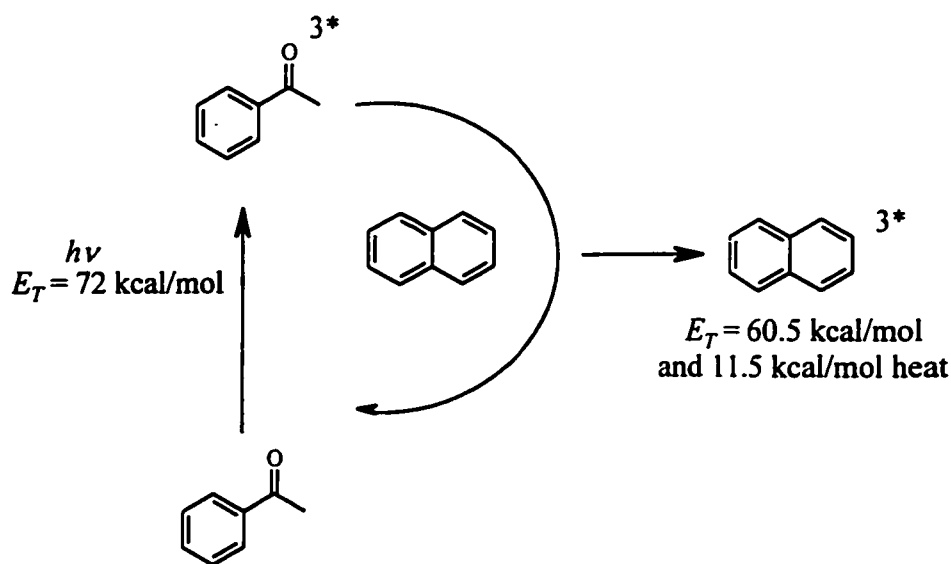
$$\Delta G = \Delta H - T\Delta S \quad (1.1)$$

In addition, in the ground state, approaching chemical species may undergo a reduction/oxidation (redox) reaction, in which a single electron is transferred from the reductant to the oxidant.

In photochemistry, this overall picture is complicated slightly in that one of the species has gained a large amount of energy from the light quantum. As a photoexcited molecule approaches a potential reactant, a reaction can occur, as can electron transfer. A third possibility is unique to excited electronic states and is called state energy transfer.

Energy transfer events are phenomena in which a photoexcited molecule with a certain state (singlet or triplet) energy transfers the energy (usually exothermically) to an acceptor, producing a new excited state of the same multiplicity (singlet or triplet). For example, Scheme 1.1 shows how acetophenone triplets (triplet energy, E_T , of 72 kcal/mol) may encounter naphthalene molecules (60.5 kcal/mol) and be quenched by

Scheme 1.1. Triplet-triplet energy transfer between acetophenone and naphthalene.



them to form ground state acetophenone molecules and triplet naphthalene. The balance is released as heat.

Several mechanisms of energy transfer have been proposed^{3,4} and this photophysical process remains a very active area of research today, over fifty years after its discovery.

Exothermic energy transfer usually involves only a small amount of molecular reorientation and consequently has a negligible barrier to reaction. This causes it to usually proceed at a very fast rate when energetically downhill. In solution, the fastest possible *intermolecular* rates are moderated by how fast molecules can physically diffuse through the condensed media and encounter each other. A simple equation which can be used to model the diffusion rate constants is the Smoluchowski-Stokes-Einstein equation (1.2)⁵, which uses the temperature T in Kelvin, the ideal gas constant R (8.314 J/mol K) and the solvent viscosity η (in Pa s) as parameters. The units of k_{diff} are $\text{M}^{-1} \text{s}^{-1}$.

$$k_{diff} = (8000/3) RT \eta^{-1} \quad (1.2)$$

The diffusion rate constant of two solutes in most common organic solvents are on the order of 10^9 to $10^{10} \text{ M}^{-1} \text{ s}^{-1}$ at room temperature.

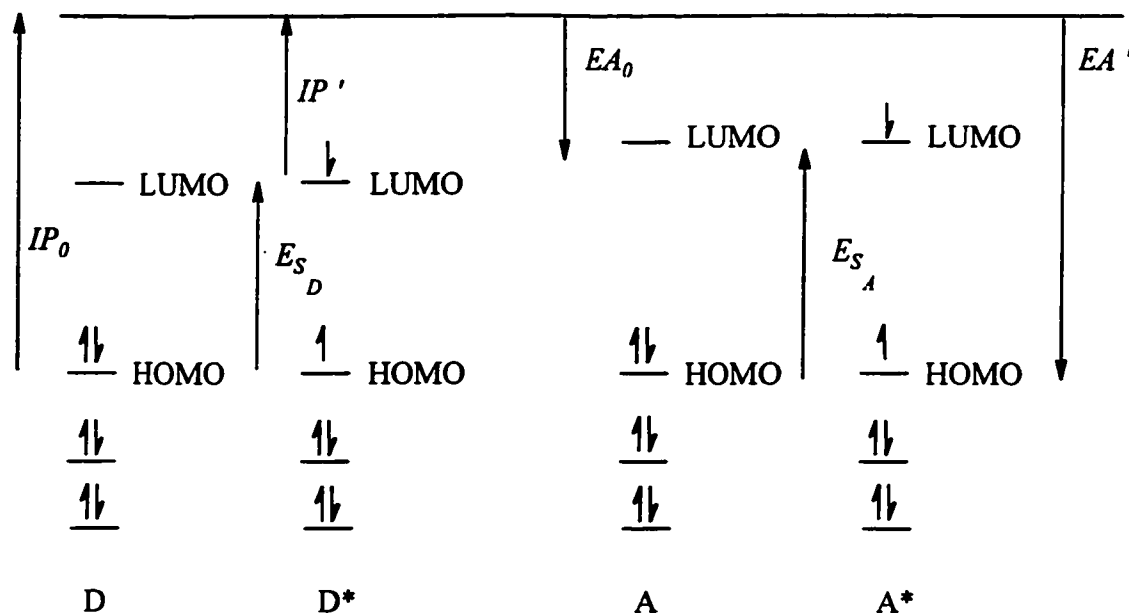
Collisions between photochemically excited molecules and ground state molecules can also result in electron transfer. This process is called photoinduced electron transfer (PET) when these events involve electronically excited states.

As Scheme 1.2 suggests, both reductants and oxidants become more reactive under photochemical conditions. For donors (D), the ionization potential IP_0 measures the ease of removal of an electron, and it is decreased by the state energy, E_{SD} . Thus $IP' = IP_0 - E_{SD}$. Similarly, acceptors (A) are made more reactive since the electron may now go into the half-vacant HOMO instead of the lowest unoccupied molecular orbital (LUMO). The thermodynamic measure is the electron affinity, EA_0 , and under PET conditions $EA' = EA_0 + E_{SA}$. Note that the effects of solvent interactions between the initial states, and the final ionic states, have not been placed in the Figure for clarity.

Rehm and Weller studied the PET reaction that led to observable singlet state quenching of aromatic compounds by a series of acceptors.⁶ From this work they discovered that the exergonicity of electron transfer reactions can be very well reproduced by the following equation, now known as the Rehm-Weller equation.

In the Rehm-Weller equation, n stands for the number of electrons transferred, F is

Scheme 1.2. Energetics of photoinduced electron transfer.



the Faraday constant, the $E(D)$ and $E(A)$ values are the half-wave oxidation and reduction potentials of the donor and acceptor, respectively, e_0 is the fundamental electric charge, ε is the permittivity of vacuum, $R_{D^+A^-}$ is the distance between the two newly formed ions (usually taken as the sum of the estimated ionic molecular radii) and E_S is the excited state energy.

$$\Delta G_{et} = nF \left[E_{1/2}^{ox}(D) - E_{1/2}^{red}(A) - \frac{e_0^2}{\varepsilon R_{D^+A^-}} \right] - E_S \quad (1.3)$$

The Rehm-Weller equation can be used to determine, in theory, if a given collision should result in exergonic PET, assuming that the thermodynamic parameters including the excited state energy are known.

1.3. Aromatic Ketone Photochemistry. Triplet States and their Configurations.

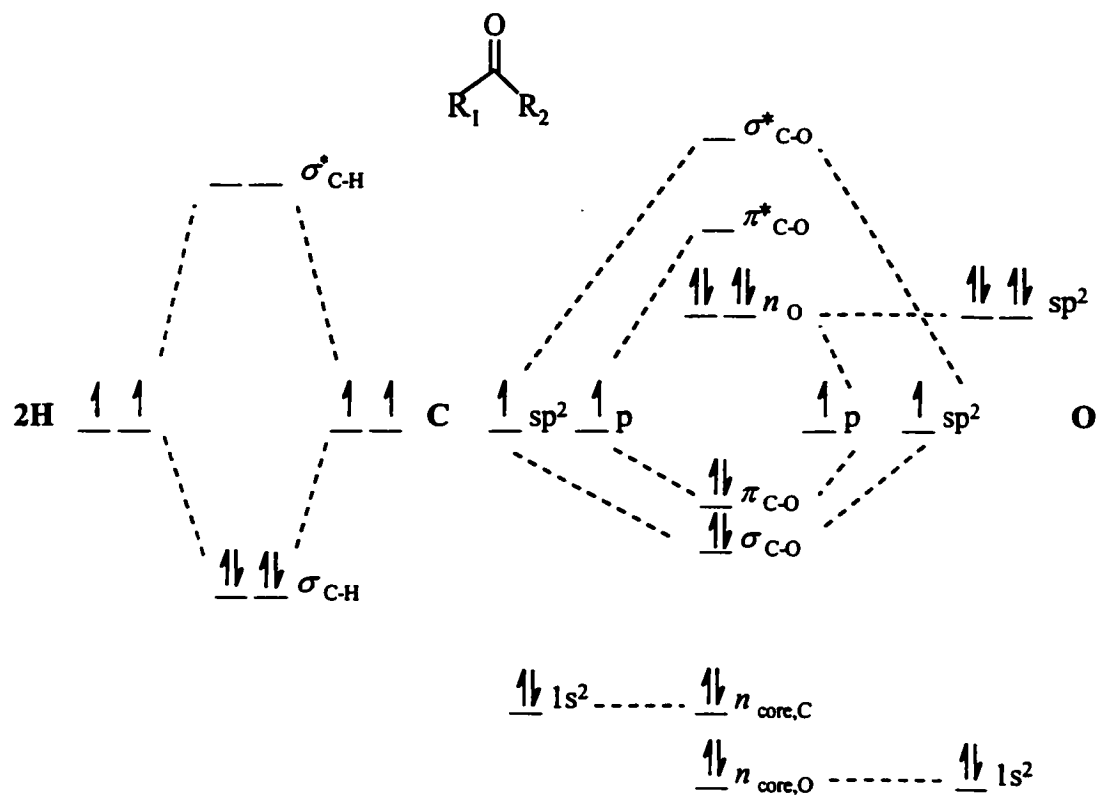
1.3.1. The formaldehyde model.

Many of the photochemical principles that are used to understand the reactivity of the ketone functional group can be gleaned from consideration of the simplest carbonyl compound, formaldehyde. Figure 1.2 depicts the formulation of the molecular orbitals of the molecule from the hybridized atomic orbitals of the four atomic building blocks. Orbitals are chosen that have the correct geometry around carbon to describe the observed molecular shape and planarity (sp^2 hybrid orbitals).

The orbital energies have been predicted *via* calculation to lie in the same qualitative ordering as represented in the figure.⁷ Thus, the S_1 transition in formaldehyde results in excitation from the fully occupied non-bonding n HOMO orbital to the LUMO, the antibonding π^* orbital. The product species is called an n, π^* singlet, the notation derived from the origins of the HOMO and LUMO orbitals, respectively.

Even if the hydrogen substituents on formaldehyde are replaced by more complicated groups, this overall orbital picture is maintained. Thus, acetone ($R_1 = R_2 = \text{Me}$), benzaldehyde ($R_1 = \text{H}, R_2 = \text{Ph}$), acetophenone ($R_1 = \text{Me}, R_2 = \text{Ph}$) and benzophenone ($R_1 = R_2 = \text{Ph}$) all have lowest excited states consisting of n, π^* configurations. The presence of an aromatic ring, however, infuses in to this picture new π and π^* orbitals with character relating to the aromatic ring. Thus, the eventual ordering of valence MOs in aromatic ketones is a HOMO of $n_{\text{C-O}}$ character followed by a ring $\pi_{\text{C-C}}$ molecular orbital directly below in energy.

Figure 1.2. Molecular orbital formulation for formaldehyde.



As will be discussed in the next section, the effect of substituents and/or solvent causes many acetophenones to actually possess a HOMO of π character, which leads to them having a first excited triplet state of π, π^* character.

1.3.2. Lowest triplet configurations: n, π^*, π, π^* and charge-transfer.

In general, aromatic ketones possess an important property that distinguishes their photochemistry from aliphatic ketones. This property is a very fast rate of intersystem crossing from S_1 to the triplet state. In benzophenone, the rate is estimated⁸ to be on the order of 10^{12} s^{-1} , resulting in an S_1 lifetime of picoseconds. As this timescale is similar to that of molecular vibrations, very little chemistry can occur from the singlet state. Instead, the photophysics and photochemistry of benzophenone is dominated by the triplet state. It turns out that this is a general result for almost all aromatic ketones.

Since substituents on an aromatic ring can affect the distribution of charge on the ring by π -conjugation, it is expected that substituents can in turn alter the energy of the ring MOs (these are π orbitals which are perpendicular to the molecular plane). On the other hand, the carbonyl n orbitals (lying in the plane of the molecule) are orthogonal to the π orbitals and are thus not affected by conjugation, to a first approximation. From this picture a very important conclusion can be drawn: the n orbital levels should be little affected by substituents, as they are only subject to (relatively minor) inductive effects. In contrast, π -conjugating substituents can raise the (HOMO-1) π_{C-C} orbital energy to such an extent that it switches place with the $n_{C=O}$ HOMO. In these ketones, electronic

excitation now results in a triplet of lowest π, π^* configuration. As mentioned above, this effect is pronounced for acetophenones and many of these triplets have lowest π, π^* character based on their phosphorescence emission. On the other hand, this effect is not present in benzophenones and almost all benzophenones have lowest n, π^* triplet states.⁹ This is perhaps due to out-of-plane twisting of each aromatic ring caused by the steric crowding of the two rings.¹⁰

Wagner's group has obtained quantitative data on the stabilization of π molecular orbitals by aromatic substituents from a study of substituted benzonitriles.^{11,12} This system was chosen since there are no n, π^* transitions to complicate the spectroscopy (even though there is a lone pair of electrons on the nitrile group, transitions involving these electrons occur at much higher energies than ketone n, π^* transitions). Additionally, since the electron-withdrawing properties of the nitrile group make it a good mimic for the acyl group, these results can be extended to include aromatic ketones as well.

Figure 1.3 shows the effect of the substituents on the π energy levels for both electron donors and acceptors. Note how both types of substituents result in a lowering of π, π^* triplet energies compared to the parent compound. The attachment geometry is also important. For donors, both *meta*- and *para*-substituents lower the energy relative to hydrogen, with *meta*-substituents having the larger effect. For acceptors, however, *meta*-groups have a smaller effect than *para*-groups.

Table 1.1 juxtaposes the benzonitrile results with the triplet energies of several

Figure 1.3. Triplet π, π^* state stabilizations by aromatic substituents modeled on benzonitriles.

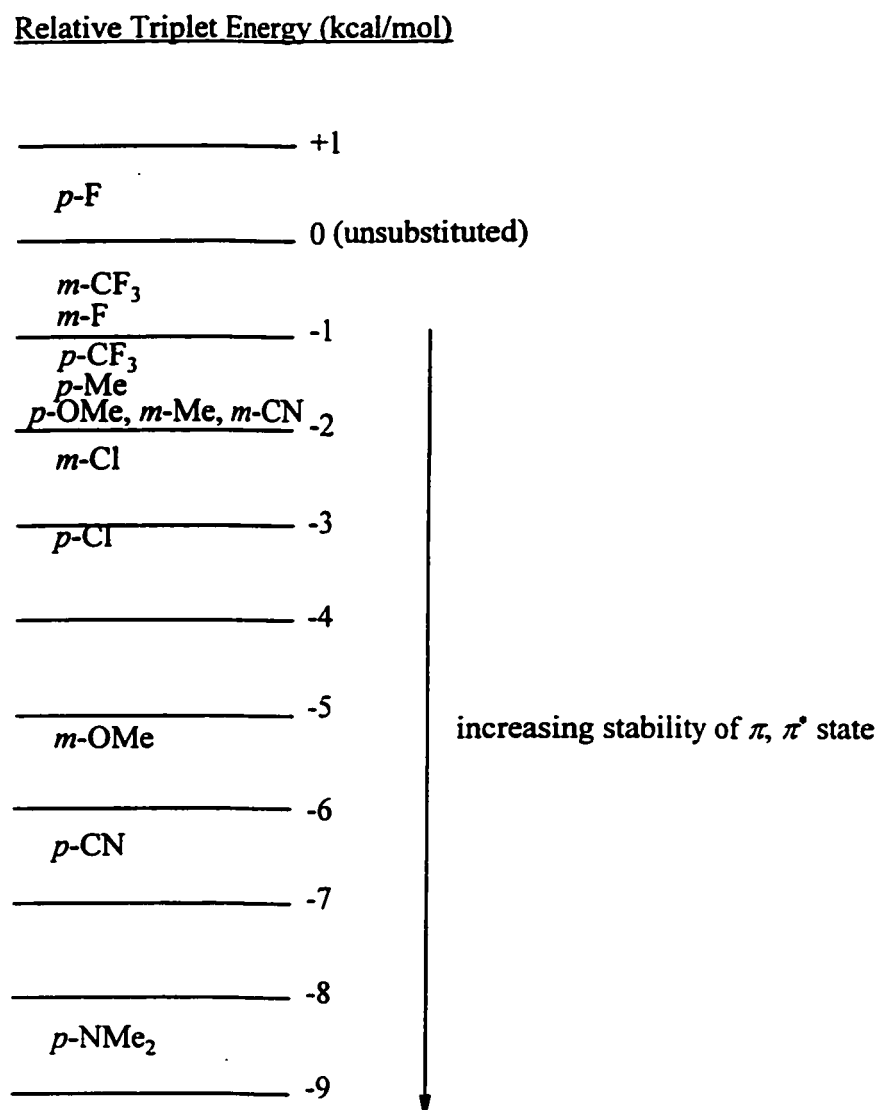
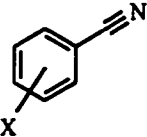
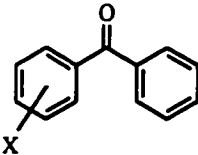


Table 1.1. Ring substituent effects on aromatic ketone triplet energies (in kcal/mol) as modeled on benzonitriles. Energies were determined at 77K in various glasses.^{a, b}

Benzonitrile (π, π^*)		Benzophenone (n, π^*)	Alkyl Phenyl Ketone Triplet	
Triplet Energy; EtOH		Triplet Energy	Energy	
			$\underline{n, \pi^*}$	$\underline{\pi, \pi^*}$
H	77.0	69.2	73.4	75.5
<i>m</i> -CN	75.5	68.5	73.3	73.8
<i>p</i> -CN	70.9	66.8	71.2	69.3
<i>m</i> -CF ₃	76.5	68.4	72.8	74.7
<i>p</i> -CF ₃	76.1	67.6	72.4	74.3
<i>m</i> -F	76.3		70.6	75
<i>p</i> -F	77.7	69.8	72.4	75
<i>m</i> -Cl	74.9	68.8	70.6	74
<i>p</i> -Cl	74.1	68.8	70.5	71.5
<i>m</i> -Me	75.5		73.5	73.2
<i>p</i> -Me	75.9	69.3	74.1	73.4
3,4-(Me) ₂			74.2	72.2
<i>m</i> -OMe	72.1	68.3	73	70
<i>p</i> -OMe	75.5	69.4	74.8	72

a. The bold font indicates lowest π, π^* triplet configurations in acetophenones.

b. Refs. 11 - 14.

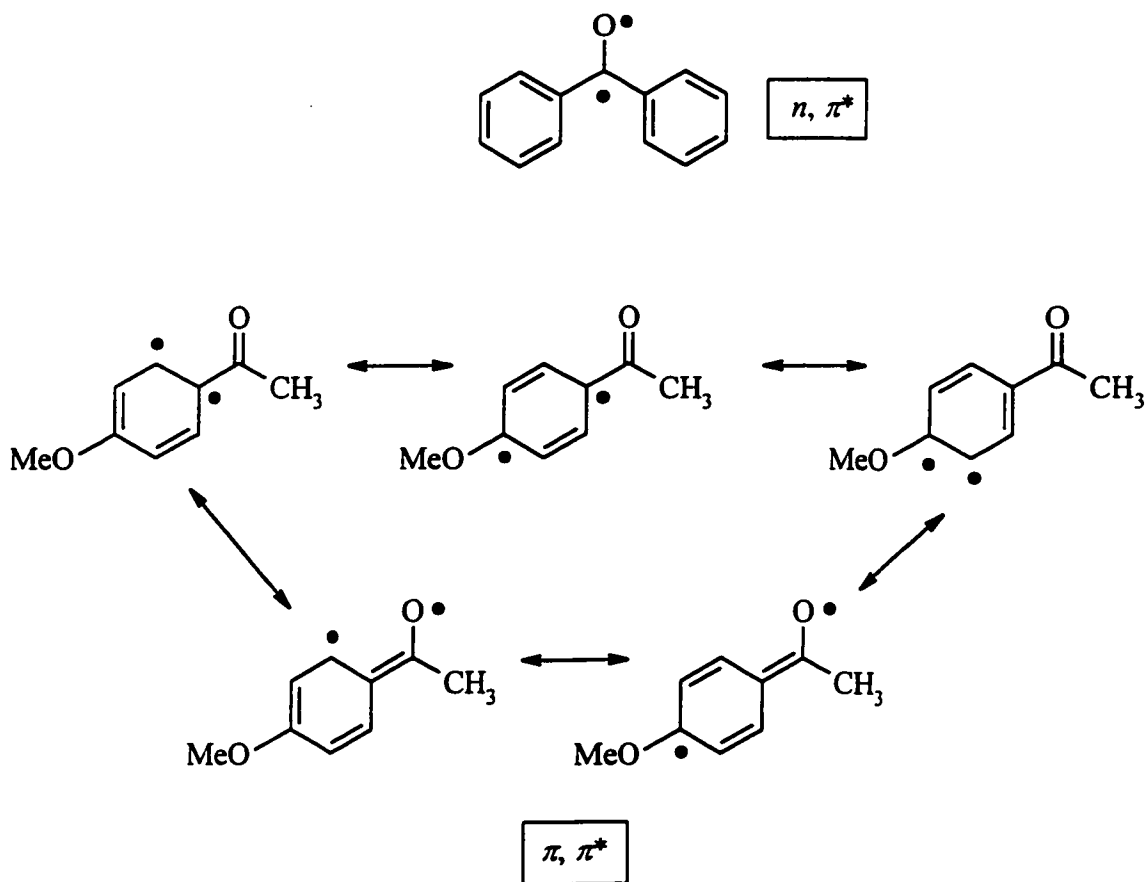
aromatic ketones. Estimated energy gaps for acetophenones are provided based on spectroscopic and reactivity data of Wagner and co-workers.¹¹⁻¹⁴ Note that in general the substituent effects on the energy levels behave as predicted from the benzonitrile model study. An interesting observation is that acetophenones with strongly electron-withdrawing groups in the *meta*-position have n, π^* lower triplets; this is an important point for later (see 2.1.8).

The above discussion has omitted any mention of the effect of the solvent on the photophysics. The solvent complicates matters since the ground S_0 state, as well as the n, π^* and π, π^* triplet states, are all solvated differently because of their different charge distributions. The result is that as solvent polarity is increased the more polar states are stabilized compared to the less polar ones. All else remaining equal, a polar solvent will lower the energies of π, π^* states relative to n, π^* states. This is an important result, since it indicates that aromatic ketone triplet sublevel energies can be highly variable. In fact, changing from a non-polar to a polar solvent can be sufficient to “switch” the character of the lowest triplet state in lowest n, π^* ketones with small $n, \pi^* - \pi, \pi^*$ gaps.¹⁵

Scheme 1.3 represents the electronic arrangement of the two different types of triplets. The n, π^* state can be pictured as a biradical species, with an electrophilic oxygen-centered radical site. This is because the transference of an n electron to the carbonyl π^* effectively breaks the double bond.¹⁶ In contrast, the π, π^* state has spin density in the aromatic ring, where the π -system causes extensive delocalization.

One prediction based upon their different electronic arrangements is that the two

Scheme 1.3. Valence bond representations of n, π^* and π, π^* triplet states.

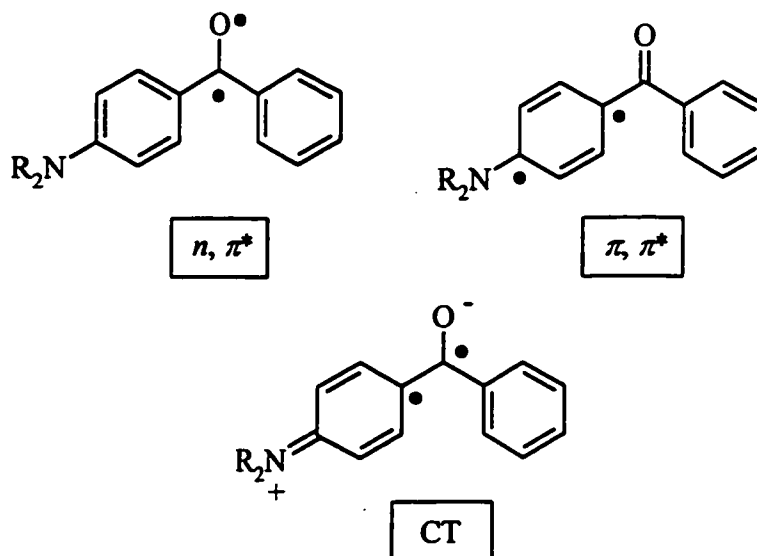


classes of ketones should display different reactivity patterns. This prediction will be explored in the next section.

Finally, a third type of triplet state should be mentioned. Porter's group observed that ketones with very electron-rich ring substituents, such as amino groups, displayed spectroscopic behaviour different from n, π^* and π, π^* species.¹⁷⁻¹⁹ These are the charge-transfer (CT) triplets, a general representation of which is depicted in Scheme 1.4.

In these species, any radical-like character from contributions by the other states is

Scheme 1.4. Comparison of CT triplets to n, π^* and π, π^* triplets.



supplanted by a very polar zwitterionic form. Experimentally¹⁸, CT-triplets are characterized by ground and excited state ultraviolet absorption spectra which display large bathochromic Stokes shifts, significant singlet reactivity resulting from less efficient ISC, and a markedly different chemical reactivity than the other two types. Also, the large buildup of negative charge at the carbonyl oxygen should make these excited states more basic than the other two classes.

Porter's group found¹⁸ that hydroxy ketones can also possess lowest CT states in basic aqueous media, where the substituents are actually phenolates.²⁰ However, methoxyketones turn out to have limited CT-character due to oxygen's lesser ability to tolerate a full positive charge than nitrogen.

1.4. Photoreduction and Hydrogen Atom Abstraction.

The photochemical reaction known as photoreduction forms the basis of the research to be discussed in this thesis. Photoreduction is a general process that follows from one of the main reaction channels of photoexcited ketones, hydrogen atom abstraction (HAA, Figure 1.4). In this process, the triplet state abstracts a hydrogen atom from a donor molecule, producing a triplet radical pair that then can undergo normal radical chemistry. The pair can undergo ISC and disproportionate to regenerate starting materials, or couple and produce a tertiary alcohol. If the ketone radical reacts with an H-donor, then photoreduced products are obtained analogous to those of metal hydride reductions of ketones. Finally, other radical-radical couplings can occur to form pinacol species and/or coupled donor fragments.

1.4.1. Energetics of hydrogen atom abstraction.

The large increase in energy that the ketone triplet possesses over the ground state makes radical-like HAA a favourable reaction process for many ketone/donor combinations.

Figure 1.5 represents a simple thermochemical cycle that allows the enthalpy of HAA to be estimated (Eq. 1.4). The bond dissociation energy of the hemipinacol C-H bond is that of a typical secondary C-H bond with aryl and oxygen substituents,²¹ and the heat of hydrogenation of the C=O group (-9 kcal/mol) is a number typical of aromatic ketones.²¹ Table 1.2 lists bond dissociation ($D_{R''-H}$) energies for potential H-donors, and Table 1.3 collects the $\Delta H_{R(HAA)}$ values calculated from the cycle.

Figure 1.4. Hydrogen atom abstraction by an aromatic ketone triplet leading to various photoreduced products.

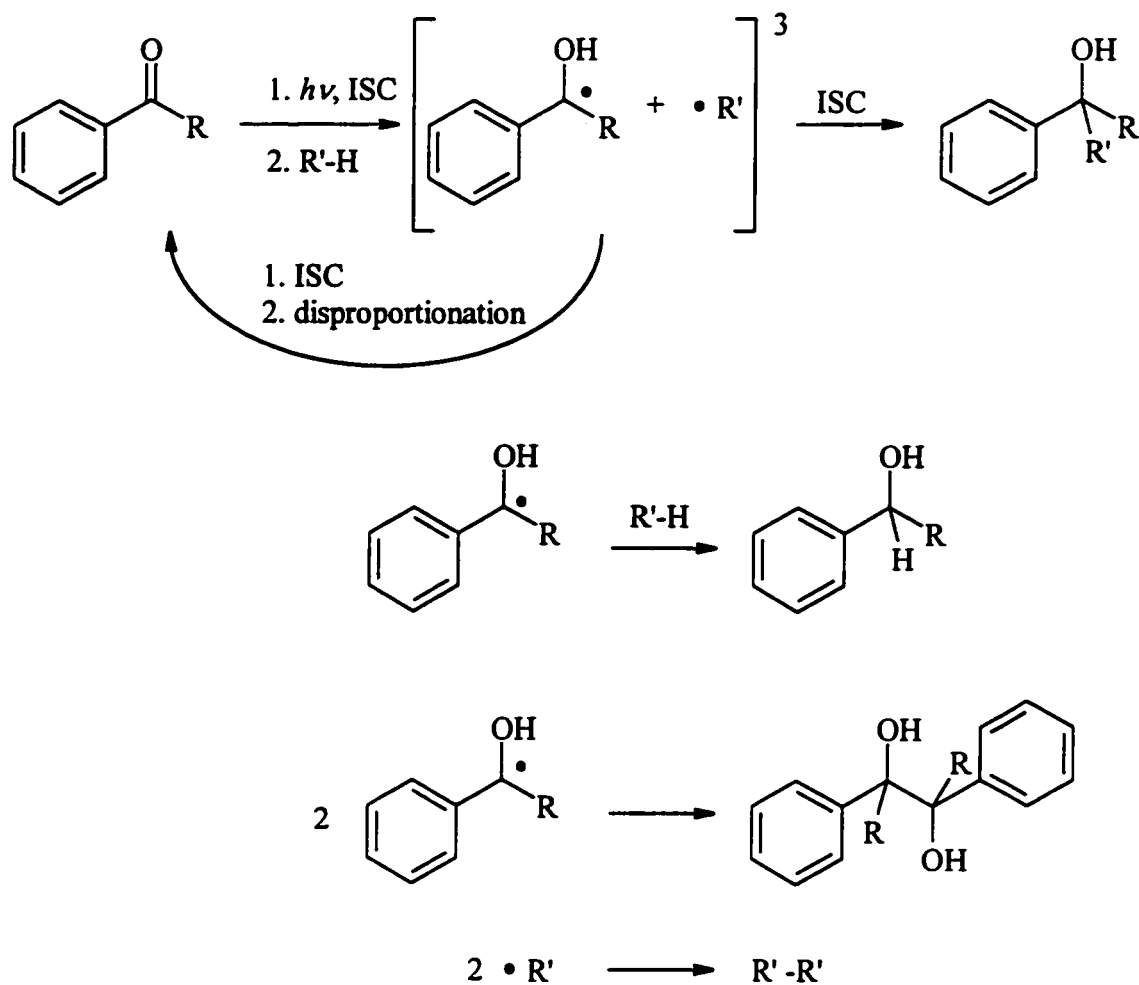
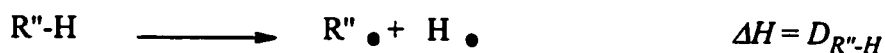
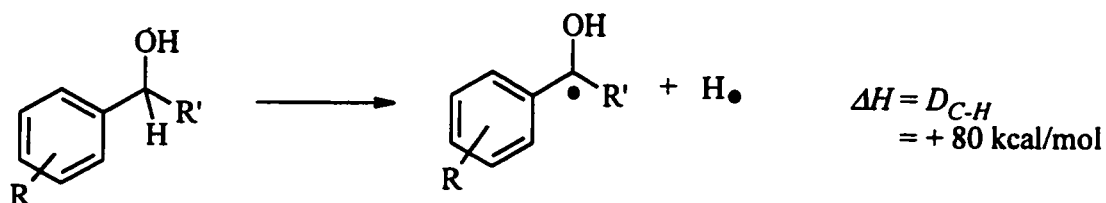
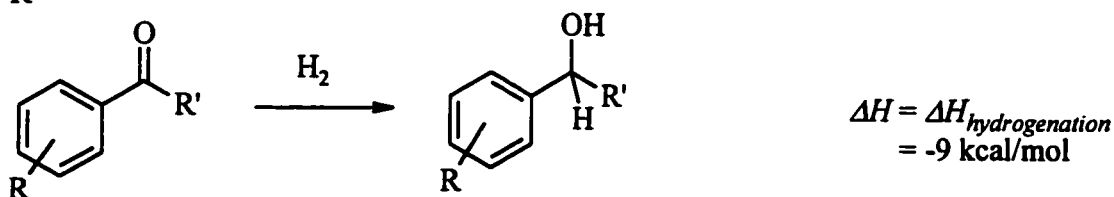
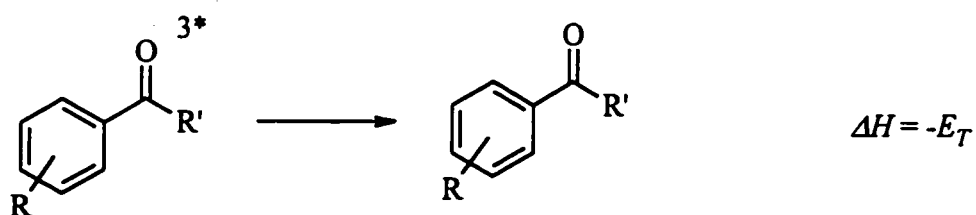
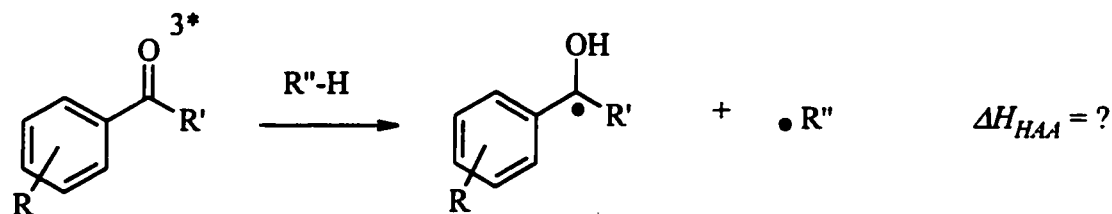


Figure 1.5. A thermochemical cycle to predict the enthalpy of HAA reactions.



$$\Delta H_{\text{HAA}} = -E_T + \Delta H_{\text{hydrogenation}} - D_{\text{H-H}} + D_{\text{C-H}} + D_{\text{R}''\text{-H}} \quad (1.4)$$

Table 1.2. $D_{R''-H}$ values for various donors. ^a

Donor	$D_{R''-H}$ (kcal/mol)
ethane (1° C-H)	98
propane (2° C-H)	94.5
benzene (sp ² C-H)	103
toluene (benzylic C-H)	85
water; methanol (RO-H)	120; 105
methanol (HOCH ₂ -H)	93
phenol (ArO-H)	88 ^b

a. Ref. 21, p. 94.

b. Ref. 58.

Table 1.3. $\Delta H_{R(HAA)}$ values for various ketones and donors. ^a

Ketone	E_T ^b	$\Delta H_{R(HAA)}$ for various donors (kcal/mol)						
		Ethane	Propane	Benzene	Toluene	Water	Methanol	Phenol
Acetophenone	73.5	-8.5	-12	-3.5	-21.5	+13.5	-13.5	-18.5
Benzophenone	69.0	-4	-7.5	+1.0	-17	+18	-9	-14
Fluorenone	53.3	+11.7	+8.2	+16.7	-1.3	+33.7	+6.7	+1.7

a. calculated from cycle (eq. 1.4 in Figure 1.4).

b. Ref. 5.

From these estimates, it is clear that simple, radical-like HAA processes will be exothermic with sp^3 C-H donors. Toluene demonstrates that factors that increase radical stability, such as resonance stabilization, will increase reactivity. As well, note that abstraction from aromatic C-H and aliphatic O-H bonds is predicted to be endothermic. As a final note, phenol is an exception since it has the ability to form a stable phenoxyl radical after HAA of the O-H bond.

1.4.2. Mechanisms of hydrogen atom abstraction.

Hydrogen atom abstraction by aromatic ketone triplets has been studied and reviewed in detail^{16,22,23} over the past three decades, and a large volume of data has been acquired on different aspects of the reaction. Since the radical processes following HAA have been relatively well understood for a long time, the mechanistic thrust of modern studies have focused on the photochemical process(es) and the actual details of the formal hydrogen atom transfer. These details have been found to be a complicated interplay of the nature of the ketone, the nature of the donor, and the solvent.

Arising from this interplay are three main mechanistic classes of photoreduction. The first involves full-electron transfer, in which the overall hydrogen atom transfer occurs stepwise as an electron transfer and then a proton transfer between fully formed radical ion pairs.²⁴⁻³¹

If the thermodynamics of electron transfer are unfavourable, then the HAA can occur *via* a single-step charge-transfer assisted mechanism, in which only partial ionization occurs.³²

The third mechanism (as well as the first to be recognized in the history of the reaction) is so-called “pure” or radical-like HAA. In this process, the abstracting ketone triplet behaves as an alkoxyl radical and the process exhibits characteristics similar to alkoxyl-radical abstractions.³³⁻³⁵

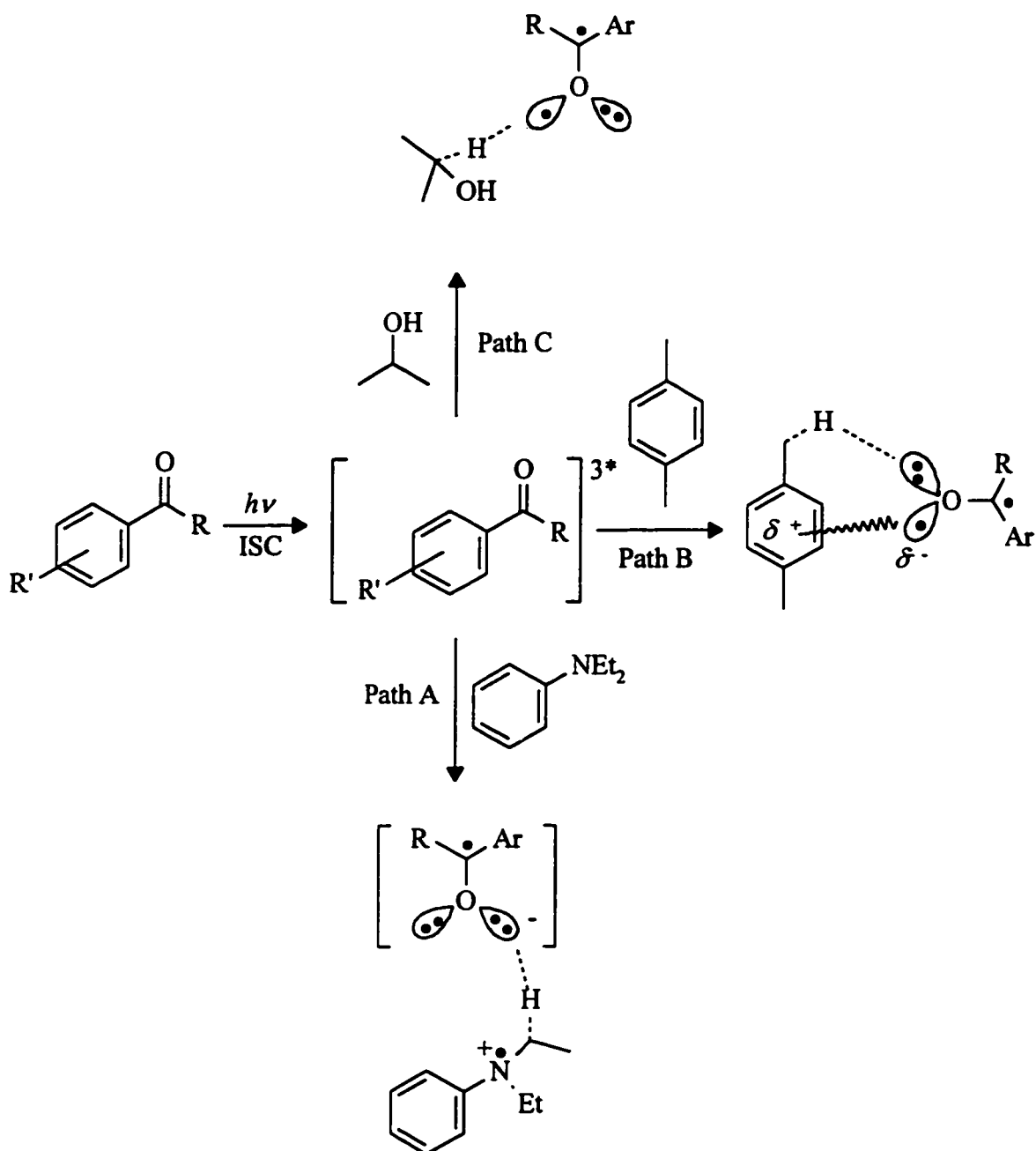
Figure 1.6 depicts these three different mechanisms.

The thermodynamic parameters of the reaction are what determine which of the pathways is followed in a particular photoreduction. These parameters in turn are dependent on the identity of the donor and the ketone, and to a lesser extent, the solvent.

Path A, the full-electron transfer case, is commonly observed in polar solvents with electron-rich donors that have low ionization potentials, such as amines and sulfides. In particular, the quenching of aromatic ketone triplets by amines has been well studied.^{19,24,25,29-31,34,36-39} The mechanistic spectrum is a complicated one, depending upon the solvent, the structure of the amine, and the possibility of secondary reactions of the primary intermediates. As well, numerous studies on the interactions of excited ketones with sulfur-containing species have been reported. Such compounds include simple alkyl and aryl thiols and thioethers,^{26,28,40-43} as well as compounds of biological importance such as amino acids and peptides.⁴⁴⁻⁴⁷ In aqueous or mixed aqueous solution, the direct detection of radical ions^{42,48} has clearly demonstrated that the mechanism involves electron transfer from the sulfur atom to the triplet ketone, and this is supported by theoretical calculations.⁴⁷

For the amine case, radical ions have also been observed by time-resolved spectroscopy down to the picosecond level and rates of quenching in these reactions are

Figure 1.6. The three main classes of hydrogen atom abstraction. Path A: full electron-transfer. Path B: charge-transfer assisted. Path C: alkoxyl-radical like abstraction.



on the order of 10^8 to $10^{10} \text{ M}^{-1} \text{ s}^{-1}$, near to that of diffusion in most solvents.

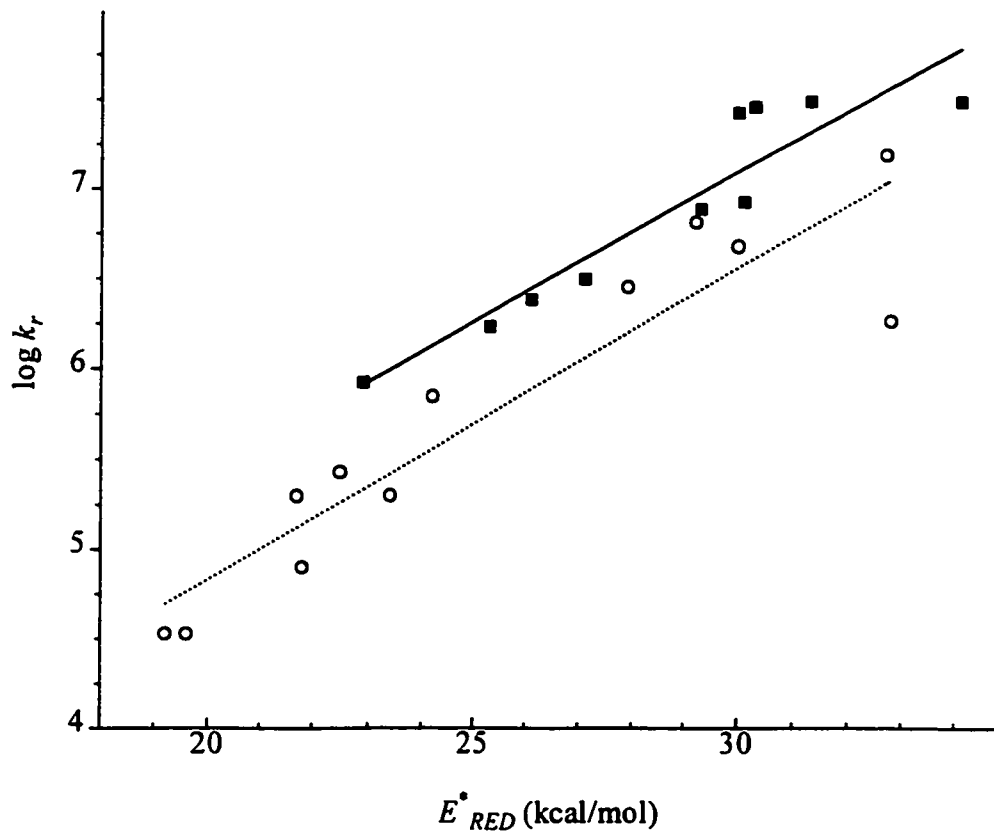
The second mechanistic class (Path B) is most commonly observed with π -conjugated donors that are less electron rich than amines or sulfides. Alkyl benzenes are an example. The formation of an arene/ketone donor/acceptor excited state complex (exciplex) occurs, in which a small amount of charge redistribution takes place to activate the benzylic C-H bond for HAA (as depicted in Figure 1.6).³²

This type of mechanism was first assigned by Singer and co-workers to the quenching reactions of donor-substituted triplet benzophenones by their ground states (self-quenching).^{49,50} As part of a much larger study, it was found that self-quenching rates increased as the benzophenone became more electron rich. For example, the rate of self-quenching of 4,4'-dimethoxybenzophenone was roughly 200 times greater than that of benzophenone itself. This trend was in agreement with the fact that triplet quenching rates of benzophenone by aromatic compounds were known to increase with increasingly electron-rich benzenes.⁵¹ It was argued that the exciplex formed had stabilization from the aromatic ring of the ground state molecule to the carbonyl n -orbital of the triplet; this was called an " n -type" exciplex.

Wagner's group found evidence consistent with the intermediacy of an " n -type" exciplex in the reactions of aromatic ketone triplets with xylenes and toluenes. Rate constants of triplet deactivation by these molecules correlated with the reduction potential of the triplet state.³² Since the electron demand on the xylene directly influenced the reactivity, some interaction with the arene nucleus and the triplet was occurring.

Figure 1.7 reproduces a plot of ketone reactivity towards *para*-xylene plotted *versus*

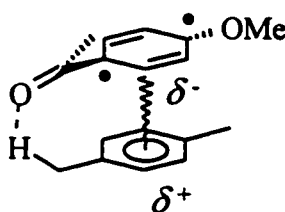
Figure 1.7. Plot of bimolecular reaction rate constants of ketone triplet quenching by *para*-xylene in acetonitrile as a function of triplet reduction potential. Squares indicate benzophenones, circles represent acetophenones. From Ref. 32.



triplet reduction potential in acetonitrile.³² The triplet reduction potential, E_{RED}^* , is defined as the sum of the ketone triplet energy and its ground state reduction potential. Linear correlations indicating a charge-transfer dependence for the mechanism are observed for both benzophenones and acetophenones. Interestingly, the lines have similar slopes, indicating a similar participation in a charge-transfer assisted HAA mechanism for both types of lowest triplet state. It is believed that the π, π^* states react *via* an exciplex of " π -type" (Scheme 1.5), similar to one which Singer's group had first assigned to the quenching of triplet benzophenone by electron-*poor* aromatic compounds.⁵⁰

In this type of exciplex, the benzoyl π -orbital can undergo efficient overlap with the donor π -orbital.

Scheme 1.5. The " π -type" exciplex.



Finally, the rest of aromatic ketone HAA reactivity falls under Path C, the "pure" radical pathway. In this mechanism, the transition state for HAA has very little polarity, and the reactions generally feature the smallest quenching rate constants of the three mechanistic types discussed. Aliphatic donors, such as hydrocarbons or aliphatic

alcohols, are the most common types of donors from which these abstractions occur.

Regardless of the process mediating these reactions, rates of reaction for the Path B mechanism are several orders of magnitude lower than the full electron transfer case.

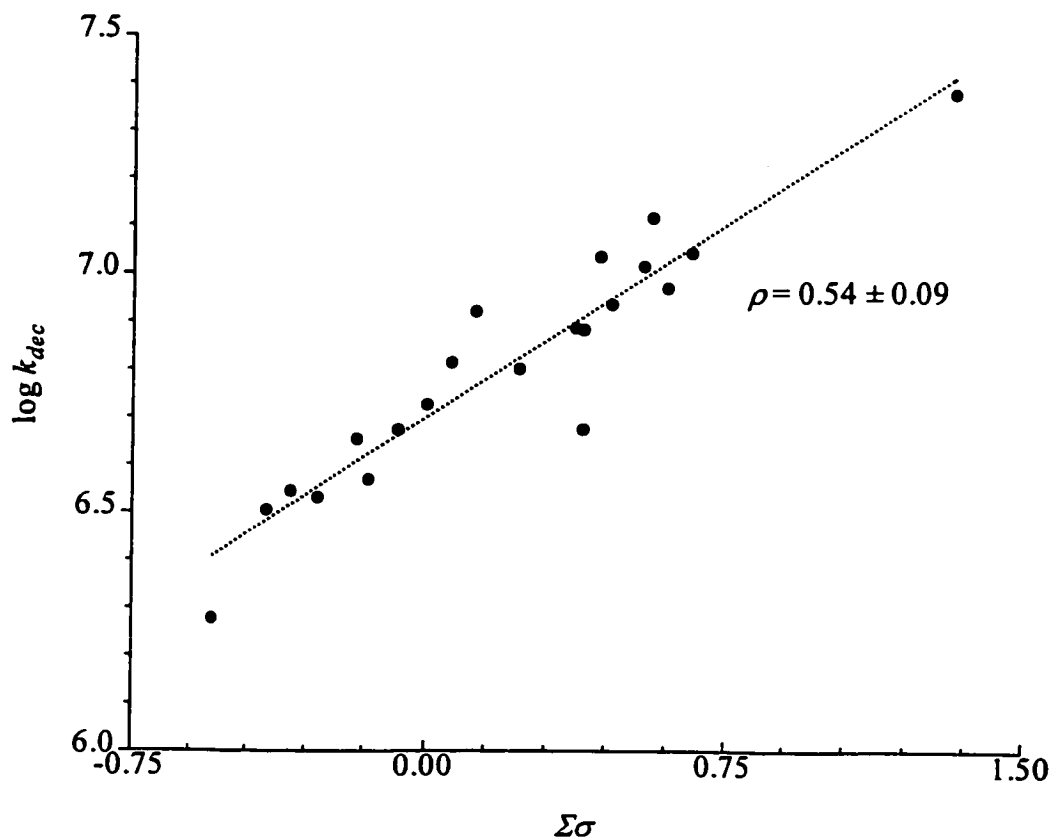
Wagner's group investigated substituent effects on this reaction.⁵² In this study, lifetimes of substituted benzophenone triplets in cyclopentane solvent were determined by NLFP; the resulting Hammett plot is reproduced in Figure 1.8. From this analysis, it was concluded that the triplets abstracted hydrogen from the hydrocarbon with a mechanism very similar to that of radical-like HAA, in agreement with the earlier findings of Padwa, Walling and Gibian, and Steel and co-workers.^{33,35,53} The small positive ρ value indicates that there is very little charge-transfer stabilization of the transition state.

1.4.3. Role of the lowest triplet state in hydrogen atom abstraction.

Over the course of the late 1960s and early 1970s, it was identified that there existed a further demarcation of aromatic ketone triplet HAA reactivity, namely the configuration of the lowest triplet state. With hydrocarbon, arene and alcohol photoreductants, it was observed that ketones with lowest n, π^* triplet states were 10 - 100 times more reactive than π, π^* ketone triplets of similar energy.^{13,19,22,23,32,33,52,54,55} For heteroatomic donors containing nitrogen or sulfur, on the other hand, the configuration of the lowest triplet state is less important.

For example, consider benzophenone (with a lowest n, π^* triplet configuration) and

Figure 1.8. Plot of benzophenone triplet decay rates in cyclopentane *versus* total Hammett sigma parameter. From Ref. 52.



para-methoxyacetophenone (lowest π, π^* triplet, with the n, π^* state lying 2.8 kcal/mol above).¹³ Both ketones abstract hydrogen from xylene at rates about ten times higher than from cyclopentane (due to the different mechanisms operative with the different donors), but benzophenone has a hundred-fold greater reactivity than 4-methoxyacetophenone in both reactions.^{32,52} Furthermore, lowest π, π^* triplets sometimes display very little reactivity or even total inertness in some reactions. CT states, as a sub-class of the π, π^* ketones, similarly show inertness in typical photoreduction reductions. The only exception, for both π, π^* and CT triplets, is quenching by the primary electron transfer mechanism (Path A, Figure 1.6). Cohen's group documented that amine donors quenched benzophenone, fluorenone (π, π^* triplet, and inert to many donors) and 4-dimethylaminobenzophenone (CT triplet, inert to most donors) efficiently and rapidly.²⁴

1.4.4. Reactivity of upper triplet levels in radical-like HAA reactions.

By the early 1970s a consensus was reached in the literature regarding π, π^* state radical-like HAA reactivity. Enough photoreduction studies involving radical-like abstractions had been done to suggest that the reactivity of the π, π^* state, if not altogether negligible, was only a mere fraction of the n, π^* reactivity. Yang's group¹⁵ was the first to propose that whatever reactivity a lowest π, π^* triplet exhibited in a radical-like HAA reaction came instead from the small population of the upper n, π^* state

available due to the thermodynamic equilibration of states, modulated by the energy gap ΔE between the first two triplet levels. Equations 1.6 and 1.7 depict the reactivity of a lowest n, π^* triplet divided between n, π^* and π, π^* *intrinsic* reactivities, and the formulation for calculation of the upper state's population based on the Boltzmann equation, respectively.

$$k_q = \chi_{n,\pi^*} k_{n,\pi^*} + \chi_{\pi,\pi^*} k_{\pi,\pi^*} \quad (1.6)$$

$$\chi_{n,\pi^*} \sim e^{-\Delta E/RT} \quad (1.7)$$

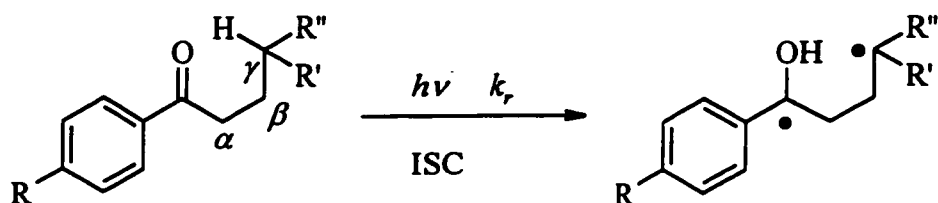
For a triplet gap of 0.5 kcal/mol, equation 1.7 predicts a partial population of over forty per cent for the upper state at 300 K. In fact, even with a gap as large as 3 kcal/mol, the resulting n, π^* population of 0.5% could be enough to account for the very small reactivity observed in some π, π^* abstractions if k_{n,π^*} was much larger than k_{π,π^*} .

Wagner and co-workers became interested in solving this problem, arguing that evidence for upper n, π^* reactivity could come from studying a well-known reaction with two series of compounds. The first series was chosen since it would react through an unambiguously assigned n, π^* lowest triplet, while the other would have a lowest π, π^* state, but with an n, π^* state not too far removed in energy. The reaction would be studied for the first series to determine the intrinsic n, π^* reactivity, and then repeated for the other series. Although the absolute reactivity may be less, if the *trends* in rate

constants were the same for both series, then that would mean that both series were reacting *via* an n, π^* state (barring coincidentally similar intrinsic reactivities).

For this study, the Norrish-Yang reaction, Scheme 1.6,¹³ was chosen. This particular reaction involves intramolecular HAA from the γ -carbon of the ketone chain, and produces a 1,4-biradical, the chemistry of which has been exhaustively studied.²³

Scheme 1.6. The Norrish-Yang reaction for substituted valerophenones.



Results for γ -substituted valerophenones and *para*-methoxyvalerophenones are listed in Table 1.4. They indicate that although the methoxy-substituted ketone has a much lower Norrish-Yang reactivity than the unsubstituted derivative, the *per-bond* reactivity ratios are nearly the same for both the $R = H$ (lowest n, π^*) and $R = OMe$ (lowest π, π^*) compounds. The rate-changes from substrate to substrate are due to the substituent effects on the C-H bond strengths. It was concluded that since the trends were similar for both series the n, π^* state was responsible for the observed reactivity in both cases. A ΔE value of 2.8 kcal/mol in benzene was calculated for *para*-methoxyvalerophenone.

Table 1.4. Norrish-Yang abstraction rates, per-bond reactivities and reactivity ratios of γ -substituted valerophenones and *para*-methoxyvalerophenones in benzene. ^a

R	R'	R''	Corrected Reactivity ^b		Ratio ^c
			$k_r / 10^7 \text{s}^{-1}$	$/ 10^7 \text{s}^{-1}$	
H	H	H	12.5	37.5	1
OMe	H	H	0.056	0.168	1
H	Me	Me	48	48	1.28
OMe	Me	Me	0.3	0.3	3.33
H	H	CO ₂ Me	1.0	2.0	0.05
OMe	H	CO ₂ Me	0.0025	0.005	0.03
H	H	CH ₂ CO ₂ Et	4	8	0.21
OMe	H	CH ₂ CO ₂ Et	0.028	0.056	0.33
H	H	CN	1.0	2	0.05
OME	H	CN	0.003	0.006	0.04

a. From ref. 13.

b. Corrected reactivity = (k_r) x (number of C-H bonds at carbon- γ).

c. Ratio = (corrected ketone reactivity) / (corrected reactivity of ketone with R' = R'' = H).

Excellent support for both the concept and the magnitude of ΔE in *para*-methoxy substituted aromatic ketones was provided in 1983 when Encinas *et al*⁵⁵ reported the temperature dependence of the rate constants for Norrish-Yang HAA in unsubstituted and *para*-methoxyvalerophenone. They observed that the Arrhenius activation energy for reaction by lowest π, π^* ketones was consistently about 3 kcal/mol higher than for the lowest n, π^* ketones. They concluded that n, π^* states were solely responsible for the reactions studied, and that the larger Arrhenius energies for the reactions of the lowest π, π^* ketones reflected the energy gap, ΔE .

1.5. Photochemical Hydrogen Atom Abstraction from Phenols.

Phenols represent a class of donors that has received relatively minor attention in the mechanistic studies of aromatic ketone triplet quenching. Prior to 1981, fewer than ten publications dealt with the photochemistry of phenols with ketones, with only two kinetic studies reported. This is interesting, as phenols occur naturally in various forms and display a rich chemistry. Examples of biological importance include the essential amino acid tyrosine that has a phenolic side chain, Vitamin E (α -tocopherol), and the lignin molecule, a building block of wood matter which contains both ketone and phenol groups, the interactions of which are partially implicated in the photoyellowing of paper.^{56,57}

Upon consideration of the structure and properties of phenol, certain predictions can be made regarding their potential reactivity with ketone triplets. As shown in Table 1.2,

the phenolic O-H bond is weaker than that of alcohols by *ca.* twenty kcal/mol.⁵⁸ This fact, coupled with the strength of aromatic C-H bonds, indicates that if phenols react with triplets *via* HAA, they will lose the phenolic hydrogen to produce a phenoxyl radical, a relatively stable species.

As far as a mechanism is concerned, several possibilities can be discussed. A simple, radical-like abstraction may occur, in analogy to alkoxyl radical abstractions from phenols, as proposed by various workers.⁵⁹⁻⁶¹

However, as an electron-rich benzene derivative, phenol can also act as a reductant under certain circumstances. While not as strongly reducing as most amines or sulfides (the estimated ionization potential of phenol (8.45 - 9.11 eV)^{62,63} is higher than normal members of these two classes of species (7.5 eV for triethylamine⁵¹ and 8.2 eV for dibutylsulfide⁶⁴), the possibility of electrophilic ketone triplets being quenched by electron-transfer from phenols is something that needs to be addressed with the Rehm-Weller equation. Even if full electron-transfer in general turns out not to be favourable, phenol's resemblance to toluene suggests that a mechanism involving charge-transfer through an "*n*-type" exciplex may also be a possibility to consider.

Finally, phenol is weakly acidic and thus mechanisms involving hydrogen-bonding with or even protonation of excited ketones can be envisioned. This is a new aspect not present with other typical donors, such as amines, alcohols or hydrocarbons. Lowest π , π^* and CT-type triplets, due to their relatively basic natures compared to lowest n , π^* triplets, could be particularly well suited to this kind of mechanism.

1.5.1. Previous studies involving phenols.

Perhaps one of the reasons why ketone/phenol photoreactions received relatively little early attention was because one of the first studies of the reaction indicated that phenol was a very poor photoreductant. Figure 1.9 shows some of the results of this study, which was an attempt at a large scale photochemical reaction between aromatic ketones and phenols by Becker⁶⁵⁻⁶⁷. These experiments indicate that with 2,6-bis(*tert*-butyl)phenol (**1**) and triplet benzophenone a reaction occurs in the presence of an acid catalyst to produce the tetraarylmethane **2**, and not the traditional photoreduction products, mixtures of benzhydrol and benzopinacol. Without the acid, only very low yields of a totally different product, fuchsone **3**, is isolated.

The mechanism Becker proposed is that HAA by triplet benzophenone leads to the hemipinacol radical **4** and phenoxy radical **5**. Compound **5** couples to radical **4** and the fuchsone then forms after subsequent dehydration. The final product is produced by acid-assisted electrophilic aromatic substitution (EAS) in the dark with another phenol molecule. This explains the need for acid catalysis. These studies were extended to substituted benzophenones and other 2,6- disubstituted phenols, with similar results.⁶⁶

The first studies of the kinetics of ketone triplet/phenol reactions were those of Turro and co-workers.⁶⁸⁻⁷¹ They used biacetyl (MeCO-COMe) exclusively, an aliphatic diketone with a lowest n, π^* triplet state and a triplet energy of 56 kcal/mol. In one paper⁷⁰ the quenching of biacetyl fluorescence and phosphorescence intensities by a wide variety of donors ranging from simple alcohols to amines and phenols is studied. A small selection of the results that focus on the triplet state are reproduced in Table 1.5, as well

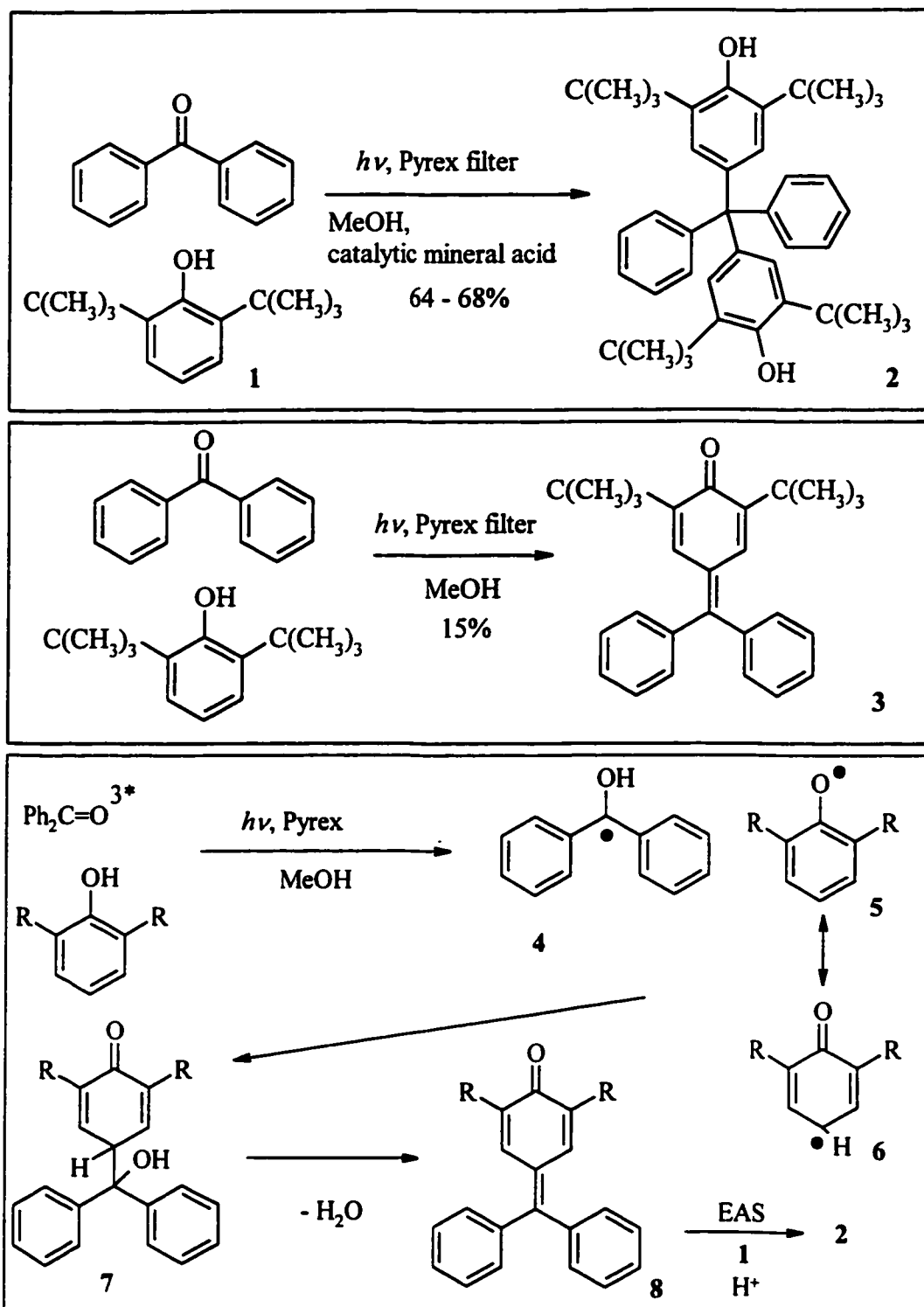
Figure 1.9. Photochemical reaction of benzophenone with 2,6-disubstituted phenols.

Table 1.5. Rate constants of quenching of biacetyl phosphorescence by various donors in benzene and acetonitrile, and proposed HAA mechanisms. ^a

Quencher	$k_q / 10^7 \text{ M}^{-1} \text{ s}^{-1}$	$k_q / 10^7 \text{ M}^{-1} \text{ s}^{-1}$	Proposed Mechanism of HAA
	Benzene, 25°C	Acetonitrile, 25°C	
Isopropyl Alcohol	3.3×10^{-4}	1.3×10^{-3}	irreversible H abstraction
Diphenylmethanol	7.0×10^{-3}	0.013	irreversible H abstraction
$(n\text{-C}_4\text{H}_9)_3\text{SnH}$	1.5		irreversible H abstraction
Phenol	34	0.79	reversible H abstraction
Phenol- <i>O</i> -d	10		
Anisole	0.013		electron-transfer
<i>meta</i> -Hydroxyphenol	250	12	reversible H abstraction
Aniline	50	150	electron-transfer
Diphenylamine	170	280	electron-transfer

a. Data and proposed mechanisms from Ref. 70.

as the assigned mechanisms for each donor. There are several important observations.

First, steady-state irradiations of mixtures of biacetyl and phenol do not result in consumption of the diketone, pointing toward a reversible quenching process for phenols. Second, the large kinetic isotope effect ($k_H/k_D = 3.4$) on the phenolic abstraction highlights the importance of the phenolic hydrogen in the quenching process; this is corroborated by the greatly diminished reactivity of anisole, a compound identical in structure to phenol but lacking this hydrogen.

The amine quenching behaviour is very typical of an electron-transfer mechanism, with very large rate constant that increases with solvent polarity. In contrast, the two phenols studied reacted as rapidly as the amines, but with an opposite solvent effect. The conclusion is that electron-transfer is not occurring for phenols; instead, the reaction proceeds *via* a 'reversible hydrogen abstraction'. The manner in which this process was occurring with such large rate constants was not explained.

The next year, Turro and Lee reported⁷¹ another kinetic study involving phosphorescence intensity quenching of biacetyl, this time by seven substituted phenols. From these data, a Hammett plot was prepared which indicated a negative slope of -1.15. The fact that electron-rich phenols interact faster than electron-poor ones is consistent with the electrophilic nature of an n, π^* triplet. No further speculation as to the nature of the triplet quenching mechanism was made.

1.5.2. The ketone triplet / phenol interaction studied by nanosecond laser flash photolysis.

True insight into the nature of the reaction was not gained until 1981, when Scaiano and co-workers used the technique of nanosecond laser flash photolysis (NLFP) to study the quenching of both benzophenone and *para*-methoxypropiophenone (MPP, lowest π , π^* triplet) by a wide variety of phenols in benzene solution.⁷²

This study gave the first direct spectroscopic evidence of the reactive intermediates involved in the reaction. The transient spectroscopy demonstrated that the primary products of the reaction are the corresponding phenoxyl and hemipinacol radicals, and it is estimated that in most cases 80-100% of quenching events give rise to the radical pair. The absolute rate constants for quenching are very high, close to $10^9 \text{ M}^{-1} \text{ s}^{-1}$ in all cases. Rate constants for quenching in water- or D_2O -saturated benzene indicated isotope effects greater than one, indicating a mechanism involving a hydrogen atom transfer in the rate-determining step for triplet deactivation, in agreement with previous results from steady state quenching experiments.⁷⁰

An extremely interesting result is found upon comparison of the reactivity of the lowest n , π^* and π , π^* triplet ketones. There is very little difference between the two; in fact MPP is quenched more rapidly than benzophenone by certain phenols. Here, for the first time, π , π^* triplets are reported to show a greater reactivity in a HAA reaction in which full-electron transfer is not occurring. Although at the time there were no grounds to rule out full-electron transfer, use of the Rehm-Weller equation will later demonstrate

(see Chapter Two, section 2.1.7) that for phenol and benzophenone, electron transfer is endergonic.

Hammett substituent analyses were prepared from the rate data, and they are reproduced in Figure 1.10. The variation in rate constants yields a negative slope for benzophenone, again consistent with its electrophilic n, π^* state. For MPP, however, a totally different result is obtained. The nearly zero slope indicates an almost total insensitivity to phenol substituent, and perhaps a potentially different mechanism of interaction for the lowest π, π^* ketone triplet. This result is tempered by the fact that the proximity of the bimolecular quenching rates to the diffusion-controlled limit is expected to have an attenuating effect on the sensitivity.

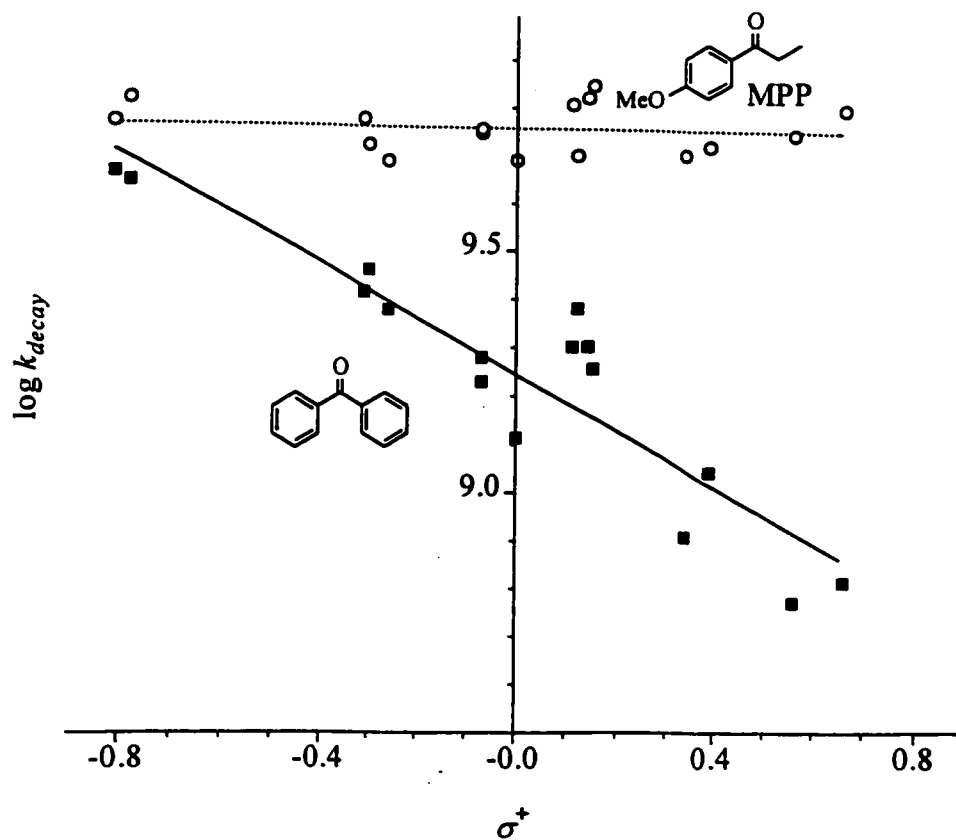
Ultimately, it was concluded that the fast overall quenching rates and lack of state dependence in the reaction indicated for both triplet classes a charge-transfer component in the quenching process, but no further mechanistic conclusions were drawn.

Since then, a number of other LFP studies have been published,⁷³ mostly focusing on aspects of spectroscopy and the behaviour of the free radical products of the reaction. A number of other techniques have also been used to study the basic HAA process.^{20,74-82}

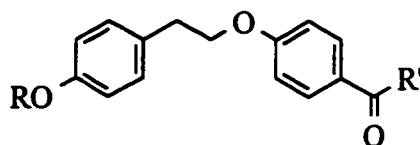
1.5.3. The photochemistry of para, para'-linked phenolic acetophenone in fluid solution and ordered media. Intramolecular phenolic hydrogen atom abstraction.

An interesting paper⁷⁴ was published almost fifteen years ago reporting the solution photochemistry of the para, para'-oxyethyl-linked phenolic ketones (LPKs) **9a** and **9c** and

Figure 1.10. Hammett plots of benzophenone and *para*-methoxypropiophenone (MPP) triplet quenching by substituted phenols in benzene. From Ref. 72.



Scheme 1.7. A series of para, para'-oxyethyl-linked phenolic ketones and their *O*-methyl ethers.



R = H; R' = Me	9a
R = Me; R' = Me	9b
R = H; R' = <i>n</i> -C ₃ H ₇	9c
R = Me; R' = <i>n</i> -C ₃ H ₇	9d

their *O*-methyl ethers **9b** and **9d**, Scheme 1.6, in deoxygenated solution.

Both compounds **9a** and **9b** appeared to be quite unreactive in solution, with the quantum yield of disappearance of compound **9a** measured at less than 0.02. On the other hand, the valerophenone derivative **9d** exhibited Norrish-Yang reactivity almost identical to *para*-methoxyvalerophenone itself. Compound **9c**, however, despite also being able to undergo intramolecular Norrish-Yang abstraction, also had a very low quantum yield.

This result points towards a very rapid competing triplet deactivation process.

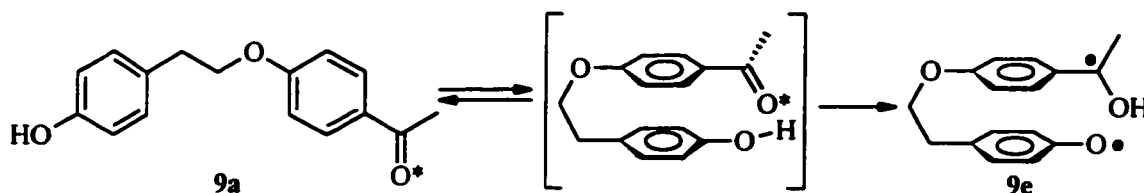
NLFP studies indicated that compound **9b** in acetonitrile behaved as a normal *para*-alkoxyacetophenone, with a similar triplet-triplet absorption spectrum⁸³ ($\lambda_{max} = 385\text{-nm}$) to *para*-methoxyacetophenone, and a triplet lifetime of 2.6 microseconds.

The 12-nanosecond triplet lifetime of compound **9a** is over two *orders of magnitude* smaller than that of compound **9b**, and the transient absorption spectrum indicates that

there are residual products which persist after the triplet decay is complete. Apparently, the presence of the phenolic hydrogen distinctly affects the photochemistry of the remote carbonyl group in compounds **9a** and **9c**.

The short triplet lifetimes of both of these LPKs is attributed to excited state deactivation by intramolecular abstraction of the remote phenolic hydrogen, *via* an intermediate 'sandwich' exciplex, leading to the formation of the expected phenoxyl-hemipinacol biradical **9e** shown in Scheme 1.8 for the case of ketone **9a**.

Scheme 1.8. Intramolecular phenolic hydrogen atom abstraction.



The observation of a deuterium kinetic isotope effect ($k_H/k_D = 1.8$) on the triplet decay rate of compound **9a** in water- or D_2O -saturated benzene solution supported the idea that hydrogen abstraction is the rate determining process in the triplet quenching.

This result is in agreement with the primary isotope effect for lowest π, π^* triplets observed previously⁷² and suggests that in fluid solution, the conformational motions required for the molecule to achieve an appropriate geometry for intramolecular hydrogen abstraction occur over a somewhat faster timescale than the actual abstraction process.

The residual absorption in the transient spectrum of LPK **9a** is assigned to the triplet biradical **9e**, whose lifetime of 120-ns was directly determined by NLFP. Based on the lack of a kinetic isotope effect on its lifetime, the mechanism of its decay was proposed to be rate determining ISC to the singlet state, followed by rapid intramolecular HAA to re-form ketone **9a**.

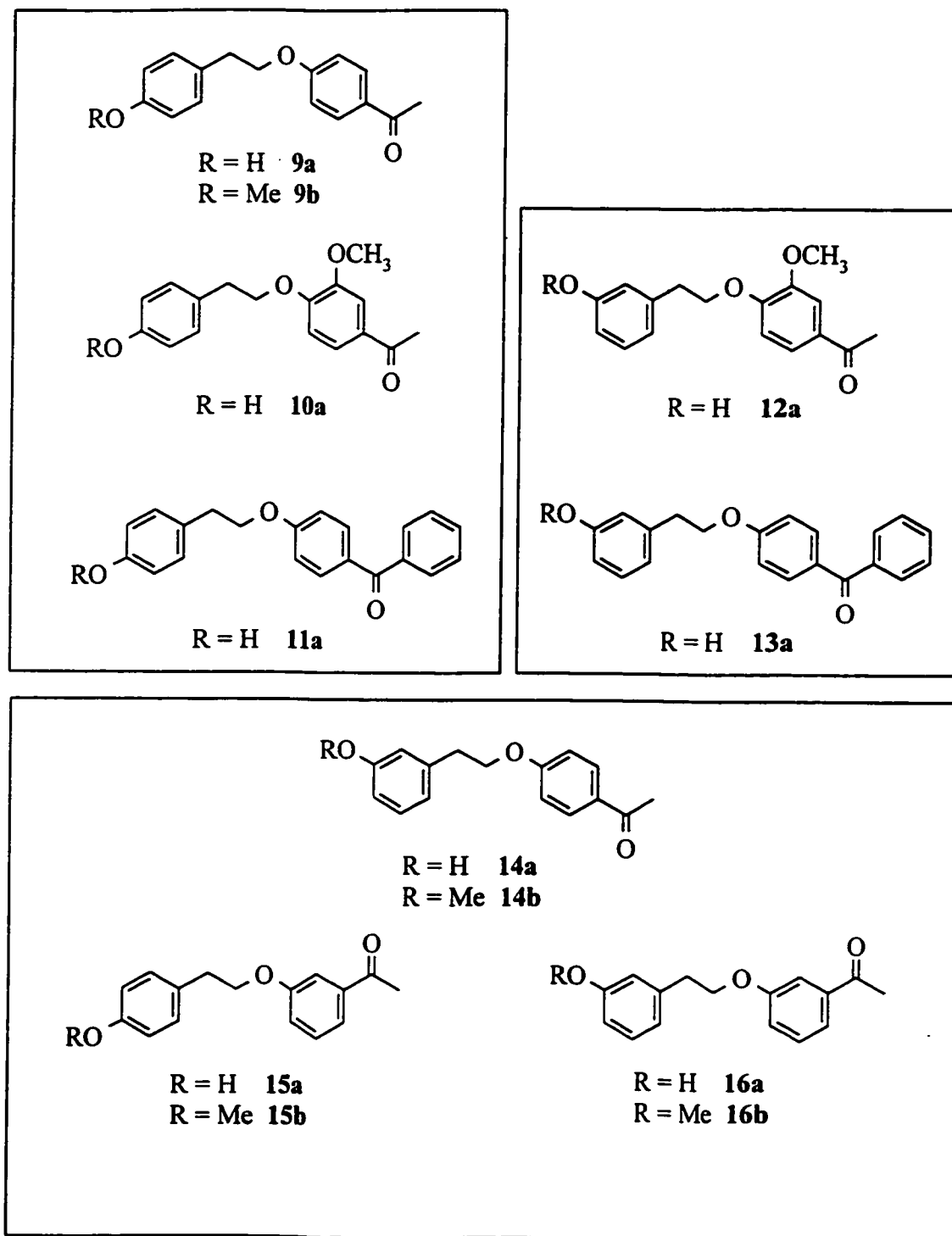
Having established the photochemistry of compound **9a**, it was used as a photochemical probe molecule in subsequent studies of organized media, such as liquid crystals⁸⁴ and cyclodextrins.⁸⁵ In these cases, the now-established propensity of the molecule to "bite its own tail" was hindered owing to the restrictive effects of these media on its conformational mobility. Thus, inclusion of compound **9a** in such environments resulted in substantial increases in the triplet lifetime.

1.5.4. Preliminary study of the effects of chromophore and geometry on intramolecular HAA.

The LPK series was dramatically expanded by Michael St. Pierre's (MSP) M.Sc. work, completed in 1994 in this laboratory.⁸⁶ He prepared ten new LPKs, as shown in Figure 1.11, and compared their photochemical behaviour, in a preliminary fashion, to ketone **9a**. The preparation of benzophenone LPKs as well as LPKs with *meta*-attachments allowed two new aspects of the intramolecular phenolic HAA reaction to be investigated.

The first was to determine the intramolecular reactivity of an n, π^* triplet. Recall that in bimolecular reactions, π, π^* triplet reactivity towards phenols is slightly higher

Figure 1.11. Linked phenolic ketones previously studied by MSP.



than n, π^* reactivity. Faced with this result, it was of interest to see if it applied in the intramolecular reaction as well.

The second aspect involved the effect of geometrical isomerism among LPKs of the same chromophore. This was of interest because in bimolecular quenching, the approaching triplet and phenol are free to adopt whatever geometry is necessary for fast HAA. Intramolecularly however, the three-atom tether greatly reduces the number of available orientations and can ostensibly hold the two rings in essentially a face-to-face arrangement in the sandwich. As a consequence, any dramatic differences in triplet lifetime between compounds **9a** and **14a-16a** could indicate that the actual geometry of the molecule inside the sandwich exciplex was important.

A summary of some of the results of MSP's thesis is given in Table 1.6.⁸⁶ They consist of triplet lifetimes of LPK series **9-16**, and kinetic isotope effects on the triplet lifetimes based on data in 5% aqueous acetonitrile compared to 5% D₂O/acetonitrile. The table also lists the lowest triplet assignment (n, π^* or π, π^*) of each ketone as determined by low temperature phosphorescence emission spectroscopy. The bimolecular rate constants listed in the table next to each LPK are from the reaction of the corresponding model ketone and phenol whose chromophores mimic the intramolecular reaction. For example, the model compounds for compound **16a** are *meta*-cresol and *meta*-methoxyacetophenone. The significance of the bimolecular rate constants will be discussed in Chapter Two.

As can be seen from the Table, the isotope effects were all found to be larger than one, and for the compounds with *O*-methyl ethers for comparison, triplet lifetimes for the

Table 1.6. Lowest triplet assignments, kinetic isotope effects, triplet lifetimes of LPKs 9-16, and bimolecular rate constants of quenching of model ketone triplets with the appropriate cresol in deoxygenated MeCN at temperatures ranging from 20 to 27°C. ^a

Compound	Kinetic Isotope	Triplet Lifetime	
	Effect ^b	(ns)	$k_q / 10^9 \text{M}^{-1} \text{s}^{-1}$
9a (π, π^*)	1.4	12	1.24
9b (π, π^*)		2600	
10a (π, π^*)	1.7	55	0.80
11a (n, π^*)	1.2	20	1.2
12a (π, π^*)	1.9	860	0.51
13a (n, π^*)	2.6	350	0.96
14a (π, π^*)	2.2	320	0.71
14b (π, π^*)		1800	
15a (π, π^*)	1.8	670	1.4
15b (π, π^*)		4800	
16a (π, π^*)	2.1	1135	1.1
16b (π, π^*)		3500	

a. all data from MSP thesis, ref. 86. Errors in lifetimes and rate constants $\pm 10\%$.

b. k_H/k_D from 5% aqueous and 5% D₂O acetonitrile mixtures. Errors are $\pm 15\%$.

phenolic species are all much shorter than for the methoxy compounds. This indicates that the triplet states of each LPK most likely react by remote phenolic HAA as established earlier for ketone **9a**.

The comparison between the triplet lifetimes for the *para*, *para'*-alkoxyacetophenone (**9a**), 3,4-dialkoxyacetophenone (**10a**), and alkoxybenzophenone (**11a**) indicate that, in the *para*, *para'*-attachment orientation at least, there is only a small chromophore effect on the abstraction. The slightly longer triplet lifetime of compound **12a** is consistent with the retarded bimolecular reactivity of 3,4-dimethoxyacetophenone towards *para*-cresol compared to *para*-methoxyacetophenone. Similarly, the slightly longer triplet lifetime for ketone **11a** mimics the smaller reactivity of *para*-methoxybenzophenone with *para*-cresol compared to *para*-methoxyacetophenone.

The trend in the triplet lifetimes of the *meta*-substituted LPKs also proved to be interesting. First, each LPK with a *meta*-hydroxyl group displays a longer triplet lifetime than its *para*-isomer. However, in the acetophenone case, a large difference (over one hundred fold) is seen if *both* the hydroxy group and the acyl group are moved into *meta*-positions on their respective rings. Furthermore, the *meta/para* and *para/meta* molecules both display reactivity intermediate between compounds **9a** and **16a**.

This presents a bit of a mystery, since the bimolecular rates of quenching of each model compound by either *para*- or *meta*-cresol vary by only a factor of three. Clearly, substituent electronic effects, *or at least those that are present in the bimolecular reaction*, are not responsible for the dramatic differences in the behaviour of the alkoxyacetophenone isomers. Ultimately it was concluded that the variation in each

molecule's ability to assume a conformation for rapid quenching had to be responsible, at least in part, for the dramatic variation in triplet lifetimes.

1.6. Thesis Goals.

MSP graduated before these data were published, and I entered the scene at the stage described above, where a fascinating, albeit preliminary, geometrical effect on intramolecular phenolic hydrogen atom abstraction had been observed.

My initial attempts at reproducing MPS's data indicated that many of the numbers listed in Table 1.6 were actually only lower limits. As will be explained, the concentrations of the LPK, of oxygen, and, as it turned out later, water, each have dramatic effects on the lifetimes of these triplets. Only by rigorously controlling each parameter could the "real" triplet lifetime be determined.

Faced with this realization, my thesis work had three main goals. The first was to repeat MSP's experiments and determine the triplet lifetimes of the previously synthesized LPKs as accurately as possible. The second goal was to design a plan of study that would bring about a better understanding of the actual ketone triplet/phenol quenching mechanism. This targeted the anomalous result of fast rates of quenching by π, π^* triplets in a system where electron-transfer can in general not occur.

The final goal was to understand the dramatic "*meta*" effect in the LPKs. While MSP's numbers describing the increase in triplet lifetime in the compound series **9, 14-16** were not absolutely correct, but he had definitely established the qualitative trend in the triplet lifetimes.

CHAPTER TWO
A STUDY OF THE BIMOLECULAR REACTIVITY OF AROMATIC KETONE
TRIPLETS WITH PHENOLS

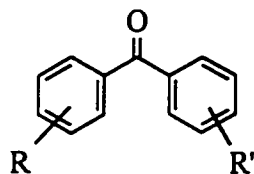
2.1. Quenching of Aromatic Ketone Triplets by *para*-Cresol.

2.1.1. Introduction. General considerations.

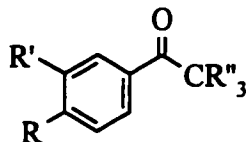
This Chapter describes a study of the bimolecular reactivity of aromatic ketone triplets with phenols. The work began with a small selection of ketones and ultimately grew to encompass a wide range of different compounds representing the three classes of lowest (n , π^* , π , π^* and CT) triplet states.

Figure 2.1 shows these ketones, grouped as benzophenones (17-30), acetophenones (31-48), and indanones/other (49-56). Tables 2.1-2.3 list the triplet energies and ground (E_{RED}) and triplet (E_{RED}^*) state reduction potentials of these species where available from the literature. Note that E_{RED}^* is defined as the sum of triplet energy and E_{RED} , thus it refers to the ease of reduction of the triplet state.

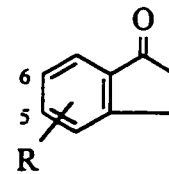
Before the actual experiments and their results are described, it is important to note that in all of these cases, irradiations were carried out under conditions where the ketone is the exclusive light absorber. This is important since phenol photochemistry is a rich and complicated area unto its own, and the generation of excited phenols would only serve to complicate any attempts to understand the ketone processes.

Figure 2.1. List of ketones studied.

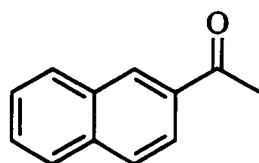
- 17; $R = R' = H$
 18; $R = R' = 3\text{-CF}_3$
 19; $R = 4\text{-Br}, R' = H$
 20; $R = 4\text{-CN}, R' = H$
 21; $R = R' = 4\text{-Cl}$
 22; $R = R' = 4\text{-OMe}$
 23; $R = R' = 4\text{-Me}$
 24; $R = 4\text{-NMe}_2, R' = H$
 25; $R = 3\text{-OMe}, R' = H$
 26; $R = 4\text{-OMe}, R' = H$
 27; $R = 4\text{-OMe}, R' = 4\text{-Me}$
 28; $R = 4\text{-Me}, R' = H$
 29; $R = 4\text{-Ph}, R' = H$
 30; $R = 4\text{-SMe}, R' = H$



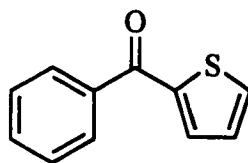
- 31; $R = R' = R'' = H$
 32; $R = Cl, R' = R'' = H$
 33; $R = H, R' = CN, R'' = H$
 34; $R = CN, R' = R'' = H$
 35; $R = R' = Cl, R'' = H$
 36; $R = R' = OMe, R'' = H$
 37; $R = R' = Me, R'' = H$
 38; $R = NMe_2, R' = R'' = H$
 39; $R = H, R' = F, R'' = H$
 40; $R = F, R' = R'' = H$
 41; $R = H, R' = OMe, R'' = H$
 42; $R = OMe, R' = R'' = H$
 43; $R = OMe, R' = H, R'' = F$
 44; $R = Me, R' = R'' = H$
 45; $R = Ph, R' = R'' = H$
 46; $R = R' = H, R'' = F$
 47; $R = H, R' = CF_3, R'' = H$
 48; $R = CF_3, R' = R'' = H$



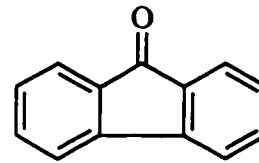
- 49; $R = H$
 50; $R = 5\text{-OMe}$
 51; $R = 6\text{-OMe}$



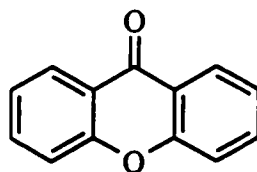
52



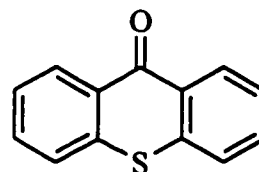
53



54



55



56

Table 2.1. Triplet energies and ground and triplet state reduction potentials of some of the benzophenones studied. ^a

Benzophenone	E_T (kcal/mol)	$-E_{RED}$ (kcal/mol)	E_{RED}^* (kcal/mol)
	MTHF	MeCN; vs. SCE	MeCN; vs. SCE ^b
unsubstituted (17)	69.2	42.1	27.1
3,3'-bis(trifluoromethyl) (18)	69.1 ^c	36.0 ^c	33.1
4-cyano (20)	66.8	32.7	34.1
4,4'-dichloro (21)	68.6	38.5	30.1
4,4'-dimethoxy (22)	69.4	46.5	22.9
4,4'-dimethyl (23)	69.1	43.8	25.3
4-methoxy (26)	69.0 ^c	45.0 ^c	24.0
4-methyl (28)	69.2 ^c	43.8 ^c	25.4
4-thiomethyl (30)	64.0 ^d	42.4 ^d	21.6

a. All data from Ref. 32 (2-methyltetrahydrofuran (MTHF) solvent for E_T measurement at 77K; E_{RED} measurement: 0.1-1.0 M tetraethylammonium perchlorate (TEAP)/MeCN at 298 K for) unless otherwise noted.

b. $E_{RED}^* = E_T + E_{RED}$.

c. Ref. 94 (4:1 EtOH/MeOH solvent for E_T measurement at 77K; E_{RED} measurement: 0.1 M TEAP/MeCN vs. Ag/0.1 M AgNO₃/0.1 M TEAP at 298 K). Corrected vs. SCE.

d. Ref. 188 (EPA solvent for E_T measurement at 77K; E_{RED} measurement: 0.1 M TEAP/MeCN vs. Ag/0.1 M AgNO₃/0.1 M TEAP at 298 K). Corrected vs. SCE.

Table 2.2. Triplet energies and ground and triplet state reduction potentials of some of the acetophenones studied. ^a

Acetophenone	E_T (kcal/mol)	$-E_{RED}$ (kcal/mol)	E_{RED}^* (kcal/mol)
	MTHF	MeCN; vs. SCE	MeCN; vs. SCE ^b
unsubstituted (31)	73.5	49.3	24.2
<i>para</i> -chloro (32)	71.7	48.3	23.4
<i>meta</i> -cyano (33)	73.0	40.3	32.7
<i>para</i> -cyano (34)	69.2	36.4	32.8
3,4-dimethoxy (36)	73	45.0 ^c	28
3,4-dimethyl (37)	70.3	50.7	19.6
<i>meta</i> -methoxy (41)	72.4 ^d	45.7 ^e	26.7
<i>para</i> -methoxy (42)	70.1	51.4	18.7
<i>para</i> -methoxy- α , α , α -trifluoro (43)	65.9	37.5	28.4
<i>para</i> -methyl (44)	72.2	50.4	21.8
α , α , α -trifluoro (46)	69.9	31.9	38.0
<i>meta</i> -trifluoromethyl (47)	73.0	43.8	29.2
<i>para</i> -trifluoromethyl (48)	71.7	41.7	30.0

a. See footnote (a) of Table 2.1, p. 52.

b. $E_{RED}^* = E_T + E_{RED}$.

c. Wayner, D.D.M. Personal communication. (*N,N*-dimethylformamide/0.1 M tetrabutylammonium perchlorate vs. ferrocene/ferrocenium. Corrected using +0.464 V vs. SCE for ferrocene in MeCN).

d. Ref. 5.

e. Workentin, M.S. Personal communication. (MeCN/0.1 M TEAP vs. ferrocene / ferrocenium. Corrected using +0.449 V vs. SCE for ferrocene in MeCN).

Table 2.3. Triplet energies and ground and triplet state reduction potentials of some of the indanones and other lowest π, π^* ketones studied.

Ketone	E_T (kcal/mol)	$-E_{RED}$ (kcal/mol)	E_{RED}^* (kcal/mol)
		MeCN; vs. SCE	MeCN; vs. SCE ^a
5-methoxy-1-indanone (50)	73.4 ^b	50.7 ^c	22.7
6-methoxy-1-indanone (51)	71.4 ^b	46.2 ^c	25.2
2-acetonaphthone (52)	59.5 ^d	39.7 ^e	19.8
fluorenone (54)	50.3 ^f	29.7 ^g	20.6
xanthone (55)	74.1 ^h	39.9 ⁱ	34.2
thioxanthone (56)	63.3 ^j	38.5 ⁱ	24.8

a. $E_{RED}^* = E_T + E_{RED}$.

b. In 4:1 EtOH/MeOH at 77 K, this work.

c. See footnote (e) of Table 2.2, p. 53.

d. Ref. 5.

e. Rajadurai, K.; Bhattacharyya, K.; Das, P. K. *Chem. Phys. Lett.* **1986**, *129*, 244.

f. In EtOH:isopentane:diethyl ether (5:2:2, EPA) at 77 K. Huggenberger, C.; Labhart, H. *Helv. Chim. Acta* **1978**, *68*, 250.

g. 0.5 M $\text{Bu}_4\text{NBF}_4/\text{N}$, *N*-dimethylformamide vs. SCE at 298 K. House, H.O.; Huber, L.E.; Umen, M.J. *J. Am. Chem. Soc.* **1972**, *94*, 8471.

h. In EPA at 77 K. Pownall, H.J.; Huber, J.R. *J. Am. Chem. Soc.* **1971**, *93*, 6429.

i. 0.1 M $\text{Et}_4\text{NBF}_4/\text{MeCN}$ vs. SCE at 298 K. Lucarini, M.; Pedulli, G.F.; Alberti, A.; Paradisi, C.; Roffia, S. *J. Chem. Soc., Perkin Trans. 2* **1993**, 2083.

j. In 2-methyltetrahydrofuran at 77 K. Meier, K.; Zweifel, H. *J. Photochem.* **1986**, *35*, 353.

2.1.2. Results. Transient ultraviolet absorption spectra.

Nanosecond laser flash photolysis (NLFP) experiments were conducted at room temperature on deoxygenated solutions in 7x7 mm or 3x7 mm Suprasil cells using a pulsed excimer laser for excitation and a microcomputer-controlled system for detection.⁸⁷ The gas mixture used was exclusively the nitrogen fill, which produces 337.1-nm pulses with six nanosecond widths and roughly four mJ doses.

Ketone solution concentrations (ranging from 10^{-4} -0.5 molar (M)) were chosen to provide an absorbance of 0.1-0.9 at 337-nm. The laser intensity was attenuated with neutral density filters to limit the concentration of transient species produced, and avoid second-order contributions to the triplet decays.

Transient absorption spectra were determined for each ketone in point-by-point fashion over several time windows after the laser pulse. For each ketone, prominent transients were observed and assigned to triplet absorptions, based on their rapid quenching by oxygen and/or phenol quenchers (*vide infra*), and general agreement of the position of triplet-triplet absorption maxima with literature data where available.⁸⁸

Figure 2.2 displays transient absorption spectra and decay traces of three representative ketone triplets: Figure 2.2a depicts the features of the benzophenone chromophore, while 2.2b shows a typical substituted acetophenone, and 2.2c represents xanthone. The black points represent the spectrum immediately after the laser pulse and show the triplet-triplet absorbance. The gray points represent the transients present at a time long after the laser pulse, after the majority of the triplet has reacted. The legend in each spectrum indicates how long these delays are in each case.

Figure 2.2. Transient absorption spectra and decays recorded by 337-nm laser flash photolysis of deoxygenated acetonitrile solutions of (a) 0.1 M benzophenone (17), (b) 8×10^{-5} M *para*-dimethylaminoacetophenone (38) and (c) 4×10^{-4} M xanthone (55) at 23 to 25 °C.

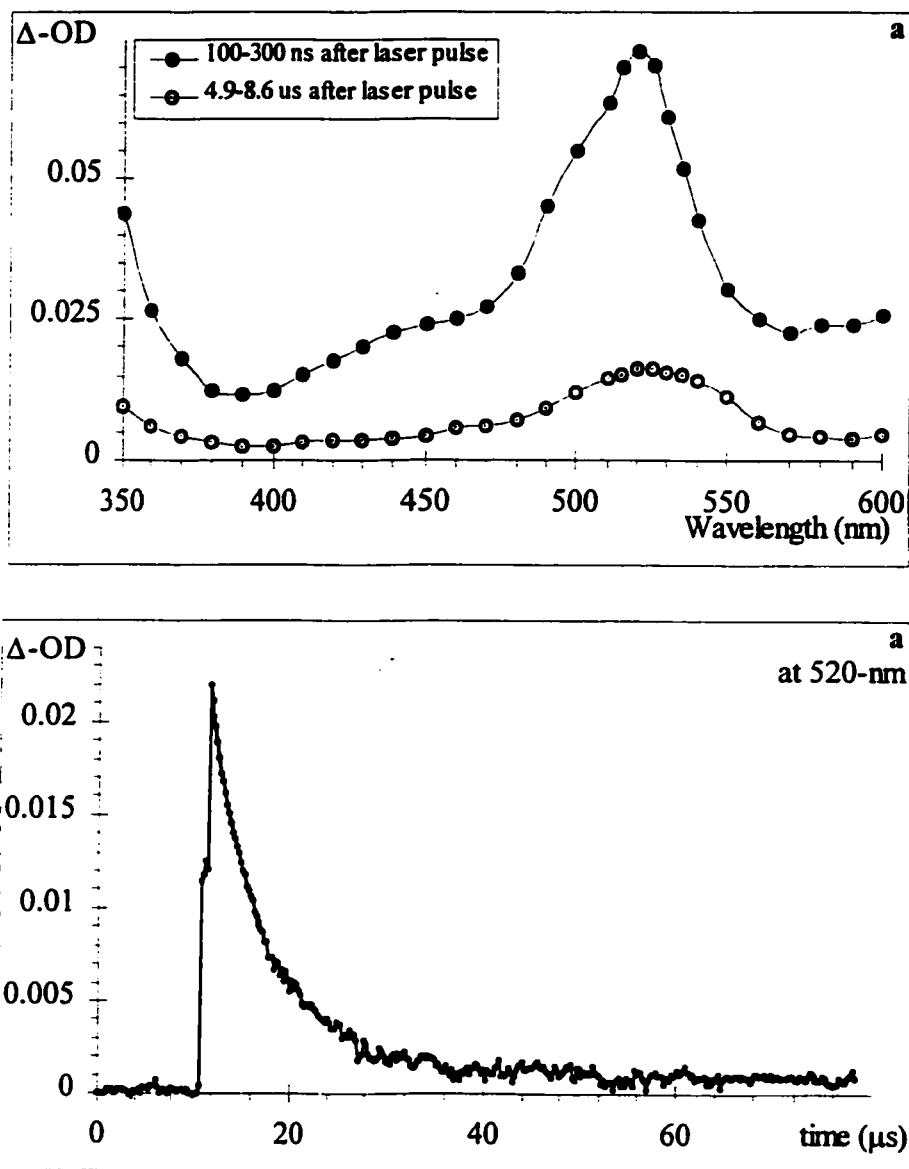


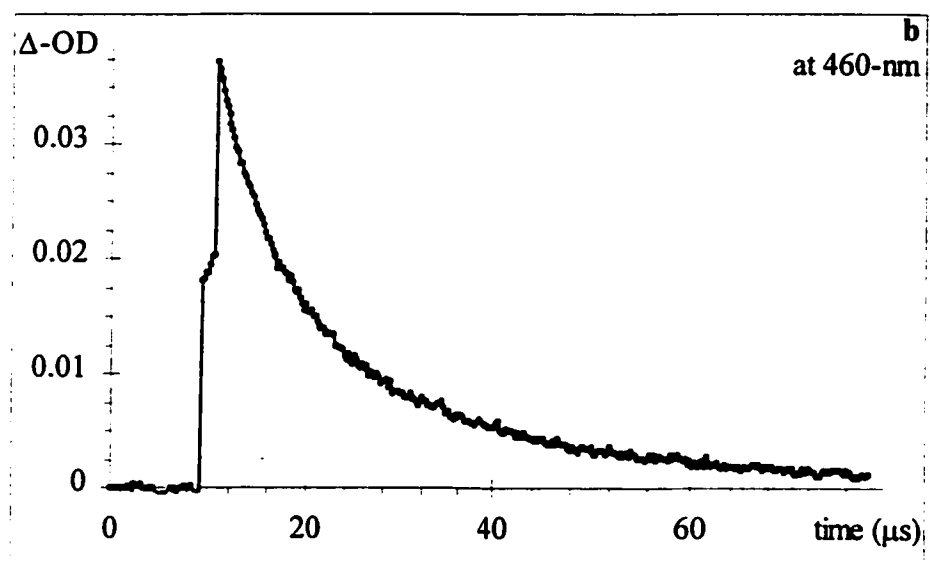
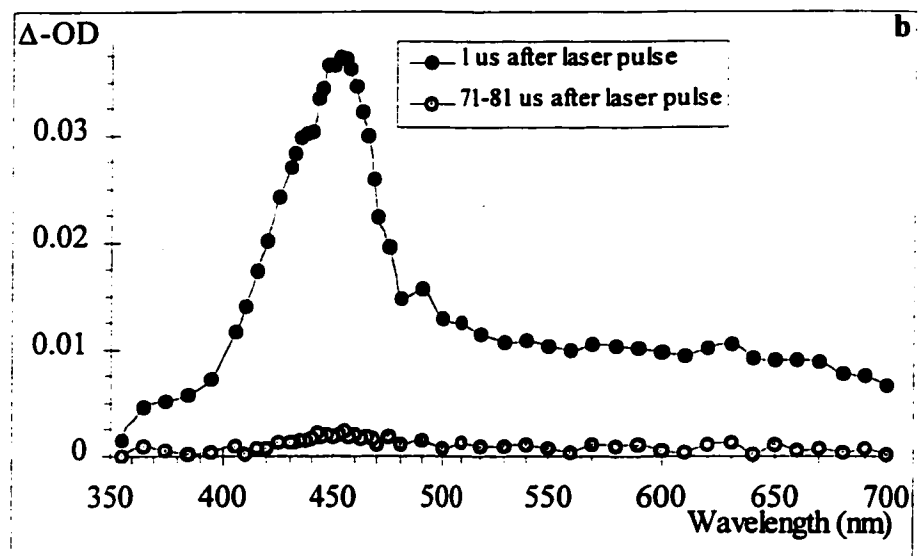
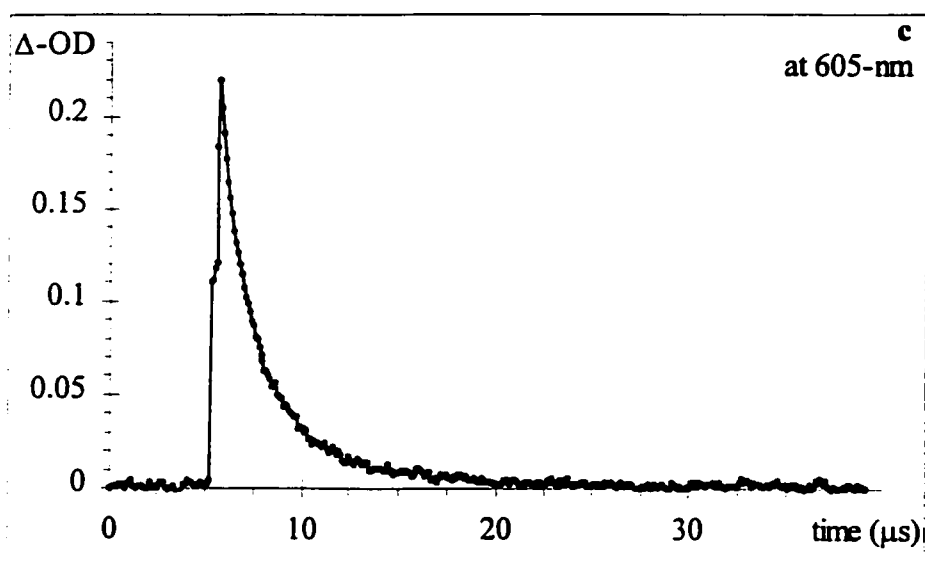
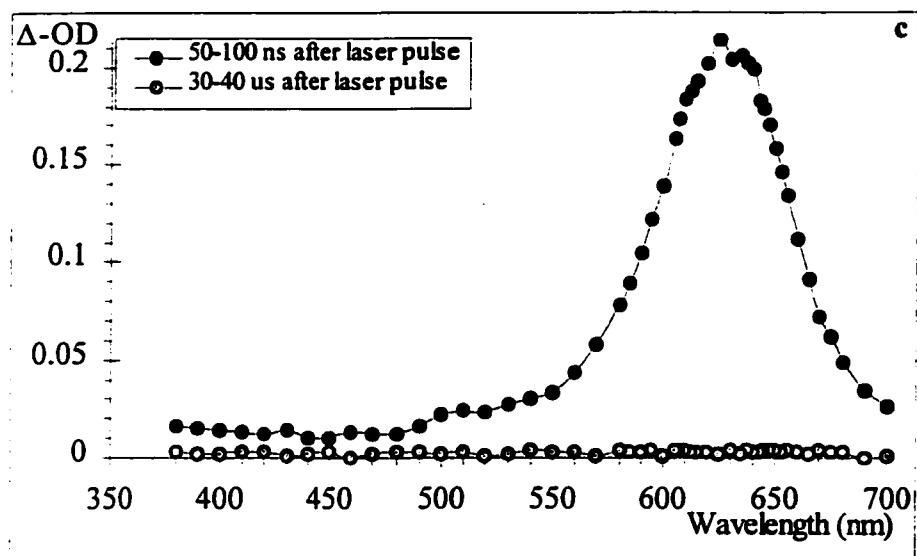
Figure 2.2. Continued.

Figure 2.2. Continued.

A short summary of the results follows, and Tables 2.4 to 2.6 list triplet maxima and typical triplet lifetimes of all species. How the triplet lifetimes were determined from the decays will be explained in the next section.

Acetophenone and indanone triplet absorptions were monitored at their maxima of approximately 380-nm; in most cases, they were readily detectable as far out as 470-nm as well.

The triplets of benzophenone and its derivatives were observed in two main bands, with well-known maxima at 300- and 525-nm.^{5,88} The longer wavelength band extended to 700-nm in some cases. Most experiments conducted with benzophenones were monitored at 525- or 600-nm. The lowest π, π^* ketones such as xanthone and fluorenone gave spectra similar to those reported previously.^{5,88}

Figure 2.3 displays transient absorption spectra of the same three representative ketones with *para*-cresol present. These spectra were recorded at the end of quenching experiments in an attempt to verify the formation of radical species.

The new absorption around 407-nm seen in each gray spectrum is characteristic^{89,90} of *para*-cresoxy \cdot . In Figure 2.3a, the apparent shift of the ketone triplet maximum is in fact due to its replacement by the benzophenone hemipinacol radical, absorbing in a position only slightly shifted from the triplet.

2.1.3. Results. Transient decays and absolute quenching rate constants.

The triplet lifetimes reported in Tables 2.4 - 2.6 are in good agreement with the literature, where available.^{5,88} Triplet lifetimes in the microsecond range were routinely

Table 2.4. Triplet-triplet absorption maxima and triplet lifetimes of the benzophenones studied. ^a

Benzophenone	λ_{max} (nm)	τ_T (μ s)
unsubstituted (17)	520	6.64 ± 0.17
3,3'-bis(trifluoromethyl) (18)	545	2.80 ± 0.10
4-bromo (19)	525	0.400 ± 0.014
4-cyano (20)	545	4.44 ± 0.11
4,4'-dichloro (21)	545 ^b	18.5 ± 0.6
4,4'-dimethoxy (22)	545 ^b	6.06 ± 0.12
4,4'-dimethyl (23)	525	16.4 ± 0.6
4-dimethylamino (24)	510	12.43 ± 0.14
3-methoxy (25)	500-600 (weak)	12.6 ± 0.4
4-methoxy (26)	520	6.45 ± 0.10
4-methyl-4-methoxy (27)	530	20.8 ± 1.1
4-methyl (28)	525 ^b	8.7 ± 0.3
4-phenyl (29)	540 ^b	18 ^c
4-thiomethyl (30)	533	14.5 ± 0.6

a. In deoxygenated acetonitrile at room temperature; literature comparisons for some ketones may be found in Refs. 5 and 88.

b. Ref. 88.

c. Presence of second-order kinetics makes this value an estimated lower limit.

Table 2.5. Triplet-triplet absorption maxima and triplet lifetimes of the acetophenones studied. ^a

Acetophenone	λ_{max} (nm)	τ_T (μ s)
unsubstituted (31)	335 ^b	4.7 \pm 0.2
<i>para</i> -chloro (32)	349	3.56 \pm 0.07
<i>meta</i> -cyano (33)	420	28.3 \pm 1.3
<i>para</i> -cyano (34)	350 ^c	11.0 \pm 0.3
3,4-dichloro (35)	348	1.43 \pm 0.04
3,4-dimethoxy (36)	375	7.72 \pm 0.10
3,4-dimethyl (37)	380	1.51 \pm 0.05
<i>para</i> -dimethylamino (38)	453	55.0 \pm 1.7
<i>meta</i> -fluoro (39)	350 ^c	2.44 \pm 0.09
<i>para</i> -fluoro (40)	350 ^c	3.32 \pm 0.08
<i>meta</i> -methoxy (41)	380	3.68 \pm 0.18
<i>para</i> -methoxy (42)	360 ^b	12.7 \pm 0.4
<i>para</i> -methoxy- α , α , α -trifluoro (43)	420	55.5 \pm 1.2
<i>para</i> -methyl (44)	331 ^b	4.00 \pm 0.09
<i>para</i> -phenyl (45)	420	36.8 \pm 1.3
α , α , α -trifluoro (46)	350 ^c	1.22 \pm 0.05
<i>meta</i> -trifluoromethyl (47)	418	4.91 \pm 0.19
<i>para</i> -trifluoromethyl (48)	425	7.2 \pm 0.6

a. In deoxygenated acetonitrile at room temperature; literature comparisons for some ketones may be found in Refs. 5 and 88.

b. Ref. 5.

c. Shoulder; maximum lies at a shorter wavelength.

Table 2.6. Triplet-triplet absorption maxima and triplet lifetimes of the indanones and other lowest π, π^* triplets studied. ^a

Ketone	λ_{max} (nm)	τ_T (μ s)
1-indanone (49)	345 ^{b,c}	0.152 ± 0.003 ^b
5-methoxy-1-indanone (50)	383	3.50 ± 0.08
6-methoxy-1-indanone (51)	383	28.6 ± 0.6
2-acetonaphthone (52)	425	6.37 ± 0.07
2-benzoylthiophene (53)	600	4.33 ± 0.19
fluorenone (54)	421	40 ± 2
xanthone (55)	620	5.65 ± 0.09
thioxanthone (56)	625	16.6 ± 0.6

a. In deoxygenated acetonitrile at room temperature; literature comparisons for some ketones may be found in Refs. 5 and 88.

b. In benzene.

c. Shoulder; maximum lies at a shorter wavelength.

Figure 2.3. Transient absorption spectra and decays recorded by 337-nm laser flash photolysis of deoxygenated MeCN solutions of (a) 0.1 M benzophenone (17), (b) 8×10^{-5} M *para*-dimethylaminoacetophenone (38) and (c) 4×10^{-4} M xanthone (55) at 23 to 25 °C in the presence of ~ 0.01 to 0.02 M *para*-cresol.

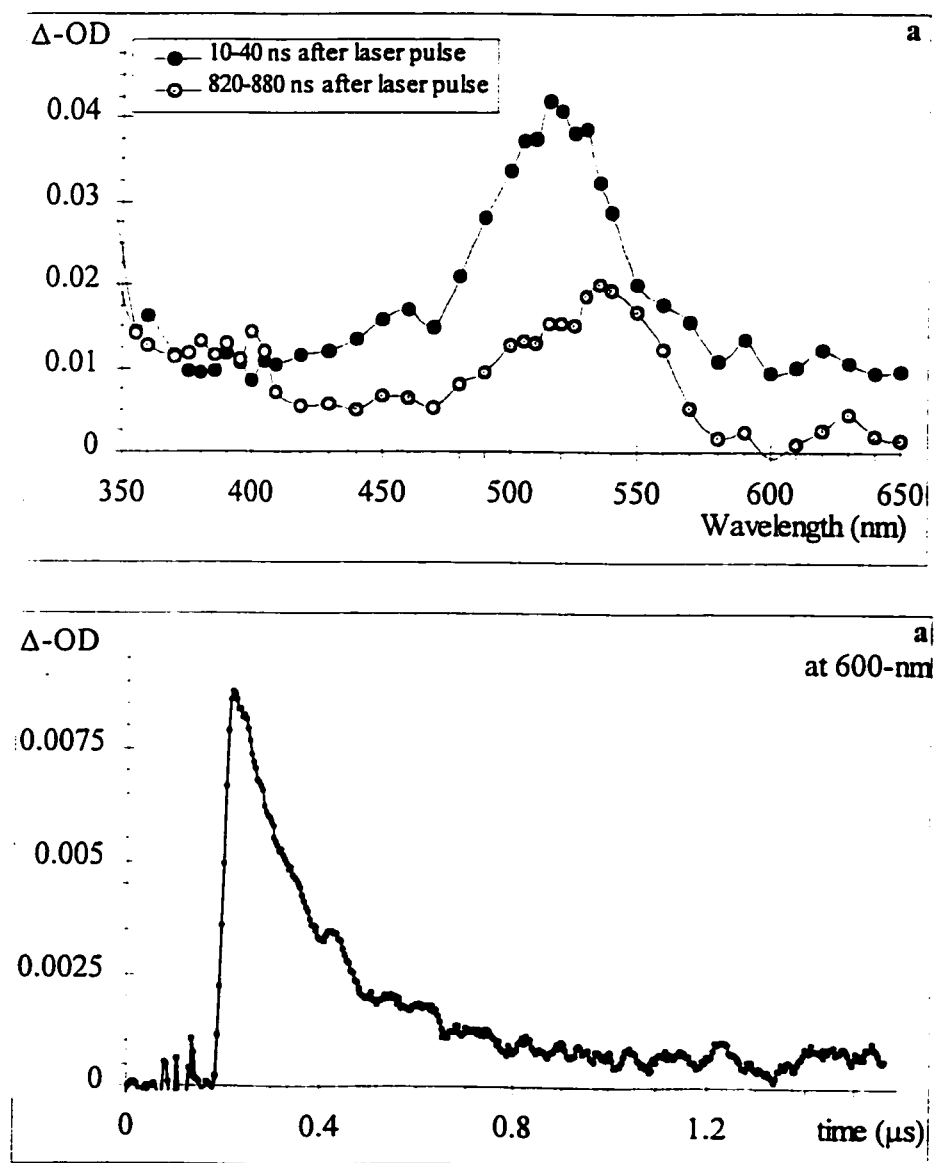


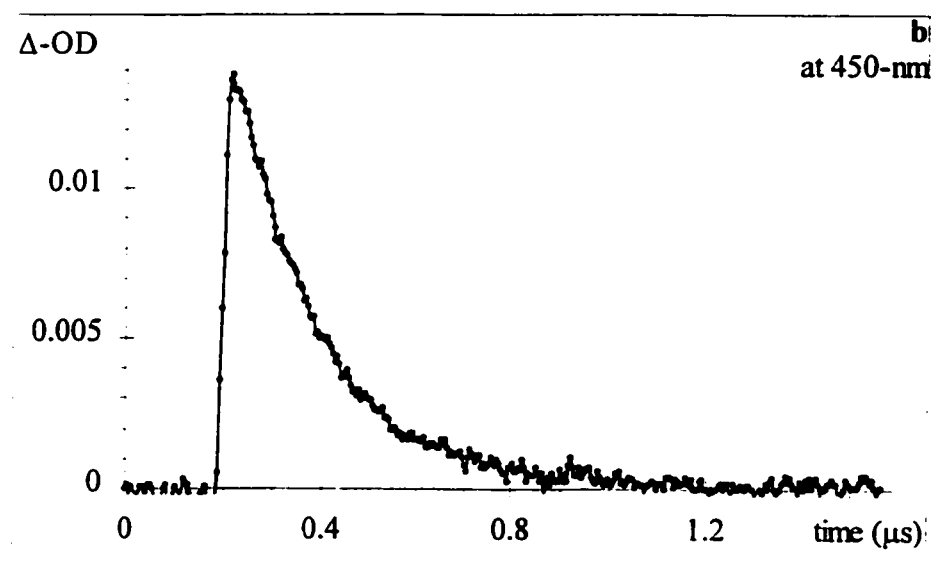
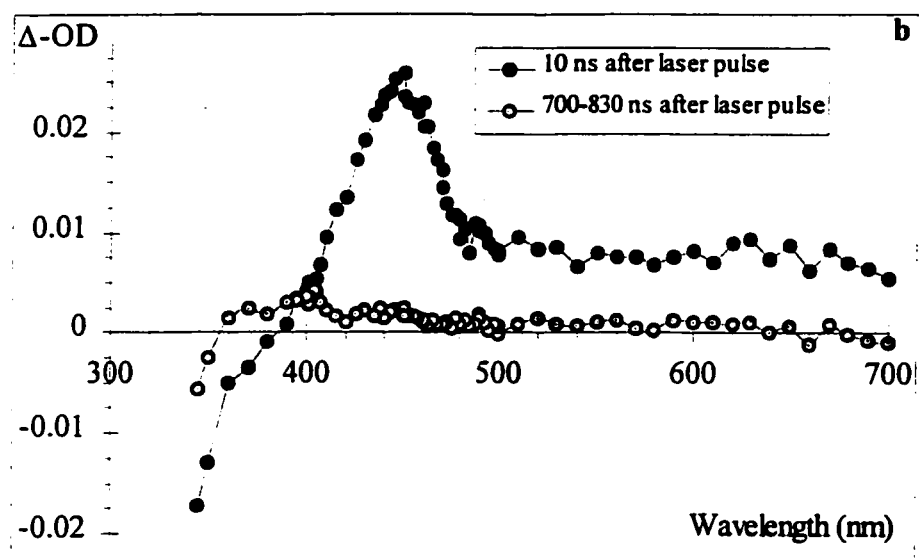
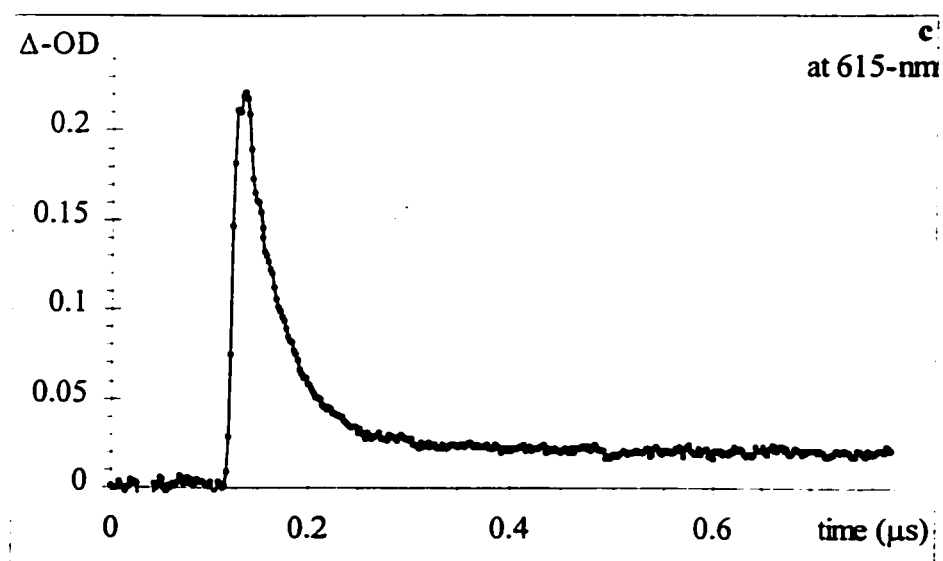
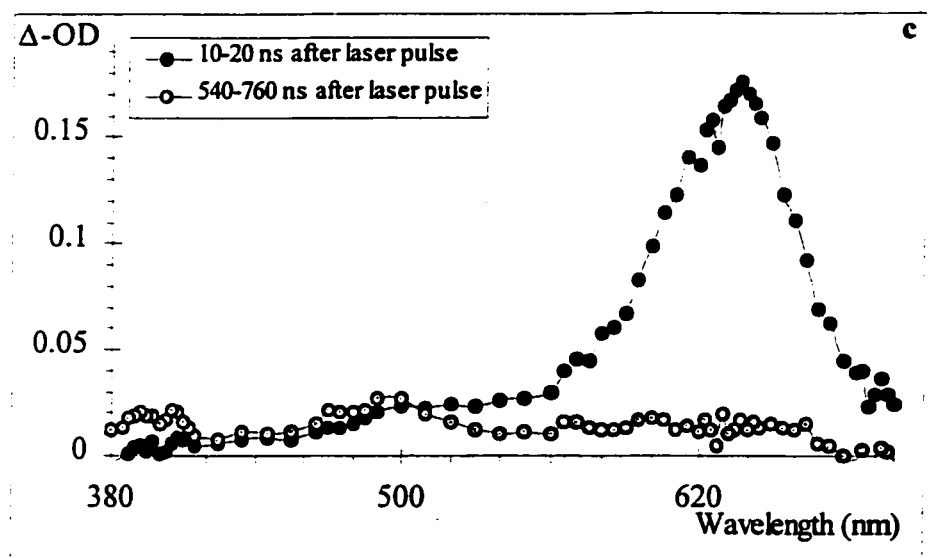
Figure 2.3. Continued.

Figure 2.3. Continued.

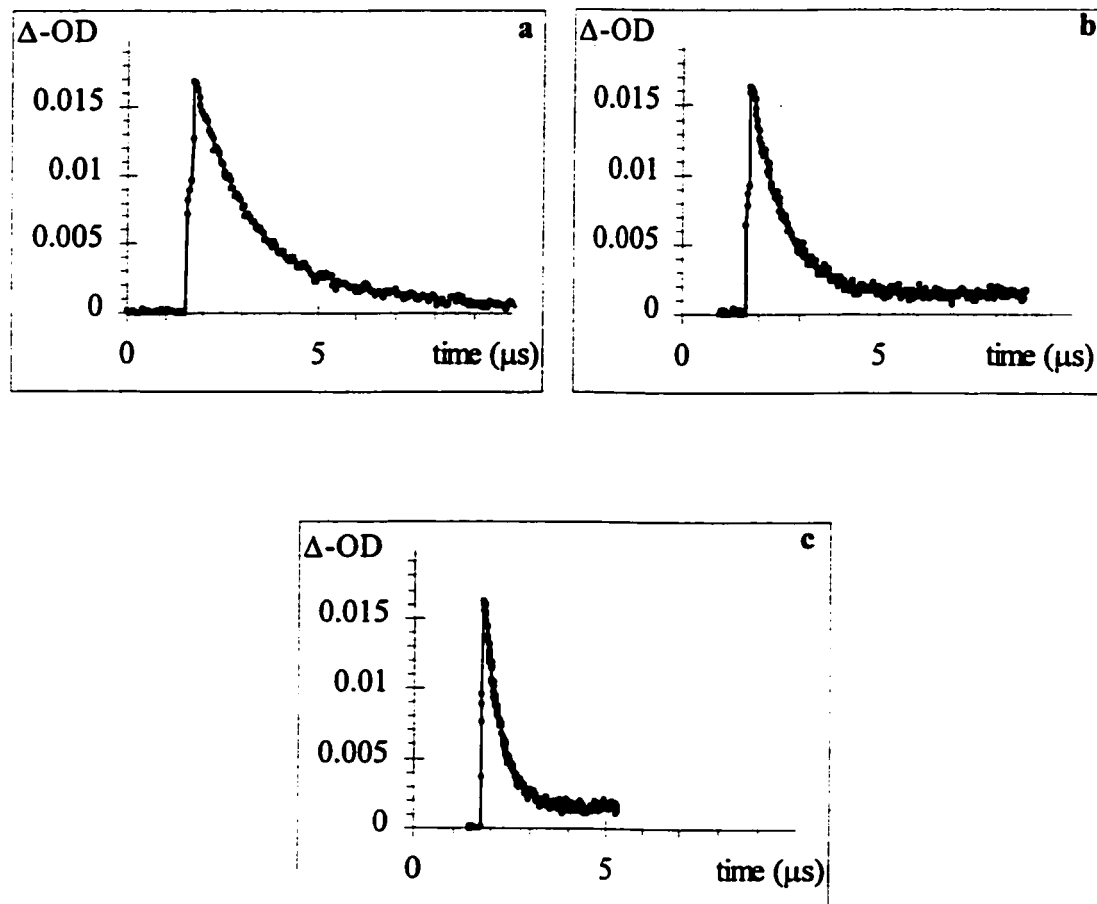
obtained, with some samples exhibiting triplet lifetimes in the tens of microseconds.

Ketone samples were purified by several distillations or recrystallizations to 98% purity or more. Rigorous purification of the ketone (in some cases to 99.5+% as determined by gas chromatography) only increased triplet lifetimes slightly past this point. During the actual NLFP experiments, triplet lifetimes measured on a particular day were a function of deoxygenation time, laser intensity and ketone concentration. While deoxygenation was always performed as rigorously as possible to produce triplet lifetimes that were as long as possible, the latter two parameters were varied from experiment to experiment to produce the smallest transient concentration necessary for the collection of data with a satisfactory signal to noise ratio. This practice led to better first-order fits of the decay profiles (see below).

Absolute rate constants for triplet quenching by *para*-cresol (*para*-methylphenol) were determined by monitoring the pseudo-first order triplet decay rate (k_{decay}) at or near the triplet maximum as a function of the concentration of added quencher. The transient decays were initially pseudo first-order but increasing the quencher concentration caused noticeable residual absorptions to grow in proportionately. An example of this is shown in Figure 2.4, which follows the kinetics of a *para*-methoxyacetophenone triplet quenching experiment. Figure 2.4a shows the kinetic trace in the absence of *para*-cresol, and Figures 2.4b and c show the triplet quenching and evolution of a residual absorption.

The effect of the residual absorption is to change the initial pseudo first-order decay to one mixed with a slower first- or second-order decay. The presence of multiple transients causes mixed kinetics, which sometimes made the determination of first-order

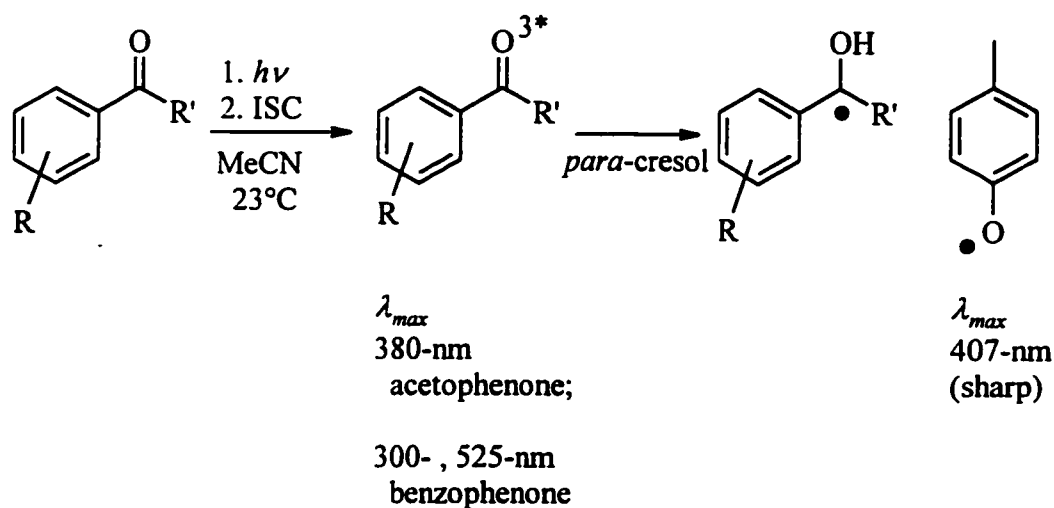
Figure 2.4. Transient decays of a 0.03 M deoxygenated acetonitrile solution of *para*-methoxyacetophenone (42) in the presence of (a) zero, (b) 3×10^{-4} and (c) 1.2×10^{-3} M *para*-cresol.



rate constants difficult. This problem was treated in several ways. One was to change the monitoring wavelength during the experiment so that the residual absorption was minimized. This was usually unsatisfactory since it usually involved employing a monitoring wavelength where the triplet signal was weaker as well. Another solution was to attempt to fit the data to more complicated kinetic expressions.

The new transients causing the residual absorption are assigned to one or both of the radical products formed by the bimolecular reaction, depending on monitoring wavelength. Scheme 2.1 delineates the process, from photochemical excitation followed by rapid ISC to the triplet state and then the HAA reaction.

Scheme 2.1. Bimolecular hydrogen atom abstraction from *para*-cresol by ketone triplets.



Data analysis begins with equation 2.1, the integrated solution to the first-order exponential decay.⁹¹

$$\Delta A_t = \Delta A_0 e^{-k_{decay} t} + \Delta A_{\infty} \quad (2.1)$$

Here, ΔA_t is the change in absorbance at any time t , ΔA_0 is the initial change in absorbance before decay begins, k_{decay} is the decay constant, and ΔA_{∞} is the change in absorbance of the system at t long enough that most of the initial transient is gone.

Rearranging and taking natural logarithms allows the change in absorbance data to be plotted linearly *versus* time according to equation 2.2. The slope is k_{decay} , and its negative sign indicates that it represents a decay process.

$$\ln (\Delta A_t - \Delta A_{\infty}) = \ln \Delta A_0 - k_{decay} t \quad (2.2)$$

As more quencher is added, the transient lifetime is observed to decrease, hence k_{decay} is a function of quencher concentration and the change in absorbance *versus* time plot is resolved at each quencher concentration, producing in the end a range of k_{decay} values.

In the case of triplet quenching by phenols, k_{decay} varies linearly with concentration and another linear least squares analysis, this time according to equation 2.3, affords the quenching rate constant k_q . The y -intercept of the plot, k_0 , represents the transient lifetime in the absence of the quencher Q .

$$k_{decay} = k_0 + k_q [Q] \quad (2.3)$$

Tables 2.7-2.9 list k_q values for all ketones studied, and several representative quenching plots are shown in Figure 2.5. Quenching studies were generally continued until triplet lifetimes were reduced from their original values by a factor of ten or more. The final concentration of *para*-cresol at the end of these experiments was usually in the millimolar range.

2.1.4. Discussion. General observations on the phenolic hydrogen atom abstraction reaction.

The direct spectroscopic detection of radical products in all bimolecular reactions studied between aromatic ketone triplets and *para*-cresol indicates that hydrogen atom transfer occurs during the reaction at some point.

The rate data indicate that triplet quenching by *para*-cresol occurs rapidly regardless of aromatic ketone structure and configuration of the lowest triplet state, with bimolecular rate constants on the order of 10^8 to $10^9 \text{ M}^{-1} \text{ s}^{-1}$. There are only three examples (2- acetonaphthone (52), fluorenone (54) and 4-phenylbenzophenone (29)) with rate constants of less than $10^8 \text{ M}^{-1} \text{ s}^{-1}$. It was observed that rate constants were two to three times larger in non-polar solvents (see Tables 2.7-2.9).

These observations are consistent with previous rate studies of ketone triplet/phenol reactions in organic solvents,^{20,72,74,75,77-80,82,83,92} including the result of generally equal or

Table 2.7. Absolute rate constants for quenching of substituted benzophenone triplets by *para*-cresol in deoxygenated acetonitrile at 23 to 25 °C; in units of $10^9 \text{ M}^{-1} \text{ s}^{-1}$. a,b

Benzophenone	$k_q, \text{para-cresol}$	$\log (k_q / \text{M}^{-1} \text{s}^{-1})$	$\Sigma\sigma^c$
unsubstituted (17)	0.299 ± 0.011	8.476	0
3,3'-bis(trifluoromethyl) (18)	3.33 ± 0.19	9.522	+ 0.86
4-bromo (19)	0.86 ± 0.12	8.93	+ 0.23
4-cyano (20)	3.9 ± 0.2	9.59	+ 0.66
4,4'-dichloro (21)	2.1 ± 0.2	9.32	+ 0.46
4,4'-dimethoxy (22)	2.4 ± 0.3	9.38	- 0.54
4,4'-dimethyl (23)	1.07 ± 0.05	9.029	- 0.34
4-dimethylamino (24)	2.10 ± 0.17	9.322	- 0.83
3-methoxy (25)	2.01 ± 0.15	9.303	+ 0.12
4-methoxy (26)	1.17 ± 0.07	9.068	- 0.27
	6.5 ± 0.3^d		
4-methyl-4-methoxy (27)	1.28 ± 0.08	9.107	- 0.44
4-methyl (28)	0.58 ± 0.5	8.76	- 0.17
4-phenyl (29)	~ 0.2	8.3	- 0.01
4-thiomethyl (30)	1.27 ± 0.13	9.104	0.00

a. Errors are given as twice the standard deviation of the least squares slope from analysis of k_{decay} vs. [*para*-cresol] according to equation 2.3.

b. Measured by 337-nm laser flash photolysis of 10^{-4} - 0.03 M solutions of the ketones.

c. Hammett substituent parameter from Ref. 93.

d. In dichloromethane.

Table 2.8. Absolute rate constants for quenching of substituted acetophenone triplets by *para*-cresol in deoxygenated acetonitrile at 23 to 25 °C; in units of $10^9 \text{ M}^{-1} \text{ s}^{-1}$. ^{a,b}

Acetophenone	k_q , <i>para</i> -cresol	$\log (k_q / \text{M}^{-1} \text{s}^{-1})$	$\Sigma\sigma^c$
unsubstituted (31)	1.09 ± 0.07	9.037	0
<i>para</i> -chloro (32)	1.23 ± 0.06	9.090	+ 0.23
<i>meta</i> -cyano (33)	0.203 ± 0.013	8.307	+ 0.56
<i>para</i> -cyano (34)	2.4 ± 0.4	9.38	+ 0.66
3,4-dichloro (35)	1.63 ± 0.05	9.212	+ 0.60
3,4-dimethoxy (36)	0.59 ± 0.04	8.77	- 0.15
3,4-dimethyl (37)	1.11 ± 0.08	9.045	- 0.24
<i>para</i> -dimethylamino (38)	0.58 ± 0.03	8.76	- 0.83
<i>meta</i> -fluoro (39)	1.71 ± 0.16	9.233	+ 0.34
<i>para</i> -fluoro (40)	1.54 ± 0.12	9.188	+ 0.06
<i>meta</i> -methoxy (41)	1.27 ± 0.13	9.104	+ 0.12
<i>para</i> -methoxy (42)	1.14 ± 0.09 ; 5.51 ± 0.10^d	9.057	- 0.27
<i>para</i> -methoxy- α , α , α -trifluoro (43)	1.98 ± 0.09	9.297	
<i>para</i> -methyl (44)	1.13 ± 0.07	9.053	- 0.17
<i>para</i> -phenyl (45)	0.0156 ± 0.0005	7.193	- 0.01
α , α , α -trifluoro (46)	8.1 ± 0.3	9.91	
<i>meta</i> -trifluoromethyl (47)	0.25 ± 0.03	8.39	0.43
<i>para</i> -trifluoromethyl (48)	0.53 ± 0.05	8.72	0.54

a. Errors are given as twice the standard deviation of the least squares slope from analysis of k_{decay} vs. [*para*-cresol] according to equation 2.3.

b. Measured by 337-nm laser flash photolysis of 10^{-4} - 0.03 M solutions of the ketones.

c. Hammett substituent parameter from Ref. 93. d. In dichloromethane.

Table 2.9. Absolute rate constants for quenching of substituted 1-indanones and other lowest π , π^* triplets by *para*-cresol in deoxygenated acetonitrile at 23 to 25 °C; in units of $10^9 \text{ M}^{-1} \text{ s}^{-1}$. a,b

Ketone	k_q , <i>para</i> -cresol
1-indanone (49)	3.9 ± 0.8^c
5-methoxy-1-indanone (50)	1.74 ± 0.13 ; 7.1 ± 0.2^d
6-methoxy-1-indanone (51)	2.18 ± 0.11
2-acetonaphthone (52)	0.0034 ± 0.0004
2-benzoylthiophene (53)	0.37 ± 0.03
fluorenone (54)	0.097 ± 0.003
xanthone (55)	3.75 ± 0.09
thioxanthone (56)	2.96 ± 0.06

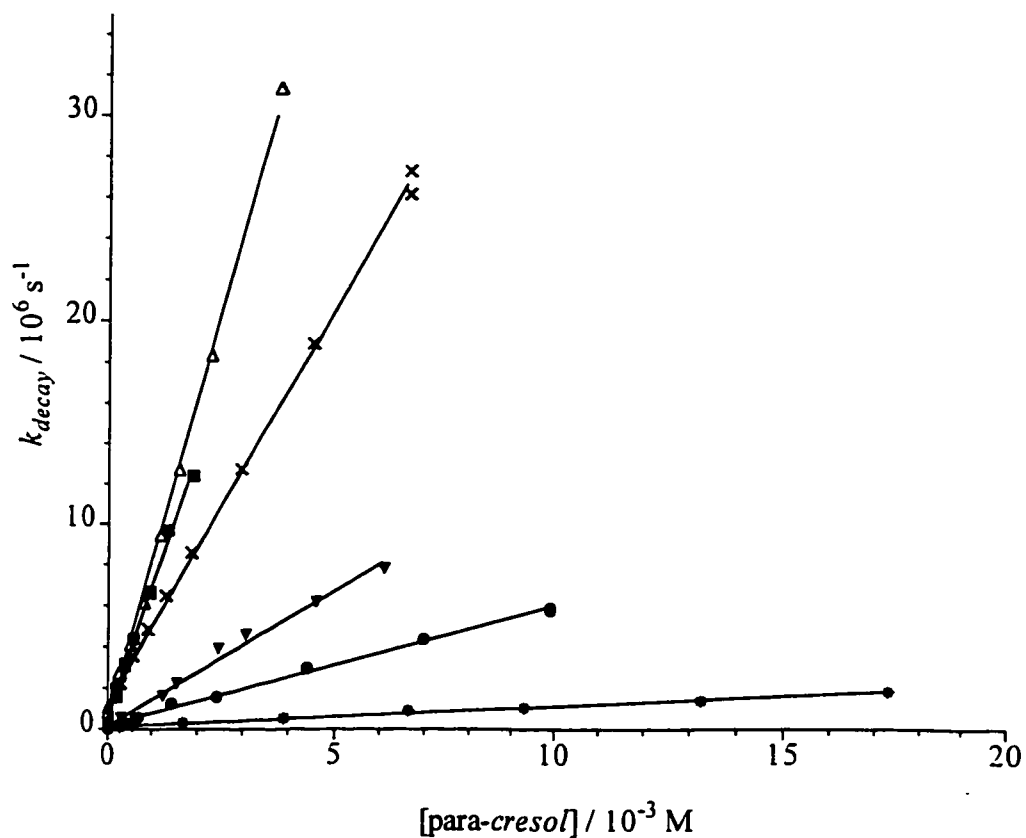
a. Errors are given as twice the standard deviation of the least squares slope from analysis of k_{decay} vs. [*para*-cresol] according to equation 2.3.

b. Measured by 337-nm laser flash photolysis of 0.01-0.03 M solutions of the ketones.

c. In benzene.

d. In dichloromethane.

Figure 2.5. Plots of k_{decay} versus *para*-cresol concentration for *para*-methoxybenzophenone (26, ■) in dichloromethane, and *para*-thiomethylbenzophenone (30, ▼), *para*-dimethylaminoacetophenone (38, ●), α, α, α -trifluoroacetophenone (46, Δ), fluorenone (54, *) and xanthone (55, X) in MeCN. Fits are according to eq. 2.3. The solutions were deoxygenated and maintained between 23 and 25 °C.



even greater HAA reactivity for π, π^* triplets over n, π^* triplets. This result has in fact been confirmed for a wide range of different ketones. The faster triplet interaction in non-polar solvents has also been reproduced in selected cases.

For the benzophenones, an odd behaviour is noted. Both acceptor-substituted and donor-substituted ketones react faster than benzophenone itself. This will be discussed in greater detail in the next section.

For the acetophenones, the electronic effect is minimal, with rate constants only slightly larger for very electron poor triplets than very electron rich ones.

A preliminary mechanistic analysis suggests that the interaction between triplet and phenol is certainly not a "normal" radical-like HAA. This is because the observed quenching rate constants of phenolic quenching are mostly $10^8 \text{ M}^{-1} \text{ s}^{-1}$ or higher, while for C-H abstractions they are on the order of $10^6 \text{ M}^{-1} \text{ s}^{-1}$ or so.^{23,33,35,52,53} The small difference in O-H bond strength versus C-H bond strength does not account for this increase (see Table 1.2), which is reflected to the fact that the phenolic quenching rate constants are also, on average, one order of magnitude higher than what has been reported for alkoxyl-radical abstractions from phenols,⁵⁹ although acetonitrile data is lacking for a more direct comparison. The proximity to diffusion control in triplet/phenol quenching points to some other process, such as electron transfer, as being important in the mechanism. This preliminary analysis is consistent with the fact that lowest π, π^* and n, π^* ketone triplets are equally reactive towards the donor, and reflects the original conclusions of previous workers.^{70,72}

2.1.5. Discussion. Benzophenone reactivity.

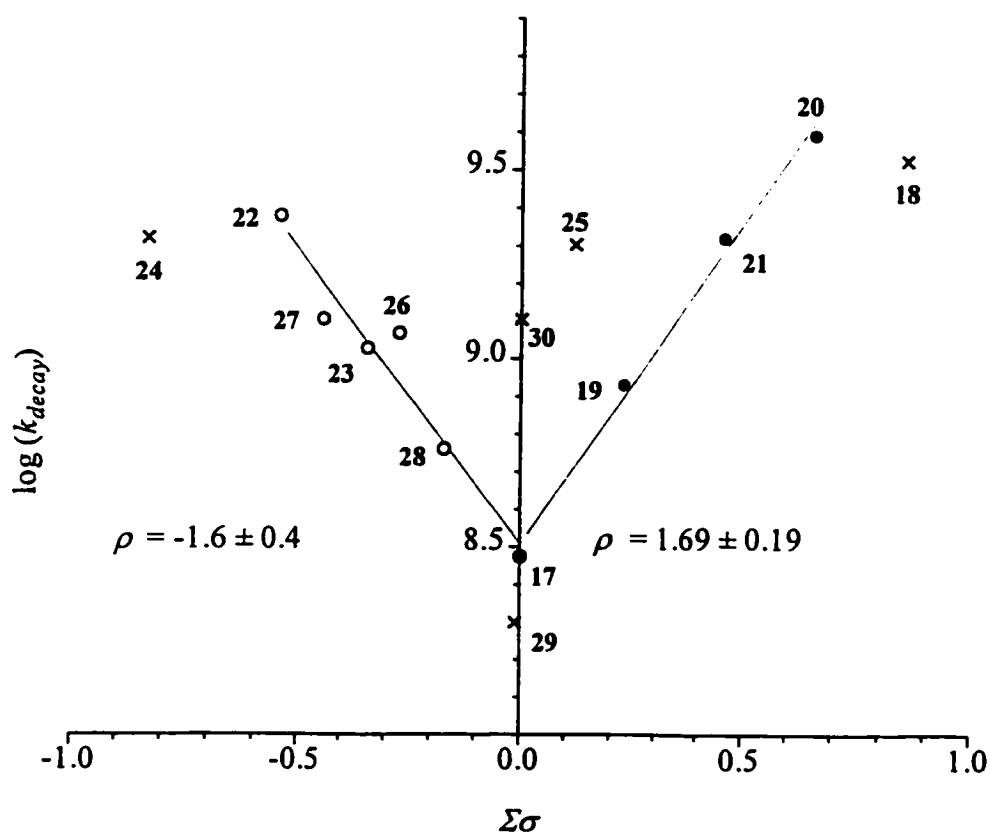
Figure 2.6 displays a plot of the logarithm of the rate constants for bimolecular quenching by *para*-cresol of the triplets of benzophenones **17** - **30** against Hammett substituent constants⁹³ in acetonitrile. The lines indicate linear regression fits for right-hand side (dark circles) data as well as left-hand side (open circles) data.

Several benzophenones (marked with an 'X' on the plot) were not included in the analyses. The 4-phenyl (**29**) and 4-thiomethyl (**30**) species were excluded since they have lowest π , π^* triplet states⁹⁴ whereas the others all have lowest n , π^* triplet states.⁹ Interestingly, the values for 3,3'-bis(trifluoromethyl) (**18**) and 4-dimethylaminobenzophenone (**24**) did not correlate with the others, perhaps displaying reactivity attenuated by their proximity to the diffusion limit.

The 'vee' shape is classic evidence of a mechanistic change that occurs as the electronic properties of the substituents are varied. In this case, the minimum at the unsubstituted compound **17** implies a fundamental difference in mechanism for the quenching of electron-rich (donor-substituted) and electron-poor (acceptor substituted) benzophenones. Since ketone **17** lies at a minimum, it is at the borderline of the two mechanisms.

The 3-methoxy compound (**25**) is a much less explicable outlier, with a quenching rate constant higher than its ground state σ_m value would predict. Zimmerman's group⁹⁵ reported a case in which the *meta*-alkoxy groups in an excited molecule were found to be more electron donating than the *para*-alkoxy groups of an isomer in the ground state.

Figure 2.6. Log rate constant *versus* sum of Hammett substituent parameter for the *para*-cresol quenching of substituted benzophenone triplets (17 - 30) in deoxygenated acetonitrile solution at 23 °C.



This result has become generally known as the photochemical "meta" effect.^{12,96-99}

This effect would imply that the ground state σ_m value of +0.12 for methoxy is not applicable for the excited state, and that the excited state value may be more negative than ground state σ_p , *i.e.*, less than - 0.27.

There are a few papers in the literature that comment on the validity of using *ground* state linear free energy parameters in excited-state reactions.¹⁰⁰⁻¹⁰² Yates and McEwen¹⁰¹ summarized previous work and found that while ground-state σ -values can sometimes provide satisfactory correlations to excited state reactivity, correlations are also sometimes very poor. They proposed a new substituent scale for linear free energy relationships, $\sigma^{h\nu}$, and showed correlations to published data as well as their own data for the photohydration of styrenes.¹⁰⁰ For 3-MeO, $\sigma^{h\nu}$ is -1.48, while for 4-MeO it is -1.17.

For our purposes, the good correlation observed for the two sides of the Hammett plot indicate that ground state parameters are satisfactory for this study.

The slope observed (1.69 ± 0.19) for the acceptor-substituted benzophenones (right-hand side of the plot) indicates a "normal" quenching mechanism for an electrophilic π^* triplet state, since the quenching accelerates as the triplet becomes more and more electron deficient. This result is similar to that reported by Wagner and co-workers for quenching of substituted benzophenone triplets by *para*-xylene in acetonitrile solution (Path B in Figure 1.6; Figure 1.7). One critical difference, however, is that in that case, linear Hammett behaviour was observed over the complete range of benzophenones studied.³² Recall that this trend was interpreted in terms of a mechanism involving the

initial formation of an “*n*-type” exciplex with substantial charge-transfer (ketone acceptor/arene donor) character.

As importantly, the positive Hammett slope for acceptor-substituted benzophenones is consistent with the negative Hammett slope observed for the quenching of benzophenone by substituted phenols, as reported by Scaiano and co-workers.⁷² Recall that this result was used to support their argument that benzophenone *n*, π^* triplets were quenched by phenols in a manner consistent with a normal charge-transfer interaction, with the phenol acting as the donor and the ketone as the acceptor.

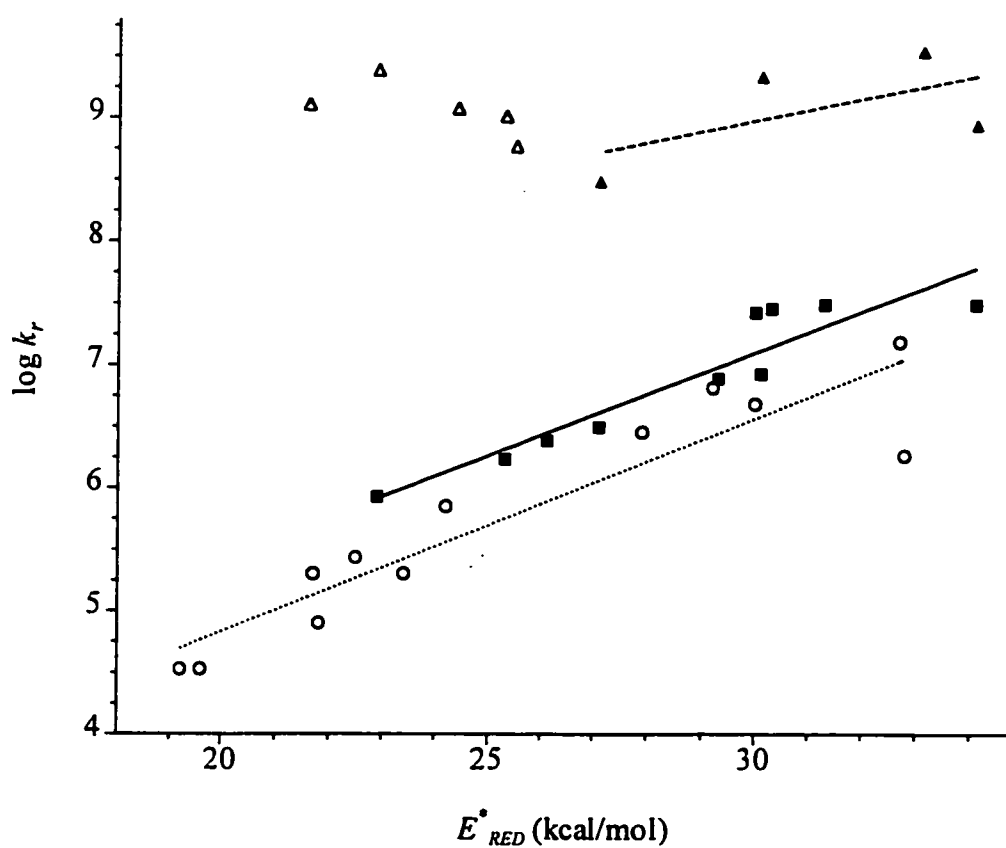
From these results, the mechanism of phenolic quenching for the right-hand side of the Hammett plot is assigned to the "normal" electrophilic triplet quenching mechanism for donors in general, similar to Figure 1.7. Figure 2.7 displays the phenol data on the same axes.

2.1.6. Discussion. A nucleophilic mechanism.

The left-hand side of the Hammett plot displays the trend observed for quenching of the donor-substituted benzophenones by *para*-cresol. The negative slope suggests that a different mechanism grows in importance and eventually takes over as the electron-donor character of the benzophenone triplet increases. Furthermore, the negative slope is consistent with a mechanism in which the dominant role of the triplet is that of a *nucleophile*. This is very odd behaviour for the electron-deficient *n*, π^* state.

Two scenarios can be envisioned. Protonation of the carbonyl oxygen involves the buildup of positive charge required to explain the negative slope, and this may seem

Figure 2.7. Updated plot of bimolecular reaction rate constants of ketone triplet quenching in acetonitrile as a function of triplet reduction potential. Squares and circles respectively indicate benzophenones and acetophenones quenched by *para*-xylene. Dark and light triangles respectively indicate acceptor- and donor-substituted benzophenones quenched by *para*-cresol.



reasonable since it is known that as a class of compounds, phenols are weakly acidic. Protonation of the ketone triplet could form a triplet acid/base pair, which could then undergo a single electron transfer event to form the observed neutral radical pair.

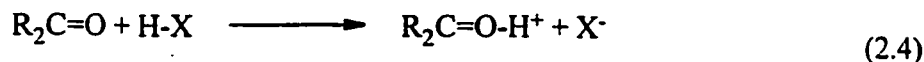
Another mechanism consistent with nucleophilic behaviour is hydrogen-bond formation. This mechanism is similar to the protonation reaction with one very important difference: hydrogen-bonding represents only *partial* protonation. Figure 2.8 describes both potential paths for donor-substituted benzophenones.

There are three factors to consider in evaluating whether either of these mechanisms are plausible:

1. Ketone *triplet* basicity in organic media.
2. Phenol acidity in organic media.
3. The thermodynamics of electron transfer within the acid/base ion pair and hydrogen-bonded complex.

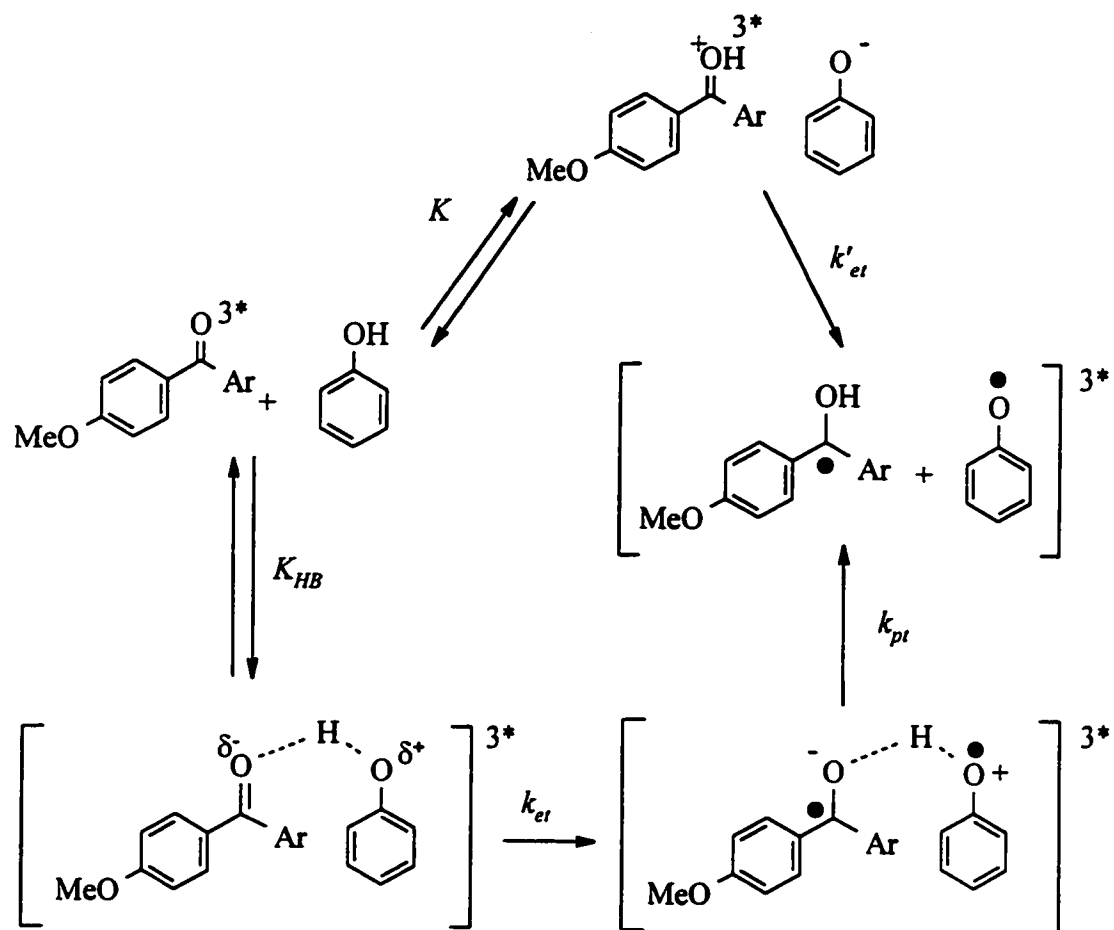
Let us consider each of these factors in turn before deciding if either mechanism is appropriate.

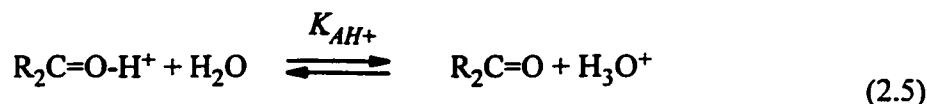
The general acid/base reaction between any ketone and acid HX can be described as:



and an equilibrium acidity constant K_{AH^+} can be defined as

Figure 2.8. Two possible pathways of nucleophilic ketone triplet interaction with phenol: acid/base (full protonation) and hydrogen-bonding (partial protonation).





Ground state ketones are thought to be slightly basic organic molecules due to the two lone pairs on the oxygen atom. They can be protonated by strong acids and display pK_{AH^+} on the order of -5. Table 2.10 lists pK_{AH^+} values for several different ketones.

Bonner and Philips studied substituent effects on benzophenone basicity and found that the pK_{AH^+} values of ground state benzophenones correlated with σ^+ , leading to a reaction constant $\rho^+ = 1.09$.¹⁰³ This electronic effect was also observed for ground state acetophenones, for which $\rho^+ = 2.17$. For both ketone classes, the positive slopes observed are most likely due to the greater ability of the resonance donor substituents to support a protonated carbonyl oxygen.

A consideration of the valence bond structures in Schemes 1.3 and 1.4 leads to the prediction that electronic excitation should cause great changes in the acid/base properties of ketones. For n, π^* states, it is not unreasonable to assume that the promotion of one of the non-bonding electrons on oxygen should result in a decrease in basicity. For π, π^* and CT-states, the non-bonding electrons on oxygen remain intact, and a likely prediction is that these species should have a basicity similar to the ground state and greater than that of the n, π^* state.

Experimentally, the acid-base properties of ground-state ketones¹⁰³⁻¹⁰⁵ and aromatic ketone triplets¹⁰⁶⁻¹¹⁴ have been studied in detail. Included in Table 2.10 are literature

Table 2.10. Ground and excited state pK_{AH^+} values for some aromatic ketones. ^a

Ketone	pK_{AH^+} S_0	pK_{AH^+} S_1	pK_{AH^+} T_1
benzophenone (17)	- 6.2 ^b , - 5.7 ^c , - 4.74 ^d	- 4.2 ^e	+ 1.5 ^d , + 0.20 ^f
4-methoxybenzophenone (26)	- 4.93 ^c		
4,4-dimethoxybenzophenone (22)	- 4.41 ^c	+ 4.0 ^e	+ 5.5 ^e
acetophenone (31)	- 6.15 ^g	- 3.2 ^h	+ 0.9 ^h , + 0.63 ^f
<i>para</i> -methoxyacetophenone (42)	- 4.81 ^c	- 1.3 ^h	+ 3.4 ^h
<i>para</i> -methylacetophenone (44)	- 5.47 ^c	- 4.4 ^h	+ 2.6 ^h
xanthone (55)	- 4.1 ^{i,j}	+ 1.0 ⁱ	+ 3.0 ⁱ

a. Values in sulfuric acid/water mixtures unless otherwise indicated.

b. Fischer, A.; Grigor, B.A.; Packer, J.; Vaughn. J. *J. Am. Chem. Soc.* **1961**, *83*, 4208.

c. Ref. 103.

d. Ref. 107.

e. Ireland, J.F.; Wyatt, P.A.H. *J. Chem. Soc. Faraday Trans. 1* **1973**, *69*, 161.

f. in aqueous acetonitrile; Ref. 108.

g. Stewart, R.; Yates, K. *Can. J. Chem.* **1958**, *80*, 6355.

h. Ireland, J.F.; Wyatt, P.A.H. *Adv. Phys. Org. Chem.* **1976**, *12*, 131.

i. Ref. 106.

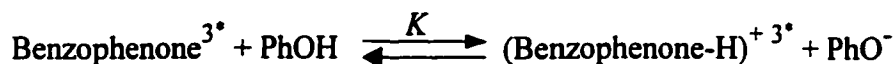
j. Tomachev, A.I.; Shulezhko, L.N.; Kisilenko, A.A. *Z. Obsch. Khim.* **1965**, *35*, 1708.

pK_{AH^+} values for several triplet ketones. The results indicate that in general, *all* aromatic ketone triplets are *more basic* than the ground state, even those with lowest n, π^* states. For example, the pK_{AH^+} value of the triplet state of benzophenone is + 1.5 in water, compared to the ground state value of -5.7.¹⁰³ One interpretation by previous workers was that since this value is considerably higher than would be expected for a lowest n, π^* triplet, protonation involves interactions with the upper π, π^* state instead.^{108,109} This proposal is consistent with the spectroscopic (phosphorescence emission) results of Leermakers and co-workers, which indicated that the lowest triplet state of benzophenone appeared to have substantial π, π^* character in protic media, including aqueous acid.¹¹⁵ Other groups have obtained similar spectroscopic evidence for other ketone systems.¹¹²⁻¹¹⁴ It seems clear that the π, π^* state plays a major role in the protonation of aromatic ketones.

Substituent effects on triplet state basicity have not been systematically examined, but are expected to follow the same trends as the ground state. It seems reasonable to expect that electron-donating groups will add to the overall basicity of lowest CT and π, π^* triplets due to the ability to directly participate in π -conjugation. The situation for lowest n, π^* states is different, since the n -orbital is orthogonal to the ring. Here, donor-substituents have two effects. The first is, as before, to increase triplet basicity due to (smaller inductive) substituent effects. However, the second, and perhaps much greater effect, is to increase the contribution from the upper π, π^* state (see Figure 1.3) due to a

reduction in the energy gap. Since π, π^* states are believed to be involved in protonation, this second effect may cause the basicity of n, π^* states to modulate greatly with the degree of donor character of the substituent, due to the varying amount of π, π^* character present.

Having established a general understanding of the basicity of ketone triplet states, phenol acidity must be considered next. In water, the pK_A value of phenol is known to be 10.0.⁹⁹ As equation 2.6 demonstrates, phenol is not sufficiently acidic to protonate triplet benzophenone to any significant extent in water.



$$K = K_{A_{\text{PhOH}}} / K_{A_{\text{TRIPLET}}} = 10^{-10} / 10^{1.5} = 10^{-11.5} \text{ (water)} \quad (2.6)$$

In acetonitrile, phenol's pK_A is 27.¹¹⁶ Presumably, despite being one of the most polar of organic solvents, its aprotic nature greatly hinders dissociation into ions compared to water. From this, it should be safe to assume that the extent of protonation in acetonitrile will be even less than in water.

Unlike full protonation, the formation of hydrogen-bonded complexes *is* likely to be significant between phenols and ketones, particularly in aprotic organic solvents where there is no solvation of the hydrogen-bonding sites.

Quantitative studies on hydrogen-bonding equilibria have been conducted by

infrared spectroscopy.¹¹⁷⁻¹¹⁹ Table 2.11 reports some equilibrium constants, K_{HB} , for the formation of 1:1 hydrogen-bonded complexes of various carbonyl compounds with *para*-fluorophenol in CCl_4 .

In general, the K values are found to be greater than 1 but do not become excessively large. Substituent effects match those on carbonyl basicity, as expected. The effect on K_{HB} of moving to a more polar solvent such as acetonitrile is suspected to cause K_{HB} values to drop as the solvent competitively hydrogen-bonds to the phenol itself.

Less is known about the hydrogen bonding of ketones in the excited state. Focusing only on triplet states here, the increase in basicity caused by excitation (as summarised above) indicates that hydrogen bonding should be more favourable in the triplet state. Literature reports have briefly described solvent effects in studies of the kinetics of phenolic quenching. For example, in wet acetonitrile, benzophenone triplet quenching by phenol is 16 times slower than in benzene. This has been ascribed to a lowering of the effective concentration of phenol by hydrogen-bonding to water.⁷² Das and Bobrowski reported a method which uses this retardation to measure hydrogen-bonding equilibria by NLFP.⁷³

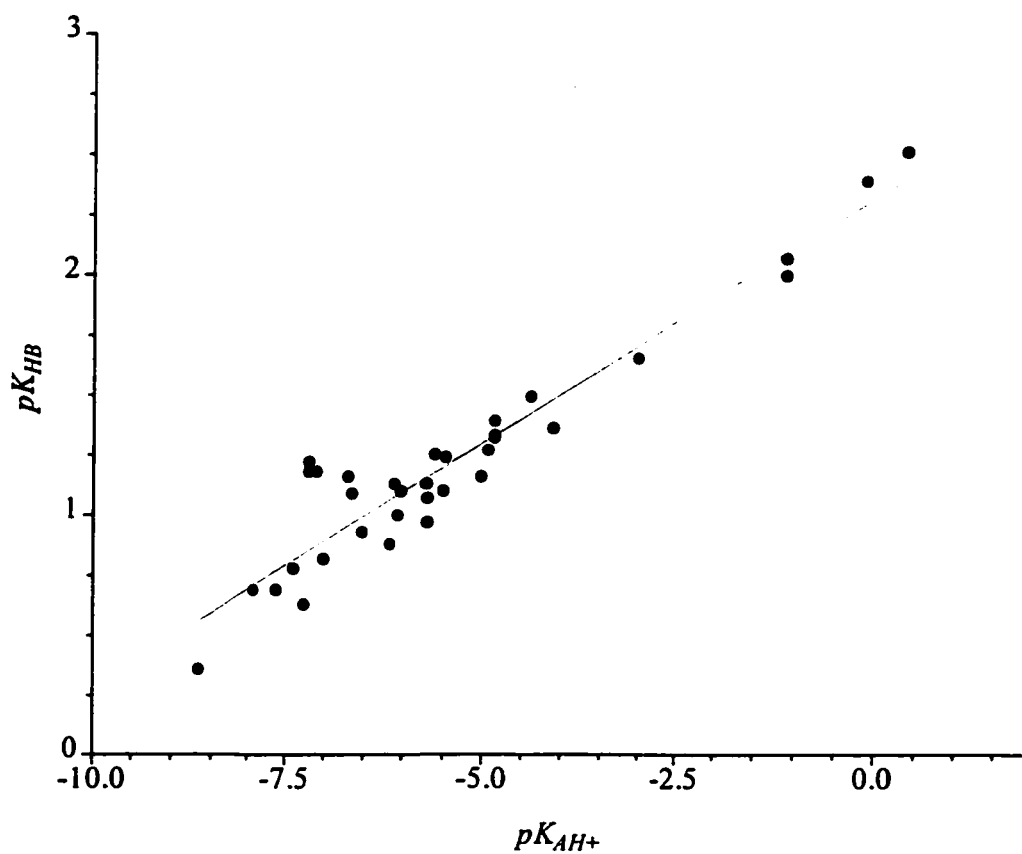
An attempt to quantify the expected effect of electronic excitation on the magnitude of ketone/phenol hydrogen bonds is displayed in Figure 2.9, which shows a plot of pK_{HB} versus pK_{AH^+} , prepared from K_{HB} data from various donors with *para*-fluorophenol in CCl_4 and aqueous acidity constants for the donors. The data used for the plot is collected in Table 2.12. Donors have been extended from aldehydes and ketones to include one

Table 2.11. K_{HB} values for the formation of 1:1 hydrogen-bonded complexes between carbonyl compounds and *para*-fluorophenol in CCl_4 at 25 °C. ^a

Compound	K_{HB}
Biacetyl	3.4
Acetone	15.1
Cyclohexanone	24.5
Benzaldehyde	6.0
<i>para</i> -Chlorobenzaldehyde	4.3
<i>para</i> -Methoxybenzaldehyde	12.6
Acetophenone (31)	12.9
<i>para</i> -Cyanoacetophenone (34)	9.3
<i>para</i> -Methoxyacetophenone (42)	21.4
<i>meta</i> -Methoxyacetophenone (41)	14.5
Benzophenone (17)	11.7
4-Methoxybenzophenone (26)	18.6
Fluorenone (54)	12.3
Xanthone (55)	22.9

a. Data from Ref. 119.

Figure 2.9. Plot of pK_{HB} (*para*-fluorophenol in CCl_4 at 25°C) versus pK_{AH^+} for various carbonyl-containing compounds. ^a



a. Data from Table 2.12.

Table 2.12. Values of pK_{HB} and pK_{AH^+} for Figure 2.9. ^a

Compound	pK_{HB}	pK_{AH^+}
<i>para</i> -Nitrobenzaldehyde ^b	0.36	-8.66
<i>para</i> -Nitroacetophenone ^c	0.69	-7.94
<i>meta</i> -Nitroacetophenone ^c	0.69	-7.62
Benzaldehyde ^b	0.8	-7.40
<i>para</i> -Chlorobenzaldehyde ^b	0.63	-7.26
2-Butanone ^d	1.18	-7.2
Acetone ^d	1.18	-7.1
3,3-Dimethylbutanone ^d	1.04	-7.1
3-Methylbutanone ^d	1.04	-7.1
<i>meta</i> -Chloroacetophenone ^c	0.82	-7.01
<i>meta</i> -Methoxyacetophenone ^c (41)	1.16	-6.70
Fluorenone ^c (54)	1.09	-6.65
<i>para</i> -Chloroacetophenone ^c (32)	0.93	-6.52
Ethyl Benzoate ^f	0.88	-6.16
Acetophenone ^c (31)	1.13	-6.15
<i>para</i> -Fluoroacetophenone ^c (40)	1.00	-6.06
<i>meta</i> -Methylacetophenone ^c	1.10	-6.02
2-Acetonaphthone ^c (52)	1.13	-5.71
Benzophenone ^g (17)	0.97; 1.07 ^h	-5.70
<i>para</i> -Ethylacetophenone ^c	1.25	-5.61
<i>para</i> -Methoxybenzaldehyde ^b	1.10	-5.50

<i>para</i> -Methylacetophenone ^c (44)	1.24	-5.47
Anthrone ^e	1.16	-5.02
4-Methoxybenzophenone ^b (26)	1.27	-4.93
Cyclohexanone	1.32	-4.85
<i>para</i> -Methoxyacetophenone ^c (42)	1.33	-4.81
4,4'-Dimethoxybenzophenone ^e (22)	1.49	-4.39
Xanthone ^e (55)	1.36	-4.10
Acetylferrocene	1.65	-3.00
Flavone	1.99	-1.10
<i>N, N</i> -Dimethylformamidine	2.00	-1.10
<i>N, N</i> -Dimethylacetamide	2.38	-0.10
2,6-Dimethyl- γ -Pyrone	2.50	+0.40

a. pK_{HB} Data from Ref. 119; pK_{AH^+} values from Ref. 119 unless otherwise noted.

b. Ref. 103.

c. Stewart, R.; Yates, K. *J. Am. Chem. Soc.* **1958**, *80*, 6355.

d. Campbell, H.J.; Edward, J.T. *Can. J. Chem.* **1960**, *38*, 2109.

e. Stewart, R.; Granger, M.R.; Moodie, R.B.; Muenster, L.J. *Can. J. Chem.* **1963**, *41*, 1065.

f. Edward, J.T.; Wong, S.C. *J. Am. Chem. Soc.* **1977**, *99*, 4229.

g. Ref. 107.

h. Ref. 119.

ester and two amides. This plot collects data from many sources, as each point represents data from two different groups of workers. A linear correlation is found between the propensity of hydrogen-bond formation and the basicity of the acceptor. Assuming that linearity extends past the last data points, then interpolating known pK_{AH^+} values of ketone triplets, *e.g.*, +3.0 for xanthone and +1.5 for benzophenone, indicates that pK_{HB} values for triplets should be quite large.

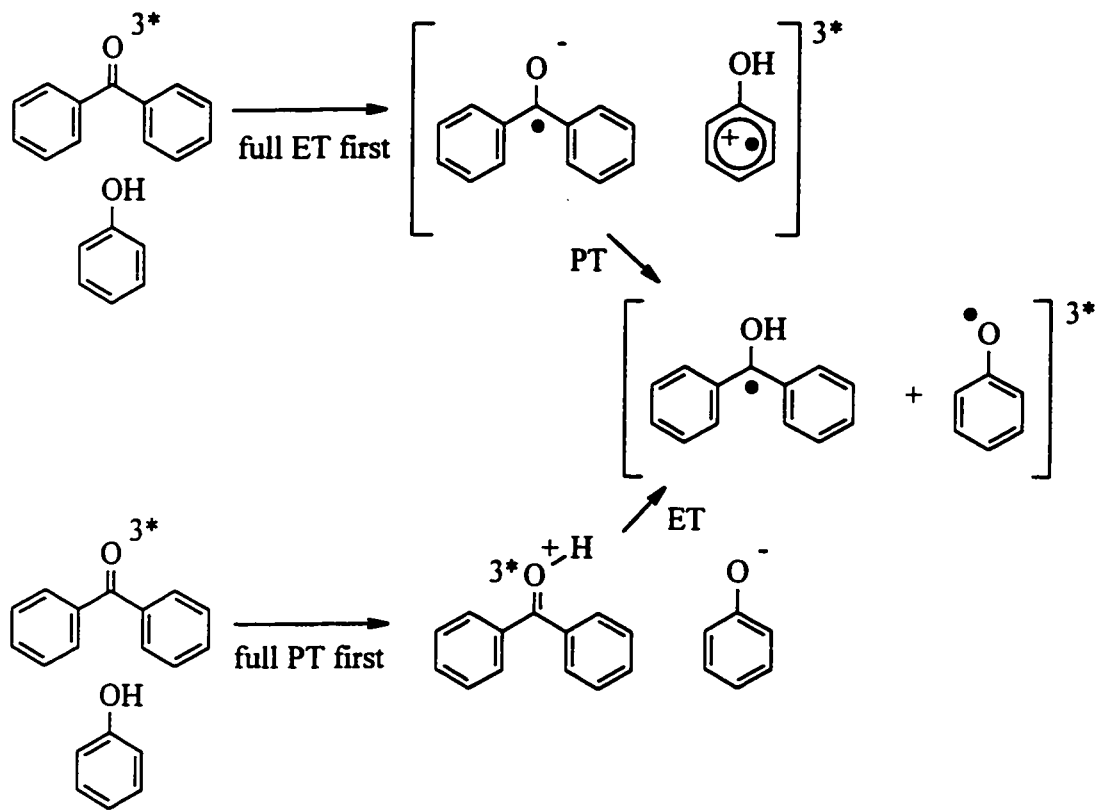
2.1.7. Discussion. Feasibility of electron transfer in a hydrogen bonded complex.

If hydrogen-bonding is favourable as a first step, the next critical question to ask is whether the thermodynamics of electron transfer within a hydrogen-bonded complex can be estimated. Clearly, if this value is unfavourable, then the overall hydrogen-atom transfer will not occur and even though hydrogen-bonded complexes freely form, some other mechanism is responsible for the observed triplet quenching.

The Rehm-Weller equation can be used in this scenario, but with a very important caveat: thermodynamically relevant reduction and oxidation potentials for hydrogen-bonded species cannot routinely be measured by the usual electrochemical techniques. Thus, an exact answer to our problem cannot be found. What can be done instead is a modeling of two extreme cases that the hydrogen-bonded mechanism falls between. Scheme 2.2 shows these two extremes, with benzophenone and phenol chosen as the two partners.

The first extreme case is full electron transfer from the phenol to triplet ketone. This

Scheme 2.2. Two extreme cases of reactivity between triplet benzophenone and phenol.



was hinted in Chapter One to be endergonic; now the calculation will be shown.

Phenol itself has an estimated half-wave oxidation potential, $E_{1/2}^{\text{ox}}$, of approximately +1.65 V vs. SCE¹²⁰ in MeCN. This value is an estimation, since the electrochemical oxidation of phenols is irreversible. This is because after one-electron oxidation, the resulting phenolic radical cation quickly deprotonates yielding phenoxide, which in turn quickly loses another electron. The value of $E_{1/2}^{\text{ox}} = +1.65$ V was interpolated from a Hammett plot of the oxidation potentials of mono- and 1,4-disubstituted benzenes.¹²¹

The reduction potential and triplet energy of benzophenone are listed from Table 2.1. Given these values, equation 1.4 predicts $\Delta G_{et} \sim +11$ kcal/mol if the Coulomb term is neglected. The unfavourable nature of ketone triplet/phenol electron transfer is thus revealed.

Now consider the other extreme case, where acid-base interaction is at a maximum and the ketone triplet is fully protonated prior to electron transfer. The Rehm-Weller equation predicts that electron transfer from phenoxide ion to protonated benzophenone triplet should be strongly exergonic, $\Delta G_{et} \sim -44$ kcal/mol. This value is based on values of +0.24 and -0.6 eV (vs. SCE) for the standard reduction potentials of phenoxyl radical¹²² and protonated benzophenone¹²³ in acetonitrile, a value of 63 kcal/mol for the triplet energy of the protonated ketone,¹¹⁵ and again neglecting the Coulombic contribution to ΔG_{et} .

Thus there is +11 *versus* -44 kcal/mol on the two sides of the hydrogen-bonding case. Clearly, as soon as even a small amount of phenoxide character builds up on the phenol due to a collision and the subsequent formation of a hydrogen-bonded complex, a large shift in the thermochemistry will occur to effectively reduce both the reduction potential of the triplet ketone and the oxidation potential of the phenol. Electron transfer should become more favorable, in essence "borrowing" some of the -44 kcal/mol value against the +11 kcal/value. Following electron-transfer, the proton then completes its migration to yield the phenoxyl-hemipinacol radical pair. The proton is presumably transferred rapidly due to the high acidity of phenol radical cations.^{124,125}

Based on the previous discussion, a mechanism for phenolic hydrogen abstraction is

proposed which involves electron transfer within a hydrogen-bonded triplet exciplex, followed by very rapid proton transfer. This new mechanism is able to explain the unusually high reactivity of π, π^* triplet ketones towards phenolic hydrogen abstraction.

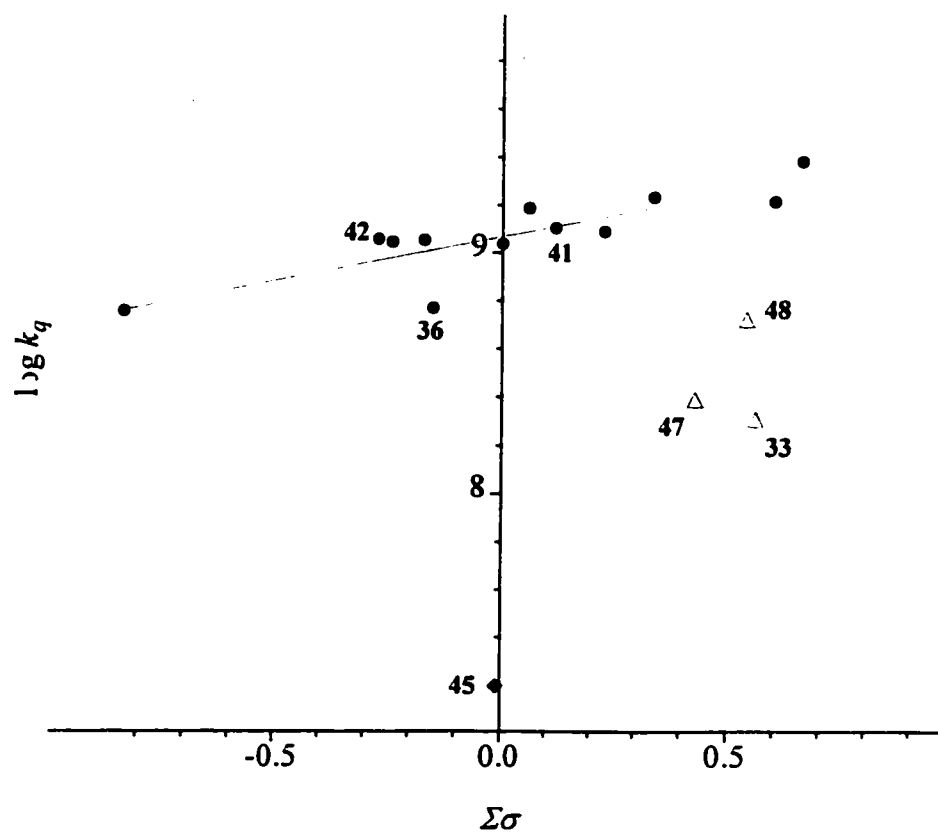
As for the benzophenones, donor substitution leads to a triplet state with increased π, π^* state character. This is caused by a reduction in the T1 (n, π^*) and T2 (π, π^*) energy gap due to the effect of donor-substitution on aromatic energy levels (see Figure 1.3). The increasing π, π^* state character with increasing donor substitution in benzophenones allows the new hydrogen-bonded mechanism to take over the reactivity for these compounds. Hence, a negative Hammett slope is observed.

This mechanism is also consistent with published data on the quenching of fluorenone triplets by certain phenols.⁹² As well, other workers have also discovered a similar role for hydrogen-bond mediated electron transfer in their study of benzophenone/naphthylamine exciplexes.¹²⁶ Very recent literature examples of proton-coupled electron transfer demonstrate such processes in a wide variety of chemical systems.¹²⁷⁻¹³¹

2.1.8. Discussion. Generality of the new mechanism.

Figure 2.10 displays a Hammett plot for acetophenones generated from the data in Table 2.8. The solid points represent ketones that possess lowest π, π^* triplets, while the n, π^* triplets are labeled with open triangles. The plot has a gentle positive slope of 0.37 \pm 0.14, and is continuous. The fit is poor ($r^2 = 0.72$), but the trends distinctly show that

Figure 2.10. Plot of $\log k_q$ versus sum of Hammett σ for the *para*-cresol quenching of substituted π, π^* (●) and n, π^* (Δ) acetophenone triplets in deoxygenated MeCN at 23 to 27 °C. Triplet 4-phenyl acetophenone (v) is also on the plot.



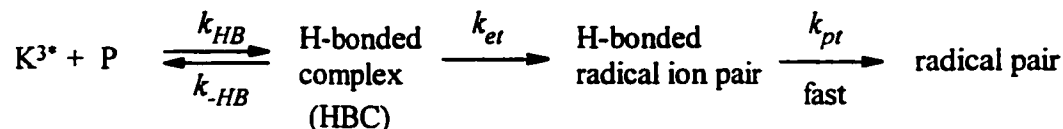
the behaviour is *very different* from the plot for benzophenones. The correlation improves ($r^2 = 0.86$) if 3,4-dimethoxyacetophenone (36) is removed from the plot.

The attempted correlation deserves several comments. First, three acceptor-substituted acetophenones are obvious outliers. The behaviour of these three ketones, *meta*-cyano- (33), *meta*-trifluoromethyl- (47), and *para*-trifluoromethylacetophenone (48), which exhibit rates much *smaller* than the Hammett line would predict, might be explained by the fact that they are in actuality lowest n, π^* triplet acetophenones.¹¹ Due to this switch of states, they possess an electrophilic triplet which does not hydrogen bond as readily, a condition exacerbated by the electron-withdrawing electronic effect of the substituents. Instead, the mechanism of their reactivity is assigned to the electrophilic mechanism for acceptor-substituted benzophenones that was described earlier.

para-Phenyl acetophenone (45) also falls far below the Hammett line. Apparently ketone 45 behaves more like a substituted biphenyl triplet than a substituted ketone triplet. Excited aromatic hydrocarbons, such as triplet biphenyls, are poor participants in HAA reactions as carbon-centered radicals are less reactive than oxygen-centered radicals.¹⁶

An argument to rationalise the magnitude of the mild slope of the Hammett plot comes after analysis of the components of the rate-determining step of the reaction. Consider Scheme 2.3, in which a ketone triplet and a phenol approach each other and form a hydrogen-bonded complex that rapidly reacts further.

Scheme 2.3. Mechanism of triplet quenching *via* a hydrogen-bonding equilibrium.



Here, k_{et} and k_{pt} are the rate constants of electron and proton transfer, respectively.

Assuming steady-state for [HBC], and $k_{pt} \gg k_{et}$, the rate law can be shown to be:

$$-d[K^{3*}] / dt = \frac{(k_{HB} k_{et})}{(k_{-HB} + k_{et})} [K^{3*}] [Phenol] = k_q [K^{3*}] [Phenol] \quad (2.7)$$

where

$$k_q = \frac{(k_{HB} k_{et})}{(k_{-HB} + k_{et})} \quad (2.8)$$

The slope of the Hammett plot gives insight into the nature of the rate-determining step. Equation 2.8 shows that the observed rate constant is a function of the hydrogen-bonding ability of the triplet/phenol pair and the rate of electron transfer upon complexation. These two fundamental aspects of the reaction suffer from opposite electronic demand, however, since as the triplet becomes more basic and hydrogen-bonding becomes more favourable, the redox reaction is predicted to slow down due to the increased difficulty in reducing a more basic triplet, and *vice versa*.

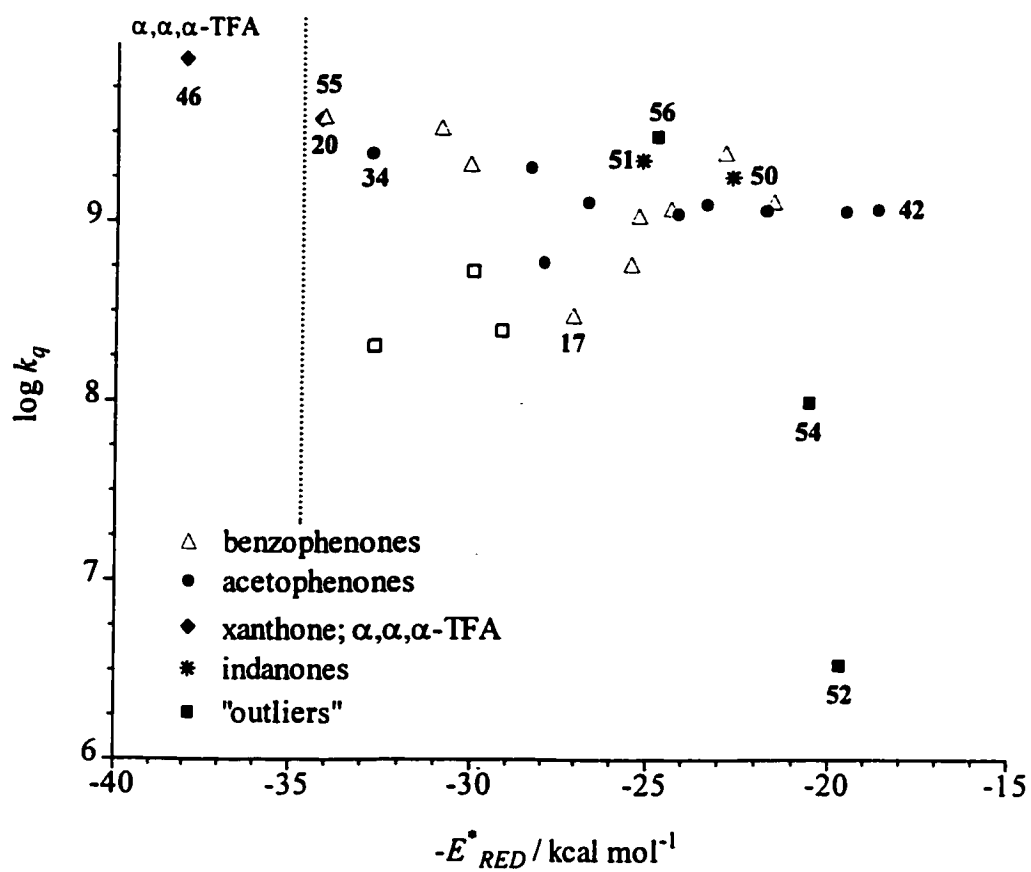
One would expect a negative Hammett slope in Figure 2.10 if the acid/base aspect dominated the mechanism, or a positive Hammett slope if the electron transfer component held an edge. What is observed is a gentle positive slope of overall small magnitude. The mild sensitivity is due to this competition, with the positive slope indicating that the redox part of the reaction is slightly more important to the overall rate constant than the hydrogen-bonding equilibrium.

One way to show that the rate-determining step of the mechanism does have a moderate component of charge transfer is to correlate the observed rate of phenolic quenching to acceptor triplet reduction potential, E_{RED}^* . Just as all ketones of similar mechanism fell on the Hammett line, it would be expected that on such a plot, those ketones that share similar redox chemistry in the reaction, would also fall on a line. The plot is shown in Figure 2.11.

The reactivity may be divided into four broad groups. On the left of Figure 2.11 is a dashed vertical line, drawn at the E_{RED}^* value such that ΔG_{et} from phenol is zero. Rehm-Weller calculations predict exergonic electron transfer for ketones quenched by *para*-cresol to occur near or to the left of the line. Xanthone (55) and 4-cyanobenzophenone (20) are each near the line, and α, α, α -trifluoroacetophenone (46) is to the left of it. The quenching rate constants of these species (3.75 , 3.9 and $8.1 \times 10^9 \text{ M}^{-1} \text{ s}^{-1}$, respectively) are among the highest observed in acetonitrile, and it is possible that a shift to a full electron transfer mechanism is occurring for these ketones.

There is no direct evidence for electron-transfer, as no radical ions are observed in

Figure 2.11. Plot of $\log k_q$ versus E_{RED}^* for the *para*-cresol quenching of ketone triplets (17 - 56) in deoxygenated MeCN at 23 to 27 °C. See legend for explanation of symbols.



the NLFP experiment. Perhaps this is not surprising considering the high acidity of phenolic radical cations, whose pK_A values are estimated to be several units less than zero in non-aqueous solvents.¹²⁵ Rate constants of deprotonation of electron-rich methoxy-substituted phenolic radical cations by water in MeCN have been recently reported by Johnston and co-workers,¹³² and are on the order of $10^8 \text{ M}^{-1} \text{ s}^{-1}$. In the phenolic quenching of ketone triplets in MeCN, the much greater base strength of the ketyl radical anion may make the deprotonation reaction even more favourable and this reaction occurs too fast to be observed on the nanosecond timescale.

The middle of the plot shows a region dominated by ketones that can definitely not undergo a one electron-transfer. As seen previously in Figure 2.7, the benzophenones (Δ) exhibit a vee pattern on this sort of plot, with benzophenone itself forming a minimum. This result may be explained by the observation that the reduction potentials of benzophenones are known to correlate with Hammett σ .^{133,134}

Lowest π, π^* acetophenone triplets (\bullet) are assigned the hydrogen-bonded mechanism, as are the donor-substituted benzophenones. The minimal scatter of the acetophenones shows clearly how the mechanism compensates for triplets of both low reducing power/high basicity (ketone 42) and high reducing power/low basicity (ketone 34), producing uniformly fast rates of reaction for a wide variety of ketones. The benzophenones show a greater sensitivity to E_{RED}^* since they have widely varying proportions of upper π, π^* reactivity to draw upon depending on substituent.

The two alkoxyindanones studied, 50 and 51 (*), fall above the acetophenone line,

indicating that they have a greater bimolecular reactivity than would be predicted based purely on E_{RED}^* values. A possible explanation is based upon the planarity induced by the carbonyl group constrained to the same plane as the attached aromatic ring, which allows the lowest triplet state of indanones to have CT triplet character. One effect that this has is to increase the basicity and hence the reactivity of the triplet state due to the resonance from the remote alkoxy group to the carbonyl oxygen.

The final group consists of the solid squares ■, which represent "outliers", such as 2-acetonaphthone (**52**) and fluorenone (**54**). The low reactivity of ketone **52** has already been discussed, but compound **54** is another species with an anomalously low reactivity. Fluorenone does not phosphoresce, and as a consequence its lowest triplet assignment^{135,136} of π, π^* is based on its long lifetime. There has been some debate as to whether an n, π^* assignment may be more applicable,¹³⁷ but recent studies using solvent and substituent effects reinforce the π, π^* assignment of Davis and co-workers based on their thorough chemical reactivity study.¹³⁸ Of course, if the excited state of fluorenone actually was of n, π^* character, then this would explain its low reactivity: it would have no access to the nucleophilic mechanism and its high triplet reduction potential would cause it to have poor charge-transfer reactivity. On the other hand, it may exist as a less reactive π, π^* triplet perhaps due to its planarity, which may cause there to be a smaller charge density on the oxygen atom than in benzophenone. This idea is something that molecular orbital calculations might be able to address.

Sulfur-containing thioxanthone **56** is an outlier in the sense that it is more reactive

than a π, π^* ketone of similar E_{RED}^* would be. It has a quenching rate constant only slightly less than xanthone despite having an E_{RED}^* value almost 10 kcal/mol lower.

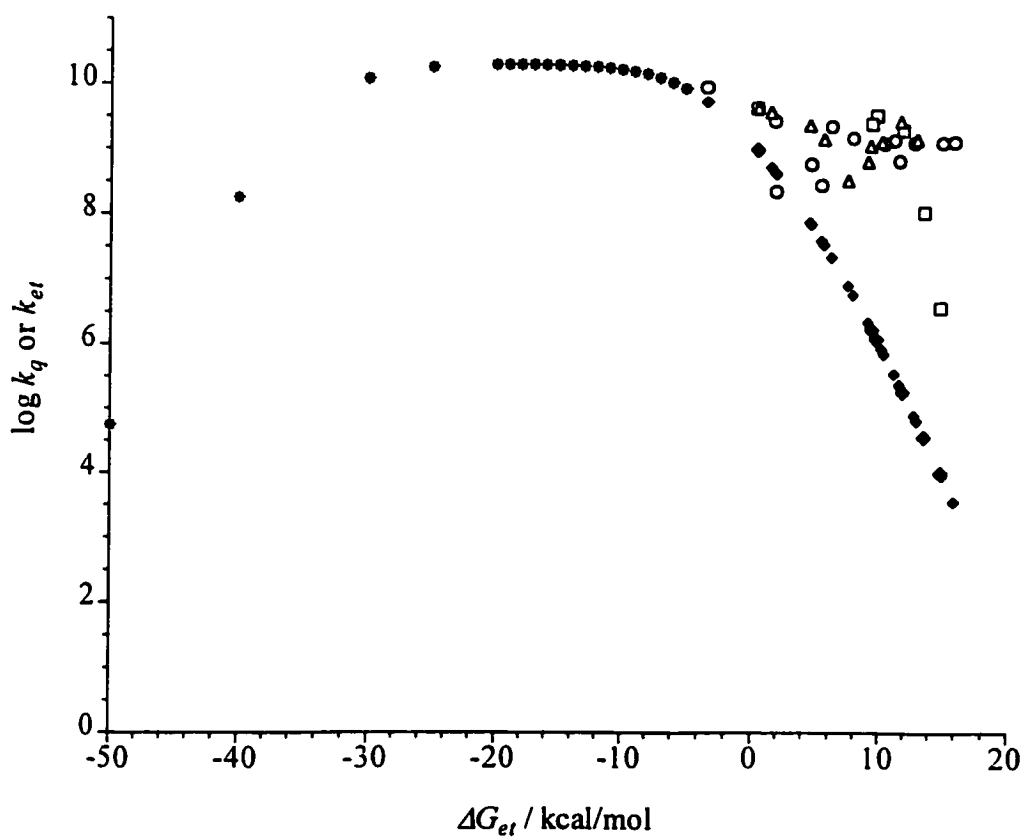
One possible explanation for this is that thioxanthone may have a more basic triplet than xanthone. Although its triplet pK_A value has not been measured, this prediction seems reasonable since the sulfur atom can allow greater stabilization of charge buildup than the ring-oxygen atom of xanthone.

Whereas Figure 2.11 displays the correlation between the rates of phenolic quenching of the triplets to their triplet reduction potential, Figure 2.12 presents a crude estimation of full electron-transfer behaviour between aromatic ketone triplets and phenols in MeCN. The open points represent the experimental rate constants for triplet quenching plotted against ΔG_{et} using the Rehm-Weller equation, equation 1.3. These values were derived from the reduction potentials and triplet energies of the ketones from Tables 2.1-2.3, and a value of +1.50 V for the oxidation potential of *para*-cresol in MeCN (estimated the same way as phenol itself; see p.93). The Coloumb term was neglected.

The curve (solid points) represents *theoretical* values for k_{et} from the Marcus equation (equation 2.9), using fit parameters from Kochi and co-workers in MeCN from their study of electron transfer between arene/quinone pairs.¹³⁹

$$k_{et} = k_{diff} / (1 + \kappa \exp (\Delta G^\ddagger / RT)) \quad (2.9)$$

Figure 2.12. Plot of $\log k_q$ or k_{et} versus ΔG_{et} for the *para*-cresol quenching of ketone triplets (17 - 56) in deoxygenated MeCN at 23 to 27 °C. The open points represent experimental values for phenolic HAA; the solid points are k_{et} values according to eq.'s 2.9 and 2.10, using $k_{diff} = 2 \times 10^{10} \text{ M}^{-1} \text{ s}^{-1}$ in MeCN from ref. 5, and the other parameters from ref. 139: $\kappa = 0.1$, $\lambda = 27.67 \text{ kcal/mol}$ and $\alpha = -9.22 \text{ kcal/mol}$.



Very briefly, the Marcus equation relates the rate of electron transfer, k_{et} , to the rate of diffusion, k_{diff} in terms of ΔG^\ddagger , the free activation enthalpy of the electron transfer. This variable is itself a function of the exergonicity and solvent reorganization energy, λ , as defined in equation 2.10. The constant shift factor, α , is used as a correction factor in triplet state electron transfers.¹³⁹

$$\Delta G^\ddagger = (\lambda / 4) [1 + (\Delta G_{et} - \alpha) / \lambda]^2 \quad (2.10)$$

A key observation is that the majority of the triplet quenching rate constants are above the ideal curve. This is excellent evidence that a full-electron transfer process is *not* occurring as a first step in the phenolic HAA reaction.

2.1.9. Conclusions.

Aromatic ketone triplet quenching by *para*-cresol has been studied and the following observations and conclusions have been made:

- 1) In agreement with previous studies, quenching rate constants are very large (on the order of $10^9 \text{ M}^{-1} \text{ s}^{-1}$) and triplets with π, π^* configuration are as reactive or even more so than n, π^* states.
- 2) Benzophenones display a minimum reactivity at the unsubstituted compound; both donor- and acceptor substituted triplets are quenched faster than benzophenone itself.
- 3) Different quenching mechanisms are proposed for these two classes of benzophenone

triplets. The one for the electron-poor triplets may be similar to the charge-transfer assisted mechanism assigned to toluene and xylene quenchers involving an "*n*-type" exciplex intermediate. The other is a fundamentally different and new mechanism, one in which initial hydrogen-bonding between the phenol and the triplet, *via* the π, π^* state, explains the nucleophilic behaviour of the triplet state and allows for an adjustment of the redox properties of the reaction to allow for fast (formal) hydrogen-atom transfer.

4) A study of the acid-base properties of ketones in the ground and excited state supports the idea that ketone triplet states should form strong hydrogen bonds to phenol in organic solvents.

5) A large variety of lowest π, π^* ketone triplets have been quenched by *para*-cresol; we propose the main mechanism of quenching is the same as that proposed for electron-rich benzophenones. Substituent effects on acetophenone triplet quenching are less pronounced due to competing forces in the proposed transition state.

6) Evidence for the need of a hydrogen-bond to adjust the thermodynamic properties of the ketone triplet/phenol interaction comes from a study of the exergonicity of the general reaction, which shows that almost all of the bimolecular reactions studied undergo charge-transfer yet lack the driving force for full-electron transfer.

CHAPTER THREE
INTRAMOLECULAR PHENOLIC HYDROGEN ATOM ABSTRACTION
REACTIONS.
PART ONE. THE STUDY OF DIFFERENT CHROMOPHORES

3.1. Bimolecular *versus* Intramolecular Reactions.

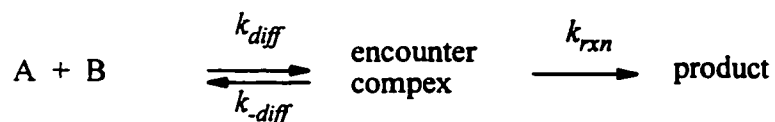
In Chapter One it was concluded that the fastest bimolecular reaction rates one could expect to encounter are those limited by diffusion in the solvent. However, this 'speed limit' for reactions applies only to bimolecular processes. Chemical change can occur inside a molecule at much faster rates. Bond vibrations, which are classically thought to be what ultimately moderate chemical processes, occur on the order of picoseconds. Thus, intramolecular reactivity can occur with rate constants on the order of 10^{11} or even 10^{12} s^{-1} . There is an extensive area of research dealing with intramolecular photochemistry and photophysics; main branches include encounter complex behaviour,¹⁴⁰⁻¹⁴² energy transfer,¹⁴³ electron transfer,¹⁴⁴⁻¹⁴⁹ and atom transfer.^{23,150-155} Wagner and co-workers¹⁵⁶ have studied the rates of various intramolecular photochemical reactions in ketones with spacers of variable length between the ketone group and a reactive terminus, and the pre-1980 work in that area has been reviewed.¹⁵⁴

A diffusion-controlled bimolecular reaction that is converted into an intramolecular one by taking the two partners and combining them into one molecule in such a way that

they can easily interact, will have a reactivity based on what is called 'conformational control', meaning that the rate of the process is moderated by how fast the reactive centers swing about and encounter each other after excitation. Conformationally-controlled lifetimes of excited states will have some dependence on temperature and viscosity.

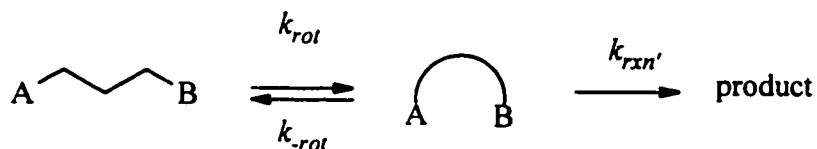
If, on the other hand, the actual reaction is relatively slow, then a conformational equilibrium will be established that will affect the transient lifetime. In this case, internal factors such as steric hindrance may be more important than the bulk properties of the system. Scheme 3.1 illustrates these concepts, and the bimolecular analogies; in the Scheme it is assumed that reaction is the only decay path of interest.

Scheme 3.1. Kinetic schemes for inter- and intramolecular reactions.



If $k_{rxn} \gg k_{-diff}$ then $k_{decay} = k_{diff}$. The reaction is under diffusion control since A and B react whenever they encounter each other.

If $k_{rxn} \ll k_{-diff}$, then an equilibrium is established and $k_{decay} = K_{diff}k_{rxn}$



If $k_{rxn'} \gg k_{-rot}$, then $k_{decay} = k_{rot}$. The reaction is under conformational control since A and B are so reactive when near each other.

If $k_{rxn'} \ll k_{-rot}$, then a conformational equilibrium is established and $k_{decay} = K_{rot}k_{rxn}'$

In the case of sandwich-structured exciplexes, various workers have concluded that the conformational motions that allow for the adoption of such geometries can proceed with rates of up to 10^8 s^{-1} in fluid solution at room temperature.^{140,157} Thus, the shortest possible intramolecular triplet lifetimes in species such as the linked phenolic ketones (LPKs, described in Chapter One, see Figure 1.11) should be on the order of nanoseconds. The very short triplet lifetime previously (Table 1.6, p.47) observed for the para, para'-linked acetophenone **9a** indicate that the deactivation reaction(s) could be under conformational control. However, the observation of kinetic isotope effects (same Table) on the triplet lifetimes rule this possibility out. This is because the isotope effects indicate that the actual hydrogen-atom transfer step, and not the conformational processes that lead up to it, is the rate-determining step in the reaction mechanism.

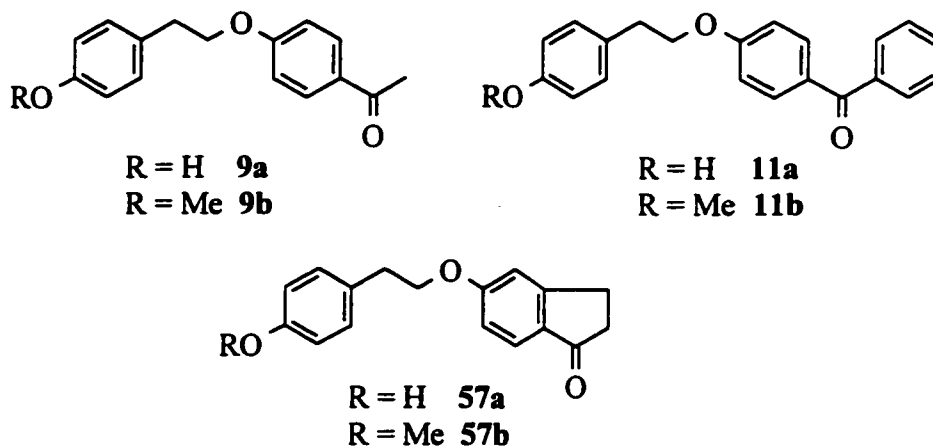
3.2. para, para'-Linked Phenolic Ketones and their Methoxy Analogues.

3.2.1. Introduction. Species of interest.

Compounds **9a**, **10a**, and **11a** represent three different LPKs that share the same para, para'-attachment geometry of the oxyethyl bridge and keto group. Figure 3.1 shows the compounds that will be discussed in this Chapter. Compounds **11b** and **57** are new, and benzophenone derivative **10a** will not be considered in detail in this thesis.

Our interest in these molecules was initially motivated by the question of whether the anomalously large reactivity of π , π^* triplets in the phenolic HAA reaction is reflected in intramolecular reactions as well. Compound **57a** has a 5-alkoxyindanone chromophore, and a lowest CT- π , π^* triplet configuration. Ketone **11a** is a

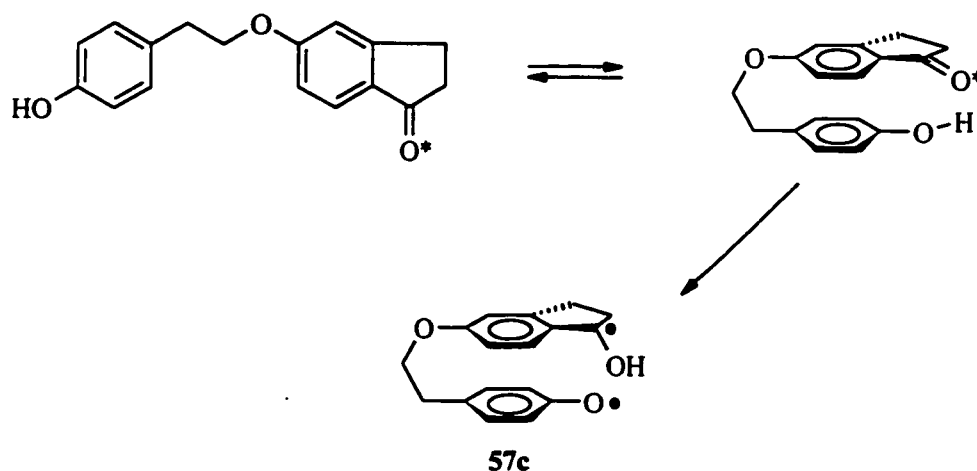
Figure 3.1. Several para, para'-oxyethyl linked acetophenones and their *O*-methyl ethers.



benzophenone derivative that has a lowest n, π^* triplet configuration.

The indanone was of interest since it has a carbonyl group that is constrained to lie flat in the molecular plane, unlike that of an acetophenone, which can twist significantly out of the plane of the aromatic ring. The effect of this is that the carbonyl n -orbitals, through which hydrogen-bonding occurs, are more freely accessible in LPK **9a** than in LPK **57a**. This leads to the expectation that if a hydrogen-bonding requirement is important in the phenolic HAA reaction, then the triplet lifetime of compound **57a** should be significantly longer than that of compound **9a**. Scheme 3.2 depicts the geometry required for intramolecular HAA in ketone **57a**.

Scheme 3.2. Configuration of intramolecular HAA in the alkoxyindanone LPK **57a**.

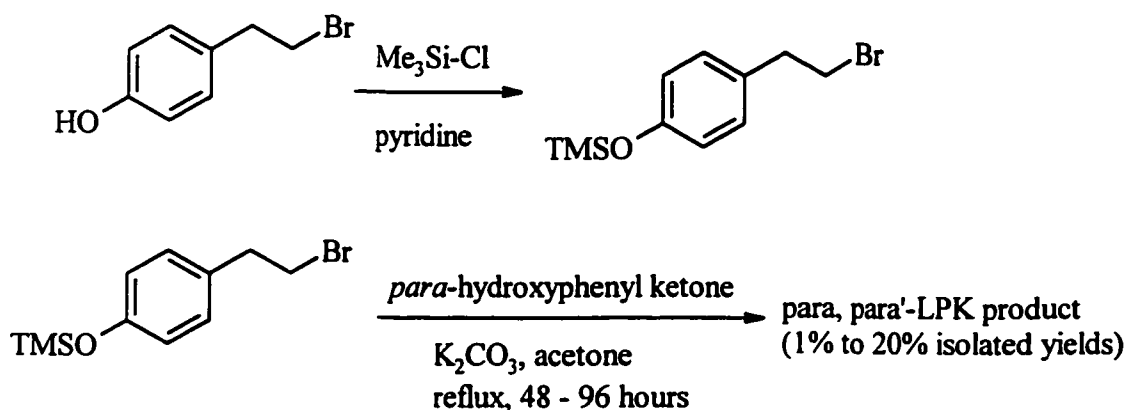


3.2.2. Results. Preparation of LPKs.

The molecules in Figure 3.1 were prepared by one or both of the following routes.

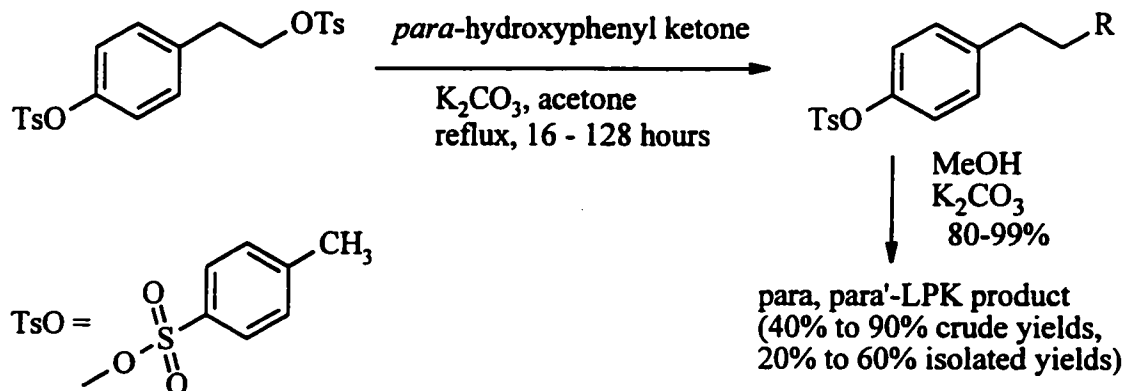
The first pathway (Scheme 3.3) begins with protection and subsequent nucleophilic substitution of *para*-trimethylsiloxyphenethyl bromide with the appropriate *para*-hydroxyphenylketone. Hydrolysis of the trimethylsilyl ether occurs coincidentally during the aqueous work-up of the second step. The methoxy compounds were prepared in analogous fashion from *para*-methoxyphenethyl bromide. Overall the yields were poor, due to competing E2 elimination to produce *para*-hydroxy- or *para*-methoxystyrene. It was found that the yields of the phenolic derivatives were highly dependent on the extent to which the pyridine from the initial silyl-protection step was removed.

Scheme 3.3. Preparation of LPKs *via* silyl-protected hydroxyphenethyl bromides.



This approach was later abandoned due to the very low yields encountered in the preparation of *meta*-substituted LPKs by this method (see Chapter Four).

Much higher yields were obtained using the ditosylate ester of *para*-hydroxyphenethyl alcohol as the substrate for the $\text{S}_{\text{N}}2$ substitution reaction (Scheme 3.4).

Scheme 3.4. Preparation of LPKs *via* a ditosylate intermediate.

For the methoxy compounds, *para*-methoxyphenethyl tosylate was used (not shown in the Scheme).

The structures of the new compounds were assigned based on their spectroscopic and analytical data. The experimental details are given in Chapter Five.

3.2.3. Results. Ultraviolet, infrared and phosphorescence spectra.

The ultraviolet (UV) absorption spectra of LPKs **9** and **11a** in acetonitrile (MeCN) are similar to those reported by Michael St. Pierre (MSP) in his thesis.⁸⁶ As found for these compounds, the UV spectra of the new compounds **11b** and **57** are typical of the alkoxybenzophenone and alkoxyindanone chromophores, respectively. The spectra are shown in Figure 3.2. UV spectra of compounds **9**, **11**, and **57** in dichloromethane (DCM) are also shown in Figure 3.2.

The static UV spectra show no new peaks that would indicate association between

Figure 3.2. Ultraviolet absorption spectra of compounds **11b**, **57a** and **57b** in acetonitrile (MeCN) and **9a**, **9b**, **11a**, **11b**, **57a** and **57b** in dichloromethane (DCM).

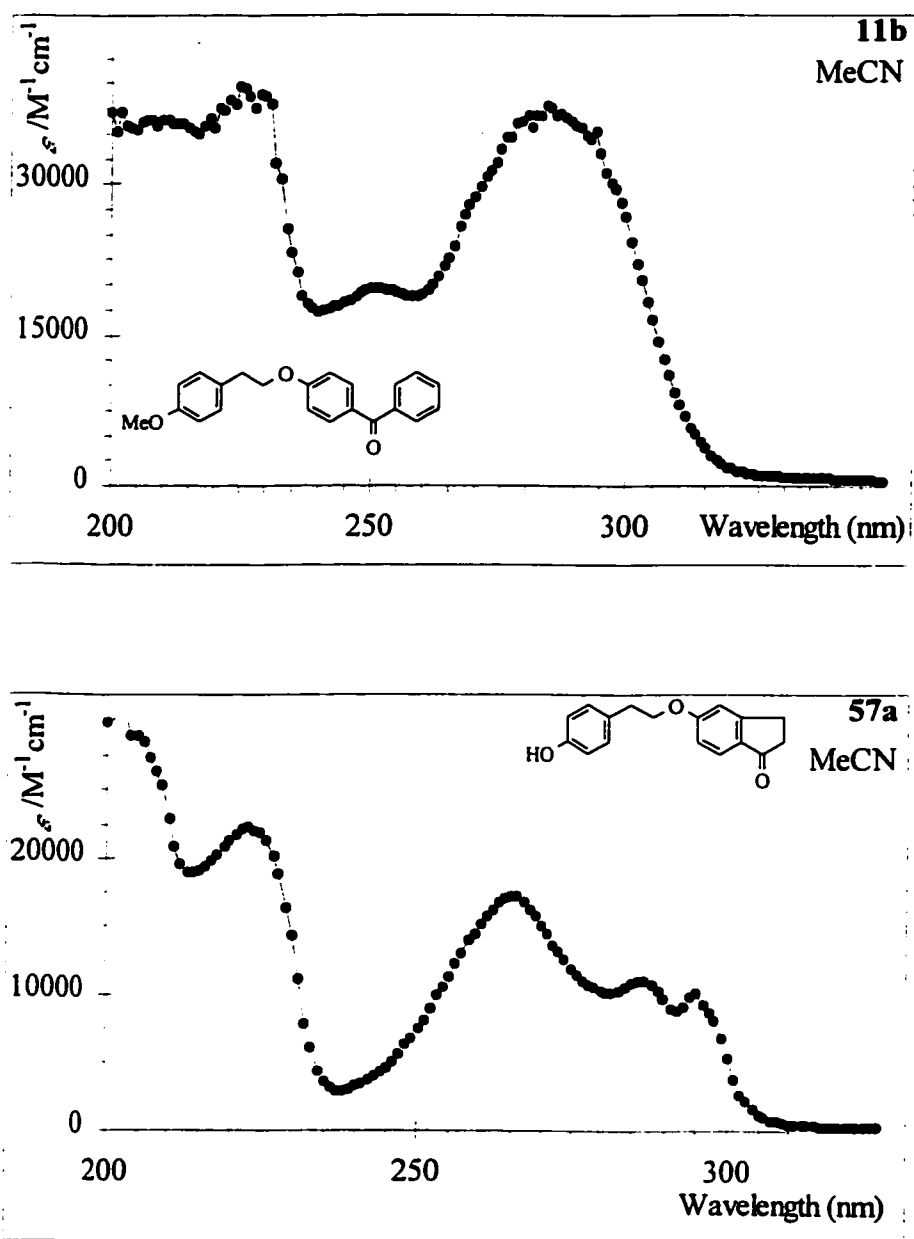


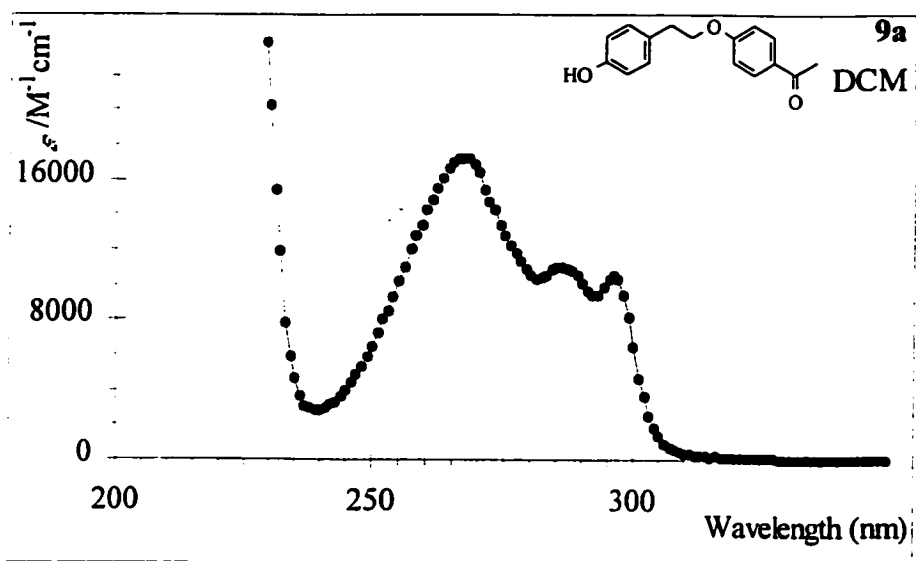
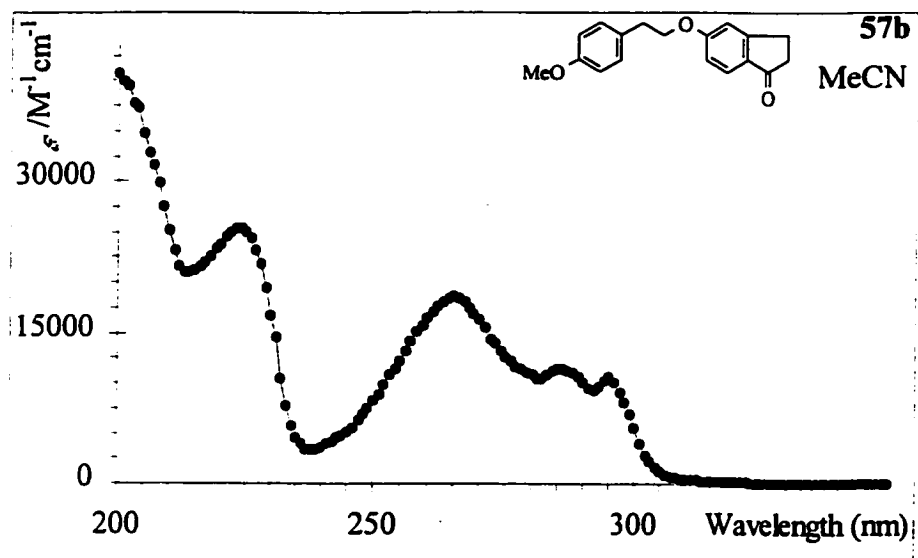
Figure 3.2. Continued.

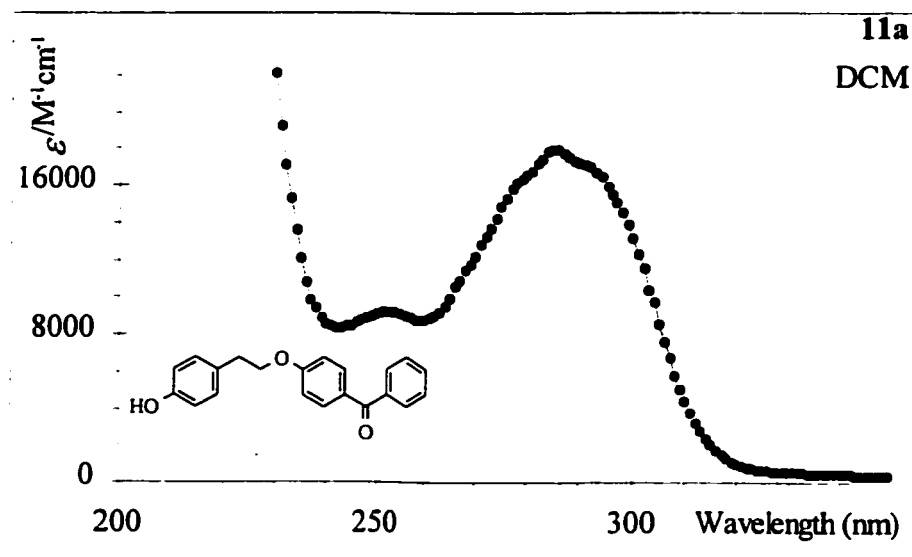
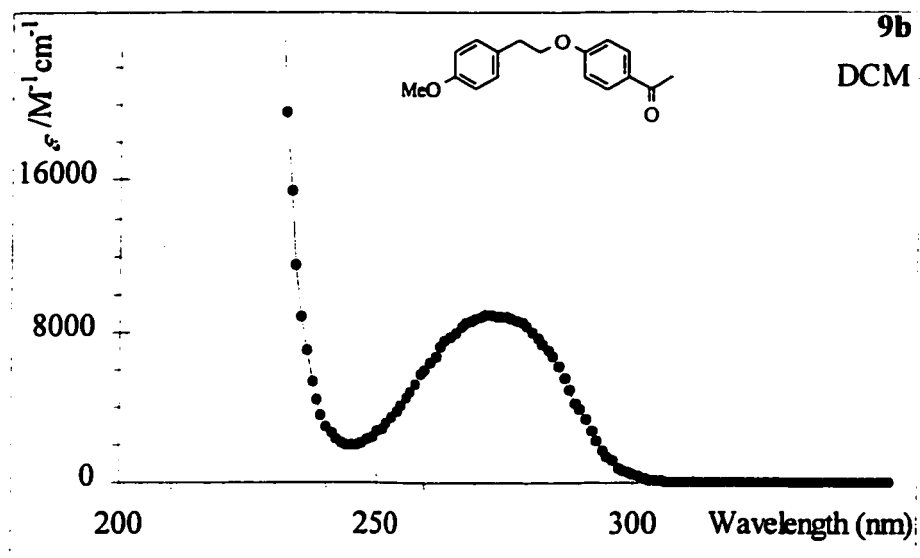
Figure 3.2. Continued.

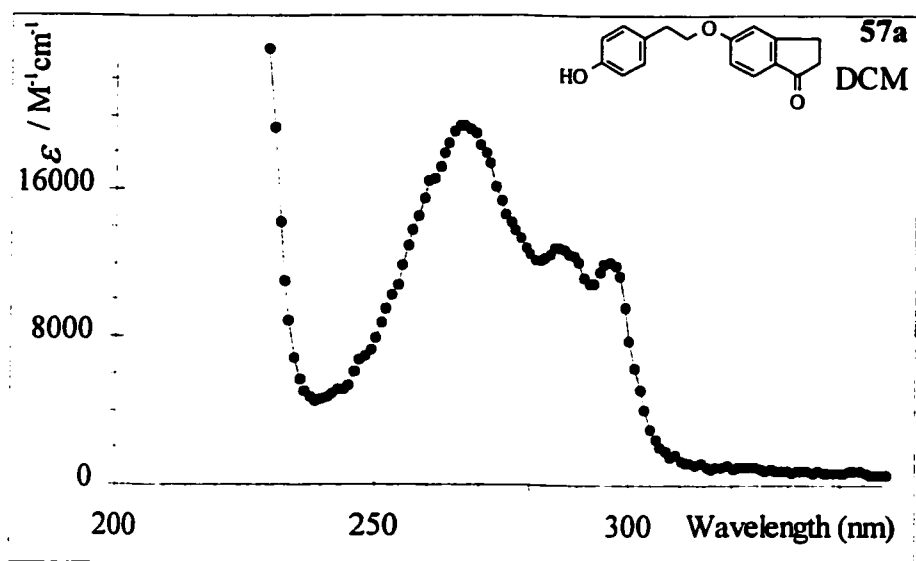
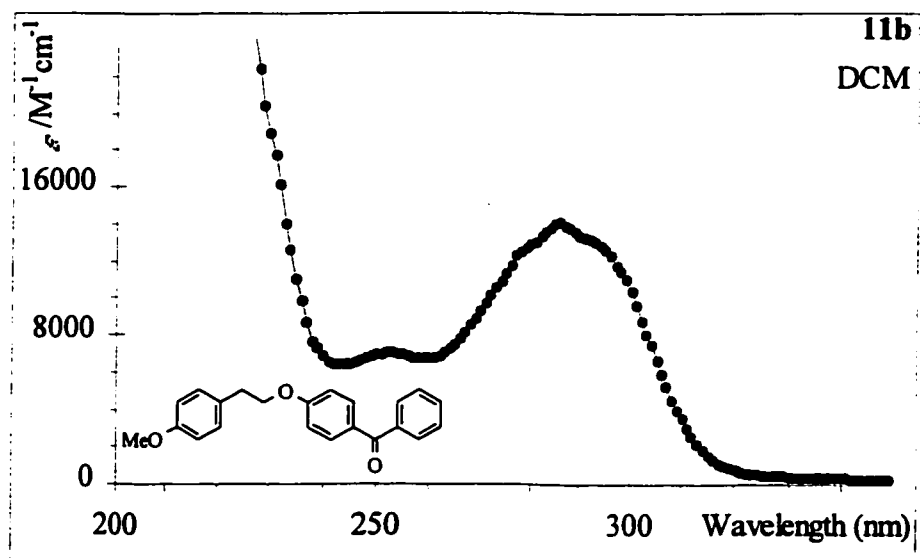
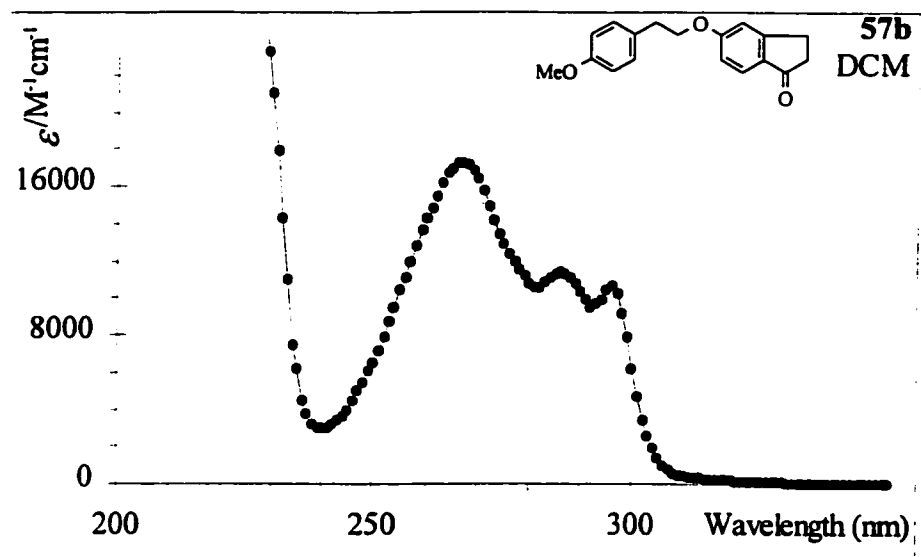
Figure 3.2. Continued.

Figure 3.2. Continued.

the carbonyl group and the remote phenolic moiety. In addition, the infrared spectra of LPKs **9a**, **11a**, and **57a** in carbon tetrachloride solution display absorptions in the region characteristic¹⁵⁸ of free phenols, 3300-3600 cm⁻¹. No evidence of hydrogen bonding is observed,¹¹⁷ except in concentrated samples (0.01 M or more) where intermolecular hydrogen-bonding is expected.

Phosphorescence emission spectra and phosphorescence lifetimes already recorded by MSP were not redetermined. The spectra for the new compounds **11b** and **57a** were recorded in 4:1 ethanol:methanol glasses at 77 K under identical conditions to those used by MSP (see Figure 3.3). The triplet energies were estimated from the onset of the 0-0 emission bands in the spectra; these and the lifetimes are listed in Table 3.1. The long phosphorescence lifetime of 360 ms for ketone **57a** and lack of fine structure is characteristic of a π, π^* configuration.¹⁵⁹ By contrast, compound **11b** has a shorter phosphorescence lifetime (8.5 ms) and an appearance which indicates that the alkoxybenzophenone species has a lowest n, π^* triplet, as expected.

The triplet lifetimes and energies for hydroxy and methoxy compounds of the same chromophore were very similar. From these results, it can be concluded that the presence of the phenolic moiety in these compounds does not effect the configuration of the lowest triplet state or the triplet lifetime in the solid matrix.

3.2.4. Results. Steady-state photochemistry.

MSP found,⁸⁶ in agreement with the original report by Scaiano *et al.*,⁷⁴ that the LPKs and their methoxy analogues are quite photochemically unreactive. His study of

Figure 3.3. Phosphorescence spectra of compounds (a) **11b**, (b) **57a**, and (c) **57b**, recorded in 4:1 ethanol/methanol mixtures at 77 K with 300-nm excitation and gated detection.

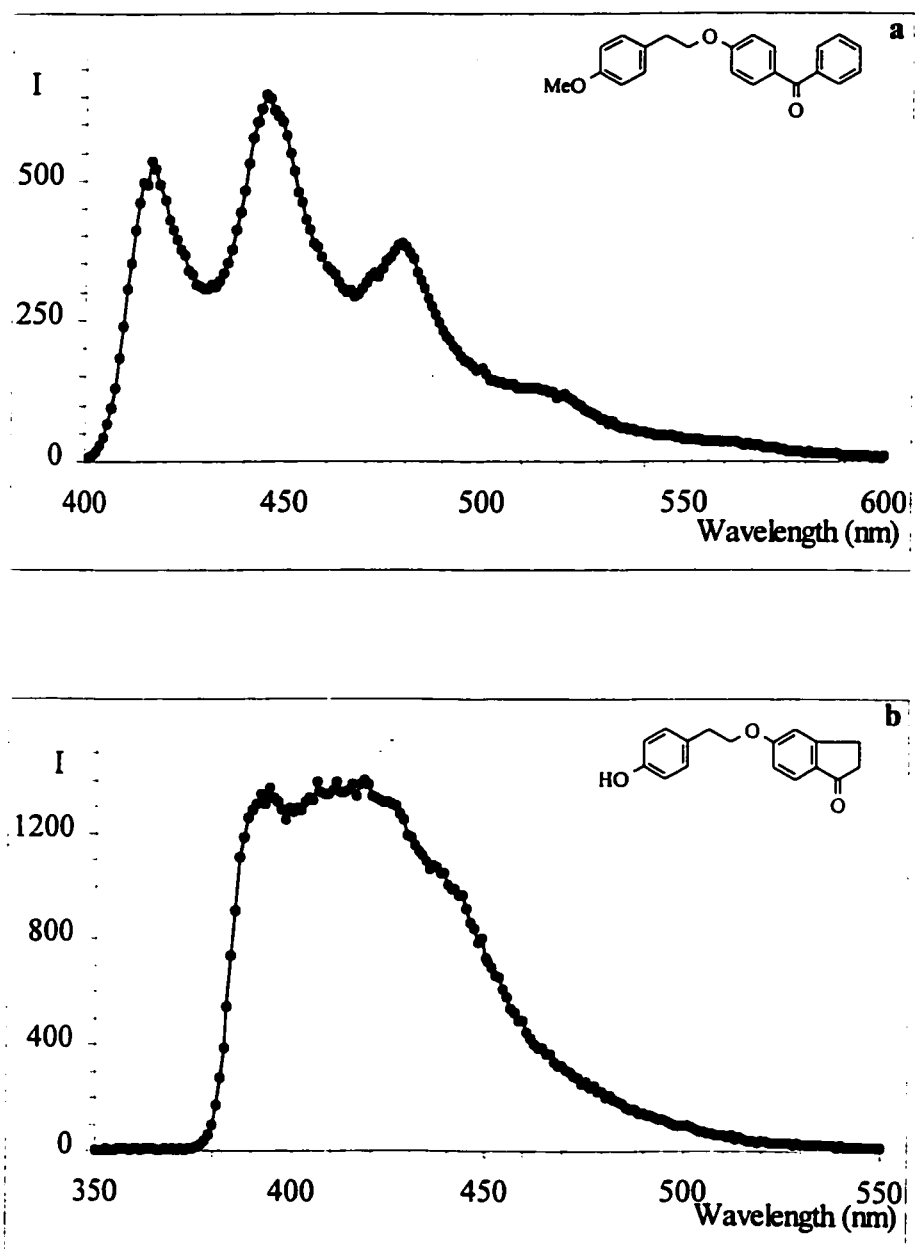


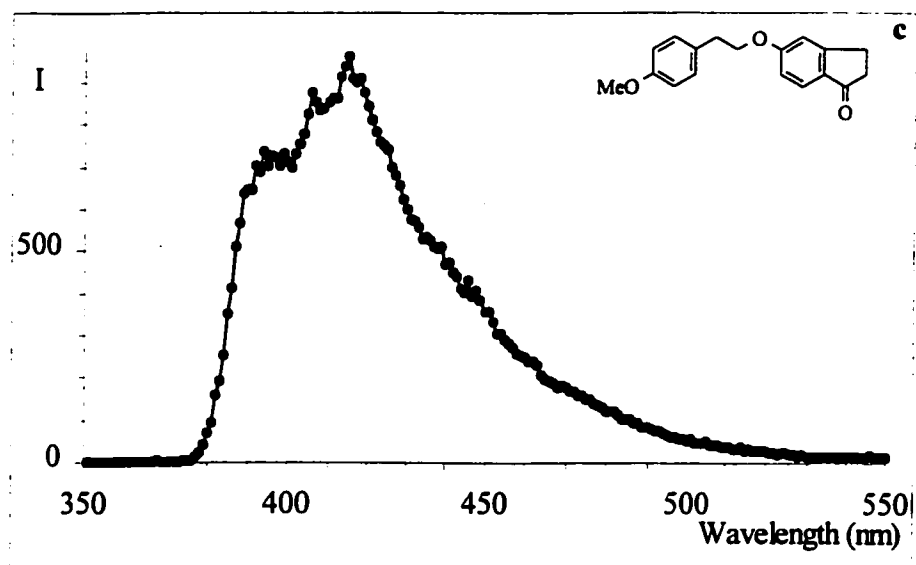
Figure 3.3. Continued.

Table 3.1. Phosphorescence data for compounds **9**, **11** and **57**.

Ketone	phosphorescence		assigned configuration of
	lifetime (ms)	E_T (kcal/mol)	lowest triplet
9a ^a	250 ± 10	70.3 ± 0.3	π, π^*
9b ^a	240 ± 10	70.1 ± 0.3	π, π^*
11a ^a	8.5 ± 0.6	68.6 ± 0.3	n, π^*
11b ^b	8.5 ± 0.6	68.6 ± 0.3	n, π^*
57a ^b	360 ± 20	72.5 ± 0.3	π, π^*
57b ^b	360 ± 20	72.5 ± 0.3	π, π^*

a. Ref. 86.

b. Measured at 77 K in 4:1 ethanol/methanol glass.

compounds **9-16** yielded quantum yields of disappearance less than 0.01 in all cases.

Compound **57** proved to be no different. Deoxygenated 0.0025 M MeCN solutions of compounds **9a** and **57** were simultaneously photolysed (300-nm) in a merry-go-round apparatus, with GC monitoring. Long irradiation times led to the formation of several products of higher molecular weight than the starting material, none of which were produced in large enough quantities to be characterized. Using ketone **9a** ($\Phi_{\text{disappearance}} = 0.006$)⁷⁴ as a secondary actinometer, the quantum yields for disappearance of compounds **57a** and **57b** were estimated to be in the range of 0.001-0.01.

3.2.5. Results. Transient spectroscopy of compounds **9**, **11**, and **57**.

Nanosecond laser flash photolysis (NLFP) experiments were performed as described in Chapter One, except that three different excitation wavelengths were used. Gas mixtures of N₂/He (337-nm, 4 mJ pulse energy, 6-ns pulse width), Xe/HCl/He (308-nm, 55 mJ, ~12-ns), or Kr/F₂/He (248-nm, 120-60 mJ, ~12-50-ns) allowed for a wide range of experiments to be conducted.

The solvents used were MeCN and DCM; MeCN was the main system. Isotope effects were determined from ratios of triplet lifetimes in 5% L₂O MeCN.

Similar to the bimolecular experiments described in Chapter Two, substrate concentrations were chosen so as to produce absorbances of 0.1 to 0.9 at the excitation wavelength. Deoxygenation was performed with either nitrogen or argon. In cases where triplet lifetimes were in the microsecond range (ethers **9b** and **11b**), neutral density filters were employed to reduce the laser intensity and avoid triplet-triplet annihilation,

which acts to shorten the transient lifetimes and reduce the quality of first-order fitting.

The first compounds studied were the methoxy ethers. From these compounds, it was hoped that model spectra and triplet lifetimes could be obtained to compare with the phenolic compounds that were expected to undergo the intramolecular HAA reaction.

NLFP of ethers **9b**, **11b** and **57b** was conducted using the 248- or 308-nm laser for excitation and low ketone concentrations (10^{-3} M or less). Compounds **9b** and **57b** gave strong transient absorptions in MeCN (Figure 3.4) in the 320- to 420-nm range that were very similar to those obtained with the simple model methoxy ketones (**42** and **50**, respectively).

The transients decayed cleanly to the pre-pulse level with pseudo first-order kinetics. They were assigned as triplet states based on quenching by 1,3-cyclohexadiene (Table 3.2) and oxygen ($k_q \sim 3 \times 10^9 \text{ M}^{-1} \text{ s}^{-1}$), and comparisons to the spectra of the model compounds. Representative transient decays in MeCN determined at the triplet maxima are shown immediately after the spectra in Figure 3.4.

NLFP of the methoxybenzophenone derivative **11b** gave transient absorptions in the 300- to 700-nm range, with maxima at 330- and 525-nm. These were identified as the triplet in a manner similar to that described above, and the spectrum and decay are shown in Figure 3.4. In DCM, similar spectra and transients were obtained (Figure 3.5). As predicted, the NLFP behaviour of the phenolic species was different from their model compounds. Instead of mono-exponential decays, the transient decays in MeCN (Figure 3.4) for LPKs **9a** and **11a** show two distinct components: a short-lived species and a longer lived one. On the other hand, the decay of LPK **57a** seems to consist of only one

Figure 3.4. Transient ultraviolet spectra and decays of $< 10^{-3}$ M ketone solutions of compounds **9a**, **9b**, **11a**, **11b**, **57a**, and **57b** in deoxygenated MeCN at room temperature.

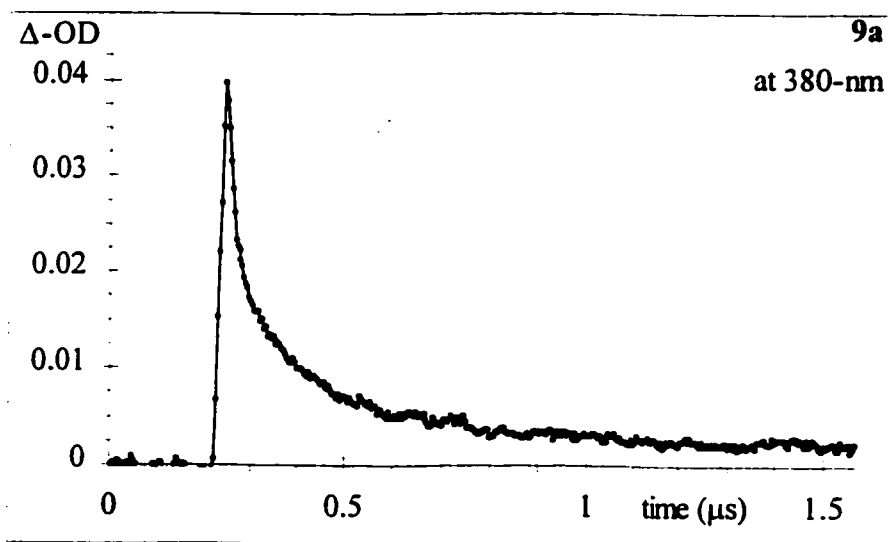
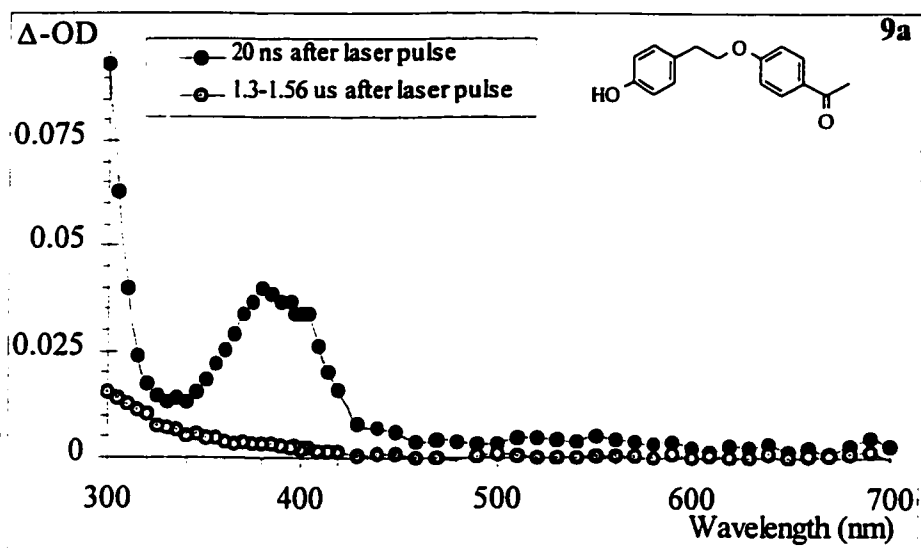


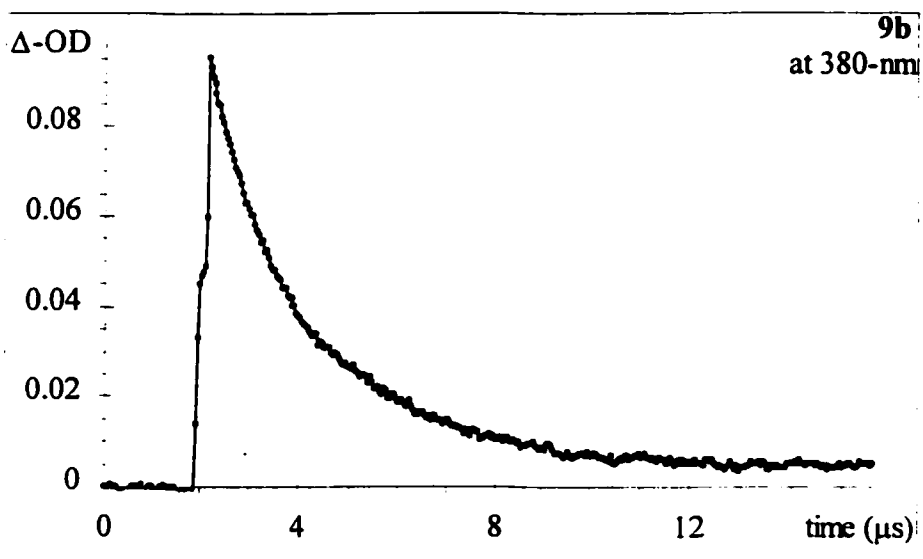
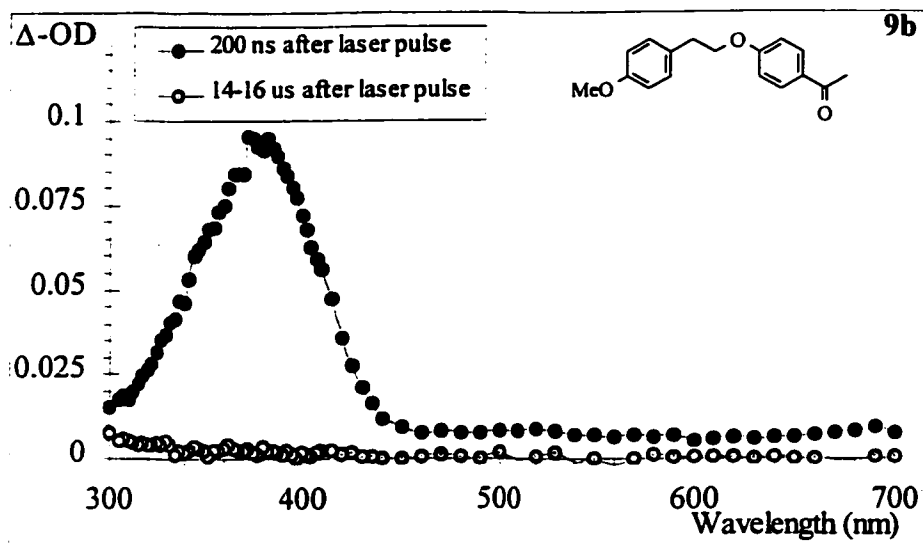
Figure 3.4. Continued.

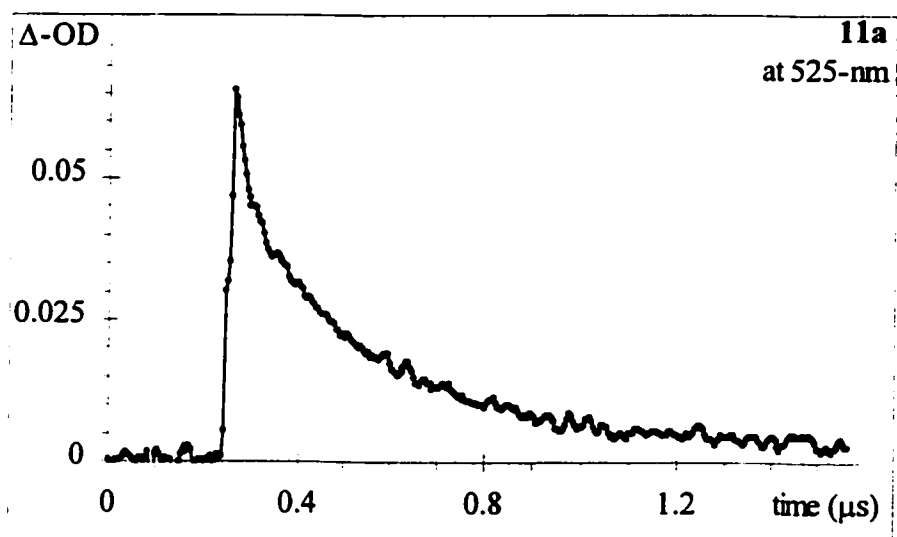
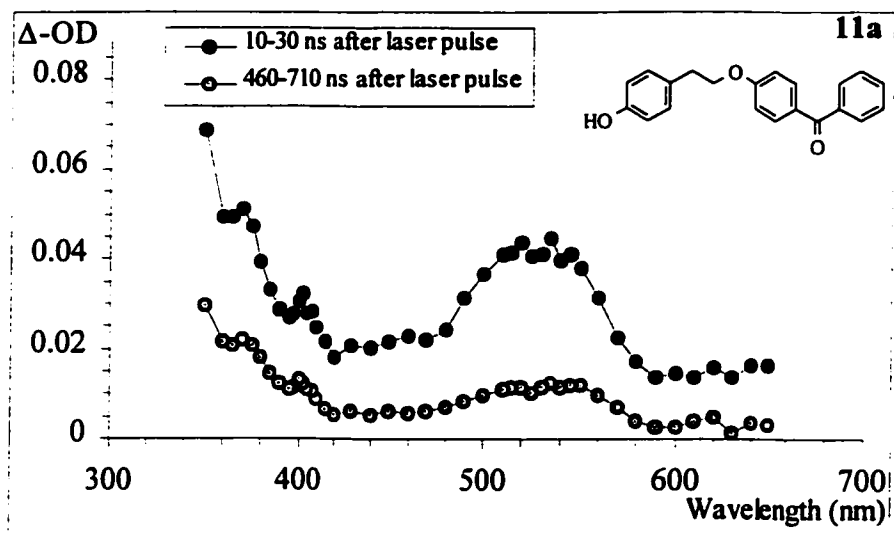
Figure 3.4. Continued.

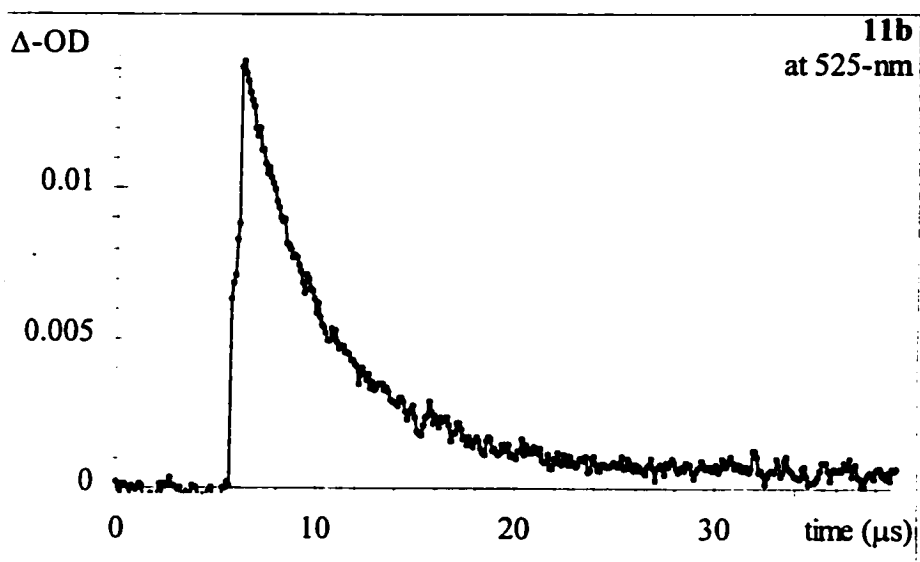
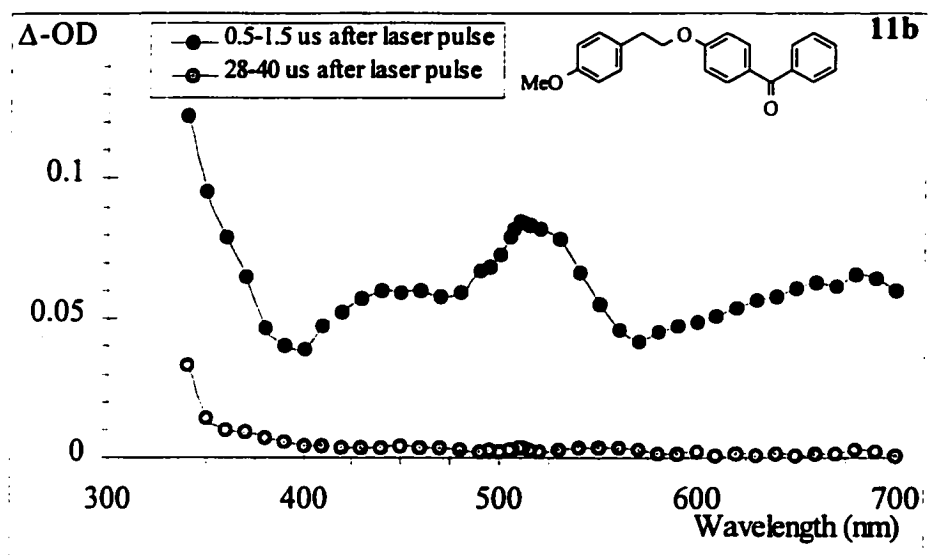
Figure 3.4. Continued.

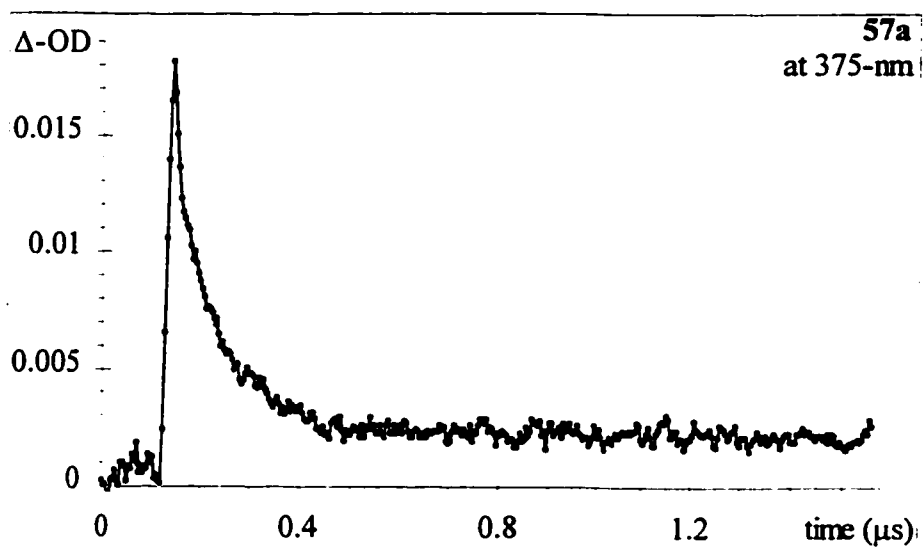
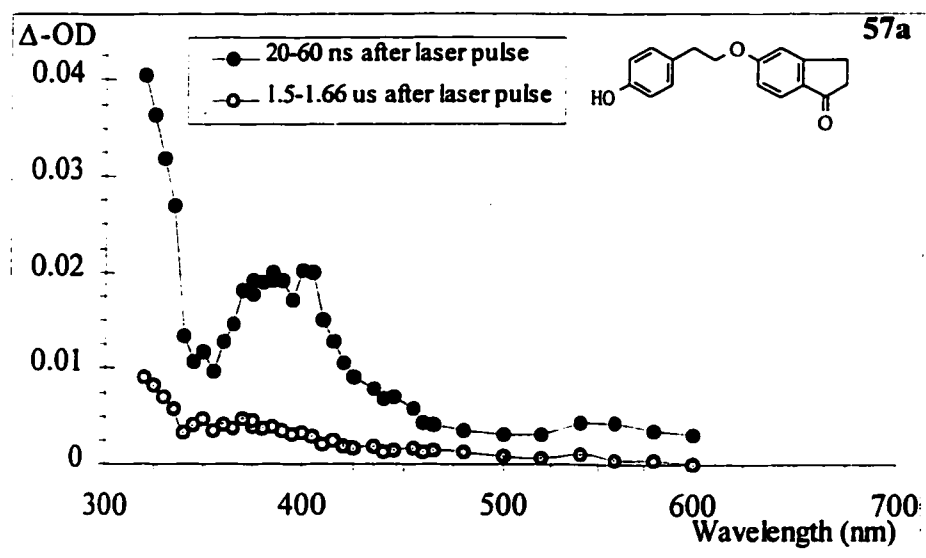
Figure 3.4. Continued.

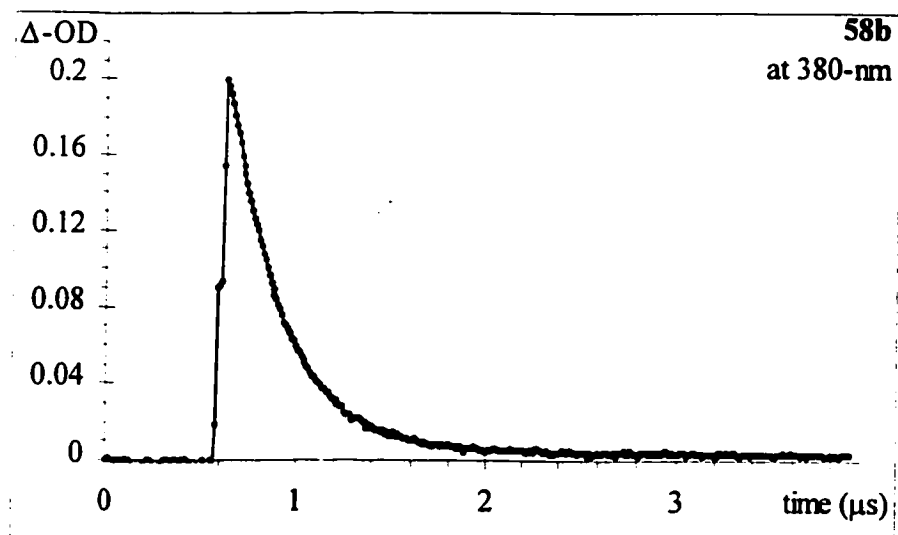
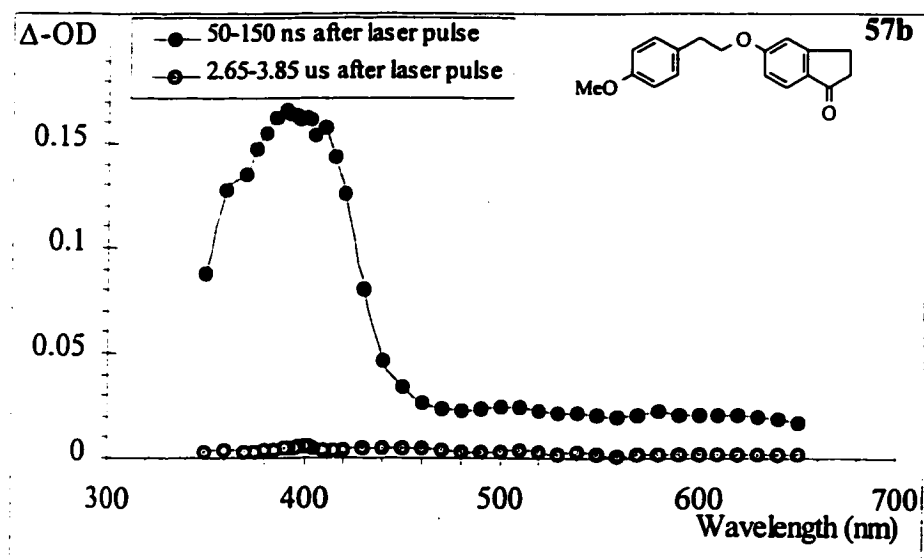
Figure 3.4. Continued.

Table 3.2. Triplet lifetimes of compounds **9b**, **11b**, and **57b** in MeCN and DCM, and triplet quenching rates by 1,3-cyclohexadiene (CHD) in MeCN. ^{a,b}

Ketone	τ_T (MeCN, μ s)	τ_T (DCM, μ s)	k_q CHD / $10^9 \text{ M}^{-1} \text{ s}^{-1}$ ^c
9b	2.4 ± 0.2 ^d , 3.3 ± 0.2 ^e	3.28 ± 0.06	6.7 ± 0.3 ^d
11b	4.85 ± 0.15	6.06 ± 0.13	7.2 ± 0.2
57b	0.283 ± 0.002	0.425 ± 0.008	7.8 ± 0.3

a. From 248-nm NLFP.

b. Errors in lifetimes are twice the standard deviation of the linear least squares line from the logarithmic fit.

c. From 308-nm NLFP; errors are twice the standard deviation of the least squares line from the quenching plot.

d. Ref. 86.

e. Rigorously dried MeCN ($[\text{H}_2\text{O}] < 10^{-4} \text{ M}$).

Figure 3.5. Transient ultraviolet spectra and decays of 10^{-4} M ketone solutions of compounds **9a**, **9b**, **11a**, and **11b** in deoxygenated DCM at room temperature.

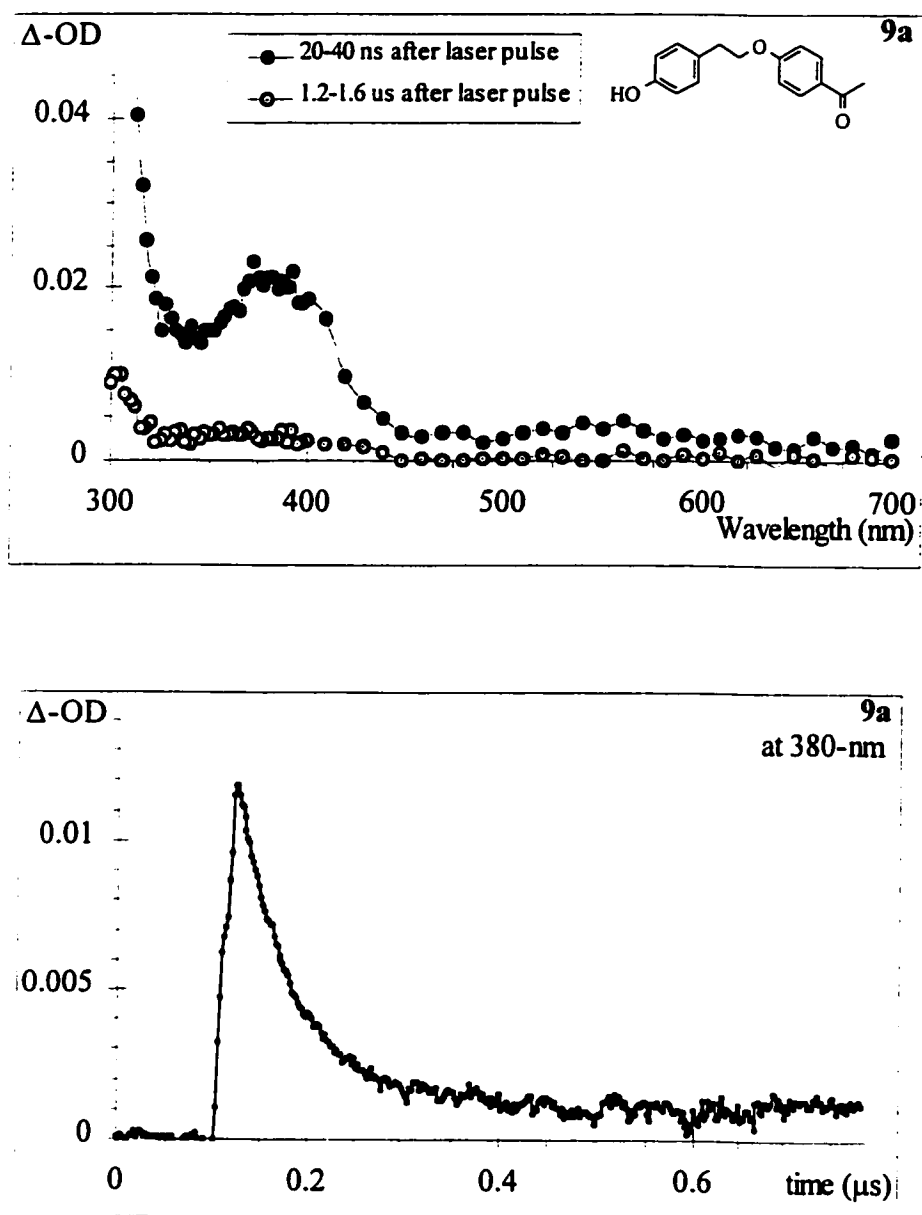


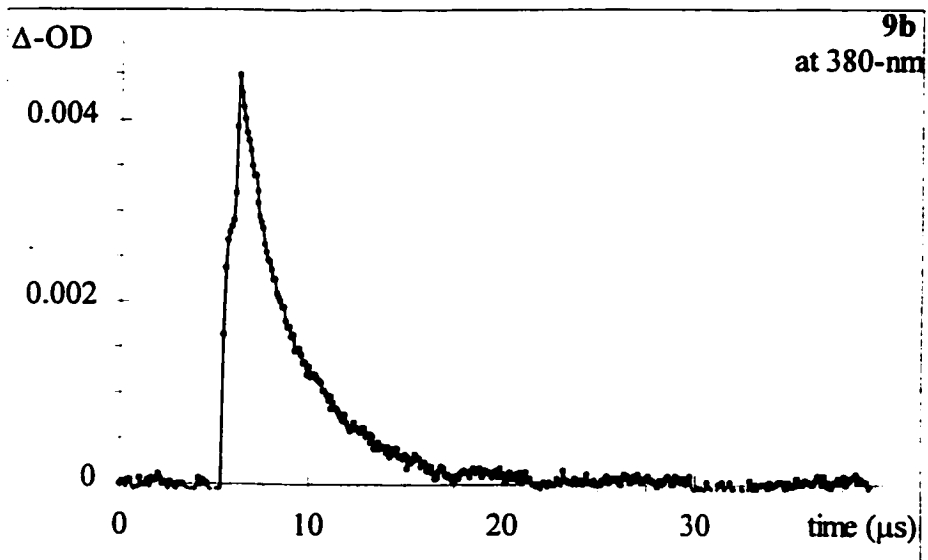
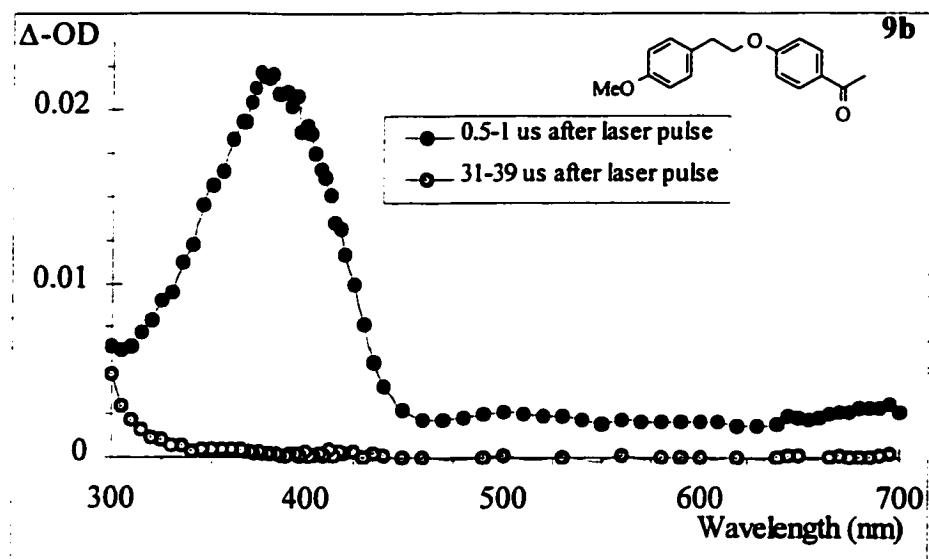
Figure 3.5. Continued.

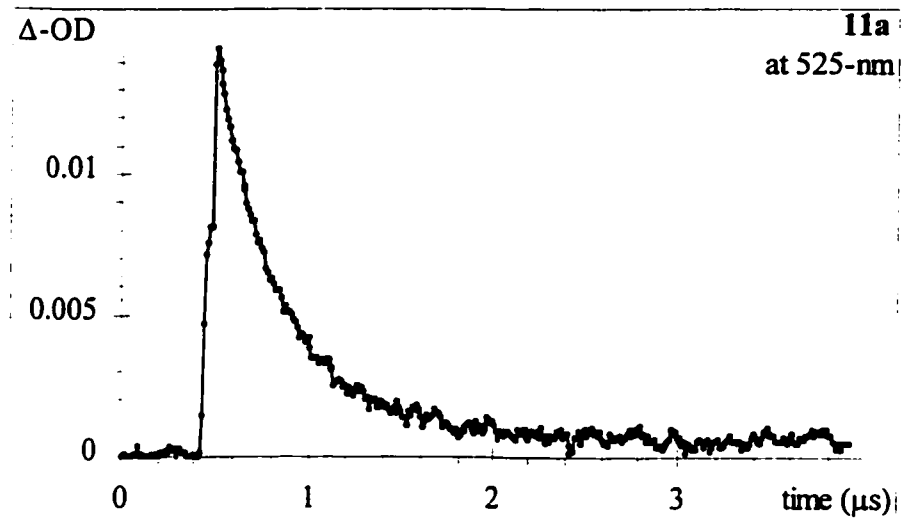
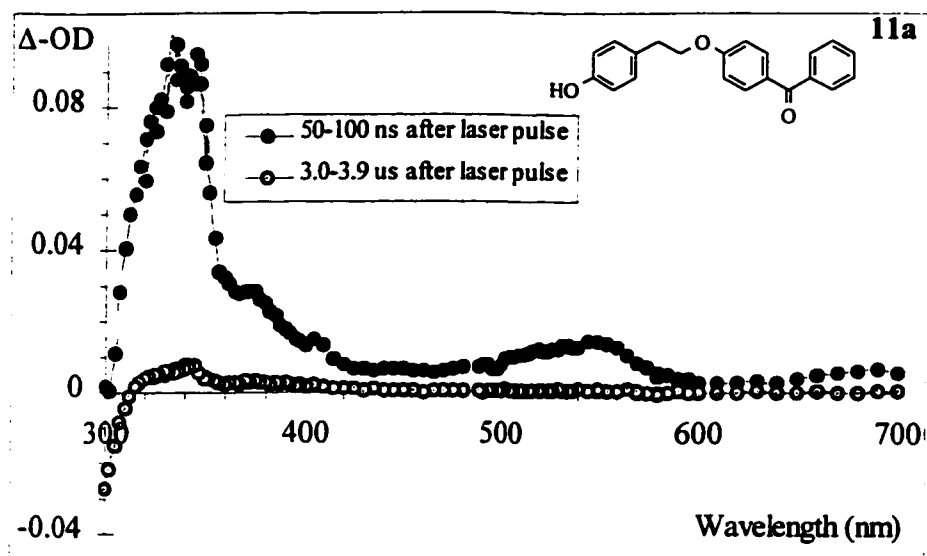
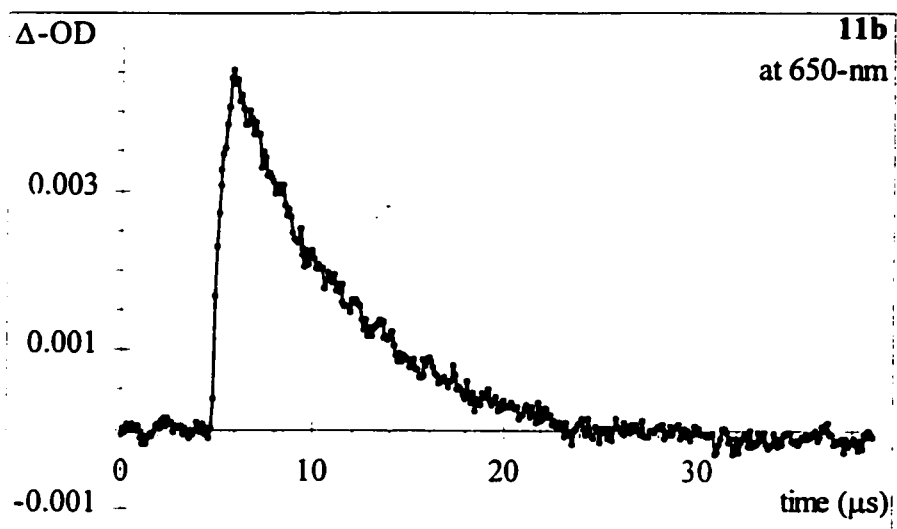
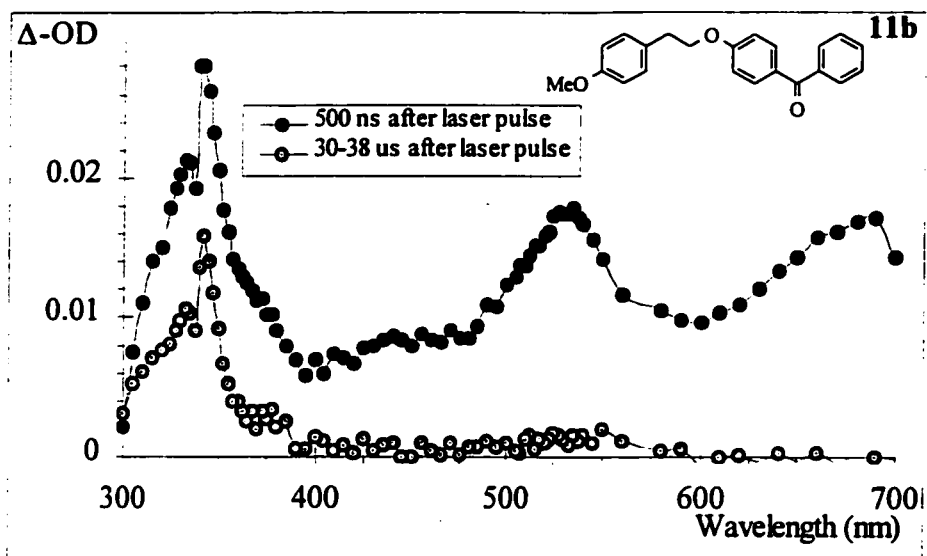
Figure 3.5. Continued.

Figure 3.5. Continued.

component. The transient absorption spectra of all three differ from the methoxy analogues, and spikes at 407-nm can be seen.

In MeCN, the quenching behaviour with diene and oxygen was used to support the assignment^{74,86} of the shorter-lived species of LPKs **9a** and **11a** as the triplet state.

Unlike the methoxy compounds, however, accurate rates of triplet quenching of these compounds were not obtained due to their very short triplet lifetimes, but it was possible to observe quenching and estimate rates on the order of $10^9 \text{ M}^{-1} \text{ s}^{-1}$. The longer-lived species was not quenched by triplet quenchers, and instead had its *top* ΔOD reduced upon their addition. This indicates that the transient is a product from a triplet state precursor, most likely a radical absorption, and the original assignment⁷⁴ as the 1,13-biradical seems valid.

The transient decay behaviour was much different in DCM. The transient decays of LPKs **9a** and **11a** changed to ones fitting mono-exponential decay kinetics. Comparing the decays in Figures 3.4 and 3.5, it appears that the short-lived component disappears in DCM. The spectra, however, recorded shortly after the laser pulse, appear similar to those recorded in MeCN. Triplet quenching indicated that in neither case was the transient the triplet.

The behaviour of ketone **57a** was different from the others. The transient exhibited a mono-exponential decay whose lifetime was not reduced by diene. The fact that its ΔOD value was suppressed by further additions of diene is consistent with a triplet-derived species, as explained above.

3.2.6. Results. Transient lifetimes of compounds 9, 11, and 57.

Triplet lifetimes of ethers **9b**, **11b** and **57b** were determined directly from their transient decays. The data are tabulated in Table 3.2. Triplet lifetimes for these compounds were dependent on laser intensity and degassing time, and the numbers listed represent the longest triplet lifetimes measured during several experiments under various conditions.

For the LPKs, the triplet lifetimes of all three compounds were so short as to make their direct measurement unreliable. This is because the values approach the order of the laser pulse width, the factor that governs the time resolution of our instrument.

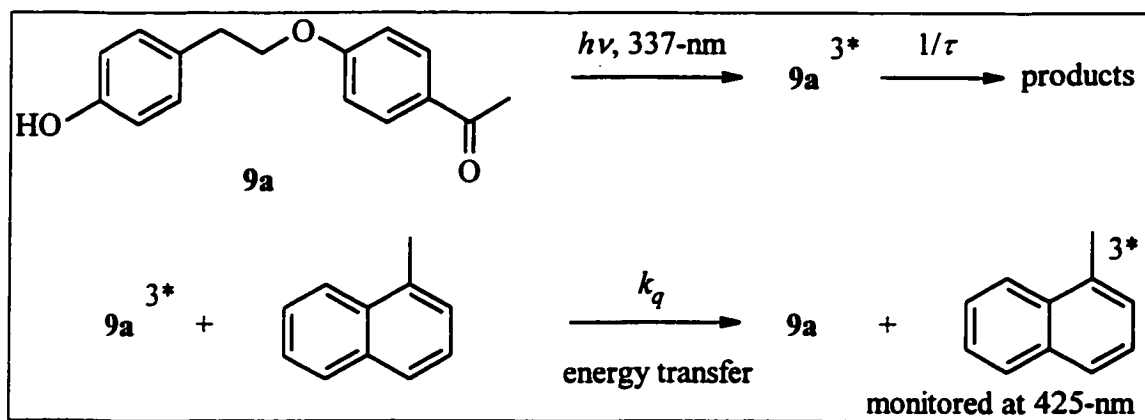
The triplet lifetimes of LPKs **9a**, **11a**, and **57a** were instead measured using what are known as probe methods. Figure 3.6 displays two common techniques, (a) the 1-methylnaphthalene (MN) probe method^{160,161} and (b) a method involving 1,3-cyclohexadiene.

These methods rely on triplet-triplet energy transfer from ketone to probe, followed by subsequent monitoring of the probe's effects on the system. For (a), irradiation of ketone/MN mixtures at a wavelength where only the ketone absorbs results in the rapid formation of the MN triplet state after triplet energy transfer to the arene occurs. The MN triplet is strongly absorbing and easily monitored, assuming there is minimal spectral overlap from the ketone.

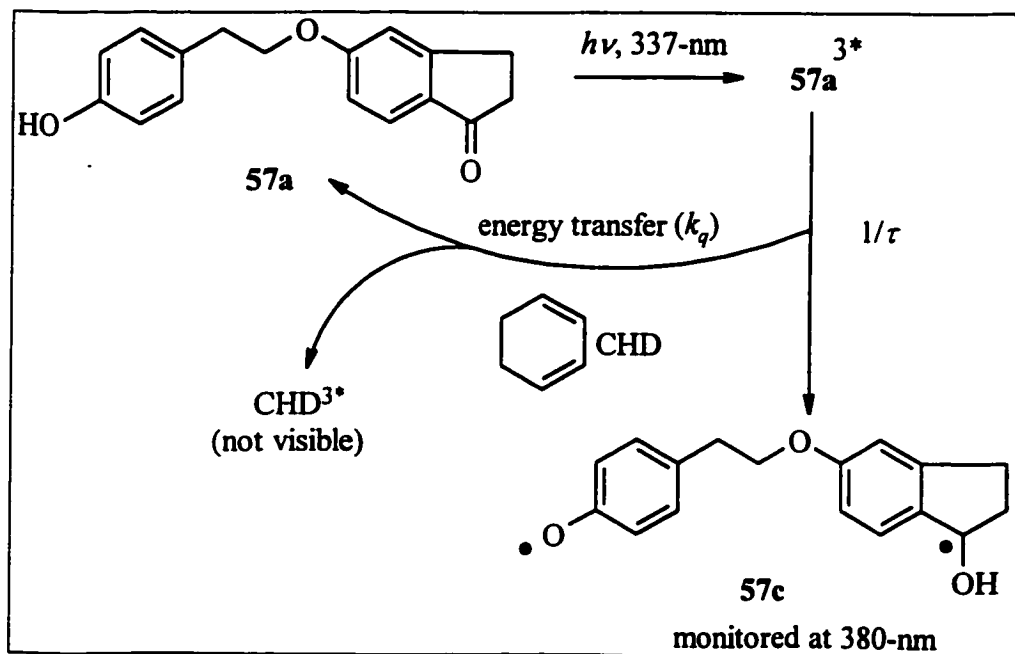
As more MN is added, the *top ΔOD* at 425-nm can be plotted *versus* concentration of arene, $[MN]$, and fit to equation 3.1, from which $k_q\tau$ values can be extracted.

Figure 3.6. Probe methods for determining triplet lifetimes.

a. The 1-methylnaphthalene probe method, illustrated for compound **9a**.



b. 1,3-cyclohexadiene as a normal Stern-Volmer probe, illustrated for compound **57a**.



$$\begin{aligned}
 (top\ \Delta - OD) &= \frac{(\phi_{isc} \varepsilon_{425} l / I_a) (k_q \tau) [MN]}{1 + (k_q \tau) [MN]} \\
 (top\ \Delta - OD) &= (constant) \frac{(k_q \tau) [MN]}{1 + (k_q \tau) [MN]}
 \end{aligned}
 \tag{3.1}$$

The k_q value is the rate of triplet energy transfer from ketone to arene, and τ is the triplet lifetime of the ketone. The k_q values used ($8.3 \times 10^9\ \text{M}^{-1}\text{s}^{-1}$) were taken from the literature.⁷⁴ The parameter $(\phi_{isc} \varepsilon_{425} l / I_a)$ is only constant under conditions of constant light intensity (I_a), since the optical path length, l , the extinction coefficient of the 1-methylnaphthalene triplet, ε_{425} , and the quantum yield of intersystem crossing of the ketone triplet, ϕ_{isc} , are all constant in the experiment.

For LPKs **9a** and **11a**, determination of the *top* Δ -OD as a function of $[MN]$ was straightforward, and fits of the data according to Equation 3.1 allowed $k_q \tau$ to be extracted. Figure 3.7 shows the plots for ketones **9a** and **11a** in both solvents. The $k_q \tau$ values, k_q values, and the derived triplet lifetimes are listed in Tables 3.3 and 3.4. For benzophenone derivative **11a** a directly-detected transient at 650-nm in MeCN had a lifetime of 18.9-ns, in good agreement with the probe result.

Study of the indanone derivative *via* this method gave poor results since its transient absorption extended farther into the red, and the resulting large residual absorption at 425-nm totally obscured the MN triplet at the beginning of the experiment.

Instead, the triplet lifetime of LPK **57a** was determined by a different probe

Figure 3.7. Fits of the 1-methylnaphthalene probe data to eq. 3.1 at 23 to 25 °C for LPKS **9a** (circles) and **11a** (squares). The filled points indicate MeCN, the open points DCM.

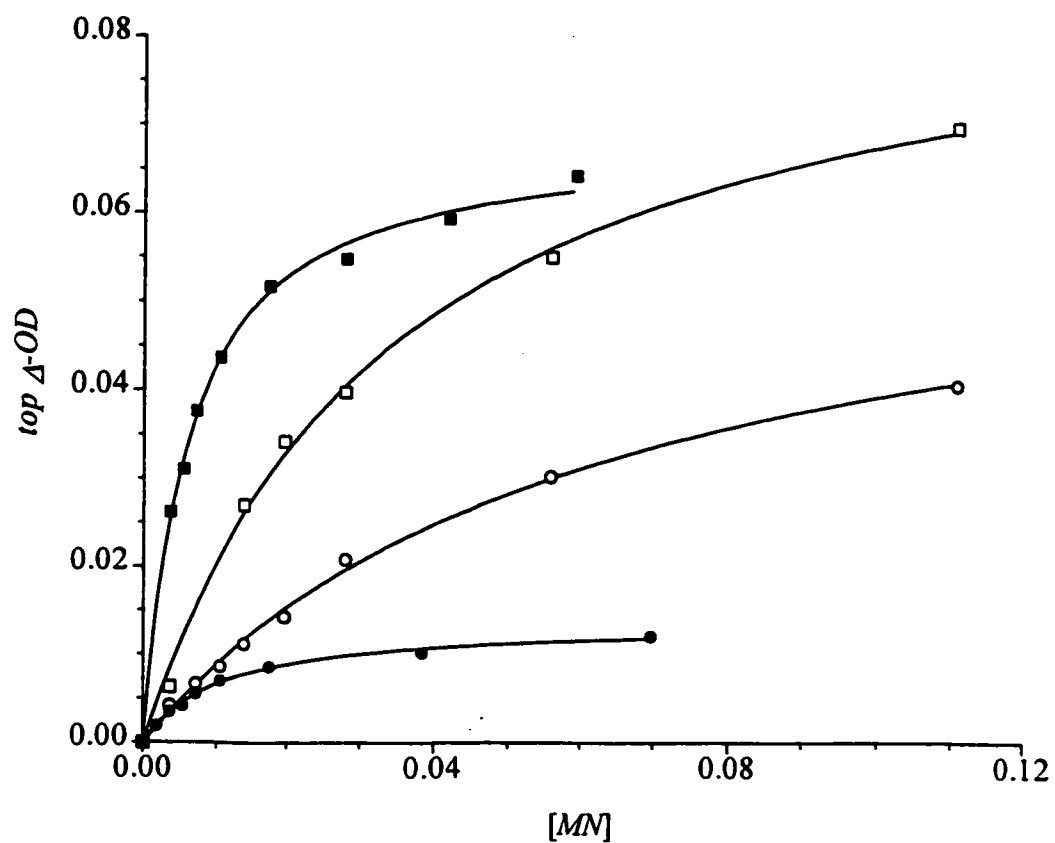


Table 3.3. Values of $k_q \tau_T$, triplet quenching rate constants of model compounds by 1-methylnaphthalene (MN) and derived triplet lifetimes of compounds **9a**, and **11a** in acetonitrile (MeCN). ^a

Ketone	model compound;		τ_T (MeCN, ns)
	$k_q \tau_T$ (MeCN) / M^{-1}	k_q MN / $10^9 M^{-1} s^{-1}$	
9a	133 ^b , 121 \pm 12 ^c , 94 \pm 13 ^d	42 ; 8.3 \pm 0.8 ^b	16 ^b , 13.3 ^b , 15 \pm 2 ^c , 11.3 \pm 1.9 ^d
11a	166 \pm 19 ^c	26 ; 8.3 \pm 0.8 ^b	20 \pm 3 ^c , 18.9 \pm 1.2 ^e

a. From 337-nm excitation, using MN as a probe.

b. Ref. 74.

c. Ref. 86.

d. Rigorously dried MeCN ($[H_2O] < 10^{-4} M$).

e. Direct detection by 248-nm excitation, monitoring at 650-nm.

Table 3.4. Values of $k_q\tau_T$, triplet quenching rate constants of model compounds by 1-methylnaphthalene (MN), and derived triplet lifetimes of compounds **9a** and **11a** in dichloromethane (DCM). ^a

Ketone	model compound;		
	$k_q\tau_T$ (DCM, M ⁻¹)	k_q MN / 10 ⁹ M ⁻¹ s ⁻¹	τ_T (DCM), ns
9a	16 ± 2	42 ; 7.4 ± 0.4	2.2 ± 0.3
11a	26 ± 3 ^b , 32.7 ± 1.4 ^c	26 ; 7.5 ± 0.4 26 ; 5.82 ± 0.17 ^d	3.5 ± 0.4 ^b , 5.6 ± 0.3 ^c

a. From 337-nm excitation, using MN as a probe.

b. The average of two runs, 22.4 ± 1.5 and 29 ± 4 M⁻¹.

c. From 1,3-cyclohexadiene (CHD) Stern-Volmer quenching (see text).

d. Quenching rate constant of triplet **26** by CHD in DCM.

technique, which was chosen on the assumption that it does not produce a transient itself.

Addition of 1,3-cyclohexadiene (CHD) to compound **57a** under dilute conditions (308-nm laser) led to a reduction in the initial *top Δ-OD* in proportion to the concentration of added CHD, verifying that the transient was indeed a species derived from the triplet state of compound **57a**.

A plot of $(top\ \Delta-OD)_0 / (top\ \Delta-OD)_{[CHD]}$ versus $[CHD]$ according to Equation 3.2, where $(top\ \Delta-OD)_0$ is the initial transient absorbance in the absence of diene and $(top\ \Delta-OD)_{[CHD]}$ is the transient absorbance in the presence of diene at concentration $[CHD]$, was linear, as shown in Figure 3.8. The results for compound **57a** are listed in Table 3.5.

$$(top\ \Delta-OD)_0 / (top\ \Delta-OD)_{[CHD]} = 1 + k_q \tau_T [CHD] \quad (3.2)$$

In order to check the consistency of the results of the two probe techniques, CHD Stern-Volmer quenching was also conducted for LPK **11a** in DCM. A slightly longer triplet lifetime for this LPK was determined by the CHD method (plot is Figure A.1 in the Appendix). This discrepancy may not be significant, due to the propagation of error in comparing the two results, each of which are derived from two slopes of quenching plots.

3.2.7. Results. Biradical lifetimes of compounds **9a**, **11a**, and **57a**.

Due to the short triplet lifetimes of LPKs **9a**, **11a**, and **57a**, transient decays

Figure 3.8. Stern-Volmer plot of the reduction of the initial yield of the transient (*top* Δ -OD) from 308-nm NLFP of compound **57a** in deoxygenated MeCN by 1,3-cyclohexadiene, monitored at 400-nm.

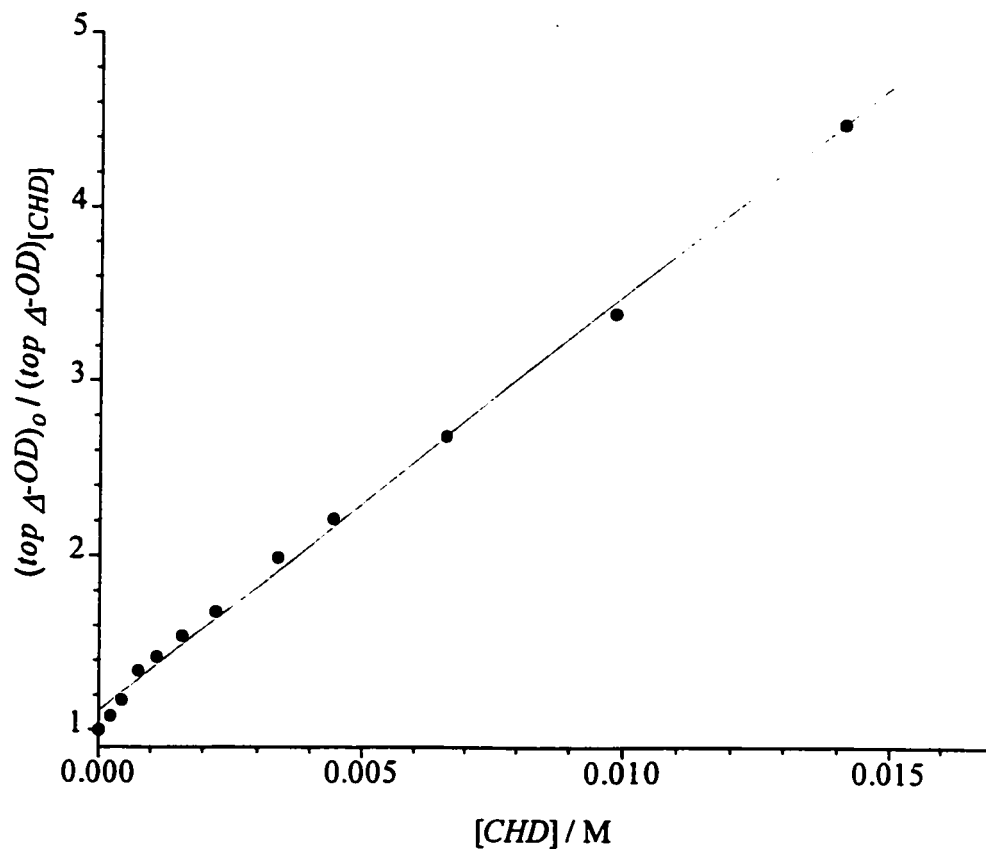


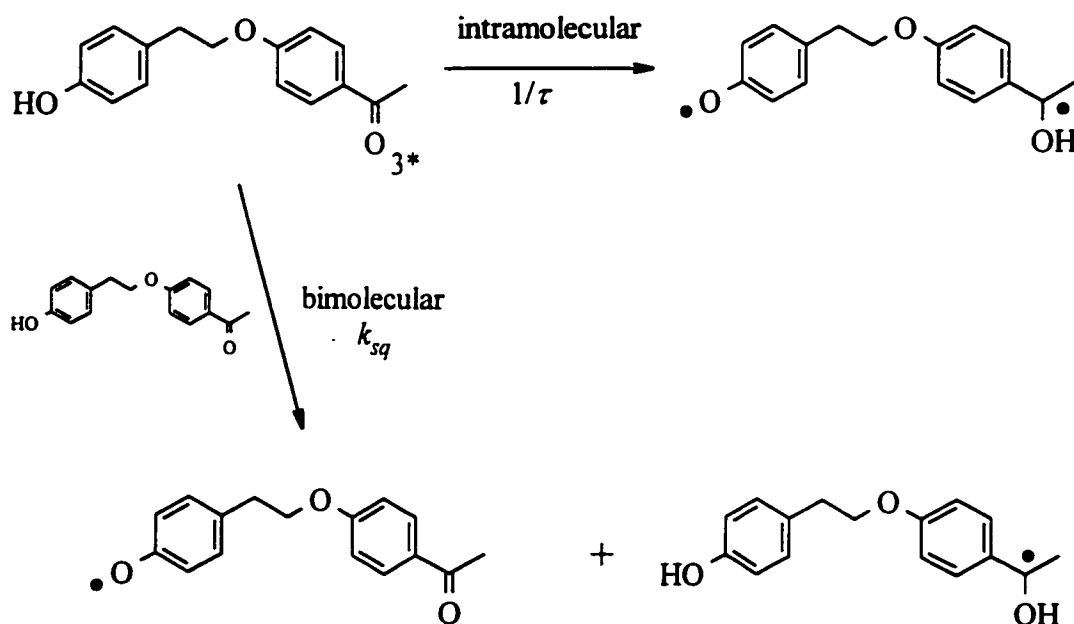
Table 3.5. Value of $k_q \tau_T$, the triplet quenching rate constant of compound **50** by 1,3-cyclohexadiene, and the derived triplet lifetime of LPK **57a** in MeCN at 23 to 25 °C. ^a

Ketone	model compound 50		
	$k_q \tau_T (\text{M}^{-1})$	$k_q \text{ MN} / 10^9 \text{ M}^{-1} \text{ s}^{-1}$	τ_T (nanoseconds)
57a	238 ± 9	11.0 ± 0.3	21.6 ± 1.0

a. From 308-nm excitation.

observed for these species consisted of residual absorptions presumably corresponding to radical products of the inter- and intramolecular hydrogen-atom abstraction reaction. An example of the latter, in the case of ketone **57a**, is 1,13-biradical **57c** in Scheme 3.2. Similar biradicals were observed in the other two cases, and each exhibited lifetimes less than 250-ns. Also observed in the transient decays were longer-lived residual absorptions whose relative intensities increased with an increasing concentration of ketone. These are assigned to mono-radical products of the "self-quenching" reaction (Scheme 3.5) where the triplet LPK undergoes bimolecular reaction with another LPK rather than react with its own phenolic hydrogen. The mono-radicals absorb in the same part of the spectrum as the biradicals (which in turn absorb in a very similar area as the triplet ketone).

Scheme 3.5. The "self-quenching" reaction of triplet LPKs.



The short triplet lifetimes of the three LPKs studied in this chapter make correction for the self-quenching reaction unimportant in the determination of the "true" ketone triplet lifetime, since the self-quenching reactions are expected to be occurring with rate constants very similar to those of the bimolecular ketone/phenol abstractions. However, in Chapter Four, the triplet lifetimes reported for some of the longer-lived LPKs will have to be corrected for self-quenching.

Finally, the rate determining step for triplet biradical decay has been assigned to intersystem crossing in the case of ketone **9a**.⁷⁴ This was because the biradical lifetimes do not change upon isotopic substitution and so a rate-determining back-hydrogen transfer reaction does not compete with ISC. This result is now also extended to the indanone and benzophenone species as well.

3.2.8. Results. Kinetic isotope effects.

Experiments in water/MeCN and D₂O/MeCN mixtures were conducted to determine kinetic isotope effects. Table 3.6 lists the results from either MN or CHD probe experiments for each ketone, as well as the previous results from the literature for comparison. The quenching plots are shown in the Appendix (Figures A.2 and A.3).

3.2.9. Discussion. NLFP Results.

The lifetimes and behaviour of the LPKs, compared to their *O*-methyl ethers, indicate that remote phenolic hydrogen atom abstraction is occurring for each ketone. The evidence for this is three-fold. First, LPK triplet lifetimes are orders of magnitude

Table 3.6. Values of $k_q\tau_T$ and triplet lifetimes and kinetic isotope effects for compounds **9a**, **11a**, and **57a** determined in 5% water/MeCN and 5% D₂O/MeCN solutions at 23 to 25 °C. ^a

Ketone	$k_q\tau_T; \tau_T$ ^b	$k_q\tau_T; \tau_T$ ^b	Kinetic Isotope Effect
	(5% H ₂ O /MeCN)	(5% D ₂ O/MeCN)	
9a ^c	$83 \pm 6 \text{ M}^{-1}; 10.0 \pm 1.2 \text{ ns}$	$128 \pm 8 \text{ M}^{-1}; 15.4 \pm 1.8 \text{ ns}$	1.54 ± 0.15
11a ^c	$105 \pm 15 \text{ M}^{-1}; 13 \pm 2 \text{ ns}$	$130 \pm 20 \text{ M}^{-1}; 16 \pm 3 \text{ ns}$	1.2 ± 0.3
57a ^d	$95 \pm 6 \text{ M}^{-1}; 8.6 \pm 0.6 \text{ ns}$	$57 \pm 9 \text{ M}^{-1}; 5.2 \pm 0.8 \text{ ns}$	1.7 ± 0.3

a. From either 337-nm excitation, using MN as a probe, or 308-nm excitation using CHD Stern-Volmer quenching.

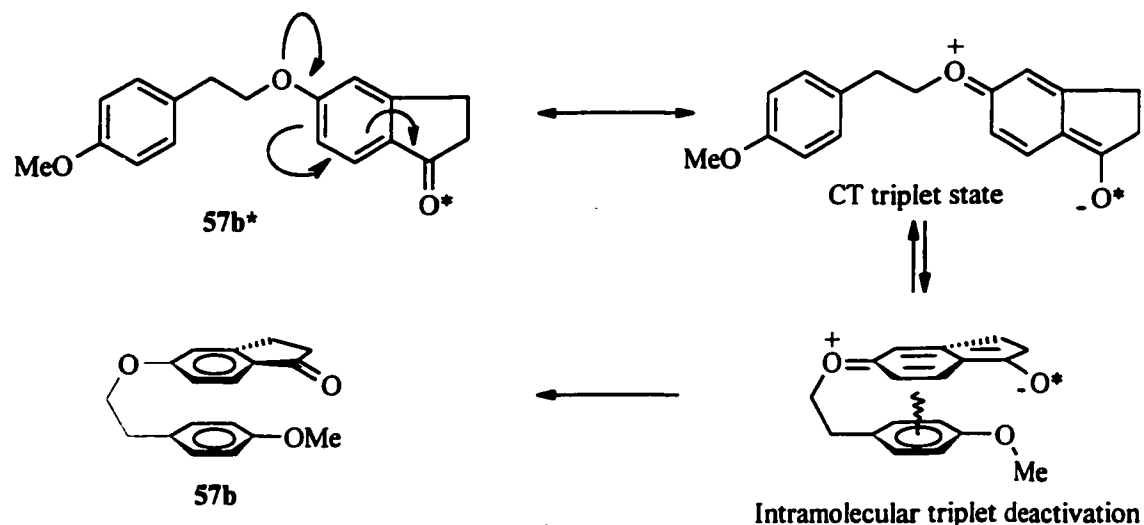
b. Using $8.3 \times 10^9 \text{ M}^{-1}\text{s}^{-1}$ as an estimation of the MN k_q value.

c. Data from MSP.

d. Using $(1.10 \pm 0.03) \times 10^{10} \text{ M}^{-1}\text{s}^{-1}$ as an estimation of CHD k_q value.

shorter than those of the *O*-methyl ether model compounds, indicating that a new decay pathway, not available to the ethers, is available to them. Next, the observation of kinetic isotope effects indicates that hydrogen-atom transfer is occurring in the rate-determining step of the reaction. Finally, good evidence for remote phenolic hydrogen atom abstraction comes from the transient spectra of each LPK, which show evidence for the formation of intermediates that match the absorption spectra of phenoxyl and hemipinacol radicals, and which are formed as products of the initially produced triplets.

The *O*-methyl ethers display triplet-triplet absorption spectra that are very similar to the base chromophores of *para*-methoxyacetophenone, 4-methoxybenzophenone or 5-methoxy-1-indanone. The only difference is that the triplet lifetimes are shorter than those of the simple model compounds. For example, the 3.5 μ s triplet lifetime of compound **9b** is significantly shorter than the value for *para*-methoxy acetophenone measured under similar conditions (5 to 10 μ s). This is possibly due to a deactivation pathway involving charge transfer quenching which has been pointed out previously.⁷⁴ This mechanism potentially plays a particularly important role in the triplet lifetime of the indanone-derived species. As explained in Chapter Two, indanone molecules will have a larger contribution from a lowest charge-transfer triplet state than either acetophenone or benzophenone chromophores since in the indanone the ketone is forced to sit co-planar with the attached aromatic ring. As Scheme 3.6 shows, the charge-buildup associated with the CT-triplet state would increase the importance of triplet deactivation *via* charge-transfer from the electron-rich attached anisyl ring. Thus, indanone **57b** has a very short triplet lifetime of less than 300-ns compared to several

Scheme 3.6. Intramolecular charge transfer deactivation in alkoxyindanone **57b**.

microseconds in the simple model compound 5-methoxy-1-indanone (**50**). The solvent effect supports this, since in DCM the triplet lifetime of ether **57b** increases by a factor of 50%, which is almost twice as great an increase as for the other *O*-methyl ethers on going from MeCN to DCM. This is due to the lesser importance of charge-transfer in a solvent of lower dielectric constant. A point to ponder, however, is that a preliminary study of triplet state deactivation by anisole and *para*-methoxyanisole indicated that *para*-methoxyacetophenone and 5-methoxy-1-indanone were quenched at roughly the same rate in acetonitrile. Whether or not a charge-transfer interaction is really what is responsible for the shortened triplet lifetimes of the indanone systems will require further study to uncover.

The triplet lifetimes of the *para*, *para'*-LPKs are all very short, indicating that the *para*, *para'*-geometry is perhaps a "good" one, and that the three-atom spacer is of

sufficient length so as not to hinder the carbonyl and phenol groups from performing the HAA reaction. Also, the fact that the benzophenone LPK has a longer triplet lifetime than the acetophenone species mirrors the initial observation made in bimolecular reactions that π, π^* species can be more reactive than n, π^* species in this reaction.

The indanone species' triplet lifetime deserves a closer look. In the bimolecular reaction with *para*-cresol, 5-methoxy-1-indanone is quenched the fastest of the model compounds. However, LPK 57a has the longest triplet lifetime of the three *para*, *para*'-species, albeit only by a slim margin. Earlier it was speculated that the planarity of the indanone chromophore would render it the least reactive of the three LPKs based on a hydrogen-bonded mechanism. However, the triplet lifetime of LPK 57a is only a factor of two greater than that of LPK 9a. It is possible that the non-radiative pathway that exists for the *O*-methyl ether 57b also contributes to the decay of LPK 57a, contributing to a shortening of the triplet lifetime to 22-ns, disguising perhaps a longer triplet lifetime in the absence of this effect. If this were correct, then the original assumption that the indanone should display a slower rate of HAA than ketone 9a has better support. In Chapter Four, another indanone molecule will be discussed which should shed more light on this topic.

3.2.10. Discussion. Solvent effect. MeCN versus DCM.

Previous workers have found that in general the phenolic HAA reaction is more favourable in non-polar aprotic solvents than in polar ones. Faster phenolic HAA in non-polar or non-hydrogen bonding solvents has also been reported for benzophenone,⁷²

para-methoxypropiophenone,⁷² and other aromatic ketone triplets,^{73,75,120} as well as biacetyl⁶⁸⁻⁷¹ triplets. This effect is attributed to a reduction in the concentration of free phenol due to hydrogen-bonding with the solvent.¹⁶² Similar effects are observed on the rate constants for alkoxyl free radical abstractions from phenol.^{59,61,75,163} A discussion of the (more complicated) effect of water on LPK triplet lifetimes and the phenolic HAA reaction is deferred until Chapter Four.

The results in this Chapter confirm the previous observations on the effect of solvent polarity on the phenolic HAA reaction. In the bimolecular reaction, both lowest n, π^* and π, π^* triplets are more reactive in DCM. Each *para*, *para'*-attached LPK studied in both solvents shows a dramatic reduction in triplet lifetime in DCM compared to MeCN, in agreement with the previous results for compound **9a** in benzene.⁷⁴ These observations confirm that hydrogen-bonding is an important aspect in the mechanism of the phenolic HAA reaction, and lend good indirect evidence to support the new mechanism for abstractions by lowest π, π^* species.

3.2.11. Conclusions.

Based on the results discussed in this Chapter, the following general conclusions can be made about the intramolecular phenolic HAA reaction:

- 1) The reaction proceeds rapidly for *para*, *para'*-species, and follows the trend where π, π^* triplets are more reactive than n, π^* triplets in phenolic HAA reactions.
- 2) The reaction involves hydrogen-atom transfer in the rate-determining step.

- 3) The indanone derivative provides tentative evidence that hydrogen-bonding is important in the reaction; however, its triplet lifetime is potentially obscured by intramolecular charge-transfer quenching, which is more important for conformationally-locked indanones than the other chromophores.
- 4) Solvent effects are consistent with the idea that hydrogen bonding is important in the intramolecular reaction. In organic solvents, decreasing polarity leads to increasing reactivity, in direct agreement with the formation of a hydrogen-bond in a kinetically significant step in the reaction.

CHAPTER FOUR
INTRAMOLECULAR PHENOLIC HYDROGEN ATOM ABSTRACTION
REACTIONS.
PART TWO. THE EFFECT OF POSITIONAL ISOMERISM IN THE
INTRAMOLECULAR PHENOLIC HYDROGEN ATOM ABSTRACTION
REACTION

4.1. Motivation for a Study of Positional Isomerism.

In Chapter Three it was shown that the fast bimolecular quenching reaction of aromatic ketone triplets by phenol donors can be reproduced in intramolecular examples. Linked phenolic ketone (LPK) triplet states with para, para'-attached acetophenone, benzophenone, and indanone moieties were created that enjoyed a brief existence mainly dictated by the speed with which they could adopt sandwich-like geometries and transfer the phenolic hydrogen-atom.

A logical next step in the study of these systems involves examining what effect geometrical isomerism has on the reaction. In chemical reactions, substrate molecules are free to approach each other in the conformation that will allow for maximal energy release and entropic increase, the two driving forces in a chemical reaction. Substituent isomerism therefore only causes differences due to electronic effects. Due to this arbitrary nature of approach, the effect of a specific interaction, such as hydrogen-bonding, cannot be easily probed by studying trends in bimolecular reactivity.

Inspection of molecular models suggests that modification of the structure of *para*, *para'*-acetophenone derivative **9a** to ones with various combinations of *para*- and *meta*-linkages should afford additional information on how the proposed hydrogen-bonded exciplex intermediate affects the rate constant for phenolic hydrogen abstraction.

Geometrical isomerism is expected to develop changes in the way a molecule such as an LPK chemically reacts since the spacer linkage restricts molecular motion greatly. Altering the attachment geometry of the molecule should change the ease with which the molecule can bring the ketone and phenol groups together. If the possibility of formation of a hydrogen-bond exists, then these forces may in turn act to change the ease with which it may be formed; this ultimately could effect the HAA process if the new mechanism is correct.

The kind of changes that provide the most information are ones subtle enough to have a negligible effect on the gross reaction process being studied while being different enough so that any changes may be tracked to the isomerism. Clearly, if the whole reaction mechanism were changed by the isomerism, then it would be very difficult to extract what change had caused what difference.

For this reason, *meta*-isomers were chosen for further study, with spacer length and constitution identical to the previous *para*, *para'*-attached series. LPKs with *meta*-substituents were thought to be different enough to probe the geometrical requirements of the intramolecular HAA process, without incurring any gross changes in the mechanism.

Substituents in the *ortho* position were not considered, as it is known that groups *ortho* to aromatic rings may affect the ability of the rings to delocalize charge due to the

steric inhibition of resonance, which is thought to be negligible for normal *meta*- and *para*-substituents.¹⁶⁴

This chapter is divided into two parts. The first is an examination of geometrical isomerism in the acetophenone chromophore. The ketones of interest had their attachment orientations systematically varied from *para*, *para'* to *meta*, *meta'*, and are shown in the first part of Figure 4.1. The latter part of the chapter deals with *meta*, *meta'*-attached LPKs of the benzophenone, **58**, and indanone, **59**, chromophores and involves a comparison of the different chromophores to the acetophenone results. These molecules are shown at the bottom of Figure 4.1.

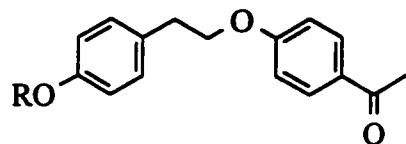
4.2. Photochemistry of LPKs with *meta* Geometries.

One goal of this study was to try to determine whether a hydrogen-bonded intermediate was present during the hydrogen atom transfer step. Good evidence for this intermediate would be a trend in triplet lifetime coinciding with the trend in apparent ease with which such a hydrogen-bonded intermediate could be formed. This ease could in turn be predicted from calculation, using known parameters of ketone/phenol hydrogen bonds and probable geometries of the sandwich exciplex.

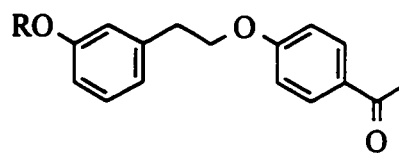
4.2.1. Introduction. Previous work and species of interest.

Previously, Michael St. Pierre (MSP) prepared the acetophenone LPKs of Figure 4.1. Preliminary NLFP experiments indicated that the triplet lifetimes of these isomers varied from the value for ketone **9a** if either linkage was altered from *para* to *meta*.

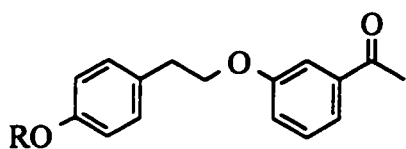
Figure 4.1. The acetophenone LPK series and meta, meta'-attached LPKs for study.



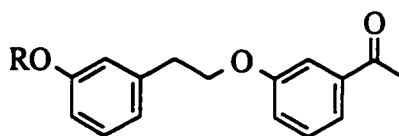
R = H **9a**
R = Me **9b**



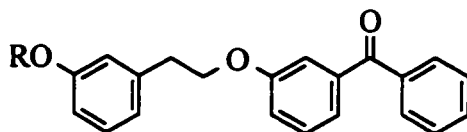
R = H **14a**
R = Me **14b**



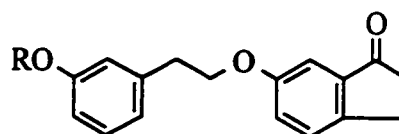
R = H **15a**
R = Me **15b**



R = H **16a**
R = Me **16b**



R = H **58a**
R = Me **58b**



R = H **59a**
R = Me **59b**

The excited state of compound **9a** had the shortest triplet lifetime of the series, and the meta, meta'-species **16a** exhibited the longest lifetime, with the others intermediary.

However, MSP's results were preliminary, as explained in Chapter One. In this section, further work conducted¹⁶⁵ on the acetophenone derivatives is presented.

No previous studies of the photochemical behaviour of compounds **58** and **59** have been reported. General expectations of the results can be considered based on the behaviour of the para, para'-attached isomers.

As reported in Chapter Three, the para, para'-attached benzophenone LPK **11a** displays a very short triplet lifetime of 19 ns, however this value is greater than the value of 12 ns for the acetophenone **9a**. This is in line with the trend in bimolecular reactivity, where the lowest n, π^* triplet 4-methoxybenzophenone is slightly less reactive than lowest π, π^* triplet *para*-methoxyacetophenone towards *para*-cresol.

The para, para'-attached indanone derivative **57a** also displays a short triplet lifetime, however it is the longest of the group **9a**, **11a**, **57a** despite the fact that the bimolecular reactivity of the indanone model compound is the greatest.

What predictions can be made about LPKs **58a** and **59a**? For the *meta*-alkoxy substituted benzophenone compound, different aspects must be considered. First, the simple model compound 3-methoxybenzophenone falls on the *acceptor* side of the Hammett plot previously discussed (Fig 2.6, p.77). Thus it is possible that the reactivity of ketone **58a** could be dominated by an n, π^* -type mechanism (the "electrophilic" mechanism discussed in Chapter Two), and not help address the question of the importance of hydrogen-bonding. However, participation of the nucleophilic mechanism

could result from the well-known photochemical "*meta*-effect" (as discussed in Chapter Two), which predicts that a *meta*-alkoxy group demonstrates a greater electron-donating capacity than *para*-alkoxy in the excited state. This means that the molecule *could* react like a π, π^* triplet and allow a direct comparison between it and acetophenone derivative **16a** to be made.

The prediction for the indanone **59a** was that it would react similarly to the acetophenone molecule **16a**, albeit slightly attenuated in analogy to the comparison of LPK **57a** to LPK **9a** due to its planar geometry.

4.2.2. Results. Preparation of LPKs and their *O*-methyl ethers.

In Chapter Three, two main methods for the preparation of LPK molecules were described (Schemes 3.3 and 3.4, pp. 112-113). As alluded to in those pages, S_N2 substitution of *meta*-substituted phenethyl bromides by *para*- or *meta*-phenoxides produced little desirable product. Instead, the majority of material was the corresponding styrene. Work by DePuy and Bishop and later by Cockerill^{166,167} on the mechanisms of S_N2 and E2 reactions in phenethyl species provided a clue that perhaps a change of leaving group was required. Upon adoption of the tosylate group as the leaving group, the S_N2 reaction became favoured, with crude yields as high as 100%. The experimental details for the preparation of the compounds in Figure 4.1, as well as the ditosylate starting materials, can be found in Chapter Five. The intermediate tosyl esters were in general not isolated, instead the crude materials were hydrolyzed and purification was then done on the final product.

4.2.3. Results. Spectroscopy and steady state photochemistry.

Experiments similar to those conducted on compounds **9-12** and **57** in Chapter Three were repeated on compounds **14-16**, **58** and **59**. Ultraviolet (UV) and infra-red spectroscopy was conducted to determine if the phenolic group had any effect on the carbonyl absorption. Figure 4.2 shows the UV spectra of compounds **14-16** in dichloromethane (DCM), which are very similar to the corresponding⁸⁶ spectra in acetonitrile (MeCN). Figure 4.3 shows the UV spectra of compounds **58** and **59** in both solvents. As before, there is no noticeable difference between phenolic and non-phenolic species.

The triplet energies of compounds **14-16** have been determined and the triplet configurations of these compounds have been assigned by low temperature phosphorescence emission spectroscopy.⁸⁶ These are each lowest π, π^* triplets.

Phosphorescence emission spectra of compounds **58** and **59** were recorded in 4:1 ethanol:methanol glasses at 77K (Figure 4.4). The spectra of ketones **58a** and **58b** are consistent with a lowest n, π^* state, while those of the indanone derivatives **59a** and **59b** exhibited the structure of a lowest π, π^* state. Triplet energies for these species, calculated from the onsets of the absorption bands, are listed as insets in the figures.

MSP showed⁸⁶ that irradiation of MeCN solutions of compounds **14-16** led to little photodecomposition. Using LPK **9a** as a secondary actinometer, quantum yields of 0.01 or less were determined for each compound. Similar results were obtained for compounds **58** and **59**.

Figure 4.2. UV spectra of compounds **14a**, **14b**, **15a**, **15b**, **16a** and **16b** in DCM at room temperature.

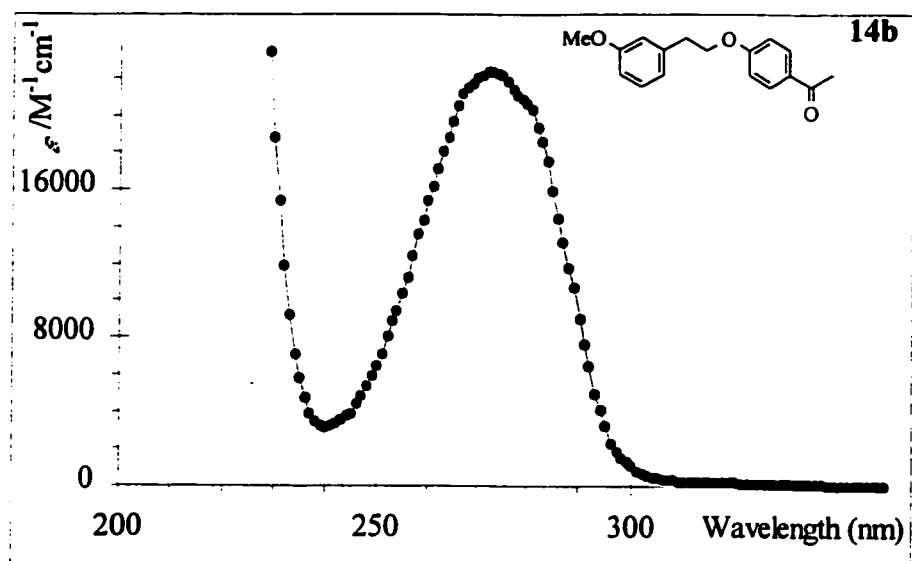
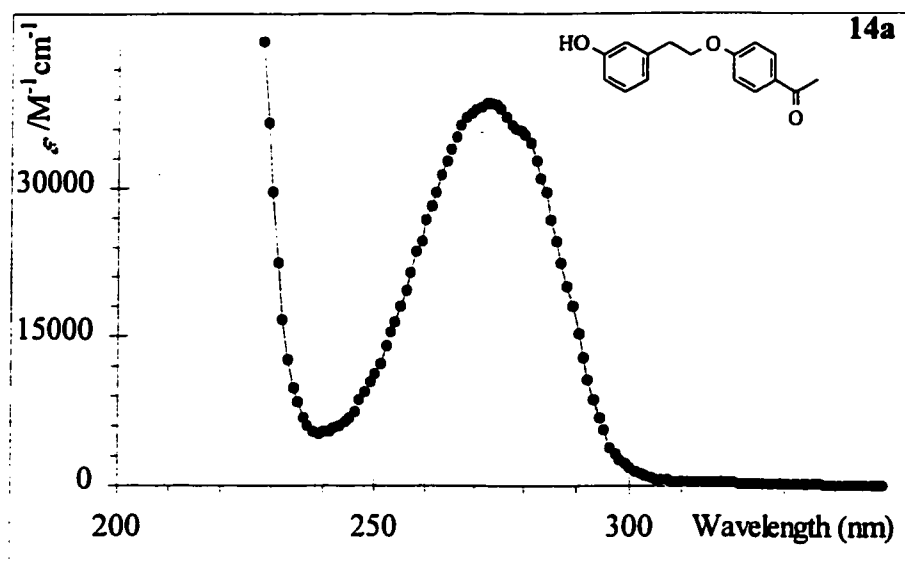


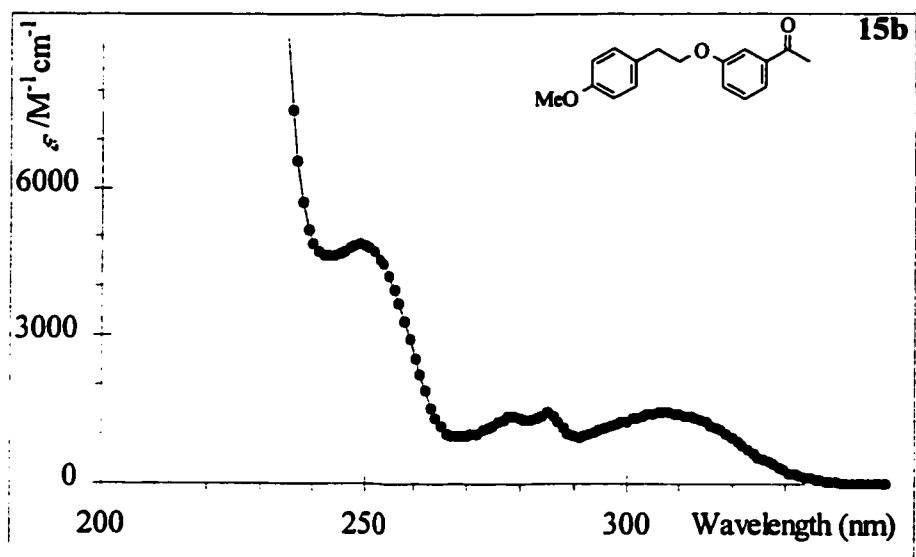
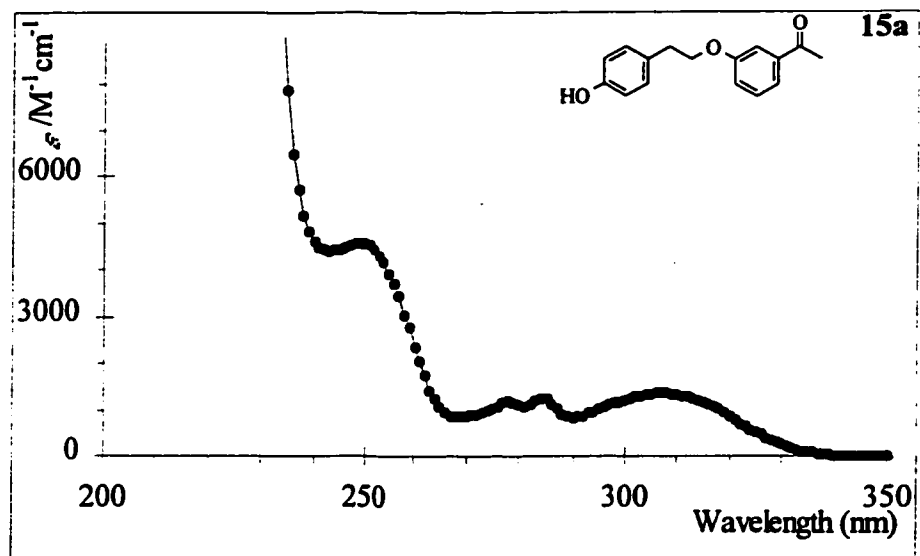
Figure 4.2. Continued.

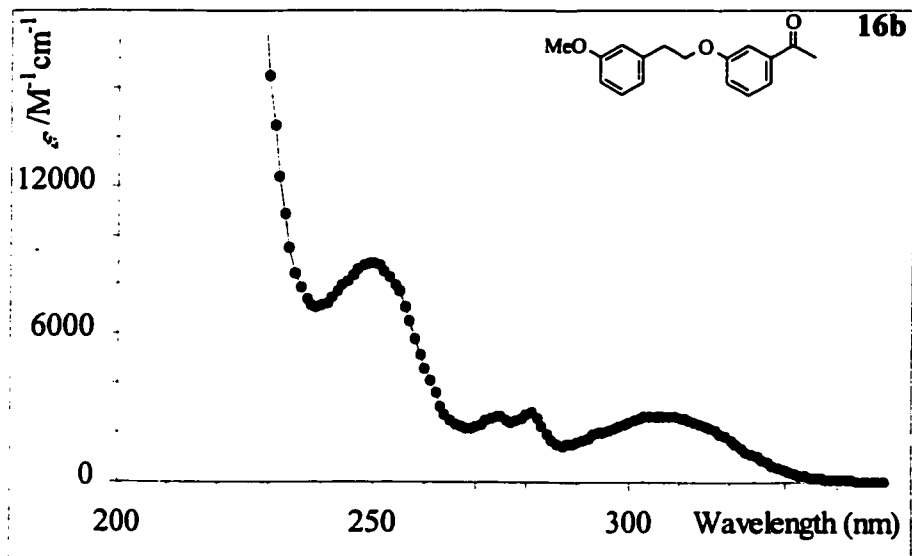
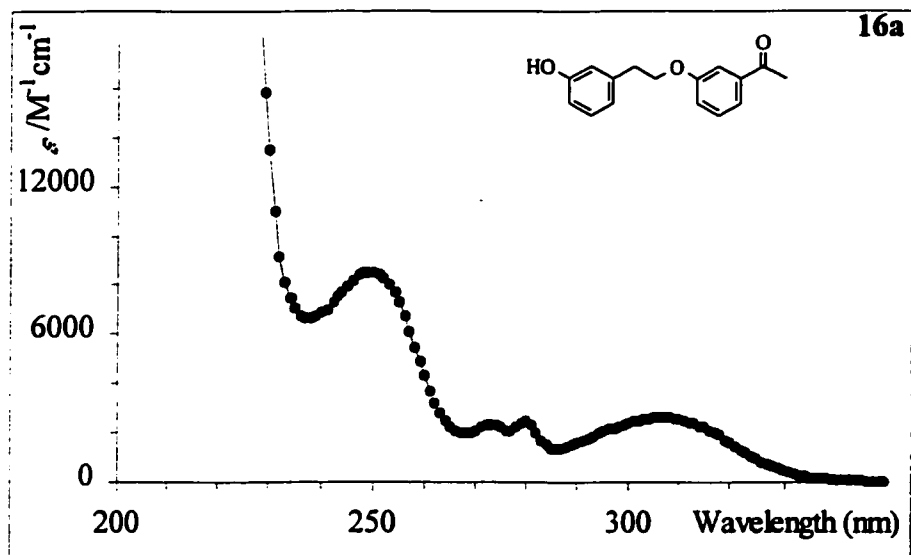
Figure 4.2. Continued.

Figure 4.3. UV spectra of compounds **58a**, **58b**, **59a**, and **59b** in MeCN and DCM at room temperature.

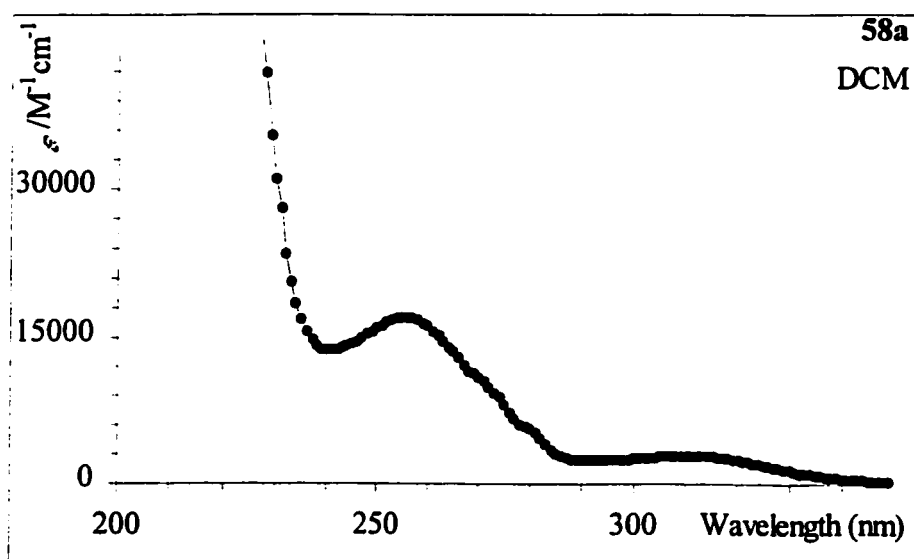
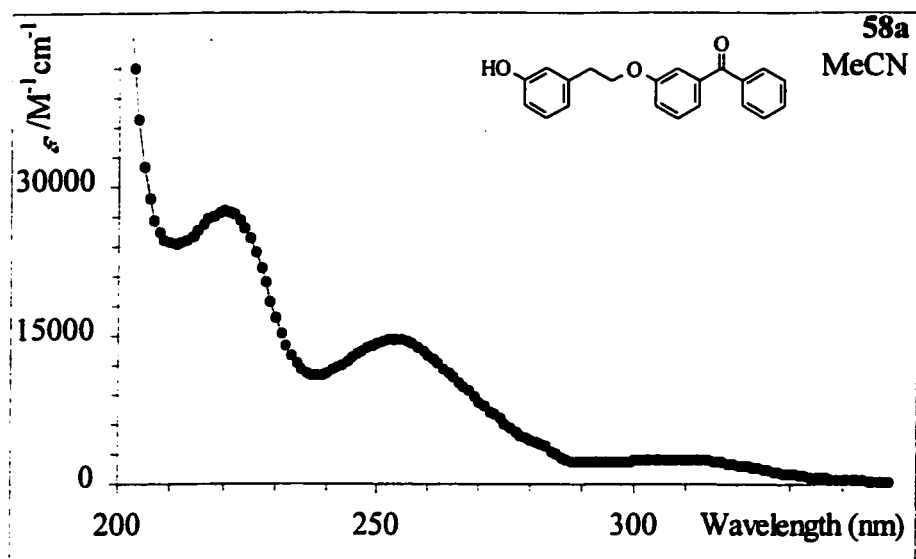


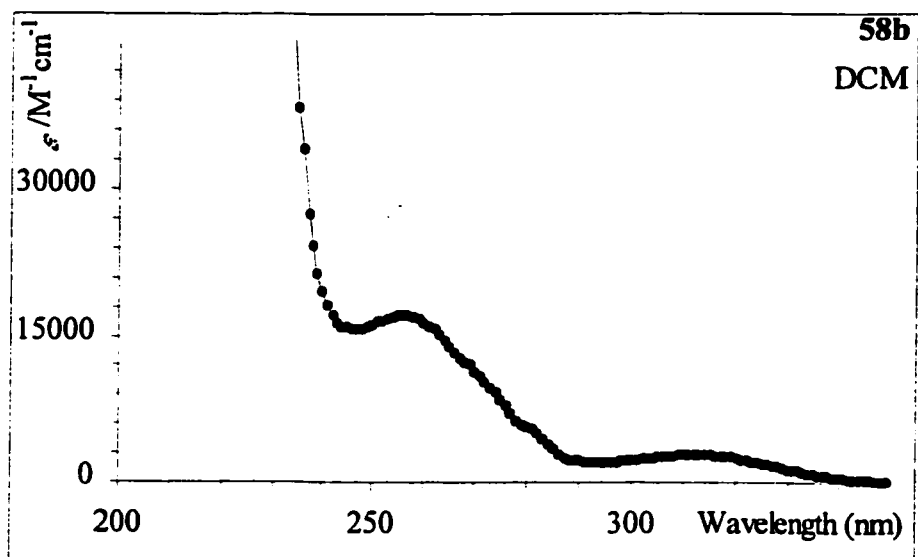
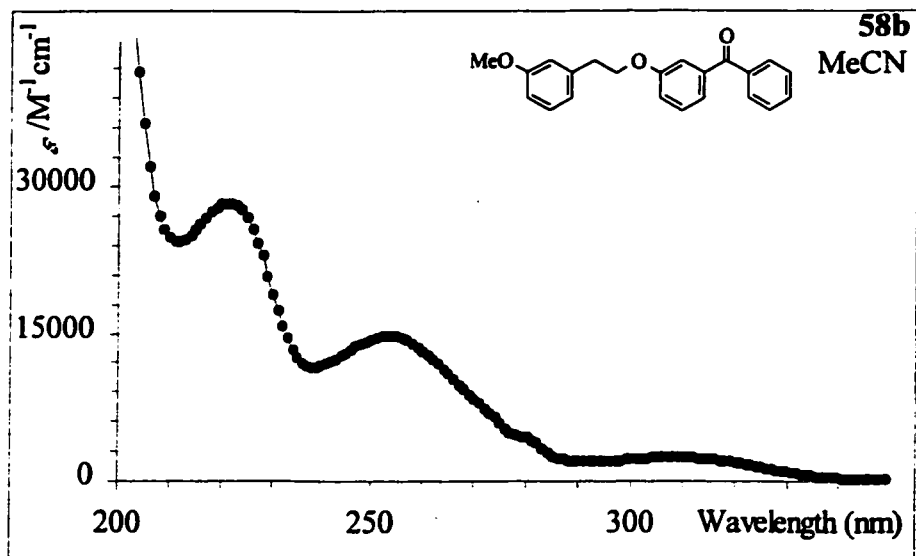
Figure 4.3. Continued.

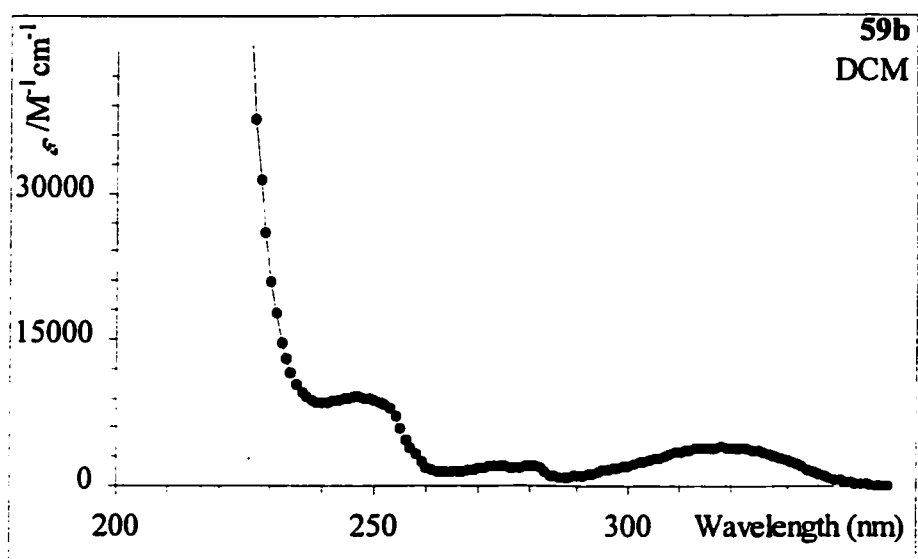
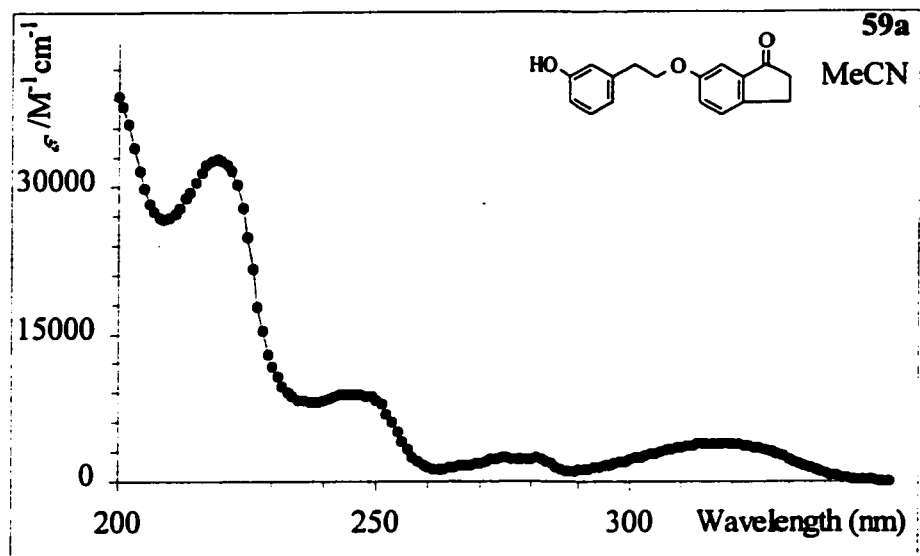
Figure 4.3. Continued.

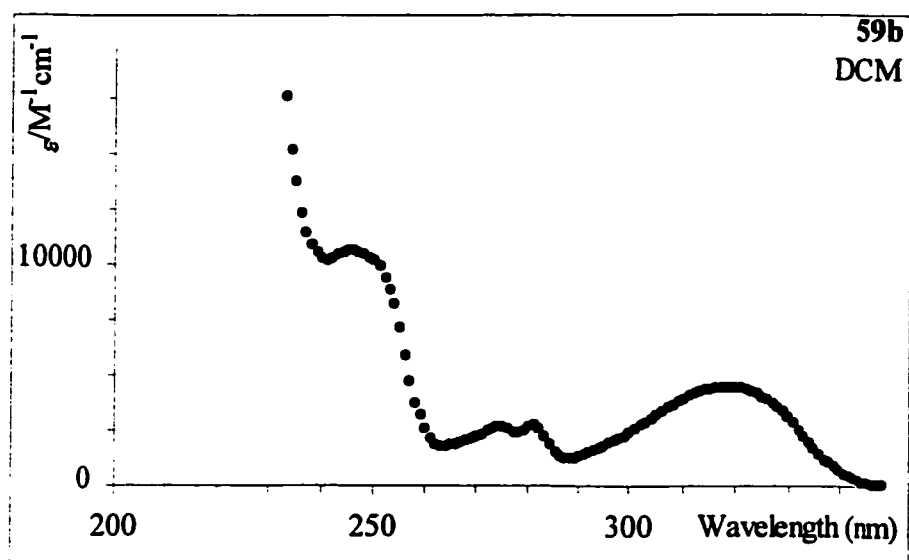
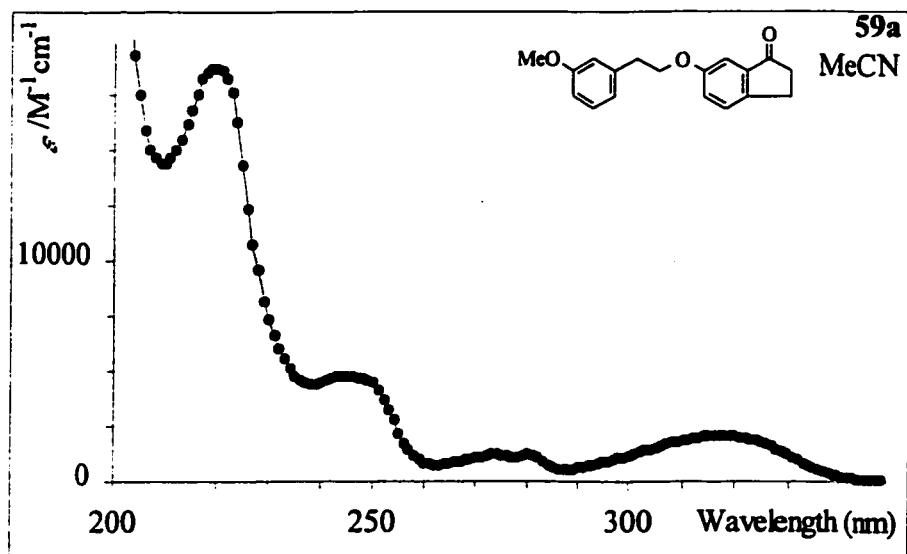
Figure 4.3. Continued.

Figure 4.4. Phosphorescence spectra of compounds (a) **58a**, (b) **58b**, (c) **59a** and (d) **59b** in 4:1 EtOH:MeOH glasses at 77 K.

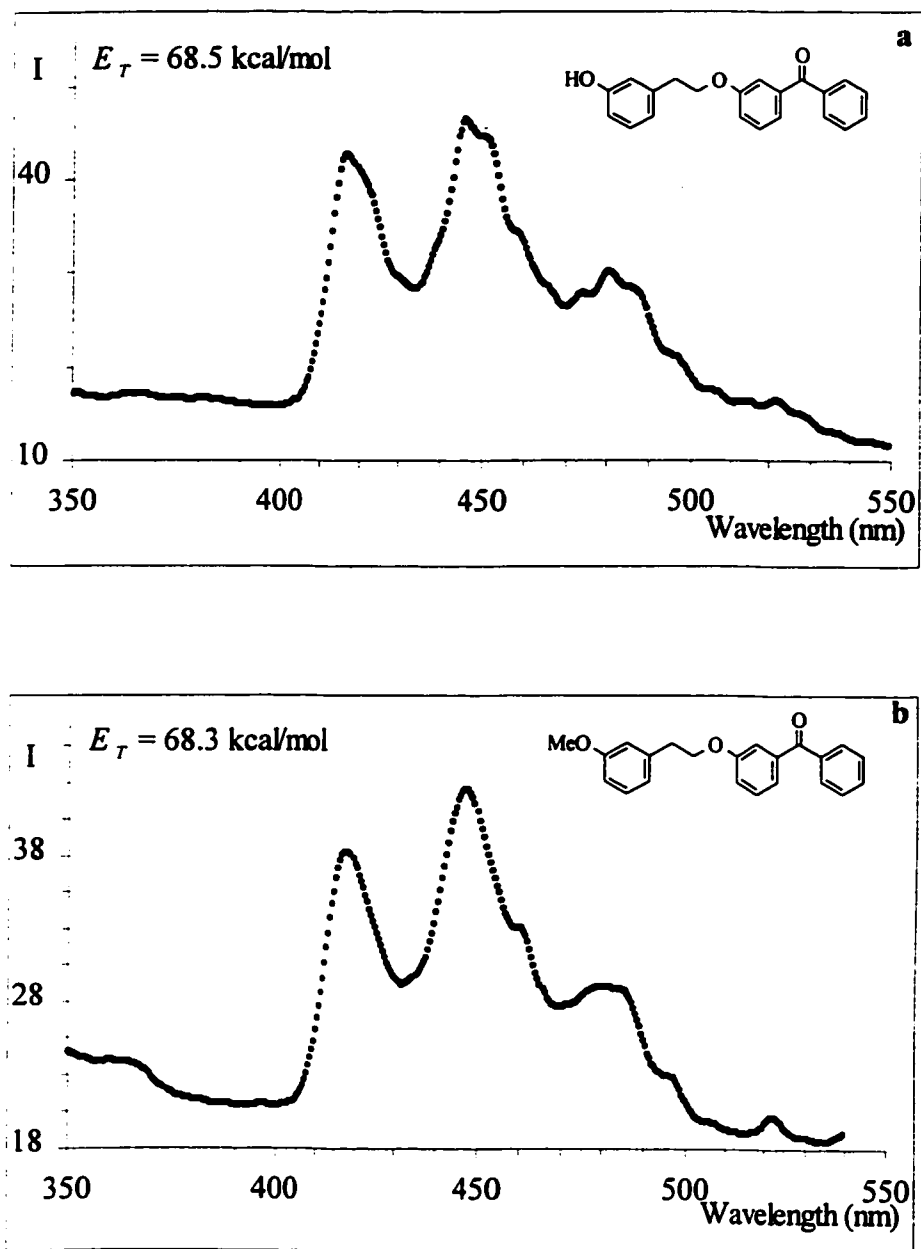
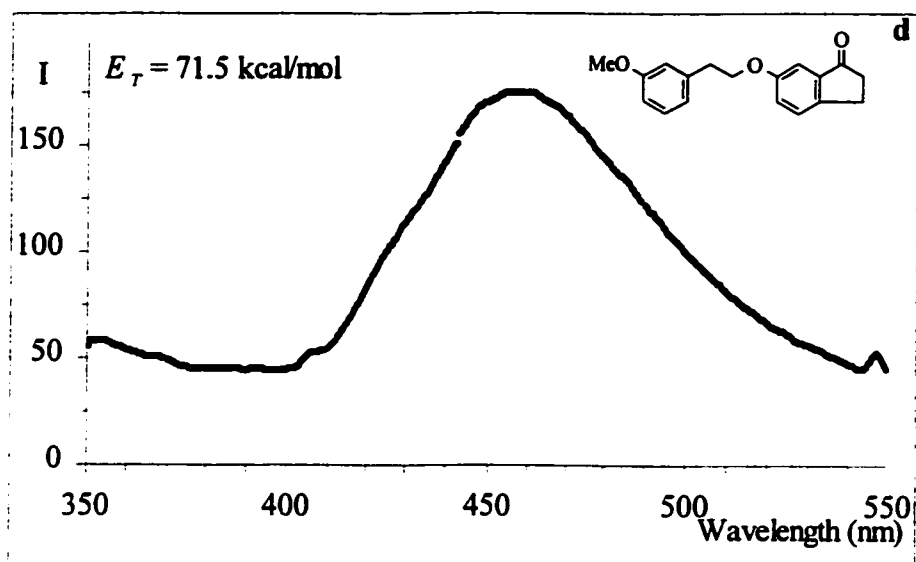
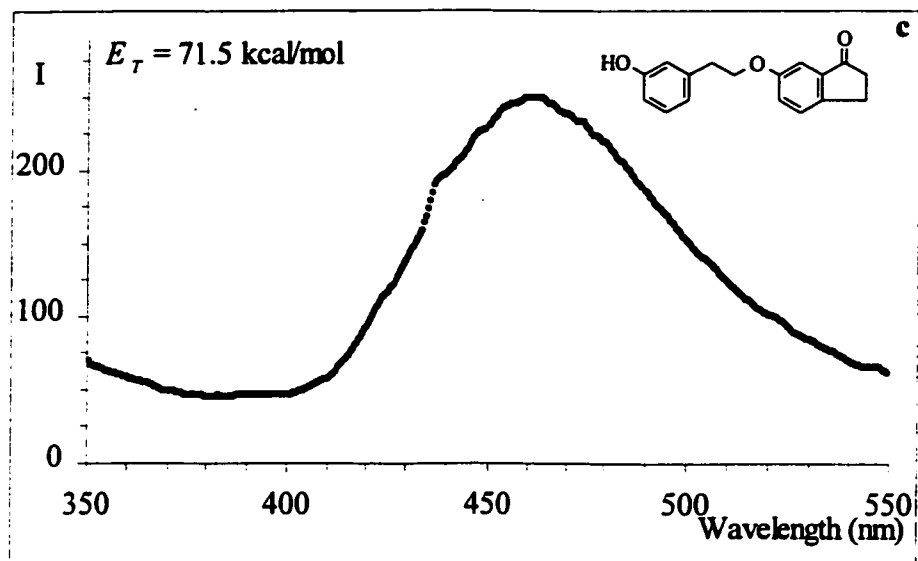


Figure 4.4. Continued.

4.2.4. Results. NLFP of compounds 14b-16b.

NLFP experiments were conducted in a similar fashion to those previously described in Chapter Three. Experiments were carried out on rigorously deoxygenated MeCN or DCM solutions in 3- or 7-mm pathlength cells, using either 337-, 308- or 248-nm excitation depending on the type of experiment to be conducted. Flash photolysis of dilute (10^{-4} M or less) solutions of the methoxy model ketones **14b-16b** using the 248-nm laser for excitation gave strongly absorbing transients in the 300- to 450-nm range which cleanly returned to the baseline with pseudo-first order kinetics, provided care was taken to keep laser intensity to a minimum.

Typical transient decays and absorption spectra are shown in Figures 4.5 (MeCN) and 4.6 (DCM).

The compounds with *meta*-acetyl attachments (**15b** and **16b**) displayed a double humped shape with maxima near 320- and 380-nm while the *para*-acetyl compound **14b** displayed a transient with only one broad absorption maximum at 375- to 380-nm. These spectra match those of the original report.⁸⁶

These transients were previously assigned⁸⁶ to the corresponding ketone triplet states on the basis of their appearance and rapid quenching by 1,3-cyclohexadiene and oxygen ($k_q = 3\text{-}10 \times 10^9 \text{ M}^{-1} \text{ s}^{-1}$); these assignments have been reconfirmed, and are also valid in DCM as qualitatively verified by their spectral similarity and behaviour in the presence and absence of oxygen.

Triplet lifetimes were determined from first order decay analyses of change in absorbance *versus* time data. The triplet lifetimes of ethers **14b-16b** in the two solvents,

Figure 4.5. Transient ultraviolet spectra and decays of 10^{-4} M solutions of compounds **14b**, **15b** and **16b** in deoxygenated MeCN at 23 to 25 °C.

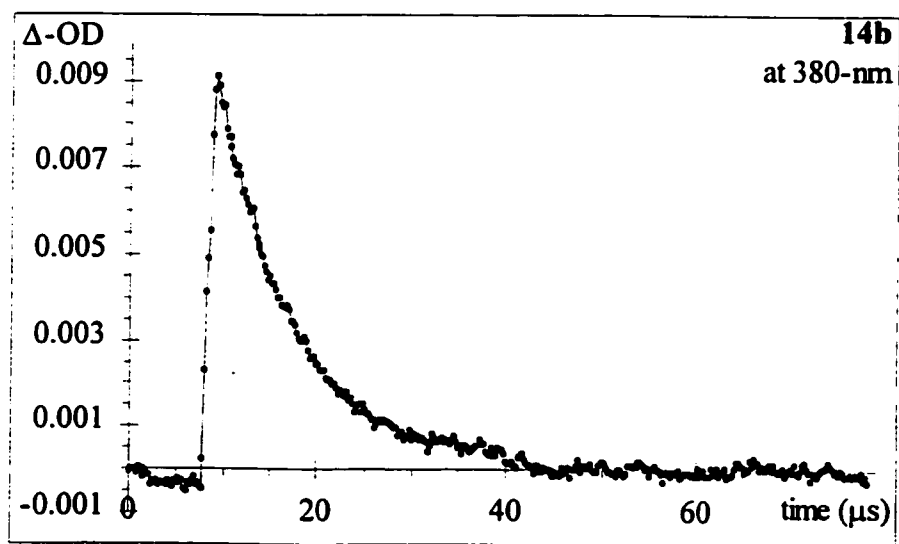
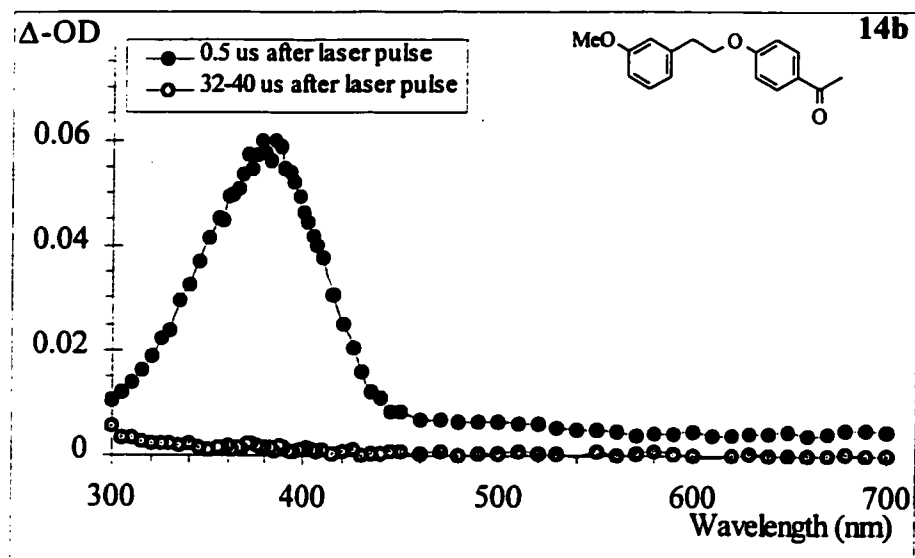


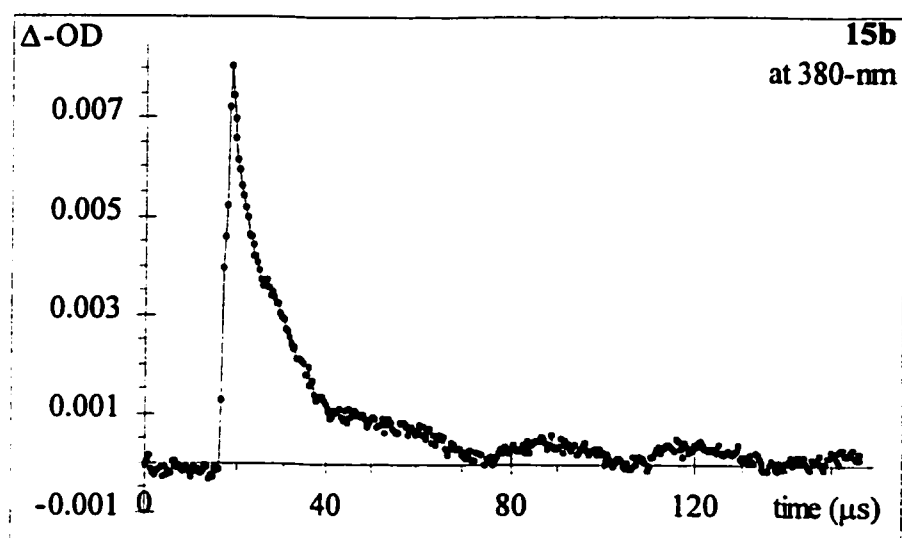
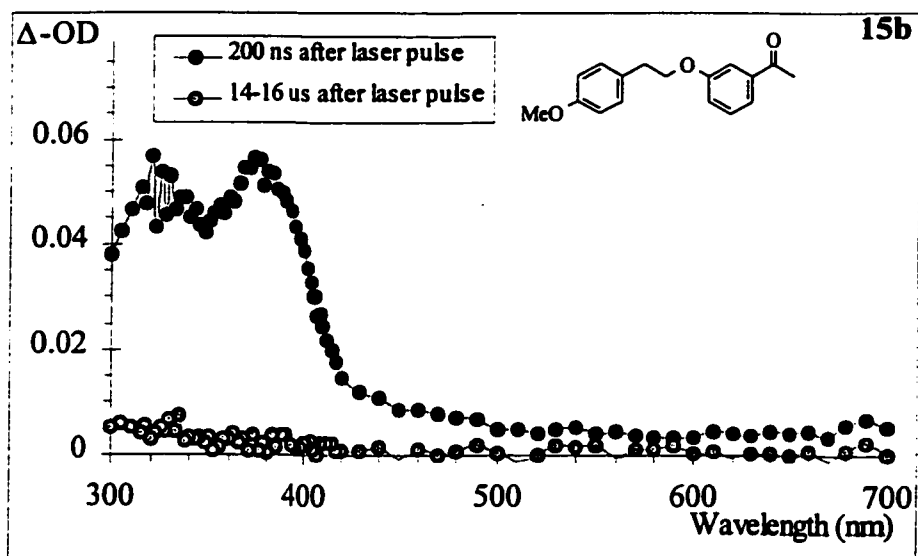
Figure 4.5. Continued.

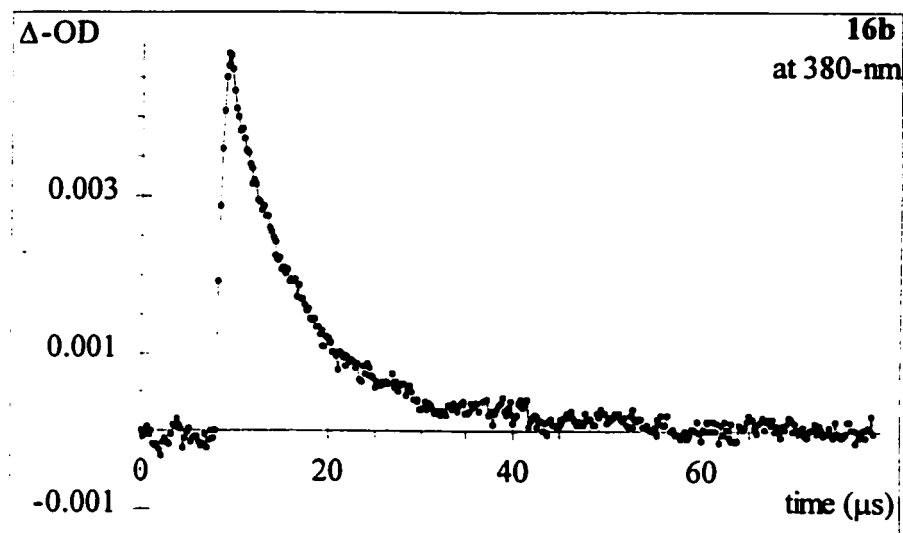
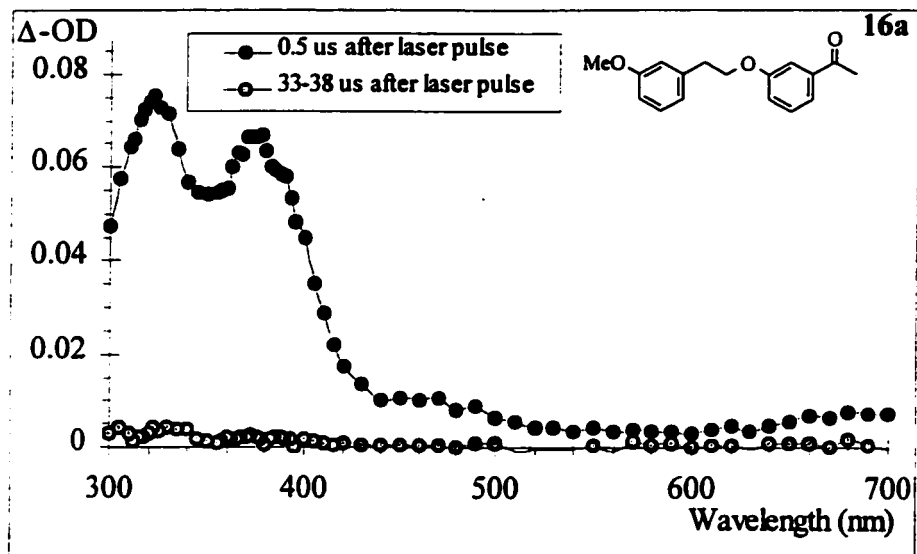
Figure 4.5. Continued.

Figure 4.6. Transient ultraviolet spectra and decays of 10^{-4} M solutions of compounds **14b**, **15b** and **16b** in deoxygenated DCM at 23 to 25 °C.

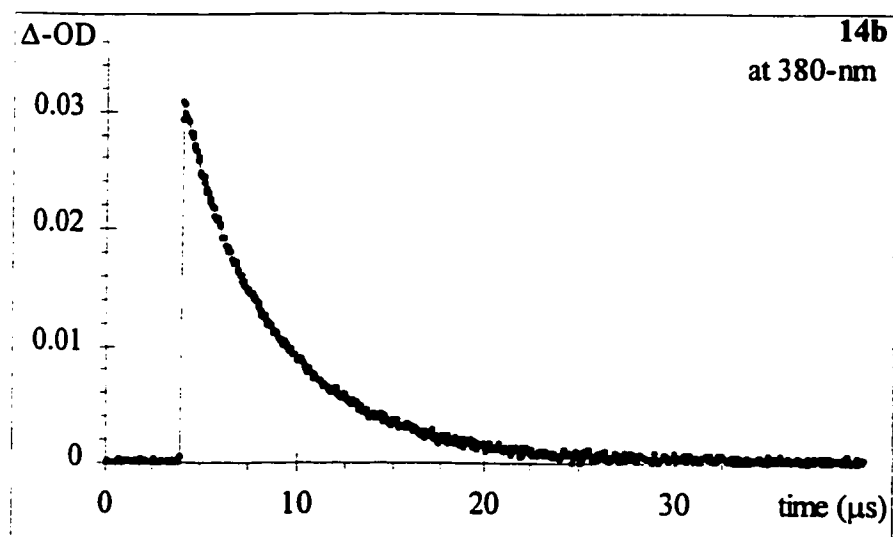
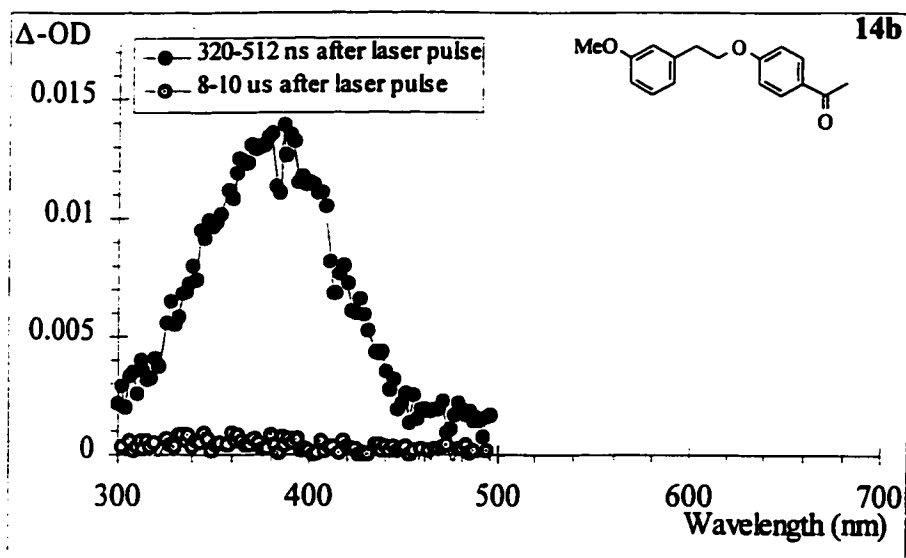


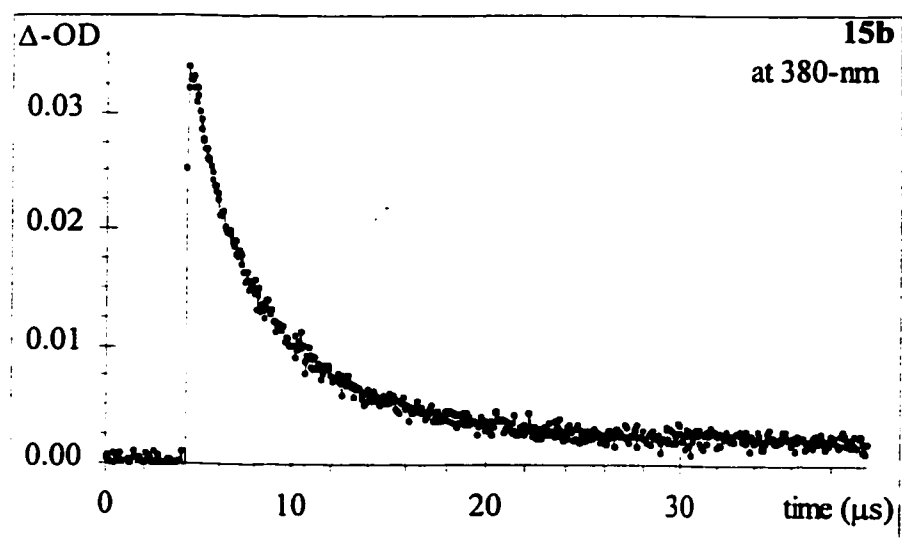
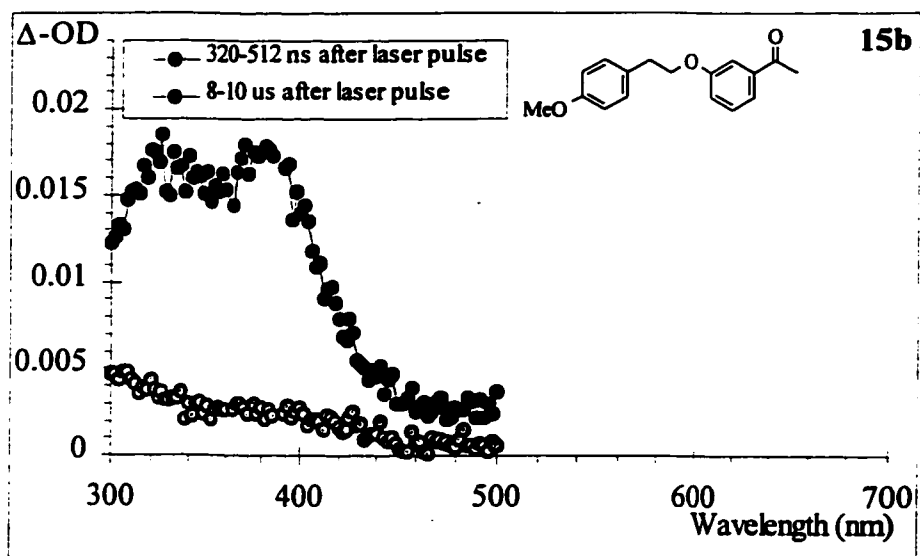
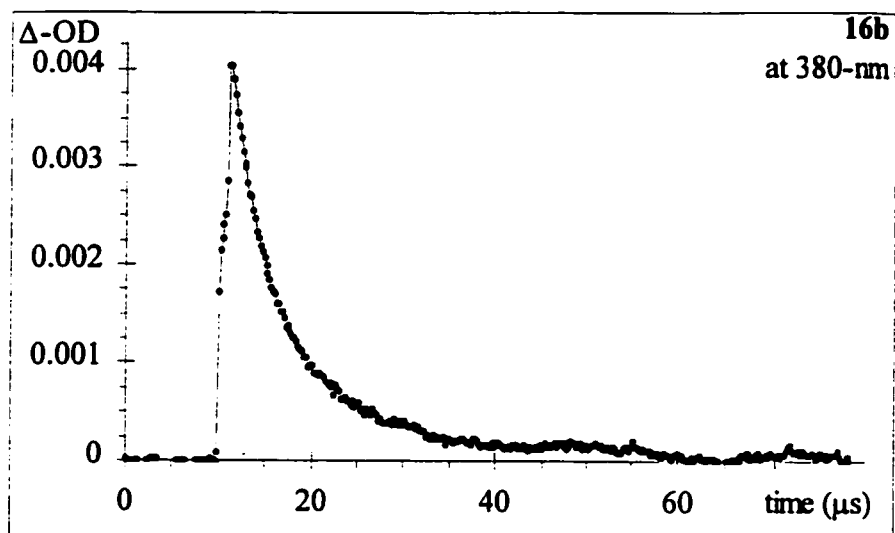
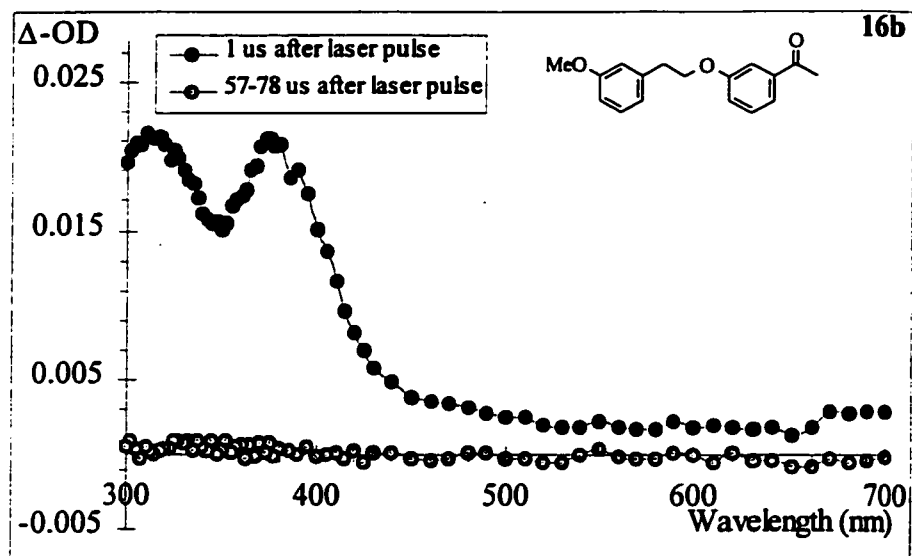
Figure 4.6. Continued.

Figure 4.6. Continued.

including wet MeCN, as well as triplet quenching rate constants, are listed in Table 4.1.

4.2.5. Results. NLFP of compounds 14a-16a.

NLFP experiments on the LPKs 14a-16a were conducted mainly at 248-nm in both solvents on deoxygenated 10^{-4} - 10^{-5} M solutions. Transient UV spectra were observed that had similar characteristics to their respective model ethers, including the double humped shapes of the *meta*-acetyl species.

Figure 4.7 shows transient absorption spectra of ketones 14a-16a in MeCN as well as transient decays for each LPK. Figure 4.8 follows after with the same data in DCM.

In contrast to the behaviour of the para, para'-acetophenone LPK 9a and in direct agreement with MSP's initial study,⁸⁶ the transients for each of the compounds 14a-16a in MeCN were long-lived enough to be directly identified as ketone triplets by the addition of oxygen or 1,3-cyclohexadiene to the solutions, although the triplet lifetimes were generally smaller than those of the *O*-methyl ethers. In addition, residual absorptions were seen in all cases. In DCM, the triplet lifetimes were much shorter.

In MeCN, triplet lifetimes were in the 0.3-8.5 μ s range for the three LPKs, as shown in Table 4.2. It was found that the triplet lifetimes were extremely sensitive to ketone concentration, decreasing rapidly if the LPK concentration increased. This is due to the self-quenching reaction, first mentioned in Chapter Three (Scheme 3.5). Self-quenching plots of triplet lifetime *versus* ketone concentration, fitted to eq. 4.1, were prepared in each case, with the slope equal to the self-quenching rate, k_{sq} , and the intercept equal to the triplet lifetime at infinite dilution, *i.e.*, without contribution from self-quenching.

Table 4.1. Triplet lifetimes of compounds **9b**, **14b**, **15b**, and **16b** in deoxygenated MeCN, 0.028 M H₂O/MeCN and DCM, and triplet quenching rates by 1,3-cyclohexadiene (CHD) in MeCN. ^{a,b}

Ketone	τ_T	τ_T	k_q CHD	
	(MeCN ^c , μ s)	(0.028 M H ₂ O/MeCN ^c , μ s)	τ_T (DCM, μ s)	/ 10 ⁹ M ⁻¹ s ⁻¹ ^e
9b	3.3 ± 0.2 ^f	2.9 ± 0.09	3.28 ± 0.06	6.7 ± 0.3 ^f
14b	8.8 ± 0.5	6.96 ± 0.14	5.00 ± 0.14	11 ± 4
15b	12.3 ± 1.1	6.1 ± 0.4	7.7 ± 0.2	8.4 ± 0.2
16b	8.5 ± 0.8	6.9 ± 0.2	7.04 ± 0.18	10 ± 2

a. Lifetimes determined from 248-nm NLFP at room temperature unless noted otherwise.

b. Errors in lifetimes are twice the standard deviation of the least squares logarithmic fit.

c. Rigorously dried MeCN ([H₂O] < 10⁻⁴ M).

d. From 308- or 337-nm NLFP, errors are twice the standard deviation of the least squares line from the quenching plot.

e. In MeCN, from Ref. 86.

f. From Table 3.2, p.131.

Figure 4.7. Transient ultraviolet spectra and decays of 10^{-4} M solutions of compounds **14a**, **15a** and **16a** in deoxygenated MeCN at 23 to 25 °C.

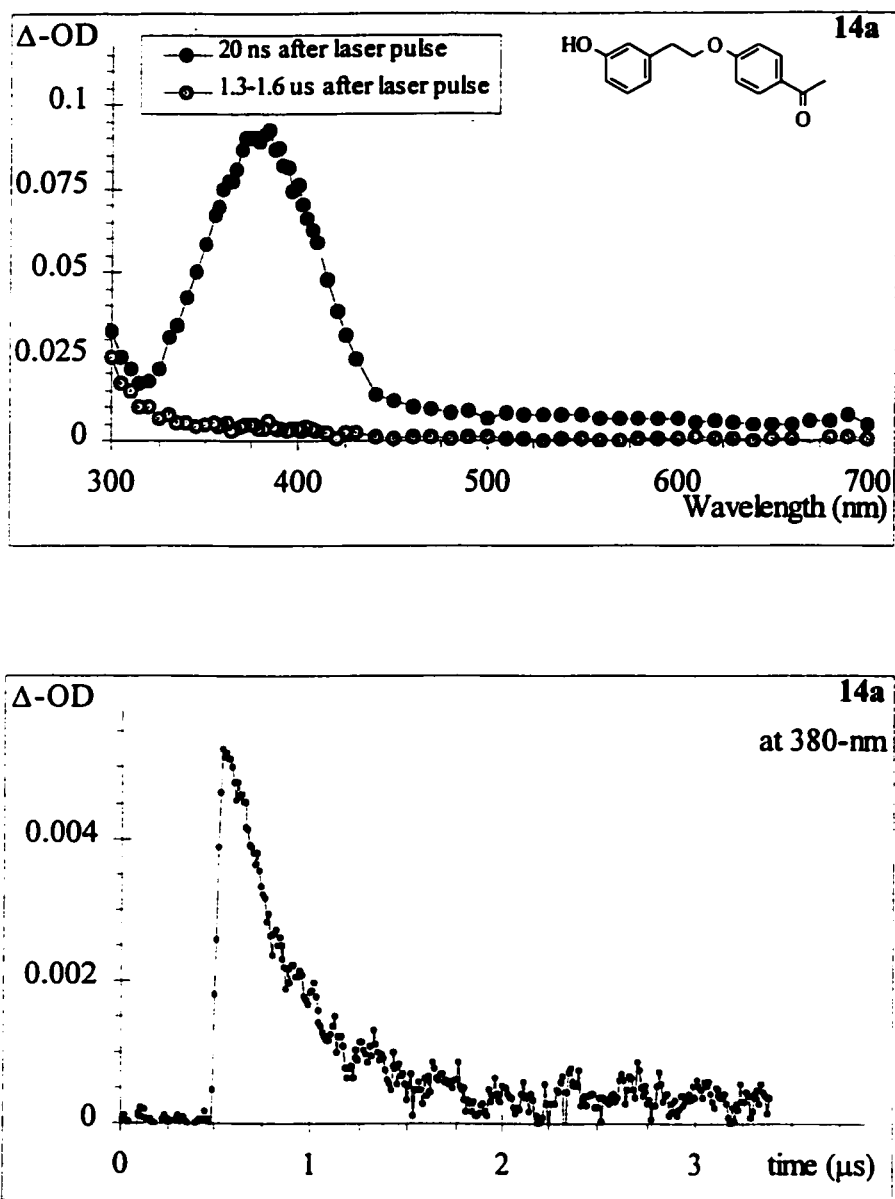


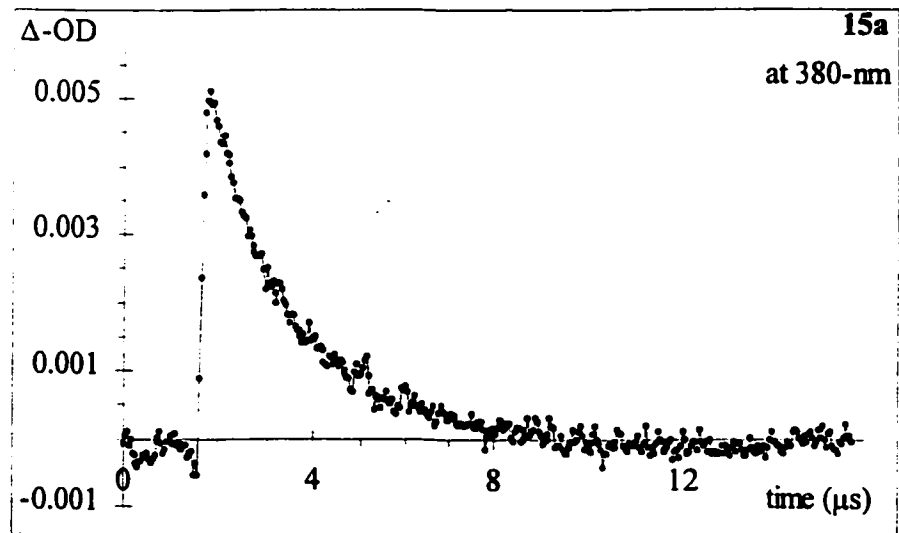
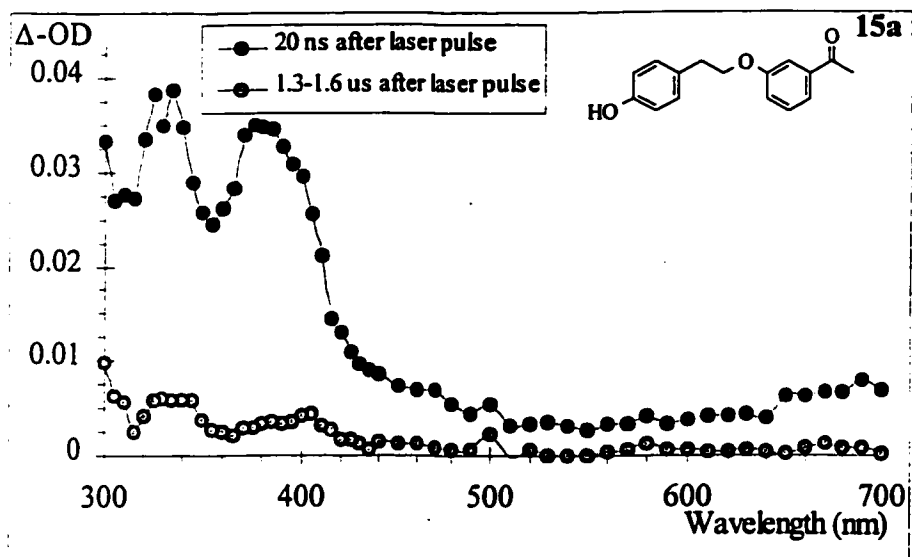
Figure 4.7. Continued.

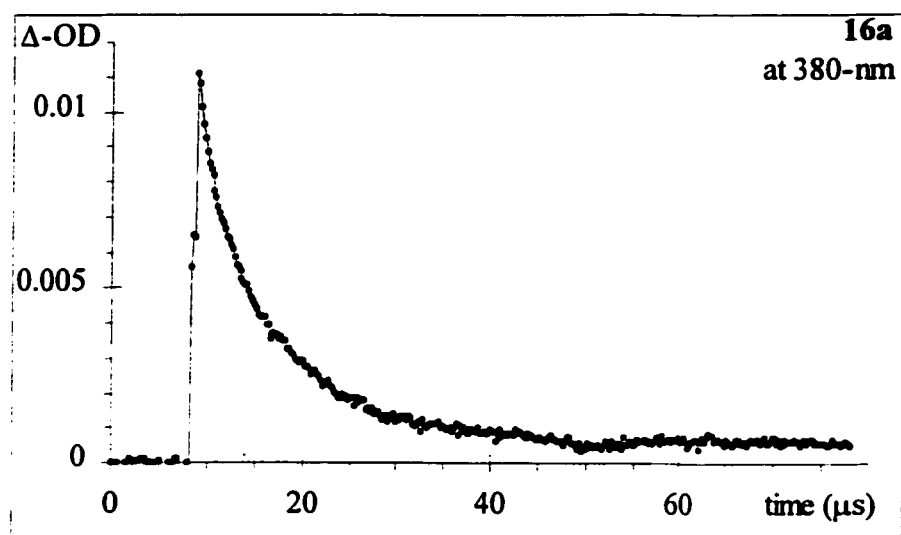
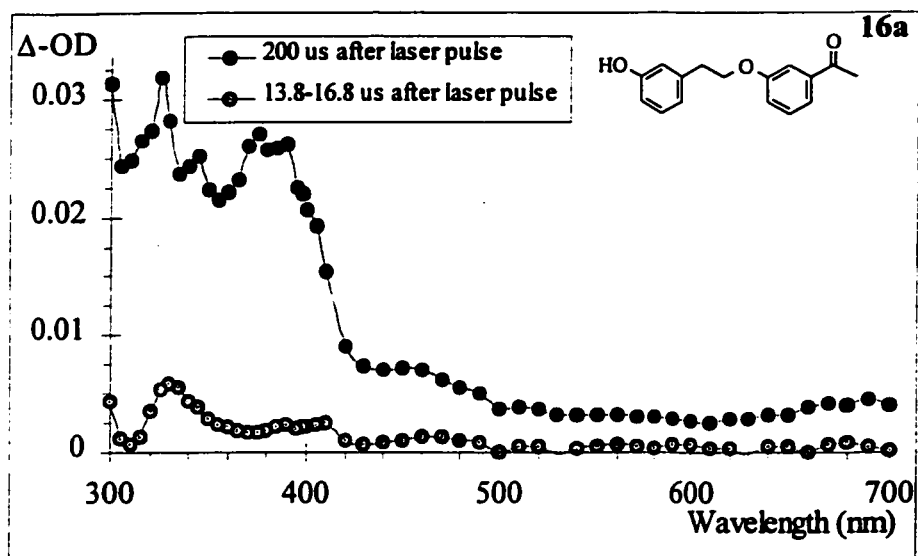
Figure 4.7. Continued.

Figure 4.8. Transient ultraviolet spectra and decays of 10^{-4} M solutions of compounds **14a**, **15a** and **16a** in deoxygenated DCM at 25 °C.

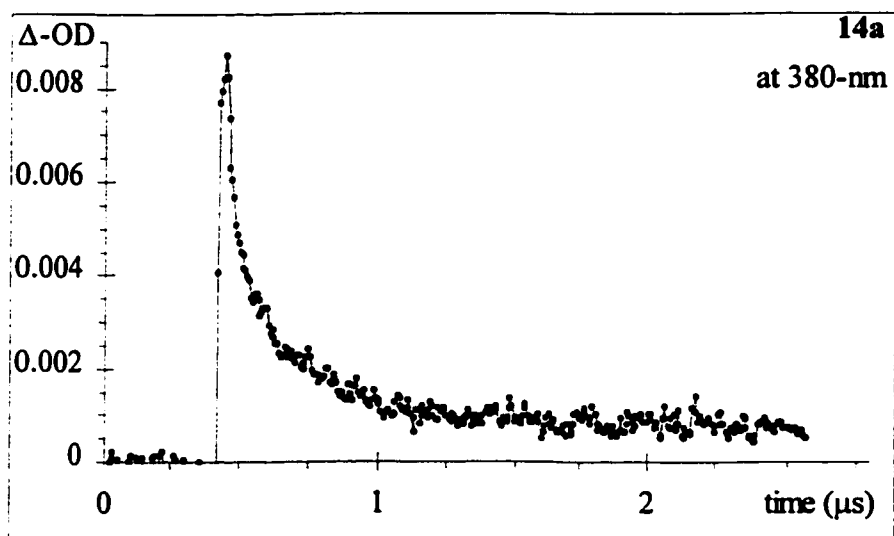
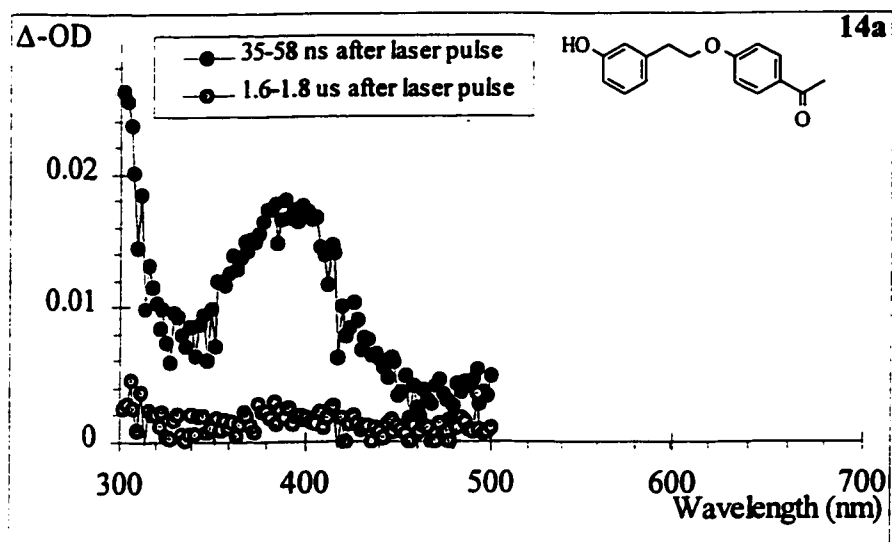


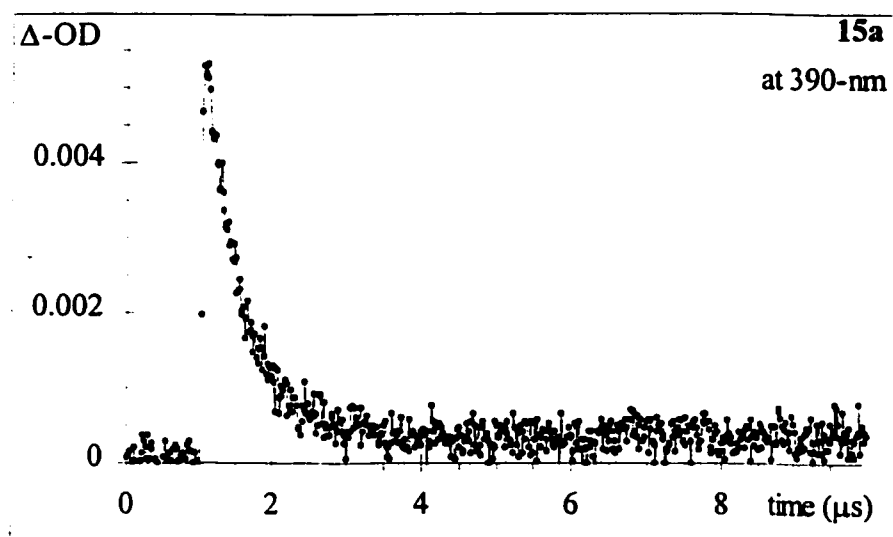
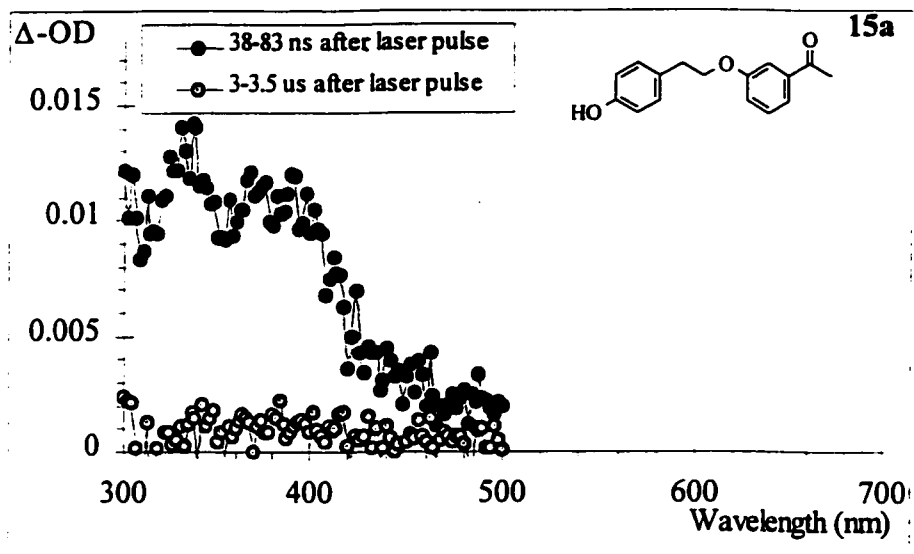
Figure 4.8. Continued.

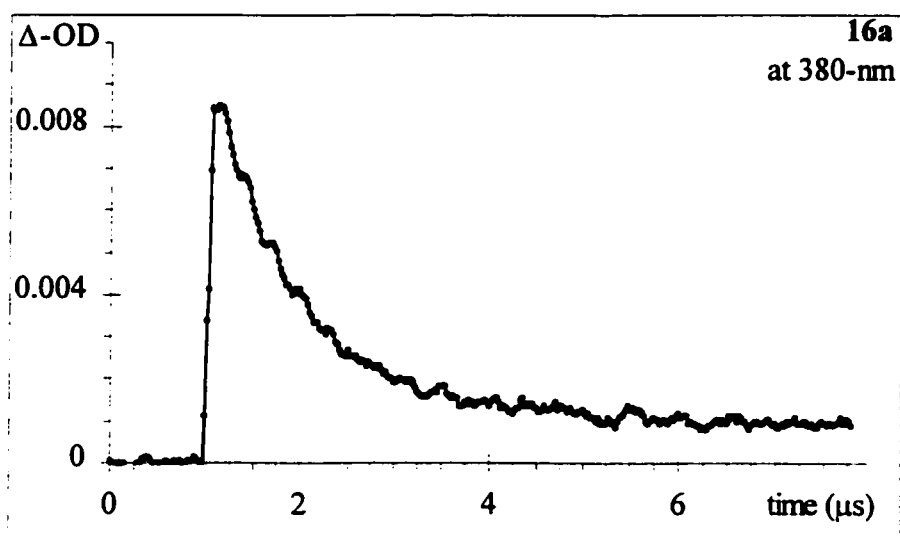
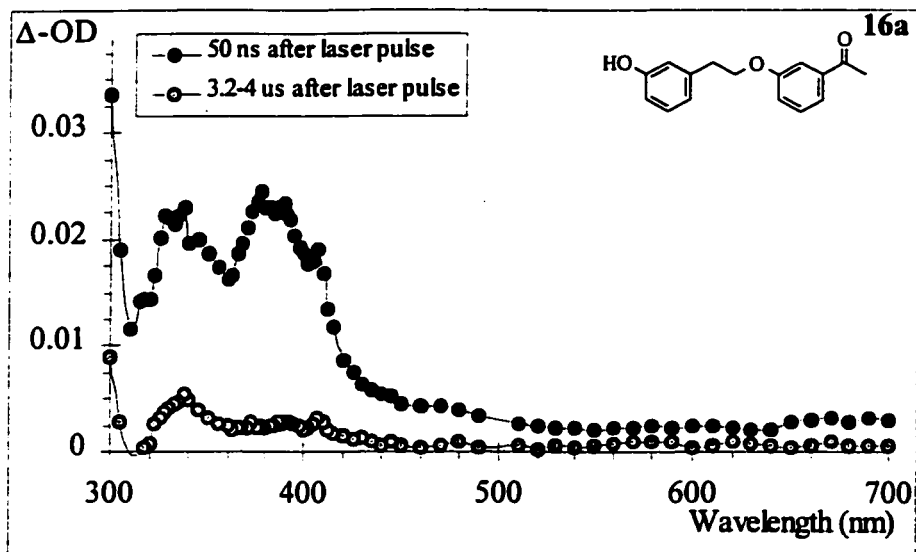
Figure 4.8. Continued.

Table 4.2. Triplet lifetimes of compounds **9a**, **14a**, **15a**, and **16a** in deoxygenated MeCN and DCM, rates of 1,3-cyclohexadiene (CHD) triplet quenching in MeCN, self-quenching rate constants in MeCN, and absolute rate constants of *para*- or *meta*-methoxyacetophenone triplet quenching by *para*- or *meta*-cresol in MeCN. ^a

Ketone	τ_T^b (MeCN, μ s)	τ_T (DCM, μ s)	k_q^c CHD / $10^{10} \text{ M}^{-1} \text{ s}^{-1}$	k_{sq}^d / $10^9 \text{ M}^{-1} \text{ s}^{-1}$	k_q^e bimol. / $10^9 \text{ M}^{-1} \text{ s}^{-1}$
9a	0.0113 ± 0.0019	0.0022 ± 0.0003^g	n.m.	--	1.24 ± 0.03
14a	0.343 ± 0.015^h	0.255 ± 0.18	0.60 ± 0.07	3.8 ± 1.2	0.71 ± 0.02
15a	1.9 ± 0.2^i	0.76 ± 0.03	1.15 ± 0.05^j	3.0 ± 0.3	1.32 ± 0.04
16a	8.5 ± 1.0^i	1.6 ± 0.3^i	0.33 ± 0.04^k	1.17 ± 0.13	1.06 ± 0.05

a. Determined by 248-nm NLFP at room temperature unless noted otherwise,

b. Rigorously dried MeCN ($[\text{H}_2\text{O}] < 10^{-4} \text{ M}$).

c. From 308- or 337-nm NLFP in MeCN; errors are twice the standard deviation of the least squares line from the quenching plot.

d. Slope of dilution plot according to eq. 4.1.

e. Either *meta*- or *para*-cresol quenching triplet *meta*- or *para*-methoxyacetophenone, depending on the LPK. Using the 337-nm laser for excitation.

f. From Table 3.3, p. 141.

g. From Table 3.4, p. 142.

h. Average of many direct determinations, error is the standard deviation.

i. From intercept of infinite-dilution plot according to eq. 4.1.

j. MSP data, average of two quenching determinations.

k. From ref. 86.

l. From CHD Stern-Volmer quenching

A sample self-quenching plot is shown in Figure 4.9 for LPK 16a, while the one for compound 15a is in the Appendix. The self-quenching rate constants are presented in Table 4.2.

$$k_{decay} = k_0 + k_{sq} [K] \quad (4.1)$$

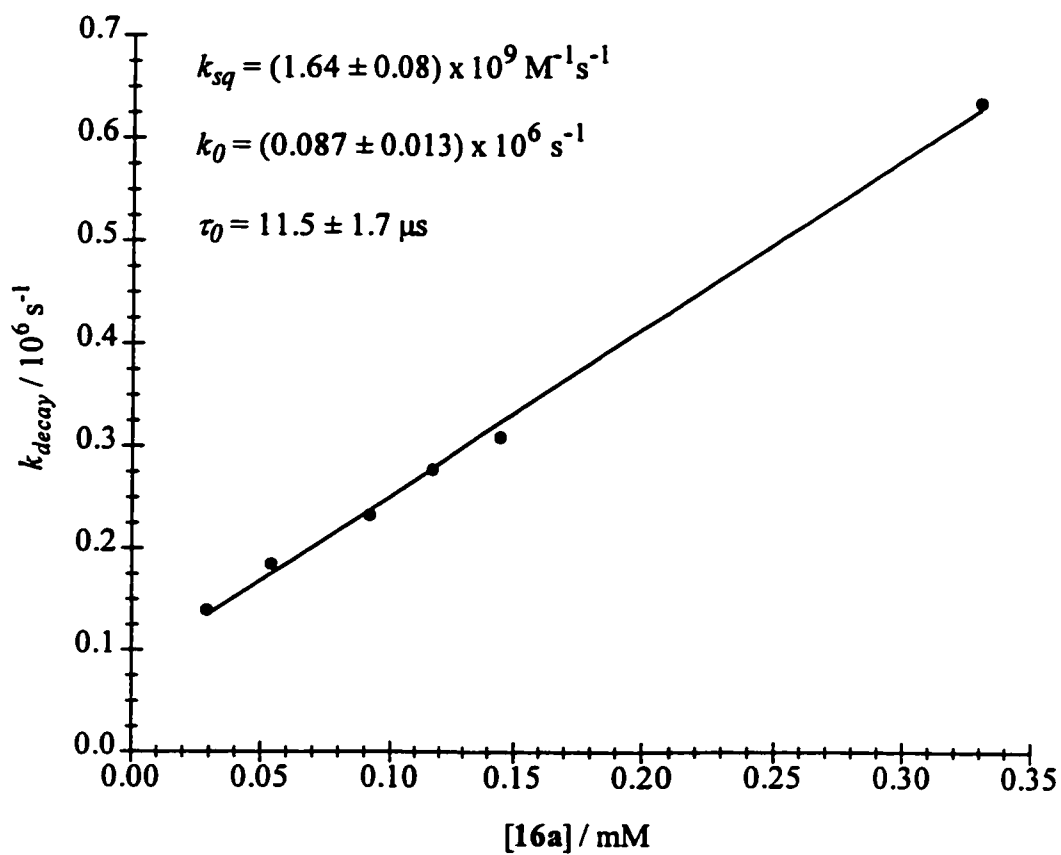
In addition, absolute rate constants for bimolecular quenching of *para*- and *meta*-acetophenone triplets by *meta*-cresol were determined in MeCN. These data are listed in Table 4.2 as well.

Unexpectedly, the concentration of water in the MeCN solvent also had a dramatic effect on the ketone triplet lifetime. This was first noticed when studying the long-lived *meta*, *meta'*-derivative 16a. It was observed that the triplet lifetime of the compound seemed to change in an irregular fashion. Only by rigorously drying the MeCN over calcium hydride and then passing the distillate over activated alumina could the water concentration be brought low enough (estimated at less than 10^{-4} M) that more or less constant triplet lifetimes could be measured. Once this effect had been noticed, analysis of the data indicated that this was a general phenomenon for compounds 14-16.

Intentional addition of water to rigorously dried MeCN solutions led to a reduction in triplet lifetime. However, rate constants for water quenching were not investigated since the triplet lifetimes became constant at water concentrations that varied for each ketone (usually at 1-5% water, but much less for LPK 15a, see below). Although each batch of MeCN was dried in more or less the same manner, there was also no guarantee

Figure 4.9. Plot of k_{decay} versus ketone concentration from 248-nm laser flash

photolysis of deoxygenated, dry ($[\text{H}_2\text{O}] \leq 10^{-4}$ M) MeCN solutions of compound **16a**.



that the same initial water levels were maintained from batch to batch. The short triplet lifetimes of the LPKs discussed in Chapter Three mostly obscured this phenomenon for the para, para'-attached species, but the reduction of triplet lifetimes of LPKs 9a, 11a and 57a observed in 5% aqueous MeCN (Table 3.6, p. 148) is consistent (*vide infra*) with this result.

Table 4.3 lists the triplet lifetimes of the LPKs in the presence of L₂O precisely added to rigorously dried MeCN solutions. The Table also lists the bimolecular quenching rate constants of the model ketones and cresols re-measured in wet MeCN.

This study was undertaken both to learn about the effect of water as well as to measure kinetic isotope effects. It was found that meaningful data for *meta*-acetyl substituted LPK 15a could only be obtained by adding very small amounts of water. Past as little as 0.05% (0.028 M) water, transient decays for compound 15a were no longer of the triplet state, as determined by diene quenching experiments. To allow valid comparisons to be made between each ketone, all KIE experiments for compounds 14a-16a were conducted at 0.028 M L₂O. Self-quenching plots are shown in the Appendix.

Another aspect of the LPK transient decays were the long-lived residual absorptions that leveled off at about 2.5-10% of the original size of the triplet signal. The residuals grew in prominence at higher ketone concentrations where self-quenching became a serious limitation of the triplet lifetime. During triplet quenching experiments with diene, the yield of the residual absorptions was lessened slightly. This behaviour is consistent with an assignment of radical species that are produced by the triplet, such as the hemipinacol and phenoxyl monoradicals formed by bimolecular hydrogen abstraction by

Table 4.3. Triplet lifetimes of compounds **9a**, **14a**, **15a**, and **16a** in deoxygenated 0.028 M L₂O/MeCN solutions, kinetic isotope effects and absolute rate constants of *para*- or *meta*-methoxyacetophenone quenching by *para*- or *meta*-cresol in 5% aqueous MeCN.^{a,b}

Ketone	τ_T	τ_T	KIE ^c	k_q bimol. ^d
	(0.028 M aq. MeCN, μ s)	(0.028 M D ₂ O/MeCN, μ s)		/ 10 ⁹ M ⁻¹ s ⁻¹
9a	0.0100 ± 0.0012 ^e	0.0154 ± 0.0018 ^e	1.54 ± 0.15 ^e	0.75 ± 0.05
14a	0.32 ± 0.03 ^f	0.88 ± 0.03 ^f	2.8 ± 0.3	0.35 ± 0.02
15a	0.88 ± 0.15 ^g	1.34 ± 0.10 ^g	1.5 ± 0.3	0.74 ± 0.05
16a	11.5 ± 1.7 ^g	8.3 ± 1.1 ^g	1.0 ± 0.3	0.49 ± 0.04

a. Determined by 248-nm NLFP at room temperature unless noted otherwise.

b. Errors in lifetimes are twice the standard deviation of the linear least squares line from the logarithmic fit.

c. This is the lifetime in the deuterated solvent divided by the lifetime in normal solvent.

d. Either *meta*- or *para*-cresol quenching triplet *meta*- or *para*-methoxyacetophenone, depending on the LPK. Using the 337-nm laser for excitation.

e. From Table 3.6, p. 148.

f. Average of three fits.

g. From intercept of infinite-dilution plot according to eq. 4.1.

the triplet from ground state ketone.

In dichloromethane solvent, LPK triplet lifetime measurements were much more straightforward owing to the fact that the solubility of water in the less-polar chlorocarbon solvent is much lower than in acetonitrile. As observed in the case of the para, para'-LPKs studied in Chapter Three, LPK triplet lifetimes were shorter in DCM as compared to values in (rigorously dried) MeCN. The triplet lifetime of LPK 16a was determined by a self-quenching plot, which is displayed in the Appendix.

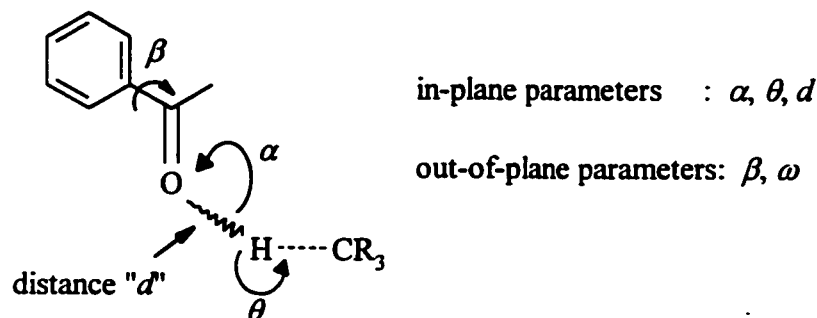
4.2.6. Results. Molecular modeling of compounds 9a and 14a-16a.

Sandwich-like structures of compounds 9a and 14a-16a were modeled by semi-empirical (PM3) geometry optimizations. For all four LPKs, preliminary calculations indicated that the most stable conformer had a geometry all-*trans* with respect to the ethylene bridge.

Bond-length and angle parameters were chosen based upon data reported by Scheffer and co-workers,¹⁵² who have studied C-H abstractions by carbonyl n, π^* triplets in the crystalline state. Scheme 4.1 represents their findings. Note that ω represents the out-of-plane angle (not shown) the n -orbital makes with the H atom. In the calculations, the carbonyl oxygen-phenolic hydrogen bond distance (d) was constrained to 2.65-Å, based on crystallographic data for hydrogen-bonded phenol-quinone pairs.¹⁶⁸ Values for α , ω , and θ were kept free from constraint. Finally, the degree of twist of the carbonyl from co-planarity with its attached phenyl ring was set to 45° (β).

In every case except for LPK 16a, the calculations performed under these conditions

Scheme 4.1. Ground-state parameters for hydrogen atom abstraction reactions in solids.



Ideal parameters: $\alpha = 90\text{-}120^\circ$, $\theta = 120^\circ$, " d " $< 2.7 \text{ \AA}$, $\omega = 0^\circ$

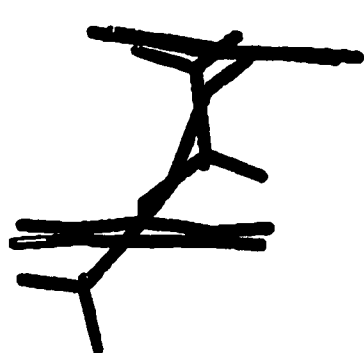
produced sandwich-like structures similar to the crude representation of Scheme 1.8, p.43. These structures are shown in Figure 4.10.

Heats of formation for the constrained geometries were compared to those of the relaxed all-*trans* conformations, and the differences are reported as $\Delta(\Delta H_f)$ in the Figure.

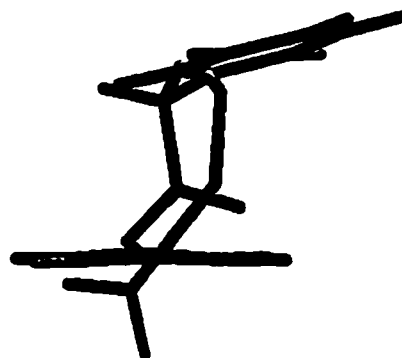
For the meta, meta'-derivative **16a**, two minima were found. One geometry has parallel, non-overlapping rings, and the other has the phenyl rings almost perpendicular.

Forcing LPK **16a** into a geometry similar to the sandwich structure for LPK **9a** was possible, at the cost of a slight rise in the calculated energy. Figure 4.10 shows the structure of such a conformer chosen so as to have a $\Delta(\Delta H_f)$ value similar to those of compounds **9a**, **14a** and **15a**.

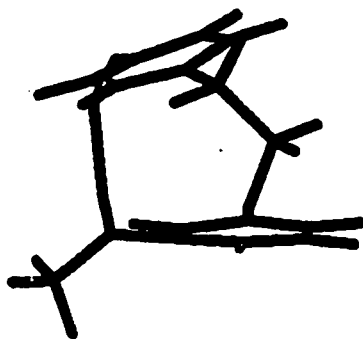
Figure 4.10. Semi-empirical (PM3) calculated geometries for compounds **9a**, and **14a-16a** and the difference in the calculated heats of formation of the indicated conformers from the relaxed all-*trans* geometries.

**9a**

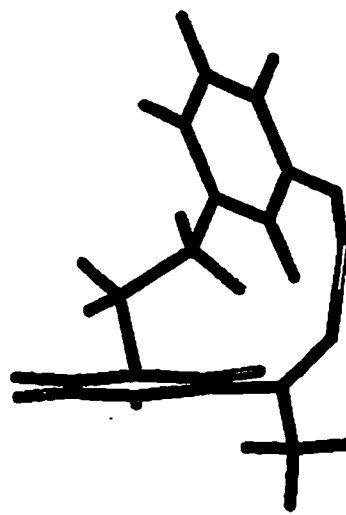
$$\Delta(\Delta H_f) = 6 \text{ kcal/mol}$$

**14a**

$$\Delta(\Delta H_f) = 5 \text{ kcal/mol}$$

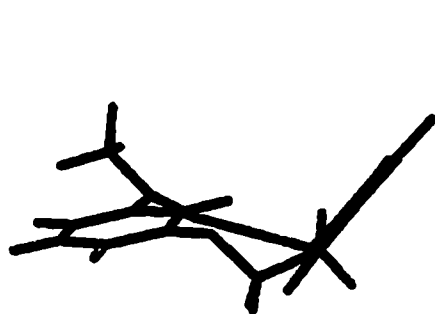
**15a**

$$\Delta(\Delta H_f) = 6 \text{ kcal/mol}$$

**16a**

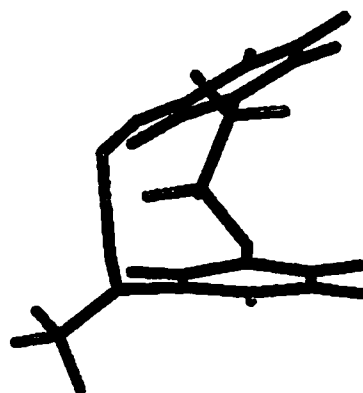
$$\Delta(\Delta H_f) = 0.9 \text{ kcal/mol}$$

Figure 4.10. Continued.



16a

$$\Delta(\Delta H_f) = 1.0 \text{ kcal/mol}$$



16a

$$\Delta(\Delta H_f) = 8 \text{ kcal/mol}$$

4.2.7. Discussion. LPK triplet lifetimes and the "meta-acyl" effect.

The data in Table 4.3 indicate that there is a dramatic geometrical effect on the triplet lifetimes for compounds **9a** and **14a-16a**. In MeCN solution, the values vary by almost three orders of magnitude, with compound **16a** displaying the longest triplet lifetime of the series. This trend is similar to what MSP originally reported (*c.f.* Table 1.6 p. 47), however the magnitude is much larger than first reported. The differences between the two sets of data are ascribed to the fact that MSP worked under conditions of greater concentrations and/or less rigorous deoxygenation, and never with dried MeCN.

Comparison of the triplet lifetimes of the phenolic species to those of the corresponding *O*-methyl ethers, as well as the presence of deuterium isotope effects on the triplet lifetimes in 0.028 M aqueous acetonitrile, indicates that intramolecular phenolic hydrogen abstraction is occurring for LPKs **14a** and **15a**, *but not 16a*.

The latter compound is different from the others in that its infinite dilution triplet lifetime does not display a KIE; moreover, its triplet lifetime is not significantly different from that of ketone **16b**. This suggests that, for some reason, the normally very fast intramolecular phenolic HAA abstraction has been turned "off" in this molecule. This is at first a bizarre observation in light of the fact that the bimolecular reactivity between *meta*-cresol and *meta*-methoxyacetophenone triplets is only 85% of that of the para isomers.

Reserving discussion for the moment, of the three LPKs that appear to undergo intramolecular reaction, it seems clear that compound **9a** is able to form a suitable exciplex geometry for fast intramolecular phenolic HAA. The fact that LPK **9a** displays

the greatest reactivity allows its structure to be used as a base against which to compare the others, and an example of the kind of geometry that leads to facile hydrogen-bonding and rapid electron-/proton-transfer to yield the corresponding biradical product if the mechanism is correct.

For the isomeric LPKs **14a** and **15a**, the trend in lifetimes seems to indicate that slight differences in geometrical arrangement can account for a lowering of reactivity by a factor of about 170 or so. However, the $\Delta(\Delta H_f)$ values from Figure 4.10 indicate that ketones **14a** and **15a** are hardly restricted from adopting an exciplex structure analogous to that of compound **9a**. For example, the slight skewing of the phenyl rings in compound **15a** does represent a slight difference from the geometry of LPK **9a**, but that it is significant enough a structural difference to cause a 170-fold difference in triplet lifetime would at first glance have seemed unlikely. One immediate conclusion from this analysis is that HAA in the LPKs seems extraordinarily sensitive to very small changes in geometry.

As mentioned in the introduction to this chapter, this is good evidence for the fact that the reaction mechanism is proceeding by something other than just a simple H-atom abstraction. If the cause of the trend in triplet lifetime of compounds **9a**, **14a** and **15a** is due to a mechanical factor affecting the ability of the molecules to reach a conformation that allows facile H-atom transfer, this points towards something of strictly defined geometry such as a hydrogen-bond.

Further evidence along these lines comes from the observation that if the hydrogen-bond distance is shortened in the calculations, the $\Delta(\Delta H_f)$ values rise across the series in a

manner similar to the increasing trend in triplet lifetimes. Thus, if the hydrogen-bond were tighter, the two rings would approach each other more closely and the geometrical effect would be more pronounced.

The lack of intramolecular reactivity of compound **16a** indicates that it stands apart in this analysis. First, while HAA can occur from (at least) two hydrogen-bonding geometries considerably lower in energy than those of the other three compounds; neither possess any overlap between the aryl rings. This overlap is presumably important for intramolecular electron-transfer compared to other competing mechanisms of triplet decay.¹⁶⁹⁻¹⁷³

Attempting to force LPK **16a** into a sandwich-like geometry causes an increase in energy; however it is not a prohibitive one. Based on our calculations, it is impossible to understand the lack of reactivity displayed by compound **16a** since it appears that it should be able to attain the requisite geometry required, albeit perhaps in a rapid equilibrium with other, non-sandwich forms.

An origin for this isomeric effect does not stem from any anomalous nature of the *meta*-cresol and *meta*-methoxyacetophenone chromophores on their own, as mentioned above. The bimolecular reactivity of substituted acetophenones towards *meta*-cresol is found to be slightly attenuated from that of *para*-cresol, but this is simply because *meta*-cresol is a slightly poorer quencher than *para*-cresol based on its slightly less electron-rich nature.

Further insight into the behaviour of compound **16a** was gained by looking at the global mechanism. If the geometrical arrangement was possibly not responsible for the

total lack of intramolecular reactivity, then another option was that something to do with the exciplex formation and/or electron-/proton transfer aspects of the overall H-atom transfer had been altered by the isomerism. In other words, perhaps the meta, meta'-orientation was causing an interesting and unexpected electronic effect.

4.2.8. Discussion. Symmetry restricted electron transfer.

It has been known for a long time in the field of electron-transfer reactions that rapid charge transfer from donor to acceptor molecules or internal parts of molecules requires good spatial overlap of the associated donor and acceptor orbitals.¹⁶⁹⁻¹⁷³

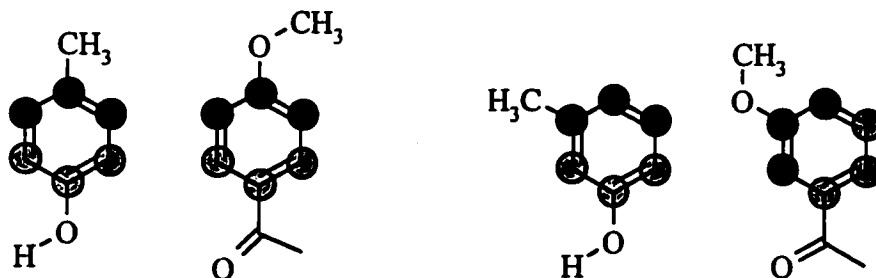
In the bimolecular phenolic HAA reaction, the orbitals of interest are the frontier molecular orbitals of the phenol (donor) and ketone (acceptor). More specifically, these can be identified as the HOMO of the phenol and the lower singly occupied molecular orbital (SOMO) of the ketone π, π^* triplet (which corresponds to the HOMO of the ground state ketone). Both of these molecular orbitals have large contributions from the benzenoid π_A molecular orbitals.

To a first approximation, potential orbital overlap in the sandwich conformations of the LPKs can be assessed by simple superposition of the orbitals of model compounds representing the aroyl and cresolic rings. This assumption is only as good as the assumption that the oxyethyl spacer does not perturb the MOs significantly from the simple model species. This question was not directly addressed.

The molecular orbitals of the appropriate MOs of *meta*- and *para*-methoxyacetophenone and *meta*- and *para*-cresol were calculated, both at the simple

Hückel level and at semi-empirical (AM1 and PM3) levels. The results at higher levels of theory are not significantly different from each other or from the results of the Hückel calculations, which are represented pictorially in Scheme 4.2.

Scheme 4.2. Results of Hückel calculation on *para*- and *meta*-substituted methoxyacetophenone and cresol molecules. Nodal properties are indicated by arbitrary shading.



The result of this simple analysis indicates that overlap of *para*-cresol with *para*-methoxyacetophenone in the same sense as in compound **9a**, *i.e.*, with both substituents in the *para*-position of the ring, results in excellent orbital overlap for all ring carbons. On the other hand, stacking *meta*-cresol above *meta*-methoxyacetophenone to form a geometry identical to LPK **16a** yields a poorer orbital overlap situation. A similar analysis for compounds **14a** and **15a** indicates that overlap is better in the former than the latter, which is consistent with the fact that ketone **15a** is the less reactive of the two. In fact, a closer look clearly indicates that the element responsible for any such MO effect is the difference between the *para*- and *meta*-acyl MOs, since the *para*- and *meta*-cresol

MOs are identical in composition.

This leads to the prediction that this "*meta*-acyl" effect could be general. Indeed, Hückel calculations on 3-methoxybenzophenone and 6-methoxy-1-indanone gave very similar results to *meta*-methoxyacetophenone.

To briefly combine ideas, the MO study suggests that fast intramolecular electron transfer between the two rings in the LPKs should occur for compounds **9a** and **14a**. Poorer overlap for compounds **15a** and **16a** results in a retardation of the reaction. This aspect, coupled with the geometrical factors detailed previously, can perhaps now explain the trend in triplet lifetimes in the entire LPK series. Compound **14a** has a slightly worse sandwich-geometry than ketone **9a** and the *meta*-cresol ring is a slightly worse quencher based on comparison of the absolute rate constants in the bimolecular case. Thus, the excited state of LPK **14a** has a slightly longer lifetime than that of compound **9a**.

In contrast, compounds **15a** and **16a** have an electronic barrier to reaction as well as a steric barrier. Compound **16a** in addition may sample a sandwich structure less readily than ketone **15a**, and this may be enough to prevent any intramolecular reaction.

The idea that geometrical factors are important as well as symmetry restricted electron transfer comes from the extensive literature on symmetry effects in photoinduced charge- or electron-transfer processes. Studies on cyclophane derivatives¹⁷⁴⁻¹⁷⁷, donor-linker-acceptor molecules,¹⁷⁸⁻¹⁸¹ and bimolecular systems¹⁸²⁻¹⁸⁴ provide good examples of the field. Many workers have shown that if the symmetries of the acceptor and donor orbitals are not the same, a retardation in electron-transfer reactions can occur. However, this retardation has never been observed to be larger than

one order of magnitude or so. The huge effect between compounds **9a** and **16a** would represent one of the largest examples yet observed. This makes an assignment of the differences between ketones **9a** and **16a** solely to electronic effects uncertain.

4.2.9 Discussion. Triplet lifetimes of the methoxy ketones in dry solvent.

Triplet lifetimes of the *O*-methyl ethers are much longer than those of their phenolic counterparts, with the exception of compounds **16a** and **16b**, which are the same within experimental error. These observations have been discussed in the context of the LPK triplet lifetimes, above.

The excited state lifetimes of ethers **14b-16b** are each longer than that of ketone **9b**, whose relatively short triplet lifetime compared to *para*-methoxyacetophenone was previously ascribed to some non-productive intramolecular mechanism based on the proximity of the two aromatic rings (see Chapter Three). Since such a process ostensibly involves charge-transfer behaviour, it should follow similar restrictions as full electron transfer^{174,177} and encounter the "*meta*-acyl" effect, albeit with a reduced importance due to the lack of hydrogen-bonding and the resulting much greater freedom of motion. This is tentatively used to explain why LPKs **15a** and **16a** are longer-lived than ether **9b**, but cannot satisfactorily explain why compound **14b** is longer-lived than compound **9b**. This latter observation may be due to the less electron rich nature of the *meta*-anisolic ring *versus* its *para*- counterpart.

4.2.10. Discussion. The effect of water.

Comparing the triplet lifetimes in Tables 4.2 and 4.3 indicates that the phenolic compounds undergoing intramolecular phenolic HAA in MeCN are extremely sensitive to the presence of water. As mentioned in the results section this was an unexpected observation, and it caused initial confusion in the determinations of the LPK triplet lifetimes.

The reason why this effect was unexpected is that it is generally accepted that ketone triplet reactivity is insensitive to the presence of water. Thermochemical cycles such as the one calculated in Chapter One (Figure 1.5, Table 1.3, p. 19, p. 20) indicate that under normal conditions ketone triplets do not abstract from the H-OH bond due to its prohibitively high energy.

The photochemistry of benzophenone in deoxygenated aqueous solution has been reported. The quantum yield of disappearance was determined to be 0.05 ± 0.02 by Ledger and Porter.¹⁸⁵ They also found that steady-state photolysis led to the formation of benzopinacol, good evidence for HAA since this is the normal photoproduct of benzophenone photoreduction (Figure 1.4, R = Ph).

Using conventional flash photolysis, they studied benzophenone and acetophenone transient behaviour. In the absence of oxygen, they determined that benzophenone had a triplet lifetime of 200 μs under these conditions, and they observed the benzophenone ketyl radical as the triplet decayed. Ultimately, a mechanism involving HAA from water was tentatively proposed with a calculated bimolecular rate constant of $5 \text{ M}^{-1}\text{s}^{-1}$, despite an admittedly unfavourable thermodynamic analysis.

Very recently, Canonica and co-workers reported a study of the quenching of three

aromatic ketones by a variety of phenols in buffered aqueous solution.¹⁸⁶ For benzophenone, absolute rate constants for bimolecular quenching were almost diffusion controlled for a wide range of phenols ($2.6\text{--}5.6 \times 10^9 \text{ M}^{-1} \text{ s}^{-1}$); the value for *para*-cresol is $4.2 \times 10^9 \text{ M}^{-1} \text{ s}^{-1}$ to compare to $0.3 \times 10^9 \text{ M}^{-1} \text{ s}^{-1}$ in MeCN (Table 2.7). Similarly, rate constants for quenching of *meta*-methoxyacetophenone and 2-acetonaphthone were all quite high. The authors concluded that the mechanism of interaction between the ketone triplets and phenols in water was full electron transfer, based upon estimated ΔG_{et} values and fits to Marcus and Rehm-Weller electron transfer expressions. Recall in Chapter Two that exactly such a process was ruled out in organic solvent, however the reduced reduction potentials of the triplets in water as well as the increased ease of oxidation of phenols is responsible for a mechanistic shift. The authors dismissed a mechanism where hydrogen bonding between ketone and phenol was occurring in pure water because the hydroxylic solvent, present in large excess, should completely solvate both reacting centers.

Thus, there is a clear hydroxylic solvent effect on the mechanism of phenolic HAA. As one moves from non-polar to polar organic media and then finally to protic media, the mechanisms of abstraction shift from one where hydrogen-bonding between the ketone and phenol is important to one where it becomes less important and finally irrelevant due to electron transfer.

Returning to the LPKs, the most obvious effect is that they have their triplet lifetimes reduced in aqueous MeCN solutions, and some, such as LPK 15a, are exquisitely sensitive.

However, small amounts of water have a *retarding influence* on the bimolecular reactivity of the simple methoxyacetophenone and cresol model compounds, as a comparison of the bimolecular data in Tables 4.3 and 4.4 indicates. This an expected result based upon the interference of the solvent in hydrogen-bonding between the reacting centers. Clearly, the presence of 5% water is not enough for full-electron transfer to occur.

The question that must be answered then is why the bimolecular reactivity decreases in solvents containing up to 5% water while intramolecular reactivity increases with even the slightest addition of water.

This question can be answered in two parts. First, the general solvent effect must be estimated in circumstances where hydrogen-bonding is not occurring. Secondly, water's ability to specifically change the intramolecular reaction must be evaluated.

The general solvent effect of water in the absence of hydrogen-bonding can be estimated from the behaviour of the *O*-methyl ether model compounds. As Table 4.1 indicates, these molecules also exhibit a reduction in triplet lifetime upon the addition of water, and the percent reductions more or less mimic the LPK behaviour in wet MeCN. This is an expected result based on an electron transfer mechanism becoming more important, since these triplets are deactivated by intramolecular charge-transfer.

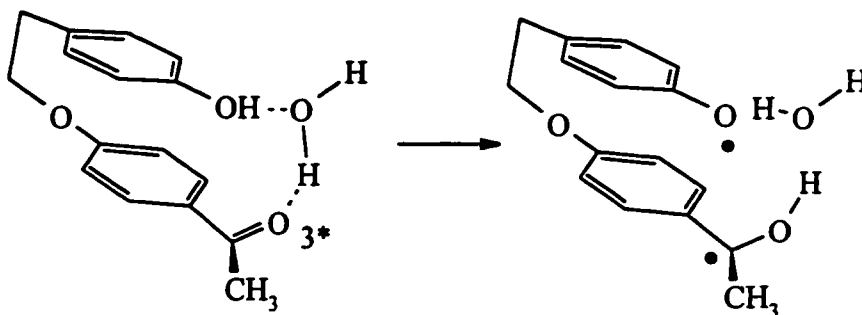
Now, several possible water-mediated mechanisms can be envisioned for an increase in intramolecular reactivity. The first is aggregation of the phenolic substrate, caused by the fact that the LPKs, while polar, are still organic compounds and not water-soluble. Aggregation would increase the effective concentration of the ketone substrate

and lower the observed LPK triplet lifetime due to an increased contribution of self-quenching to the decay.

This mechanism can be ruled out because the dilution plots of LPKs **14a** and **15a** in aqueous MeCN are linear.

A possible solvent-specific mechanism to explain a greater intramolecular reactivity for LPKs is water bridging. In this mechanism, water-phenol hydrogen bonds form that do not interfere with the HAA reaction, allowing the reaction to occur through them instead. This is illustrated in Scheme 4.3.

Scheme 4.3. A representation of "water-assisted" quenching.



Such a process would enhance triplet decay by loosening the geometrical requirement for abstraction, allowing it to occur from a greater number of hydrogen-bonded conformations.

4.2.11. Conclusions on the acetophenone study.

The results discussed in this part of the chapter allow the following general conclusions to be made:

- 1) Intramolecular phenolic hydrogen atom abstraction has been observed in an isomeric series based on the acetophenone chromophore.
- 2) There is a dramatic geometric effect caused by *para*/*meta* isomerism; this is taken as good evidence for the requirement of a strict geometry for rapid hydrogen-atom transfer and good indirect evidence for the requirement of a hydrogen-bond. The reactivity of the *meta*-acyl isomers is much less than that of their *para*-acyl counterparts. The *meta*, *meta'*-derivative **16a** exhibits no intramolecular reactivity.
- 3) Theoretical calculations show that all molecules have a reasonable ability to adopt a sandwich-like geometry similar to the one for the *para*, *para'*-derivative **9a**. Evidence for an electronic barrier to HAA exists for the *meta*-acyl isomers based on orbital overlap considerations.
- 4) Solvent effects are again consistent with a hydrogen-bonding process. The effect of water has been determined to be three-fold. First, the increased polarity of water/acetonitrile mixtures increases the gross charge-transfer reactivity of the molecules based on the methoxy model compounds. Water competes with ketone-phenol hydrogen-bonding and is expected to lower the overall reactivity as long as hydrogen-bonding is still important. Finally, water increases the reactivity of the LPKs, most likely by providing a means to overcome the stringent geometrical requirements of the intramolecular reaction.

4.3. Positional Isomerism in the Benzophenone and Indanone Chromophores

The final section of this thesis deals with the study of meta, meta'-isomerism in the benzophenone and indanone LPK series, and compares the results to the previous work on the acetophenones. These results will help determine whether symmetry-restricted electron transfer can retard the reactivity of systems that either do not possess a lowest π , π^* lowest triplet state or have much charge-transfer character in the lowest π , π^* state.

4.3.1. Results. NLFP of compounds 58a and 58b.

Benzophenone derivatives **58a** and **58b** were studied by 248-nm and 337-nm NLFP on rigorously deoxygenated MeCN or DCM solutions in 3- or 7-mm pathlength cells.

The absorption spectra and transients are shown in Figures 4.11 and 4.12, and the triplet lifetime data are displayed in Table 4.4.

Compound **58b** yielded a surprisingly featureless spectrum not typical of a benzophenone transient absorption spectrum (see Figure 2.2, p.56). A long-lived transient which decayed cleanly to baseline was seen with a maximum at 320-nm.

Oxygen and diene quenching indicated that this was the triplet; the values for the diene quenching are also in Table 4.4.

The LPK **58a** in MeCN, under similar conditions, yielded a similar transient absorption spectrum to ether **58b**, but gave a shorter-lived transient decay that analysed to a single exponential. This is different from the para, para'-benzophenone **11a**, which displayed two components: a short-lived triplet and a long-lived biradical species. Interestingly, diene quenching showed that the signal from 300-nm to just under 600-nm

Figure 4.11. Transient ultraviolet spectra and decays of 10^{-4} M solutions of compounds **58a** and **58b** in deoxygenated MeCN at 23 to 25 °C.

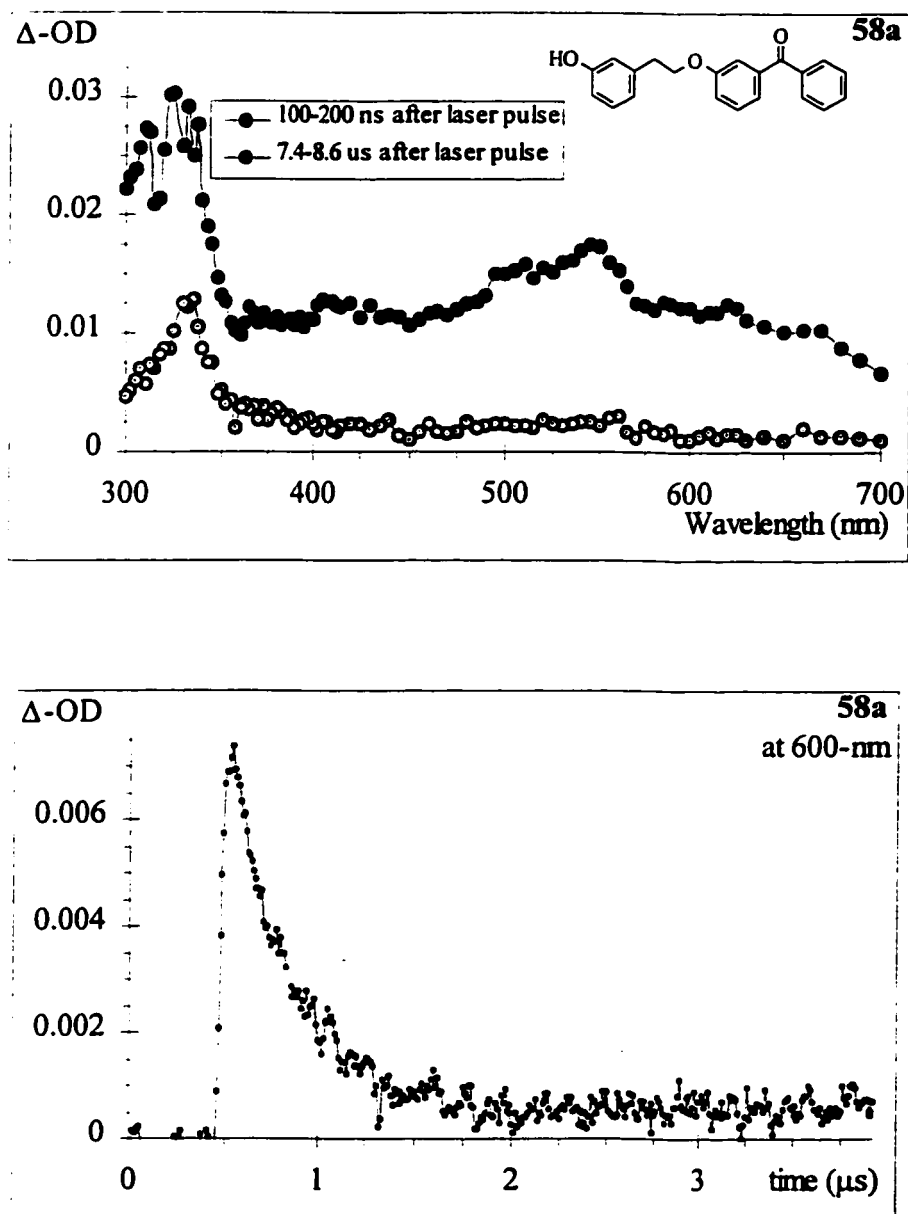


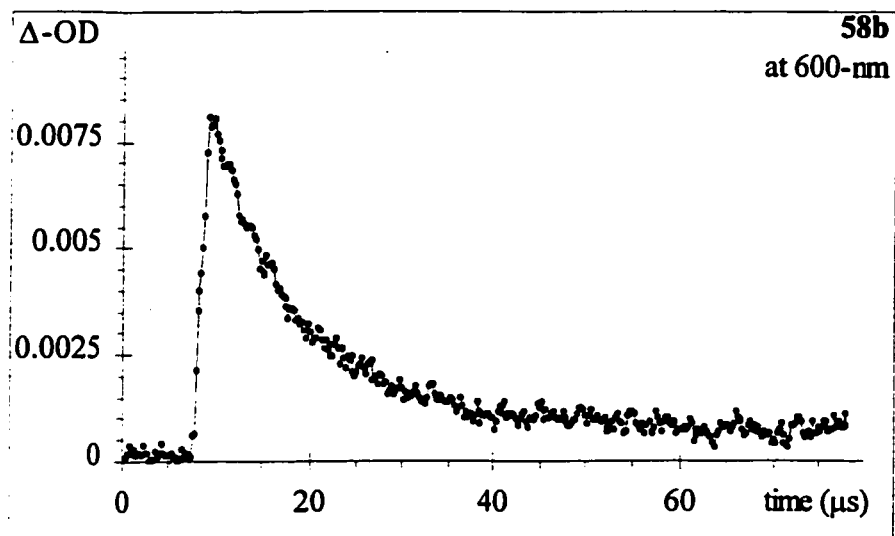
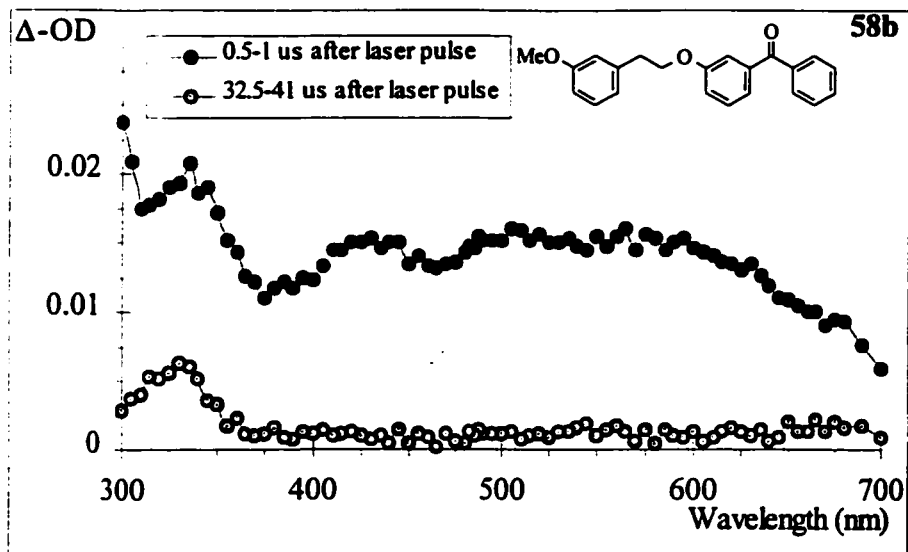
Figure 4.11. Continued.

Figure 4.12. Transient ultraviolet spectra and decays of 10^{-4} M solutions of compounds **58a** and **58b** in deoxygenated DCM at 23 to 25° C.

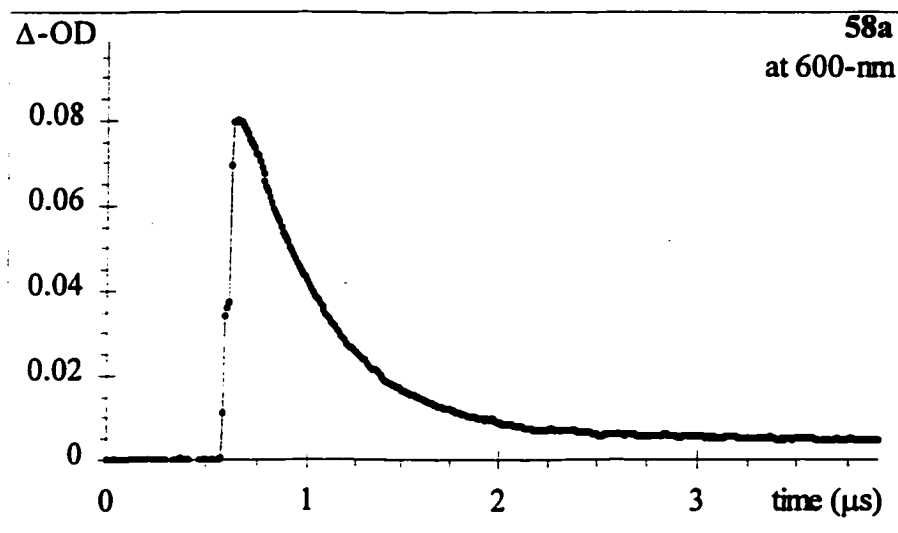
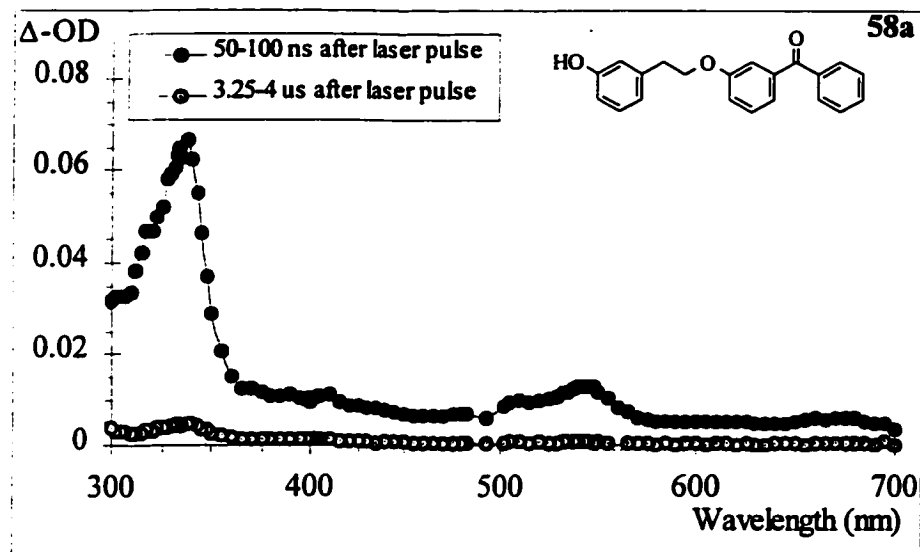


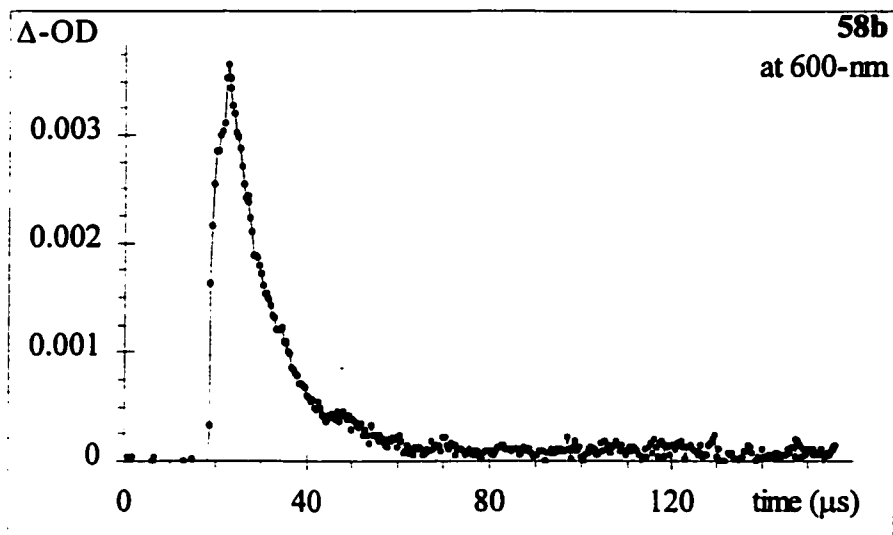
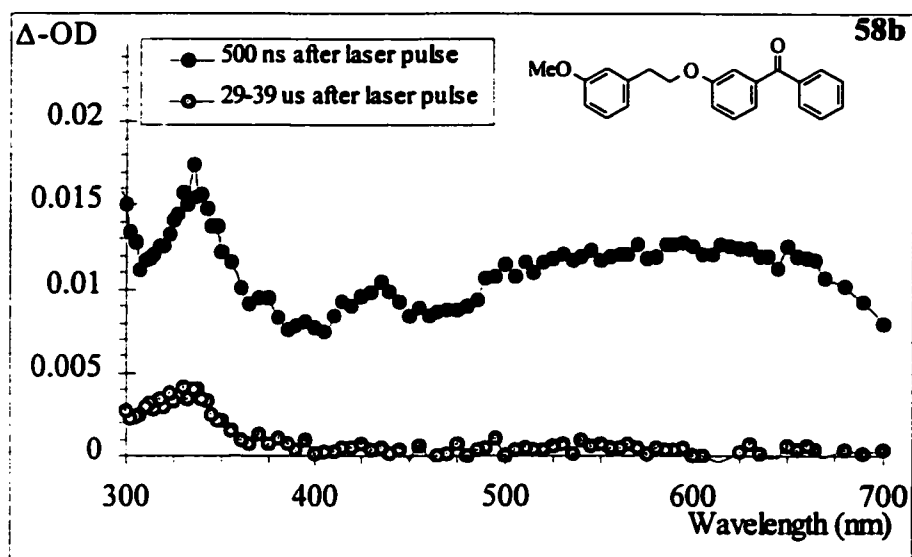
Figure 4.12. Continued.

Table 4.4. Triplet lifetimes of compounds **58a** and **58b** in MeCN and DCM, and rate constants for triplet quenching by 1,3-cyclohexadiene (CHD) in MeCN at 23 to 25 °C. ^{a,b}

Ketone	τ_T (MeCN ^c , μ s)	τ_T (DCM, μ s)	k_q (CHD) / $10^9 \text{ M}^{-1} \text{ s}^{-1}$
58a	0.362 ± 0.017	0.100 ± 0.003	7.5 ± 1.2
58b	9.8 ± 0.3	10.5 ± 0.4	7.4 ± 0.3

a. Lifetimes were directly determined from 248-nm NLFP. Diene quenching experiments were conducted at 337-nm.

b. Errors in lifetimes are twice the standard deviation from the logarithmic fit. Errors in rate constants are twice the standard deviation from the quenching plot.

c. Rigorously dried MeCN ($[\text{H}_2\text{O}] < 10^{-4} \text{ M}$).

was not a triplet species. From 600- to 700-nm (the limit of detection), however, rapid quenching by diene was observed. In DCM, similar results were obtained, except that the triplet had become shorter-lived.

From the analysis of the triplet lifetimes of compound **58a** in $L_2O/MeCN$ mixtures, a kinetic isotope effect was measured for this compound, starting from rigorously dried solvent and adding precise amounts of water or D_2O . These data are collected in Table 4.5, and the dilution plots are in the Appendix.

4.3.2. Results. NLFP of compounds **59a** and **59b**.

The final compounds studied were the indanone derivatives **59a** and **59b**. Transient absorption spectra and decays in both solvents from 248-nm NLFP are shown in Figures 4.13 and 4.14, and the triplet lifetimes are collected in Table 4.6. Diene and oxygen quenching was again used to characterise the triplet states; diene quenching data are in Table 4.6.

The transient absorption spectrum of ether **59b** is similar to that of the para, para'-derivative **57b**, however it is observed that the triplet state of compound **59b** had an appreciably longer lifetime than that of isomer **57b**. For the phenolic compound **59a**, the triplet could not be directly detected in dried MeCN and the 1,3-cyclohexadiene probe technique (Figure 3.6b, p. 138; plot in Appendix) was required for the determination of its triplet lifetime.

Finally, the kinetic isotope effect for **59a** was again measured from triplet lifetimes in $L_2O/MeCN$ mixtures, starting from the rigorously dried solvent and adding precise

Table 4.5. Triplet lifetimes of compounds **58a** and **59a** in 0.05% L₂O/MeCN and kinetic isotope effects.

Ketone	τ_T (0.05% aq. MeCN ^a , μ s)	τ_T (0.05% D ₂ O/MeCN ^a , μ s)	KIE
58a	0.315 ± 0.008 ^b	0.39 ± 0.04 ^b	1.24 ± 0.13
59a	0.030 ± 0.005 ^c	0.048 ± 0.006 ^c	1.6 ± 0.3

a. Rigorously dried MeCN.

b. From the intercept of dilution plots from 248-nm NLFP.

c. From 1,3-cyclohexadiene Stern-Volmer quenching at 337-nm using $1.05 \times 10^{10} \text{ M}^{-1} \text{ s}^{-1}$ as k_q .

Figure 4.13. Transient ultraviolet spectra and decays of 10^{-4} M solutions of compounds **59a** and **59b** in deoxygenated MeCN at 23 to 25 °C.

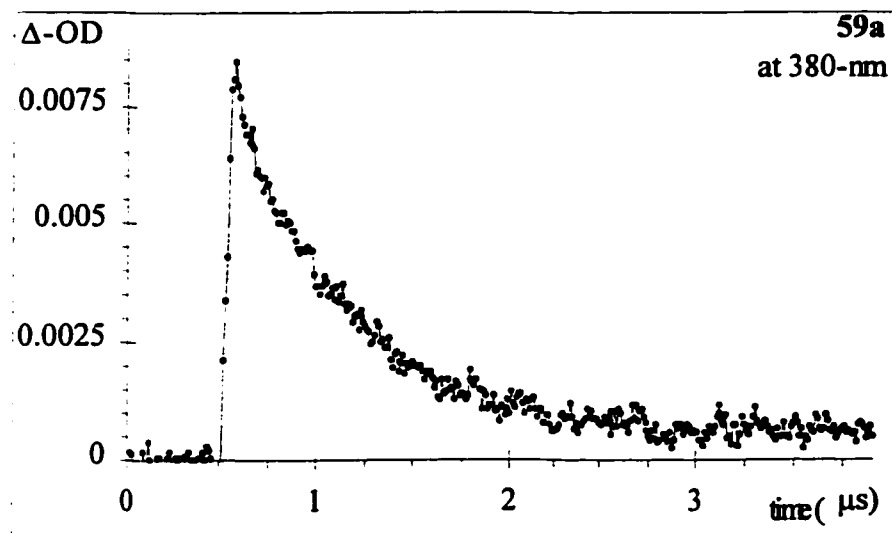
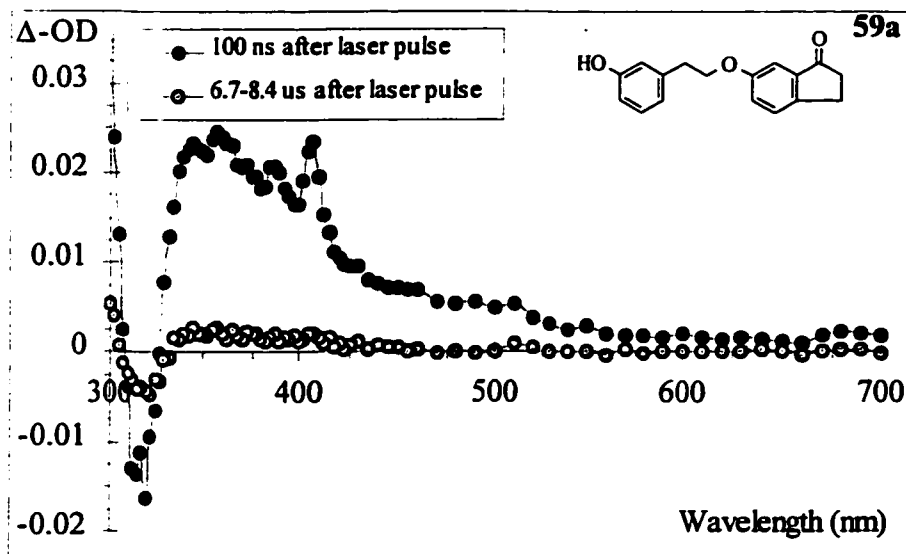


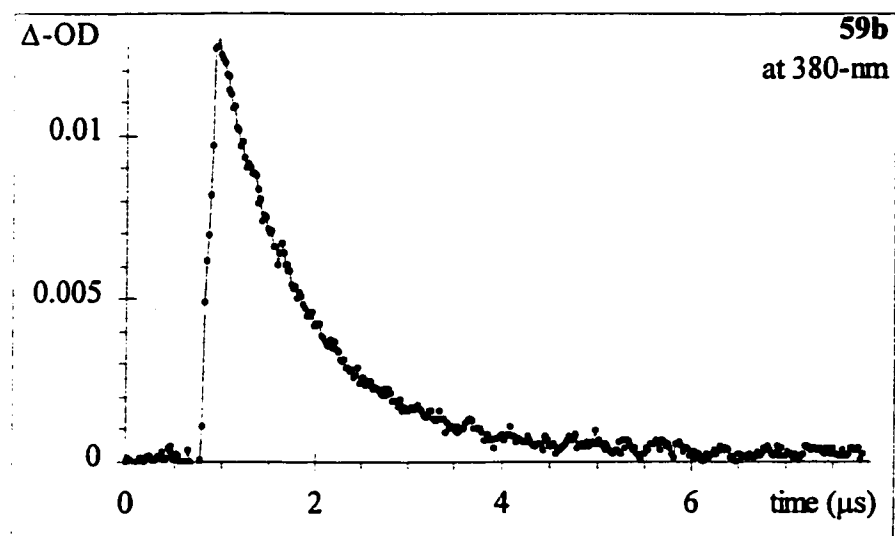
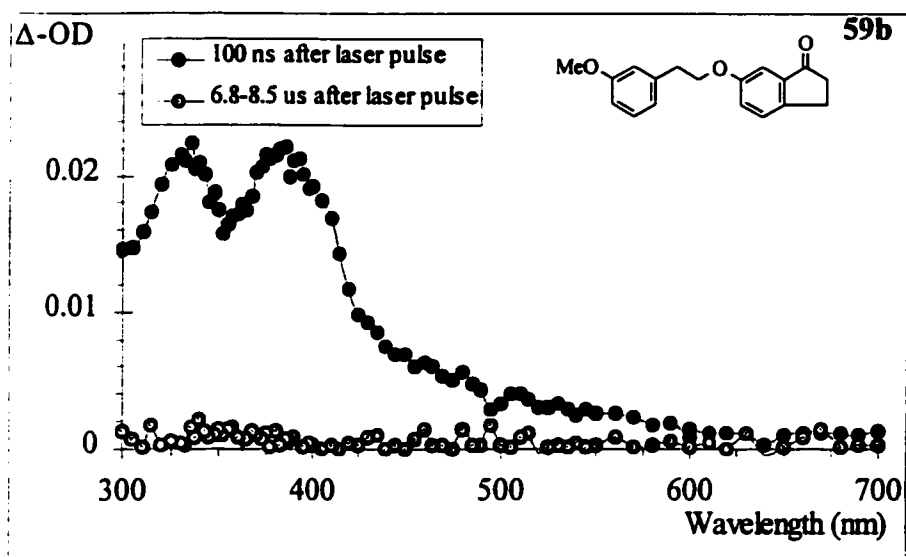
Figure 4.13. Continued.

Figure 4.14. Transient ultraviolet spectra and decays of 10^{-4} M solutions of compounds **59a** and **59b** in deoxygenated DCM at 23 to 25 °C.

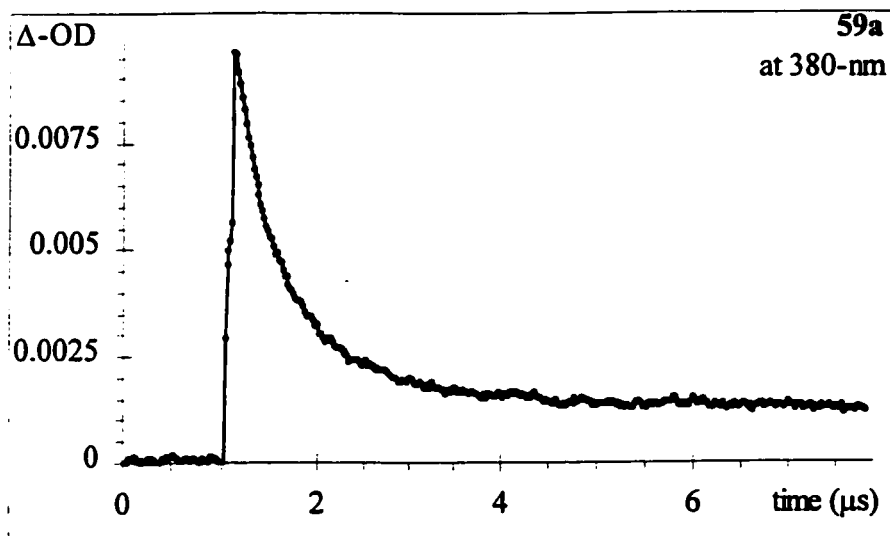
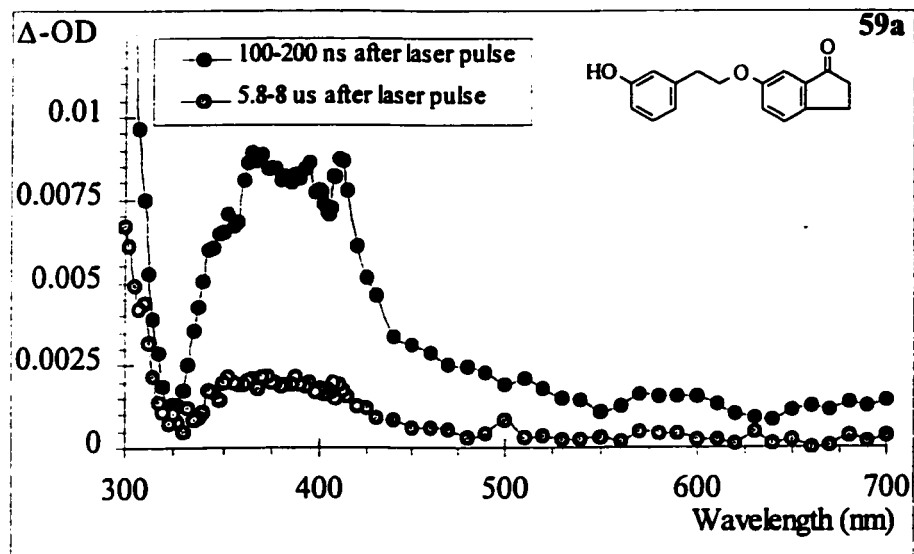


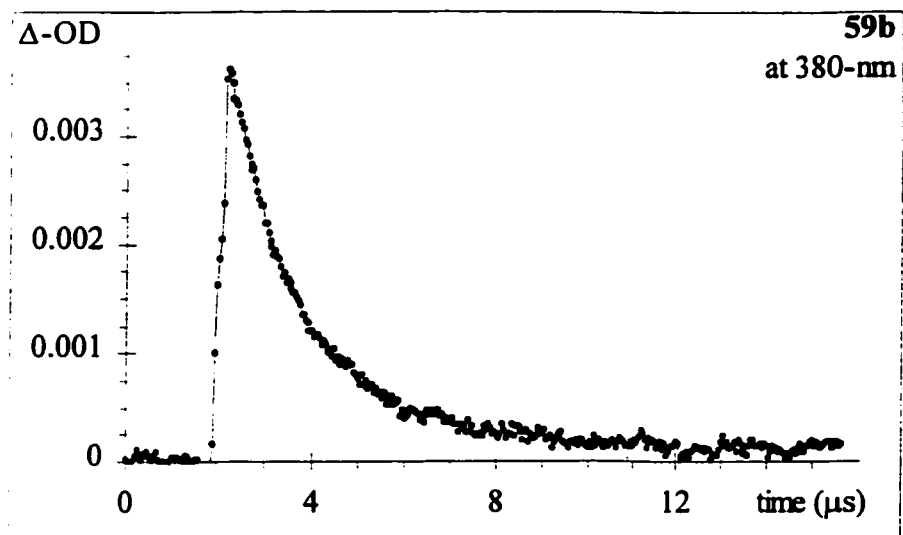
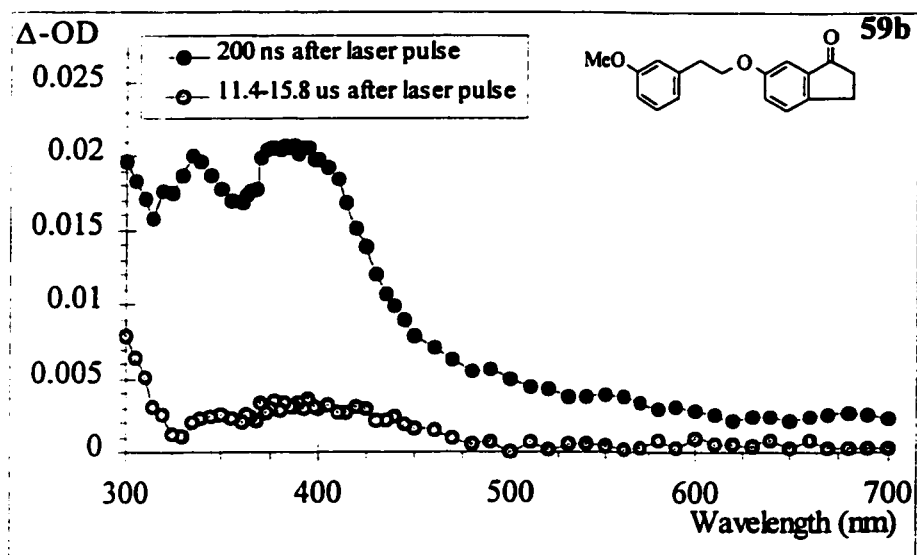
Figure 4.14. Continued.

Table 4.6. Triplet lifetimes of compounds **59a** and **59b** in MeCN and DCM and triplet quenching rate constants by 1,3-cyclohexadiene (CHD) in MeCN at 23 to 25 °C. ^{a,b}

Ketone	τ_T (MeCN ^c , μ s)	τ_T (DCM, μ s)	k_q (CHD) / $10^9 \text{ M}^{-1} \text{ s}^{-1}$
59a	$0.058^d \pm 0.004$	n.m.	--
59b	0.97 ± 0.02	1.63 ± 0.03	7.1 ± 0.4

a. Lifetimes were directly determined from 248-nm NLFP. Diene quenching experiments were conducted at 337-nm.

b. Errors in lifetimes are twice the standard deviation from the logarithmic fit. Errors in rate constants are twice the standard deviation from the quenching plot.

c. Rigorously dried MeCN ($[\text{H}_2\text{O}] < 10^{-4} \text{ M}$).

amounts of water or D₂O. These data are appended into Table 4.5, and all plots are in the Appendix.

4.3.3. Discussion. Mechanistic assignment.

From the transient spectra, isotope effects, and a comparison of the triplet lifetimes of the LPKs **58a** and **59a** with their methoxy analogues **58b** and **59b**, it is clear that for the LPKs the mechanism of triplet state deactivation is dominated by phenolic hydrogen atom abstraction. Evidence of HAA comes from the appearance of the radical absorptions in the transient spectra, as well as much shorter triplet lifetimes for the phenolic species than the *O*-methyl ethers. That H-atom transfer occurs in the rate-determining step of the mechanism comes from the primary isotope effects that are seen.

The solvent effect again emphasizes the importance of hydrogen-bonding on the mechanism of transfer, as LPK triplet lifetimes in DCM are shorter than in MeCN.

4.3.4. Discussion. Chromophore effect on the "*meta*-acyl effect".

Irrespective of chromophore, those LPKs with meta, meta'-attachment geometries exhibit longer triplet lifetimes than their para, para'-positional isomers. Table 4.7 displays a ratio comparison of the difference in triplet lifetimes between the para, para'- and meta, meta'-attached compounds of each chromophore. This ratio is largest (> 500) for acetophenone and smallest (~ 2) for indanone, and remains more or less constant for all chromophores in either MeCN or DCM. The trend of smaller reactivity for the *meta*-alkoxy isomers is opposite to what is observed in the bimolecular quenching of model

Table 4.7. Comparison of para, para'-/meta, meta'-attached LPK pairs **9a** and **16a**, **11a** and **58a**, and **57a** and **59a** in MeCN and DCM.

Ketone	τ_T (MeCN, μ s)	τ_T (DCM, μ s)	Ratio meta, meta' / para, para'
Acetophenone			750 \pm 150 (MeCN)
9a	0.0113 \pm 0.0019	0.0022 \pm 0.0003	727 \pm 170 (DCM)
16a	8.5 \pm 1.0	1.6 \pm 0.3	
Benzophenone			19.2 \pm 1.5 (MeCN)
11a	0.0189 \pm 0.0012	0.0035 \pm 0.0004	28.5 \pm 0.9 (DCM)
58a	0.362 \pm 0.017	0.100 \pm 0.003	
Indanone			2.7 \pm 0.2 (MeCN)
57a	0.0216 \pm .0010	n.m.	
59a	0.058 \pm 0.004	n.m.	

compounds by *para*-cresol, where each *meta*-alkoxy ketone triplet proved more reactive than its *para*-alkoxy isomer.

A discussion of the chromophore effect on the reaction begins by taking the acetophenone case as the base system. In this case, there exists a lowest π, π^* triplet with a retarded reactivity in the *meta*-isomer ascribed to symmetry-restricted electron transfer. This phenomenon acts to retard the electron-transfer step of the electron-proton transfer aspect of the hydrogen-bonded mechanism.

Benzophenones (11a and 58a) and indanones (57a and 59a) each possess a different type of lowest triplet state that should, at least in principle, allow a different emphasis of the importance of the symmetry-restricted electron transfer aspect of the mechanism.

As explained in Chapter Two for their bimolecular reactions, and Chapter Three for the behaviour of LPK 11a, electron-rich benzophenones have been assigned a reaction mechanism of "fast" phenolic HAA in large part due to the accessibility of an upper triplet of π, π^* character. This allows the benzophenone to participate in the same mechanism that acetophenones do. In addition, for all benzophenones there must still exist a "latent" reactivity *via* a mechanism involving the n, π^* state (the electrophilic mechanism of Chapter Two).

A reasonable explanation for the smaller reactivity ratio between *para*- and *meta*-substituted LPK isomers in the benzophenone chromophore compared to acetophenone is that the symmetry restriction exists for the hydrogen-bonded mechanism, but the latent n, π^* reaction continues unchecked. This is because the different geometry of the "*n*-type"

exciplex can better relax the need for the adoption of a sandwich-like geometry.

The indanone chromophore exhibits the smallest reactivity difference (factor of two between the indanones **57a** and **59a**) and potentially the most complicated mechanistic situation. Both isomers possess lowest π, π^* triplet states with strong charge-transfer character. As well, the geometries of indanones are very restrictive as far as facile H-atom transfer is concerned *in a sandwich exciplex*. However, this restriction should be much greater in the para, para'-attached isomer than in compound **59a**. Molecular modeling to show that ketone **59a** has access to alternate quenching geometries similar to compound **16a** has not been done, but it is a reasonable assumption that similar opportunities should exist for this molecule.

A second complication is that the greater CT-character of the alkoxyindanone triplet state compared to that of alkoxyacetophenone means that the indanones will have a more basic triplet state. As supported by the greater bimolecular reactivity of indanones, this will enhance the equilibrium constant for formation of the hydrogen-bonded exciplex and cause a greater intrinsic reactivity.

Finally, the CT-character also manifests itself in a greater intrinsic reactivity for indanones based upon the enhanced radiationless decay that these molecules seem to undergo. While the triplet lifetime of ether **59b** is much longer than its isomer **57b**, it is still considerably shorter than that of acetophenone derivative **16b**.

Taken together, the unique properties of the indanone triplet state can account for the apparent attenuation of the “*meta*-acyl” effect in the indanone chromophores.

However, a conclusive comment on the absolute magnitude cannot be made due to

the likely participation of other mechanisms.

4.3.5. Conclusions.

Several conclusions may be drawn from this last study. First, it appears that for all chromophores, a mechanism involving hydrogen-bonding is important, at least in part, in the HAA reaction. This is mostly based upon the solvent effect on the reaction.

As importantly, retardation of the phenolic HAA reaction by meta, meta'-isomerism is a general result for the three chromophores studied. However, the magnitude of the effect varies greatly and is believed to be directly dependent on the ability of the LPK to react *via* pathways other than the hydrogen-bonded mechanism, which holds the rings in a tight sandwich and emphasises the orbital mismatch in the meta, meta'-attached cases.

CHAPTER FIVE

EXPERIMENTAL SECTION

5.1. General Instrumentation.

^1H and ^{13}C NMR spectra were recorded on Bruker AC200 (200 MHz ^1H) or AC300 (300 MHz ^{13}C) spectrometers in deuterated solvents, and are reported in parts per million downfield relative to tetramethylsilane ($\delta = 0.00$). Ultraviolet absorption spectra were recorded on either a Hewlett-Packard HP8451, a Perkin-Elmer Lambda 9 spectrometer equipped with a Model 3600 data station, or Cary 50 or 300 spectrometers using standard software. Mass spectra were recorded on a VG Analytical ZABE mass spectrometer, as were exact masses that employed a mass of 12.000000 for carbon. Infrared spectra were gathered on a Biorad FTS-40 FTIR spectrometer. Melting points were determined with a Mettler hot stage controlled by a Mettler FP80 Central Processor and viewed through an Olympus BH-2 polarizing microscope. Melting points are uncorrected.

Gas chromatographic analyses employed Hewlett-Packard 5890 series II gas chromatographs equipped with a flame ionization detector, a Hewlett-Packard 3396A recording integrator, and various columns (mostly DB-1 and DB-17A) from Chromatographic Specialties. Thin-layer chromatography was conducted exclusively with silica-backed sheets (Merck). Radial (thick-layer) chromatographic separations were carried out on a Harrison Research Chromatotron[®] using 4 mm Silica Gel 60/PF

254 (EM Science) thick-layer plates. Column chromatography was performed with silica gel 60 from Aldrich or Silicycle (100 to 400 mesh), mostly under an inert nitrogen atmosphere. Elemental analyses were performed by Guelph Chemical Laboratories, Ltd.

Semi-empirical (PM3) calculations were performed using Spartan 5.0.3 (Wavefunction) on a dual-processor Silicon Graphics Octane workstation. Extended Hückel calculations were done on a Pentium PC with Hyperchem 5.0 (Hypercube).

Phosphorescence spectra were acquired on a Photon Technologies International LS-100 luminescence spectrometer utilizing the manufacturer's software. Sample concentrations were ~ 1 mg/mL and were contained in 2-mm i.d. Suprasil (Vitro Dynamics) quartz tubes that were sealed with rubber septa and deoxygenated with dry nitrogen or argon.

5.2. Photochemistry.

5.2.1. Steady state photolysis.

Steady state photolyses were done in a Rayonet reactor (New England Ultraviolet Co.) containing five to ten RPR-300 or RPR-254 lamps and a merry-go-round apparatus (Southern New England Ultraviolet Co.). Nitrogen- or argon-saturated 0.0025 M acetonitrile solutions containing ketone and dodecane or hexadecane as internal standards were irradiated simultaneously in 3- or 10-mm i.d. quartz tubes for periods up to 90 min. GC analyses were conducted before, during, and after irradiation under these conditions. No products of retention time shorter than that of the starting materials could be detected in any experiment. Quantum yields for photolysis of the ketones were estimated by

comparing the extent of photolysis of each one to that of compound **9a**.⁷⁴

5.2.2. Nanosecond laser flash photolysis.

Nanosecond laser flash photolysis experiments employed the pulses from three different excimer lasers. Pulses of 308-nm light (15 ns pulsewidth, 100 mJ per pulse) were induced from a Lumonics TE-861M filled with Xe/HCl/H₂/He. A N₂/He fill gave 337 nm (6 ns, 2-4 mJ) pulses, and 248-nm light was provided by either a Lumonics 510 or a Lambda Physik Compex filled with Kr/F₂/He (20 ns, 60 mJ or 25 ns, 100-140 mJ, respectively).

The optical array and computer-controlled detection systems have been described elsewhere.⁸⁷ Temperature control was precise. The NLFP system incorporates a brass sample holder whose temperature is controlled to within 0.1 °C by a VWR 1166 constant-temperature circulating bath. Sample temperatures were measured using a Cole-Parmer Type K digital thermocouple thermometer, also accurate to ± 0.1 °C.

Samples were contained in Suprasil quartz cells (Vitro Dynamics) of 3x7 mm (1 mL volume) or 7x7 mm (2 mL volume) dimensions. Substrate concentrations were adjusted to yield absorbances between 0.05 to 0.9 at the excitation wavelength. The cells were sealed with rubber septa and degassed with dry nitrogen or argon until constant transient lifetimes were achieved. Quenchers were added *via* syringe as aliquots of standard solutions.

5.3. Chemicals.

5.3.1. Solvents.

Acetone (Caledon Reagent) was stored over and distilled from anhydrous potassium carbonate, acetonitrile (Caledon Reagent) was used as received or dried by first distilling from calcium hydride and then either standing over activated (flamed for 15 minutes) 4 Å molecular sieves or repeated passage through a bed of activated Brockmann neutral alumina (Aldrich). The alumina was activated by heating to 300 °C under high vacuum until water no longer collected in the trap.

Benzene (BDH, Fisher or Caledon, thiophene-free) was purified by washing three times with concentrated sulfuric acid, followed by successive washings with saturated aqueous sodium bicarbonate, water and brine, and then finally distilled from sodium.

Hexane (Caledon Reagent) was distilled before use. Pyridine (BDH Reagent) was distilled from barium oxide. All other solvents were spectroscopic or HPLC grade and used as received from the suppliers (Caledon or Fisher).

5.3.2. Ketones and quenchers.

Ketones 17 - 56 were mostly obtained from Aldrich Chemical Co. or Lancaster Chemicals and either used as received or recrystallized from ethanol, methanol, ethanol/water, methanol/water or ethyl acetate/hexane mixtures. However, compounds 25, 27, 30, 38, and 43 are not commercially available. Compound 25 was prepared by Friedel-Crafts acylation of the acid chloride of *meta*-anisic acid in benzene, following the procedure described in the literature.⁹⁴ Compounds 27 and 30 were prepared by Ms.

Susannah Shaw following the same procedures and using thioanisole and anisole, respectively, as the electrophiles in the Friedel-Crafts reactions. Compound **38** was prepared by methylating *para*-aminoacetophenone according to a literature procedure.¹⁸⁷ Compound **43** was generously donated by Professor Peter Wagner, Michigan State University. Each of compounds **25**, **27**, and **38** were identified based on their NMR spectra and melting points. Compound **25**: 37.3-38.2 ° C(lit.¹⁸⁸ 44 °C), **27**: 76-77.1 ° C(lit.¹⁸⁹ 76-77.5 °C), **38**: 100-103 °C (lit.¹⁸⁸ 105.5 °C).

The purity of compound **43** was determined by GC to be less than 80%, radial chromatography using 30/70 ethyl acetate/hexanes as eluant provided a solution of 99.4% purity by GC.

1,3-Cyclohexadiene (Aldrich) was purified by freeze-pump-thaw cycles under vacuum to remove stabiliser. *para*-Toluenesulfonyl chloride(Aldrich) was purified according to the method of Fieser and Fieser¹⁹⁰ and stored under nitrogen.

para-Cresol was vacuum distilled and stored in the freezer under an argon atmosphere. Phenol was vacuum distilled. *para*-Cyanophenol was recrystallized from water and dried in a desiccator over P₂O₅. All other reagents were used as received from the suppliers.

5.3.3. Synthetic reagents.

5-Hydroxy-1-indanone was synthesized by demethylation of compound **50** according to the method of Miyake,¹⁹¹ and identified based on its spectral data.¹⁹²

6-Hydroxy-1-indanone was prepared by the same procedure (demethylation of

compound **51**) and similarly identified..

1-Bromo-2-(4-methoxyphenyl)ethane was prepared by phosphorous tribromide treatment of the ethanol according to the method of Bachmann and Thomas.¹⁹³

1-Bromo-2-(4-hydroxyphenyl)ethane was prepared by refluxing a mixture of the ethanol in 48% aqueous hydrobromic acid according to the procedure of Moreau and Roussac.¹⁹⁴

The tosylate esters were prepared following the guidelines set out in Fieser and Fieser.¹⁹⁰

A typical procedure is given for **1-tosyloxy-2-(3-tosyloxyphenyl)ethane**: in an oven-dried 250-mL ground-joint Erlenmeyer flask suspended in an ice/salt bath at -3.5 °C was placed 2-(3-hydroxyphenyl)ethanol (2.64 g, 0.019 mol), freshly distilled pyridine (70 mL) and an oven-dried stirbar. After stirring for 10 minutes, *para*-toluenesulfonyl chloride (15.2 g, 0.08 mol) was added all at once. The clear yellow solution was stoppered and stirred for 90 minutes at 0 to 2 °C, during which time a fine white precipitate of pyridinium hydrochloride was formed. The mixture was then stored at -15 °C for 12 hours and at 9 °C for 36 hours. The orange reaction mixture was poured into ice water (400 mL) and then extracted with ether (2x200 mL, 1x50 mL). The combined organic fractions were washed with ice cold 50% HCl (2x200 mL) and then water (2x200 mL), dried over anhydrous magnesium sulfate and filtered through a coarse frit. The pale yellow solution was stripped of solvent on the rotary evaporator to yield a solid residue, which was recrystallized from 10:3:2 ligroin (30-60):ether:dichloromethane to give colorless plates of the desired product (4.05 g, 0.0095 mol, 48%). m.p. 81-84 °C; ¹H

NMR (CDCl₃) δ 2.42 (s, 3H), 2.43 (s, 3H), 2.85 (t, J = 6.8 Hz, 2H), 4.11 (t, J = 6.8 Hz, 2H), 6.71 (m, 1H), 6.83 (m, 1H), 6.98 (d, J = 7.7 Hz, 1H), 7.14 (t, J = 7.9 Hz, 2H), 7.25-7.31 (m, 2H), 7.62-7.69 (m, 2H); ¹³C NMR (CDCl₃), δ 21.6 (2 carbons), 34.9, 69.8, 120.8, 122.8, 127.7, 127.8, 128.5, 129.7, 129.8 (2 carbons), 132.3, 132.7, 138.4, 144.9, 145.5, 149.7; IR (CDCl₃; cm⁻¹) 3157 (w), 2985 (w), 2256 (m), 1795 (w), 1653 (w), 1600 (w), 1487 (w), 1375 (m), 1191 (m), 1179 (m), 1133 (w), 1095 (w), 909 (s), 734 (s); MS, m/e (I): 274 (25), 155 (68), 119 (26), 91 (100), 65 (73), 52 (14), 41 (14); HRMS: Calc'd. for C₂₂H₂₂O₆S₂: 446.08586. Found: 446.085776.

1-Tosyloxy-2-(3-methoxyphenyl)ethane. This material was obtained in ~ 82% yield as a yellow oil, and contained ~ 5% 1-chloro-2-(3-methoxyphenyl)ethane as an impurity.

The IR and ¹H NMR spectra were similar to those reported in the literature for this compound.^{195,196} ¹³C NMR: (CDCl₃) δ 21.6, 35.4, 55.1, 70.6, 112.4, 114.5, 121.3, 127.8, 129.6, 129.9, 132.9, 137.8, 144.8, 159.8.

1-Tosyloxy-2-(4-tosyloxyphenyl)ethane. Using the general procedure outlined above for the tosylate preparation, the major product here was 1-chloro-2-(4-tosyloxyphenyl)ethane. The reaction was not optimised, but the amount of this impurity could be reduced with shorter reaction times and keeping the temperature below 5 °C.

Yield: 16%; m.p. 75.7-76.8 °C; ¹H NMR: (CDCl₃) δ 2.42 (s, 3H), 2.43 (s, 3H), 2.89 (t, J

6.8 Hz, 2H), 4.14 (t, $J = 6.8$ Hz, 2H), 6.83 (d, $J = 6.6$ Hz, 1H), 7.00 (d, $J = 8.7$ Hz, 2H), 7.25-7.31 (m, 4H), 7.65 (t, $J = 8.0$ Hz, 4H); ^{13}C NMR: (CDCl_3) δ 21.6, 21.7, 34.6, 70.0, 122.4, 127.7, 128.4, 129.8 (2 carbons), 130.0, 132.3, 132.7, 135.4, 144.9, 145.4, 148.5; IR (KBr; cm^{-1}): 3094 (w), 3056 (w), 2954 (w), 1718 (m), 1605 (m), 1497 (m), 1374 (s), 1202 (m), 1178 (s), 1089 (m), 967 (m), 899 (m), 866 (m), 844 (m), 814 (m), 766 (m), 709 (m), 664 (m), 558 (m); MS, m/e (I): 274 (16), 155 (38), 120 (17), 91 (100), 65 (26).

5.3.4. Linked phenolic ketones and their *O*-methyl ethers.

Compounds **9a**, **11a**, **14** - **16** were prepared and purified according to published methods.^{74,86} Spectroscopic data for these compounds matched the literature. Every compound described above except for ether **15b** was also later prepared by routes involving the appropriate tosylate esters, the routes followed closely mimic those to be described for the other LPKs below, and will not be given here. Yields were usually 20-30% higher than with the bromides. New procedures are outlined below.

4-[2-(3-Hydroxyphenyl)ethoxy]acetophenone (14a). In an oven-dried 100-mL round bottom flask equipped with a magnetic stirring bar and reflux condenser were placed 1-tosyl-2-(3-tosyloxyphenyl)ethane (1.0 g, 2.24 mmol), anhydrous potassium carbonate (0.42 g, 3.04 mmol), *para*-hydroxyacetophenone (0.29 g, 2.13 mmol) and dry acetone (30 mL). The mixture was refluxed for one week, filtered, and the solvent was removed on the rotary evaporator. The resulting light brown oil was diluted with aqueous HCl (3 M, 10 mL) until acidic and taken up into ether (2x20 mL) and ethyl acetate (20 mL). After

separation, the orange organic fraction was washed with brine (30 mL), aqueous HCl (1 M, 30 mL) and brine again (25 mL), dried over anhydrous MgSO_4 , filtered, and the solvent removed on the rotary evaporator. Analysis by ^1H NMR indicated that the crude mixture consisted largely of the tosylate ester of LPK 14a, contaminated with a small amount of unreacted *para*-hydroxyacetophenone. This mixture was hydrolysed by refluxing in methanol (20 mL) containing anhydrous potassium carbonate (2.6 g, 20 mmol) for 6 days. Work-up in similar fashion to that described above yielded crude compound 14a as a dark oil (0.53 g). The compound was purified by radial chromatography using 20% ethyl acetate in hexanes as eluant, and recrystallized twice from methanol to give compound 14a as a white powder (0.1 g, 0.4 mmol, 20%). m.p. 117.4-118.5 °C, Anal. Calc'd. $\text{C}_{16}\text{H}_{16}\text{O}_3$: C, 74.98; H, 6.29. Found: C, 74.84; H, 6.42.

3-[2-(4-Hydroxyphenyl)ethoxy]acetophenone (15a). In an oven-dried 100-mL round bottom flask equipped with a magnetic stirring bar and reflux condenser were placed 1-tosyl-2-(4-tosyloxyphenyl)ethane (1.63 g, 3.7 mmol), anhydrous potassium carbonate (0.76 g, 5.5 mmol), *meta*-hydroxyacetophenone (0.45 g, 3.3 mmol) and dry acetone (20 mL). The mixture was refluxed for 48 hours, filtered, and the solvent was removed on the rotary evaporator. The resulting light brown oil was dissolved in ether (20 mL) and shaken with aqueous HCl (3 M, 10 mL). After separation, the bright yellow ether layer was washed with water (2x20mL) and the original aqueous layer was extracted with ether (2x15mL). The combined ether extracts were dried over anhydrous MgSO_4 , filtered, and

the solvent removed on the rotary evaporator. Analysis by ^1H NMR indicated that the crude mixture consisted largely of the tosylate ester of LPK **15a**, contaminated with a small amount of *para*-tosyloxystyrene and unreacted *meta*-hydroxyacetophenone. This mixture was hydrolysed by refluxing in methanol (20 mL) containing anhydrous potassium carbonate (3.8 g, 27 mmol) for 72 hours. Work-up in similar fashion to that described above yielded crude compound **15a** as an oily solid (0.9 g). The compound was purified by radial chromatography using chloroform as eluant, and recrystallized from 30% ethyl acetate in hexanes to give colorless needles of **15a** (0.85 g, 0.33 mmol, 10%). m.p. 71.9-72.6 °C; Anal. Calc'd. $\text{C}_{16}\text{H}_{16}\text{O}_3$: C, 74.98; H, 6.29. Found: C, 74.85; H, 6.22.

3-[2-(3-Hydroxyphenyl)ethoxy]acetophenone (16a). This compound was prepared in a similar fashion to compound **15a**, except that *meta*-hydroxyacetophenone (0.22 g, 1.6 mmol) was coupled to 1-tosyl-2-(3-tosyloxyphenyl)ethane (0.805 g, 1.80 mmol) in the presence of anhydrous potassium carbonate (0.26 g, 1.9 mmol) in refluxing acetone (10 mL) over 48 hours. After workup in similar fashion to that of compound **15a**, the crude tosylate ester was hydrolysed by refluxing with anhydrous potassium carbonate (5.0 g, 36 mmol) in methanol (13 mL) for four days. Final workup yielded a mixture of compound **16a** and *meta*-hydroxystyrene, which were separated by column chromatography utilizing 30% ethyl acetate in hexanes as eluant to yield the desired material as a colorless solid. Recrystallization from methanol yielded compound **16a** as colorless plates (0.15 g, 0.6 mmol, 36%). m.p. 88.7-90.6 °C; Anal. Calc'd. for $\text{C}_{17}\text{H}_{18}\text{O}_3$: C, 75.53; H, 6.71. Found:

C, 75.61; H, 6.80.

3-[2-(3-Methoxyphenyl)ethoxy]acetophenone (16b). To 1-tosyl-2-(3-methoxyphenyl)ethane (6.27 g, 20.5 mmol) in the presence of anhydrous potassium carbonate (2.89 g, 20.9 mmol) in 20 mL dry acetone was added *meta*-hydroxyacetophenone (2.51 g, 18.4 mmol). The reaction was complete after 48 hours. Isolation as above yielded crude ether **16b**, which was further purified by radial chromatography using chloroform followed by column chromatography using 30% ethyl acetate in hexanes as eluant. This yielded the product as a colourless oil (3.2 g, 12 mmol, 65%). Anal. Calc'd. C₁₇H₁₈O₃: C, 75.53; H, 6.71. Found: C, 75.89; H, 6.78.

5-[2-(4-Hydroxyphenyl)ethoxy]-1-indanone (57a) was synthesized from 1-bromo-2-(4-trimethylsiloxyphenyl) ethane (prepared from 1-bromo-2-(4-hydroxyphenyl)ethane¹⁹⁴) and 5-hydroxy-1-indanone, by an identical procedure to that for compound **9a**. This species was isolated in 48% overall yield by silica gel column chromatography using chloroform as the eluant and recrystallized from chloroform/dichloromethane mixtures. m.p. 121-123 °C; ¹H NMR (CDCl₃) δ = 2.67 - 2.63 (m, 2H), 3.06-3.01 (m, 4H), 4.18 (t, 2H), 5.31 (s, 1H), 6.79 (td, 2H), 6.86 (dd, 2H), 7.13 (td, 2H), 7.66 (dd, 1H); ¹³C NMR (CDCl₃) δ = 25.9, 34.7, 36.4, 69.4, 110.3, 115.5, 115.8, 125.5, 129.1, 130.0, 155.0, 158.6, 164.8, 206.4; IR (KBr, cm⁻¹), 3400 (b), 3015 (w), 2926 (w), 2863 (w), 1741 (s), 1678 (s), 1596 (s), 1516 (w), 1440 (w), 1363 (w), 1309 (w), 1258 (s), 1223 (s), 1102 (w),

837 (w); UV, λ_{max} (MeCN) = 195 nm (ϵ = 52000), sh = 223, 265, 285, 295; MS, m/e (I) = 268 (15), 121 (100), 107 (15), 83 (21), 45 (45); Exact Mass: Calc'd. for $C_{17}H_{16}O_3$: 268.1100. Found: 268.10998.

5-[2-(4-Methoxyphenyl)ethoxy]-1-indanone (57b) was prepared as LPK 57a except the reagents were 2-(4-methoxyphenyl)-1-bromoethane and 5-hydroxy-1-indanone.

Purification was begun with silica gel column chromatography using chloroform as the eluant and purified material was recrystallized from methanol or petroleum ether/ethyl acetate. m.p. 65.3-67.0; 1H NMR ($CDCl_3$) δ = 2.64 - 2.62 (m, 2H), 3.06 - 3.02 (m, 4H), 3.78 (s, 3H), 4.18 (t, 2H), 6.88 - 6.83 (m, 4H), 7.18 (dt, 2H), 7.65 (dd, 1H); ^{13}C NMR ($CDCl_3$) δ = 25.8, 34.7, 36.4, 55.2, 69.3, 110.4, 114.0, 115.6, 125.3, 129.8, 129.9, 130.4, 158.0, 158.4, 164.5, 205.1; IR (KBr, cm^{-1}), 3004 (w), 2980 (w), 2840 (w), 1699 (s), 1602 (s), 1515 (s), 1435 (w), 1304 (m), 1259 (s), 1089 (m), 1037 (m), 829 (w); UV: λ_{max} (MeCN) = 196 nm (ϵ = 50000), sh = 223, 265, 285, 295; MS, m/e(I) = 282 (12), 135 (100), 121 (39), 105 (8), 91 (11), 77 (11); Exact Mass: Calc'd. for $C_{18}H_{18}O_3$: 282.1256. Found: 282.1265.

4-[2-(4-Methoxyphenyl)ethoxy]benzophenone (11b) was prepared as ether 57b except the reagents were 2-(4-methoxyphenyl)-1-bromoethane and *para*-hydroxybenzophenone. m.p. 67-68°; 1H NMR ($CDCl_3$) δ = 3.06 (t, 2H), 3.78 (s, 3H), 4.19 (t, 2H), 6.86(dt, 2H),

6.93 (dt, 2H), 7.20 (dt, 2H), 7.47-7.44 (m, 2H), 7.55 (tt, 2H), 7.74 (dt, 2H), 7.79 (dt, 2H); ^{13}C NMR (CDCl_3) δ = 34.7, 55.3, 69.1, 114.0, 114.1, 128.2, 129.7, 129.8, 130.0, 130.1, 131.9, 132.6, 138.3, 158.4, 162.5, 195.5; IR (KBr, cm^{-1}), 3006 (w), 2943 (w), 2835 (w), 1715 (s), 1647 (s), 1598 (w), 1507 (w), 1316 (w), 1223 (m), 1172 (w), 1027 (w), 886 (m), 626 (m), 530 (w); UV, λ_{max} (MeCN) = 198 nm (ϵ = 60000), sh = 224, 285; MS, m/e (I) = 332 (8), 135 (100), 121 (30), 105 (10), 91 (8), 77 (15); Exact Mass: Calc'd. for $\text{C}_{22}\text{H}_{20}\text{O}_3$: 332.1413; Found: 332.1419.

3-[2-(3-Hydroxyphenyl)ethoxy]benzophenone (58a). This material was prepared in a similar manner to compound **57a** above except that *meta*-hydroxybenzophenone (1 g, 0.005 mol) was coupled to 1-tosyloxy-2-(3-tosyloxyphenyl)ethane (4.50 g, 0.010 mol) in acetone in the presence of anhydrous potassium carbonate (0.87 g, 0.006 mol). The mixture was refluxed for 72 hours, after which ^1H NMR monitoring indicated that the ditosylate was consumed. After workup in a manner similar to that described above, hydrolysis of the crude tosylate ester was performed by dissolving in methanol (100 mL), adding potassium carbonate (10 g, 0.07 mol) and refluxing for 80 hours. Workup as before yielded 2.54 g of a beige oil that was mostly product contaminated with *meta*-hydroxystyrene. Purification by radial chromatography (30% ethyl acetate in hexanes eluant) followed by column chromatography (3% ether in dichloromethane with 10 drops acetic acid/100 mL eluant) yielded pure compound **58a** (1.2 g, 0.0038 mol, 75%) as an oil which has not crystallized. ^1H NMR: (CDCl_3) δ 3.00 (t, J = 7 Hz, 2H), 4.14 (t, J = 7

Hz, 2H), 6.2 (s, 1H), 6.7-6.85 (m, 3H), 7.1-7.2 (m, 2H), 7.3-7.6 (m, 6H), 7.79 (d, $J = 8$ Hz, 2H); ^{13}C NMR (CDCl_3) δ 35.4, 68.6, 113.6, 115.0, 116.0, 119.6, 121.1, 123.0, 128.3, 129.2, 129.6, 130.1, 132.6, 137.3, 138.6, 139.7, 155.9, 158.7, 197.2; UV λ_{max} (MeCN) 220 nm (ϵ 27600 $\text{M}^{-1}\text{cm}^{-1}$), sh. 253, 307 nm; IR (KBr, cm^{-1}) 3413 (br m), 3064 (w), 2934 (w), 2875 (w), 1716 (s), 1661 (s), 1594 (s), 1489 (w), 1451 (m), 1363 (m), 1287 (s), 1224 (s), 1161 (w), 1039 (w), 876 (w), 787 (w), 728 (m), 708 (m), 535 (w); MS, m/e (I): 318 (10), 199 (3), 121 (100), 105 (23), 91 (16), 77 (45), 65 (8), 51 (8); HRMS: Calc'd. for $\text{C}_{21}\text{H}_{18}\text{O}_3$: 318.12564. Found: 318.125592; Anal. Calc'd. $\text{C}_{21}\text{H}_{18}\text{O}_3$: C, 79.23; H, 5.70. Found: C, 79.52; H, 5.85.

6-[2-(3-Hydroxyphenyl)ethoxy]-1-indanone (59a). To a 100 mL round-bottom flask attached to a reflux condenser and equipped with a magnetic stir bar was added 50 mL acetone and 6-hydroxy-1-indanone (0.68 g, 0.00459 mol). The clear solution was chilled in an ice bath to 0°C and then anhydrous potassium carbonate (0.71 g, 0.00514 mol) and 1-tosyloxy-2-(3-tosyloxyphenyl)ethane (2.24 g, 0.00510 mol) were added. By TLC, stirring at ice temperature (2.5 hours) followed by room temperature (16 hours) did not result in any reaction. After heat was applied and another batch of potassium carbonate was added (0.71 g, 0.005 mol), the consumption of the ditosylate was observed by TLC after several hours. More of this reagent (1.02 g, 0.0023 mol) was added and the reflux continued. After three days, ^1H NMR monitoring confirmed the total disappearance of the hydroxy indanone starting material. The reaction mixture was stripped of acetone on

the rotary evaporator and then acidified with dilute HCl until gas evolution ceased. The aqueous mixture was extracted with ethyl acetate (50 mL), which caused an emulsion that was clarified upon the addition of brine (25 mL). The orange organic phase was washed with water and brine, dried with anhydrous magnesium sulfate, filtered, and concentrated under reduced pressure. The tosylate ester was hydrolyzed by reflux in a mixture of methanol (25 mL) and potassium carbonate (5 g, 0.04 mol). After 48 hours the hydrolysis was complete by TLC. Workup was performed similar to that described above, yielding 1.76 g crude material as a deep brown oil. Purified LPK **59a** was obtained in the form of yellow stars after silica gel column chromatography using chloroform as eluant. (0.34 g, 0.0013 mol, 30%). m.p.: 135.5-136.0, ^1H NMR: (CD_3CN) δ 2.60-2.64 (m, 3H), 2.97-3.06 (m, 4H), 4.22 (t, $J = 7$ Hz, 2H), 6.65-6.70 (m, 1H), 6.8 (m, 2H), 7.08-7.2 (m, 2H), 7.41 (d, $J = 8$ Hz, 1H), 7.74 (d, $J = 3$ Hz, 1H); ^{13}C NMR (CD_3CN) δ 25.4, 35.9, 37.3, 69.6, 95.0, 106.5, 114.0, 116.6, 121.0, 124.2, 128.4, 130.1, 139.0, 140.9, 148.7, 158.0, 159.3; UV λ_{max} (MeCN) 219 nm (ϵ 32700 $\text{M}^{-1}\text{cm}^{-1}$), sh. 244, 275, 317 nm; IR (KBr, cm^{-1}) 3417 (br m), 3278 (w), 3051 (w), 3009 (w), 2938 (w), 1716 (s), 1690 (m), 1623 (w), 1590 (w), 1493 (w), 1364 (m), 1287 (m), 1224 (m), 1161 (w), 1090 (w), 1040 (w), 951 (w), 838 (w), 703 (w), 527 (w); MS, m/e (I): 268 (25), 121 (100), 103 (31), 91 (39), 77 (44), 65 (12); HRMS: Calc'd. for $\text{C}_{17}\text{H}_{16}\text{O}_3$: 268.1072. Found: 268.1099; Anal. Calc'd. $\text{C}_{17}\text{H}_{16}\text{O}_3$: C, 76.10; H, 6.01. Found: C, 75.50; H, 6.07.

3-[2-(3-Methoxyphenyl)ethoxy]benzophenone (58b). This material was prepared

similarly to compound **9b** above, except that *meta*-hydroxybenzophenone (2.50 g, 0.0126 mol) was coupled to 3-methoxy- β -phenethyl bromide (4.79 g, 0.0223 mol) in the presence of anhydrous potassium carbonate (1.74 g, 0.013 mol) in 20 mL acetone. After 16 hours, the reaction was not complete, and more potassium carbonate (0.50 g 0.0036 mol) was added. After four more days refluxing, the reaction was still not complete and another 0.25 g potassium carbonate (0.0018 mol) and 2.02 g bromide (0.009 mol) were added. After another 5 days (10 total), monitoring by ^1H NMR indicated only 80% consumption of the *meta*-hydroxy benzophenone starting material. At this time another 1.09 g bromide (0.005) mol was added to the mixture and it was refluxed for a final three days, after which the reaction mixture was poured into a 50/50 mixture of ether and ethyl acetate (50 mL) and stirred. Water was added (50 mL) to produce a creamy beige emulsion, and the basic aqueous layer was acidified with 3 M HCl and extracted with 50 mL ether and 2x25 mL ethyl acetate. The combined organic layers were washed with water (200 mL), 5% aq. sodium bicarbonate (100 mL) and brine (100 mL), then dried (magnesium sulfate), and filtered. Removal of the organic solvents on the rotary evaporator yielded an orange/brown oil which was purified by silica gel column chromatography employing 50% hexane in dichloromethane as eluant to yield compound **58b**, 2.73 g, 0.008 mol, 65%) as an oil which has not crystallized. ^1H NMR: (CDCl_3) δ 3.07 (t, 2H, $J = 7$ Hz), 3.77 (s, 3H), 4.20 (t, 2H, $J = 7$ Hz), 6.75-6.86 (m, 3H), 7.08-7.12 (m, 1H), 7.20 (d, 1H, $J = 8$ Hz), 7.31-7.35 (m, 3H), 7.42-7.47 (m, 2H), 7.53-7.58 (m, 1H), 7.76-7.79 (m, 2H); ^{13}C NMR (CDCl_3) δ 35.6, 55.0, 68.6, 111.7, 114.7, 115.0, 119.2,

121.2, 122.7, 128.1, 129.1, 129.4, 129.9, 132.3, 137.7, 138.7, 139.5, 158.6, 159.6, 196.3;
 UV λ_{max} (MeCN) 220 nm (ϵ 28600 M⁻¹cm⁻¹), sh. 252, 305 nm; IR (KBr; cm⁻¹) 3060
 (vw), 2939 (vw), 2835 (vw), 1658 (m), 1596 (m), 1488 (m), 1438 (m), 1281 (s), 1164
 (m), 1043 (s), 971 (w), 872 (w), 781 (s), 724 (s); MS, m/e (I): 332(10), 135(100), 120(7),
 105(56), 91(28), 77(68), 65(12), 51(16); HRMS: Calc'd. for C₂₀H₂₂O₃: 332.1413.
 Found: 332.1413; Anal. Calc'd. C₂₀H₂₂O₃: C, 79.50; H, 6.06. Found: C, 79.90; H, 5.93.

6-[2-(3-Methoxyphenyl)ethoxy]-1-indanone (59b). To a 25 mL round-bottom flask attached to a condenser with a nitrogen inlet was added anhydrous potassium carbonate (0.47 g, 0.0034mol) and 10 mL acetone. To the stirred suspension was added 6-hydroxy-1-indanone (0.46 g, 0.0034 mol) and the resulting mixture was brought to a gentle reflux for 90 minutes. After cooling, 3-methoxy- β -phenethyl bromide (1.51 g, 0.007 mol) was added and the mixture (now a light yellow) was brought to boil again. After ten days of reflux, the reaction was still incomplete by TLC. Ten more mL of acetone and another 0.50 g of potassium carbonate were added, and after five more days of stirring the reaction was worked up by filtration and then removal of the acetone under reduced pressure. The resulting red oil was taken up into ether (50 mL) and then acidified with dilute HCl (50 mL). The aqueous layer was extracted with ether (2x50 mL) and the combined organic extracts were washed with water (100 mL) and brine (100 mL) and then dried with magnesium sulfate. Removal of the ether under reduced pressure yielded 1.4 g of an orange oil, which was purified by successive column chromatography using 10% ethyl acetate in hexanes as eluant followed by chloroform. This yielded purified

ether **59b** as a yellow oil (0.47 g, 0.0016 mol, 53%) which has not crystallized. ^1H NMR: (CDCl_3) δ 2.61 (m, 2H), 3.00 (m, 4H), 3.71 (s, 3H), 4.12 (t, $J = 7$ Hz, 2H), 6.65-6.72 (m, 1H), 6.8 (m, 2H), 7.08-7.2 (m, 2H), 7.22 (d, $J = 8$ Hz, 1H), 7.74 (d, $J = 3$ Hz, 1H); ^{13}C NMR (CDCl_3) δ 25.1, 35.6, 37.0, 68.9, 105.9, 111.9, 114.8, 121.3, 124.3, 127.4, 128.3, 129.5, 138.2, 139.6, 148.0, 158.6, 159.8, 206.9; UV λ_{max} (MeCN) 218 nm (ϵ 29250 $\text{M}^{-1}\text{cm}^{-1}$), sh. 243, 272, 279, 315 nm; IR (KBr, cm^{-1}) 3005 (w), 2925 (w), 2837 (w), 1711 (s), 1613 (w), 1492 (m), 1446 (w), 1296 (m), 1275 (m), 1222 (m), 1168 (w), 1155 (w), 1040 (m), 837 (w), 785 (w), 697 (w), 558 (w), 530 (w); MS, m/e (I): 282 (18), 135 (100), 120 (8), 105 (25), 91 (30), 67 (27), 65 (22), 51 (12), 43 (33); HRMS: Calc'd. for $\text{C}_{18}\text{H}_{18}\text{O}_3$: 282.1256. Found: 282.1256; Anal: Calc'd. $\text{C}_{18}\text{H}_{18}\text{O}_3$: C, 76.57; H, 6.43. Found: C, 76.74; H, 6.61.

APPENDIX

Figure A.1. Stern-Volmer plot of the reduction of the initial yield of the transient (*top* Δ -OD) from 337-nm NLFP of compound **11a** in deoxygenated DCM by 1,3-cyclohexadiene, monitored at 380-nm. Page reference p.142.

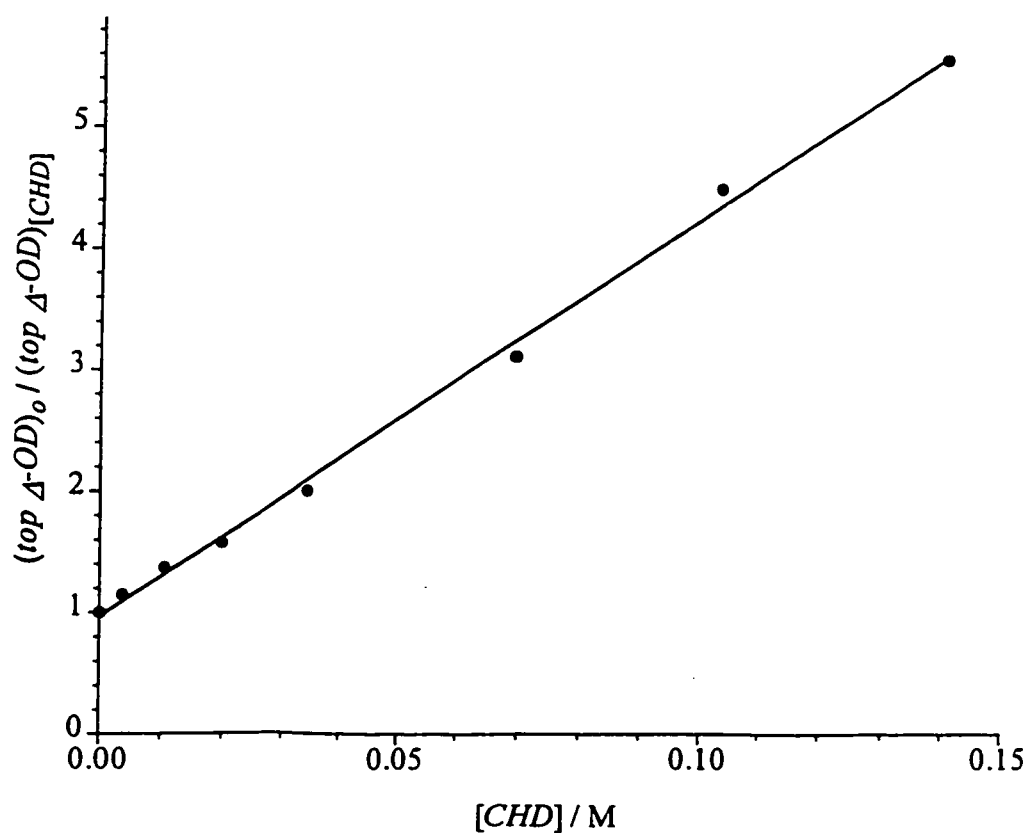


Figure A.2. Fits of the 1-methylnaphtalene probe data to eq. 3.1 at 23 to 25 °C for LPKs 9a (circles) and 11a (squares). The filled points indicate 5% D₂O/MeCN, the open points 5% H₂O/MeCN . Page reference p.148.

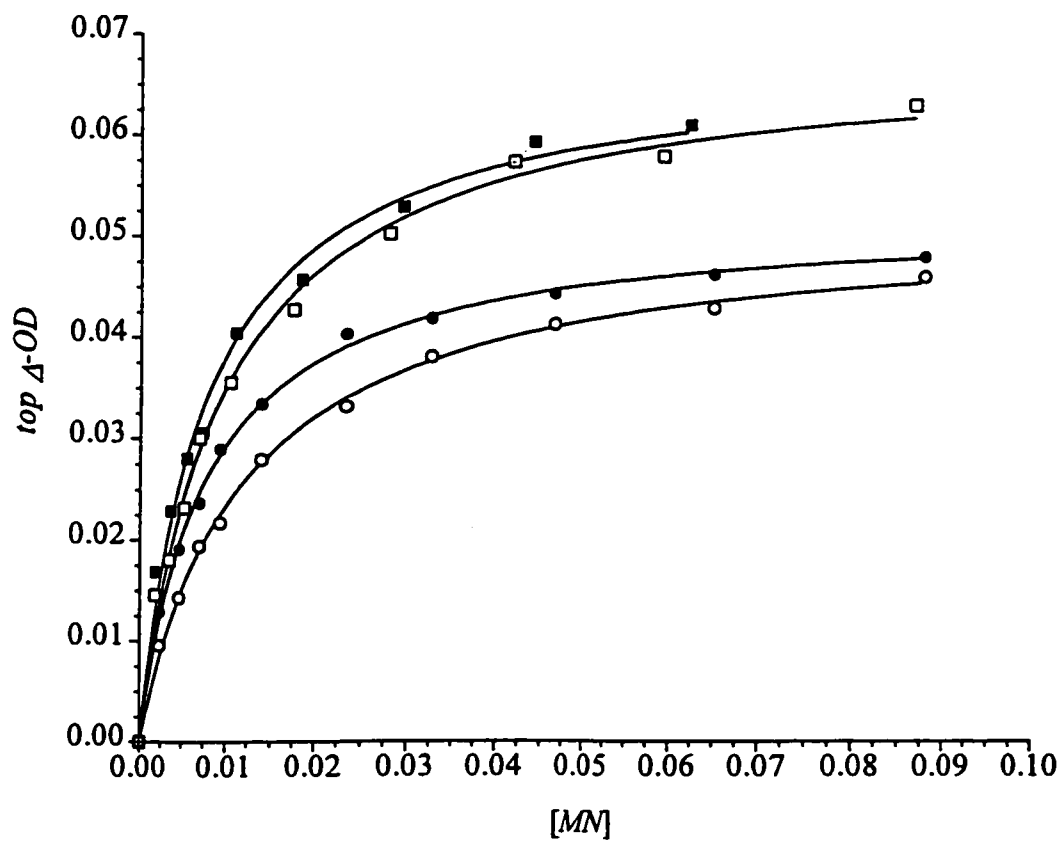


Figure A.3. Stern-Volmer plot of the reduction of the initial yield of the transient (*top* ΔOD) from 337-nm NLFP of compound **57a**. The filled points indicate 5% $D_2O/MeCN$, the open points 5% $H_2O/MeCN$. Page reference p.148.

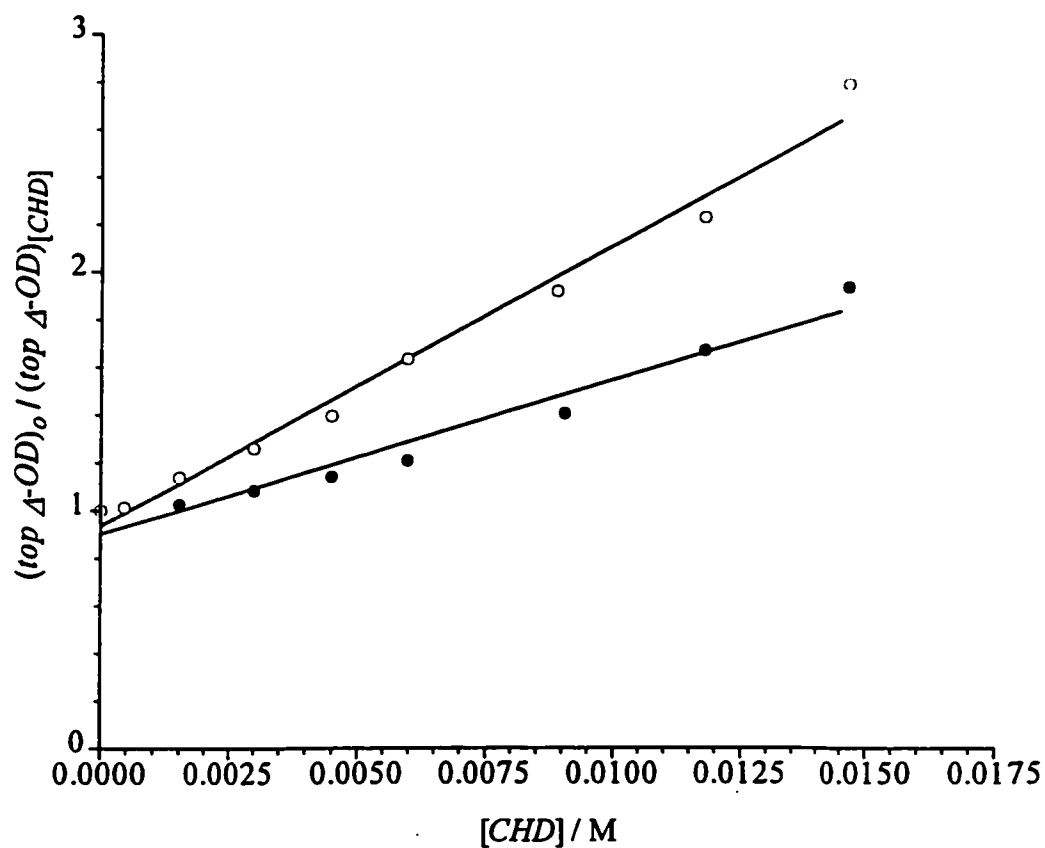


Figure A.4. Plot of k_{decay} versus ketone concentration from 248-nm NLFP of deoxygenated, dry ($[H_2O] < 10^{-4}$ M) MeCN solutions of compound **15a**. Page reference p.185.

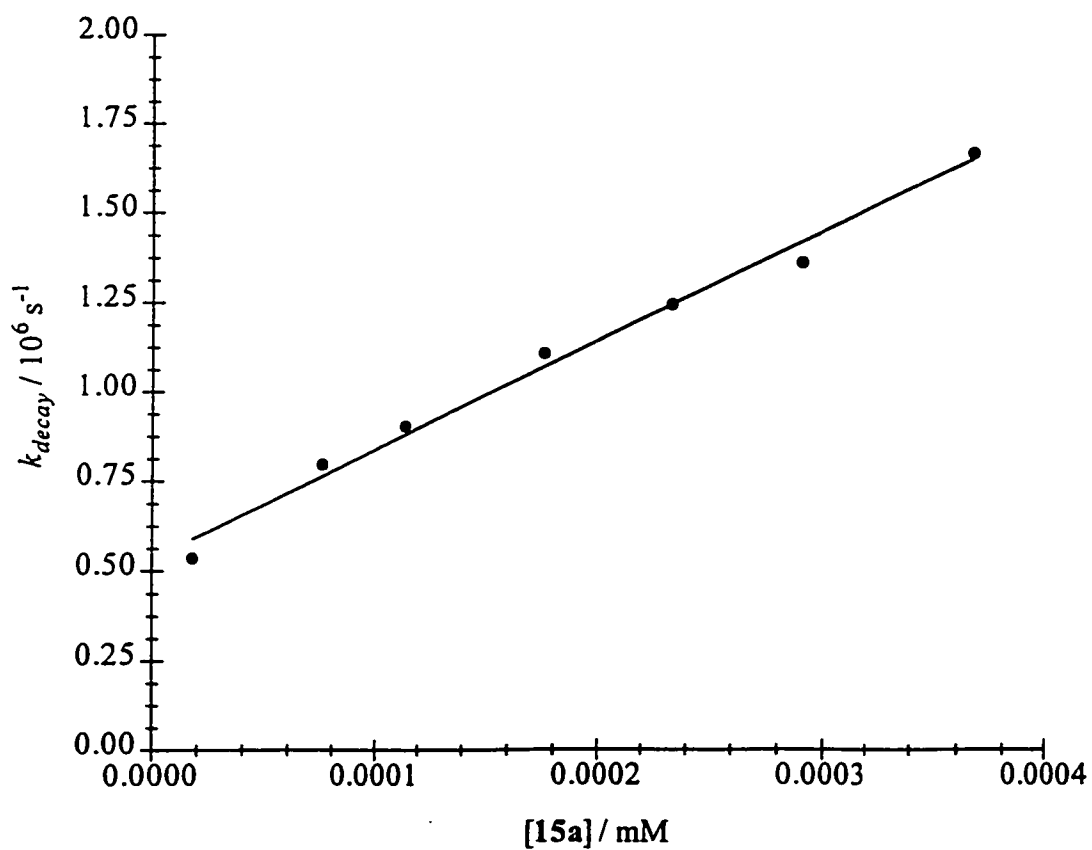


Figure A.5. Plot of k_{decay} versus ketone concentration from 248-nm NLFP of

deoxygenated 0.028 M L_2O /MeCN solutions of compound **15a**. Open circles are H_2O ,

filled circles are D_2O . Page reference p.189.

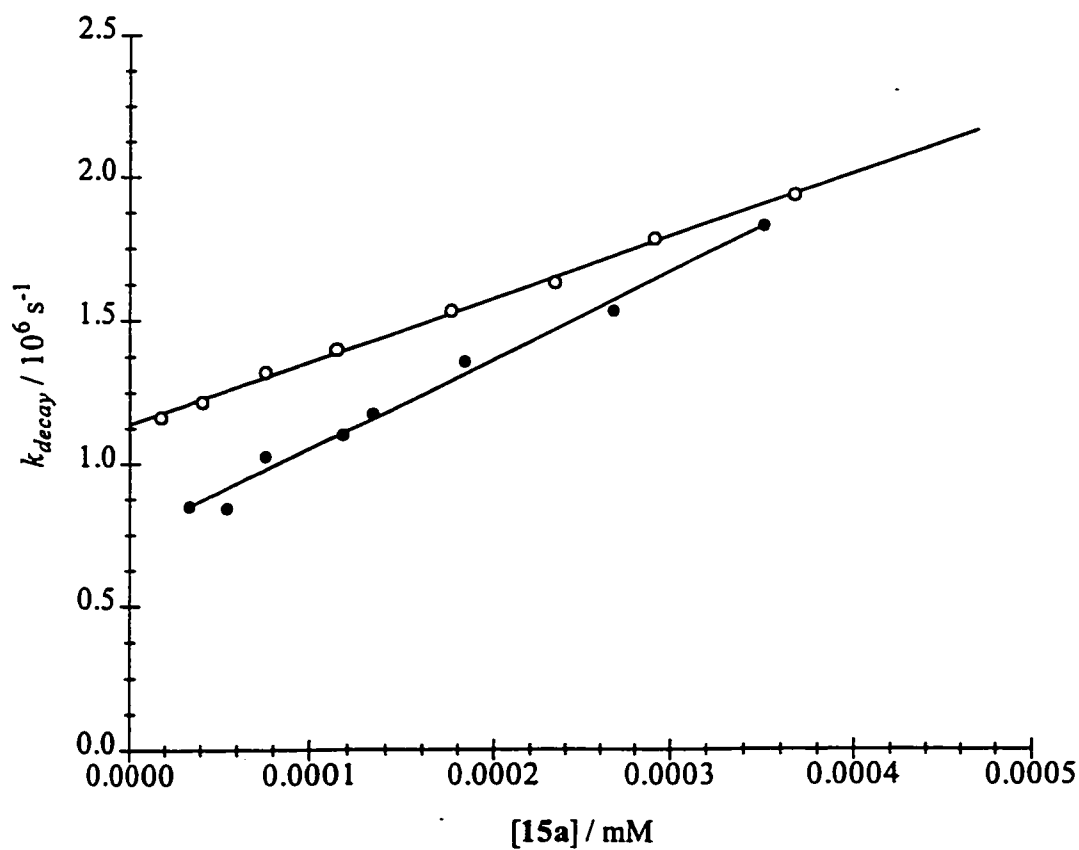


Figure A.6. Plot of k_{decay} versus ketone concentration from 248-nm NLFP of deoxygenated 0.028 M L₂O/MeCN solutions of compound **16a**. Open circles are H₂O, filled circles are D₂O. Page reference p.189.

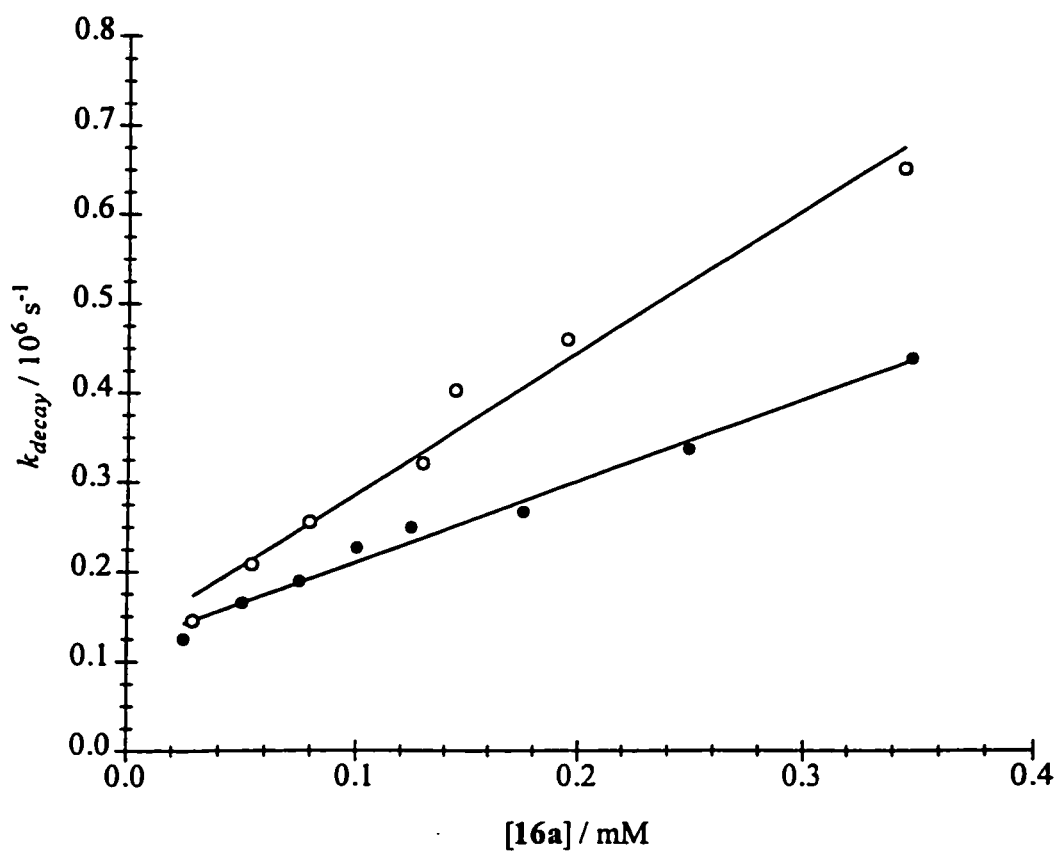


Figure A.7. Plot of k_{decay} versus ketone concentration from 248-nm NLFP of deoxygenated DCM solutions of compound **16a**. Open circles are H_2O , filled circles are D_2O . Page reference p.185.

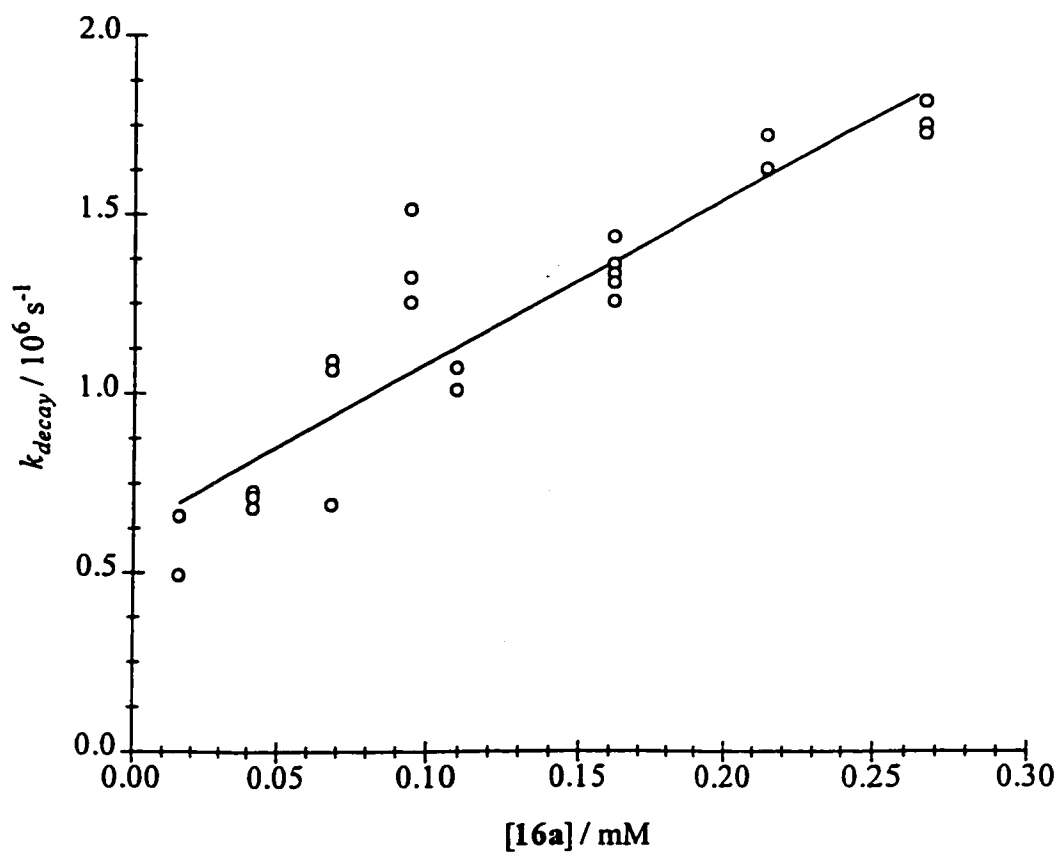


Figure A.8. Plot of k_{decay} versus ketone concentration from 248-nm NLFP of deoxygenated 0.028 M L₂O/MeCN solutions of compound **58a**. Open circles are H₂O, filled circles are D₂O. Page reference p.213.

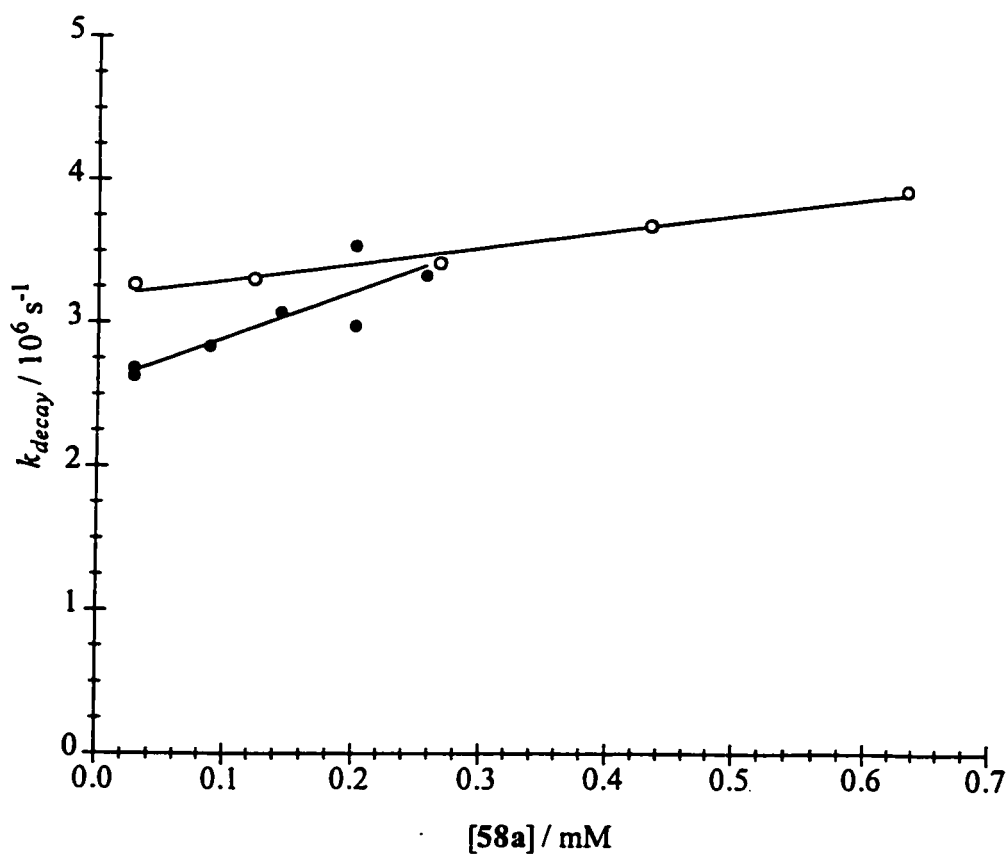


Figure A.9. Stern-Volmer plot of the reduction of the initial yield of the transient (*top* Δ -OD) from 337-nm NLFP of compound **59a** in MeCN. Page reference p.218.

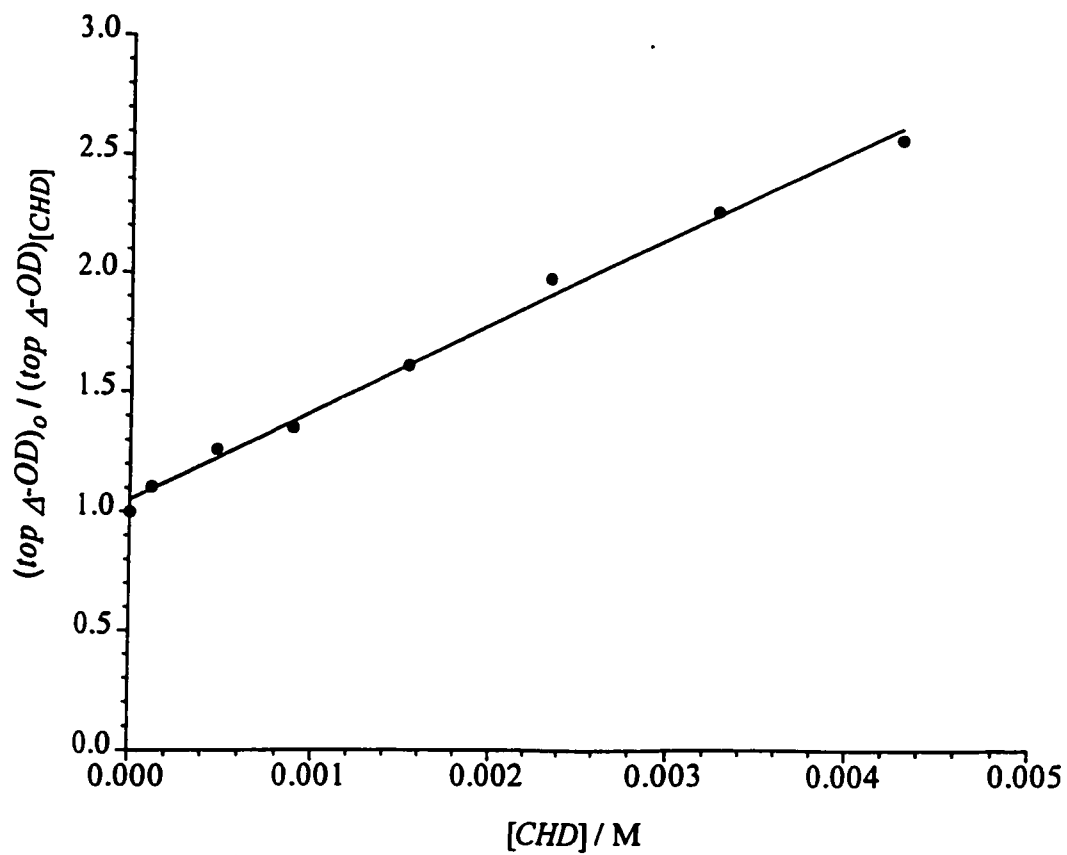
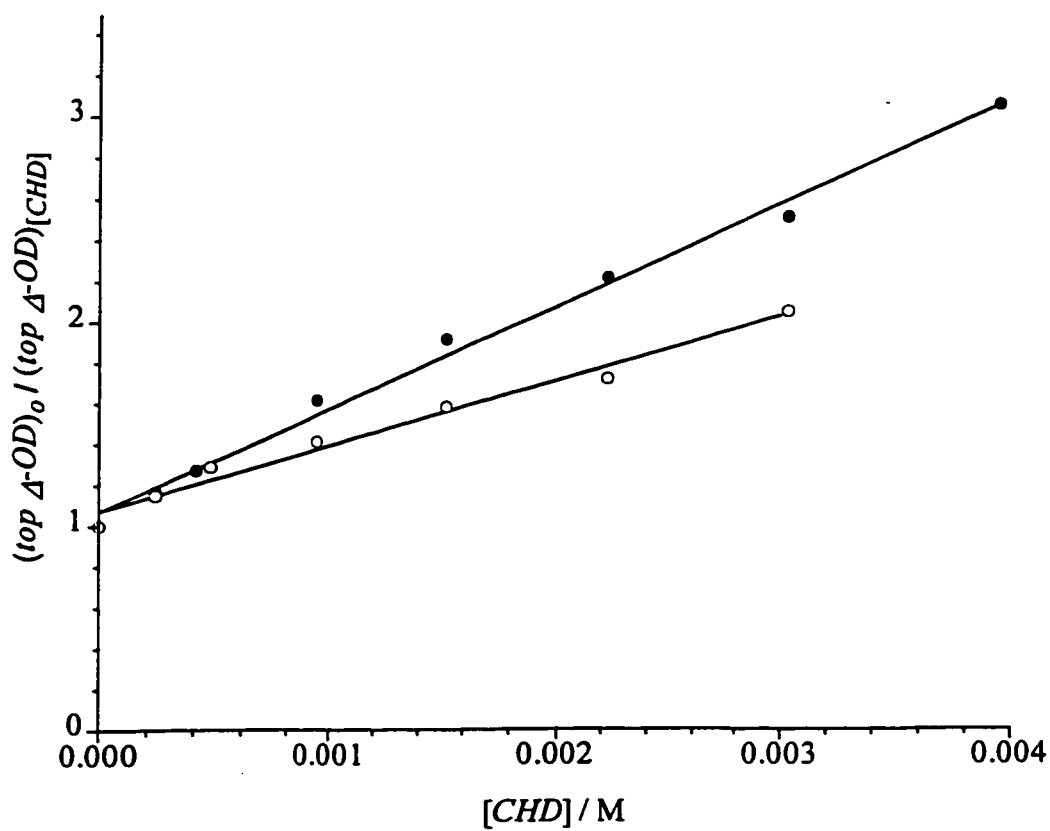


Figure A.10. Stern-Volmer plot of the reduction of the initial yield of the transient (*top* Δ -OD) from 337-nm NLFP of compound **59a**. The filled points indicate 0.05% $D_2O/MeCN$, the open points 0.05% $H_2O/MeCN$. Page reference p.213.



REFERENCES

1. Turro, N. J. *Modern Molecular Photochemistry*; Benjamin/Cummings: Menlo Park, 1978.
2. Atkins, P. W. *The Elements of Physical Chemistry*; W.H. Freeman: New York, 1993.
3. Forster, Th. *Discuss. Faraday Soc.* **1959**, 27, 7.
4. Dexter, D. L. *J. Chem. Phys.* **1953**, 21, 836.
5. Murov, S. L.; Carmichael, I.; Hug, G. L. *Handbook of photochemistry*; Dekker: New York, 1993.
6. Rehm, D.; Weller, A. *Isr. J. Chem.* **1970**, 8, 259.
7. Gilbert, A.; Baggott, J. E. *Essentials of Molecular Photochemistry*; CRC Press: Boston, 1991.
8. Dym, S.; Hochstrasser, R. M. *J. Chem. Phys.* **1969**, 51, 2458.
9. Kearns, D. R.; Case, W. A. *J. Am. Chem. Soc.* **1966**, 88, 5087.
10. Hoffman, R.; Swenson, J. R. *J. Phys. Chem.* **1970**, 74, 415.
11. Wagner, P. J.; Siebert, E. J. *J. Am. Chem. Soc.* **1981**, 103, 7329.
12. Wagner, P. J.; May, M. L. *J. Phys. Chem.* **1991**, 95, 10317.
13. Wagner, P. J.; Kemppainen, A. E.; Schott, H. N. *J. Am. Chem. Soc.* **1973**, 95, 17, 5604.
14. Wagner, P. J.; Thomas, M. J.; Harris, E. *J. Am. Chem. Soc.* **1976**, 98, 7675.
15. Yang, N. C.; Dusenbery, R. L. *J. Am. Chem. Soc.* **1968**, 90, 5899.
16. Wagner, P. J. *Topics Curr. Chem.* **1976**, 66, 1.

18. Porter, G.; Suppan, P. *Trans. Faraday Soc.* **1965**, *61*, 1664.
19. Aspari, P.; Ghoneim, N.; Haselbach, E.; von Raumer, M.; Suppan, P.; Vauthey, E. *J. Chem. Soc. , Faraday Trans.* **1996**, *92*, 1689.
20. Bhasikuttan, A. C.; Singh, A. K.; Palit, D. K.; Sapre, A. V.; Mittal, J. P. *J. Phys. Chem. A* **1998**, *102*, 3470.
21. Cowan, D. O.; Drisco, R. L. *Elements of Organic Photochemistry*; Plenum Press: New York, 1976.
22. Scaiano, J. C. *J. Photochem.* **1973**, *2*, 81.
23. Wagner, P. J.; Park, B.-S. *Org. Photochem.* **1991**, *11*, 227.
24. Cohen, S. G.; Parola, A.; Parsons, Jr. G. H. *Chem. Rev.* **1973**, *73*, 141.
25. Inbar, S.; Linschitz, H.; Cohen, S. G. *J. Am. Chem. Soc.* **1981**, *103*, 1048.
26. Inbar, S.; Linschitz, H.; Cohen, S. G. *J. Am. Chem. Soc.* **1982**, *104*, 1679.
27. Peters, K. S.; Li, B. L.; Lee, J. *J. Am. Chem. Soc.* **1993**, *115*, 11119.
28. Bobrowski, K.; Marciniak, B.; Hug, G. L. *J. Photochem. Photobiol. A:Chem.* **1994**, *81*, 159.
29. Miyasaka, H.; Morita, K.; Kamada, K.; Mataga, N. *Chem. Phys. Lett.* **1991**, *178*, 504.
30. Haselbach, E.; Jacques, P.; Pilloud, D.; Suppan, P.; Vauthey, E. *J. Phys. Chem.* **1991**, *95*, 7115.
31. Peters, K. S.; Lee, J. *J. Phys. Chem.* **1993**, *97*, 3761.
32. Wagner, P. J.; Truman, R. J.; Puchalski, A. E.; Wake, R. *J. Am. Chem. Soc.* **1986**, *108*, 7727.
33. Walling, C.; Gibian, M. J. *J. Am. Chem. Soc.* **1965**, *87*, 3361.

34. Griller, D.; Howard, J. A.; Marriott, P. R.; Scaiano, J. C. *J. Am. Chem. Soc.* **1981**, *103*, 619.
35. Padwa, A. *Tet. Lett.* **1964**, 3465.
36. Simon, J. D.; Peters, K. S. *J. Am. Chem. Soc.* **1982**, *104*, 6542.
37. Devadoss, C.; Fessenden, R. W. *J. Phys. Chem.* **1991**, *95*, 7253.
38. Miyasaka, H.; Kiri, M.; Morita, K.; Mataga, N.; Tanimoto, Y. *Chem. Phys. Lett.* **1992**, *199*, 21.
39. von Raumer, M.; Suppan, P.; Haselbach, E. *Helv. Chim. Acta* **1997**, *80*, 719.
40. Guttenplan, J. B.; Cohen, S. G. *J. Org. Chem.* **1973**, *38*, 2001.
41. Ronfard-Haret, J. C.; Bensasson, R. V.; Gramain, J. C. *Chem. Phys. Lett.* **1983**, *96*, 31.
42. Jones, G.; Malba, V.; Bergmark, W. R. *J. Am. Chem. Soc.* **1986**, *108*, 4214.
43. Wakasa, M.; Hayashi, H. *J. Phys. Chem.* **1996**, *100*, 15640.
44. Cohen, S. G.; Ojanpera, S. *J. Am. Chem. Soc.* **1975**, *97*, 5633.
45. Bhattacharyya, S. N.; Das, P. K. *J. Chem. Soc., Far. Trans. 2* **1984**, *80*, 1107.
46. Encinas, M. V.; Lissi, E. A.; Olea, A. F. *Photochem. Photobiol.* **1985**, *42*, 347.
47. Marciniak, B.; Bobrowski, K.; Hug, G. L. *J. Phys. Chem.* **1993**, *97*, 11937.
48. Marciniak, B.; Andrzejewska, E.; Hug, G. L. *J. Photochem. Photobiol. A: Chem.* **1998**, *112*, 21.
49. Singer, L. A.; Brown, R. E.; Davis, G. A. *J. Am. Chem. Soc.* **1973**, *95*, 8638.
50. Wolf, M. W.; Brown, R. E.; Singer, L. A. *J. Am. Chem. Soc.* **1977**, *99*, 526.
51. Guttenplan, J. B.; Cohen, S. G. *J. Am. Chem. Soc.* **1972**, *94*, 4040.

52. Wagner, P. J.; Truman, R. J.; Scaiano, J. C. *J. Am. Chem. Soc.* **1985**, *107*, 7093.
53. Giering, L. P.; Berger, M.; Steel, C. *J. Am. Chem. Soc.* **1974**, *96*, 953.
54. Berger, M.; McAlpine, E.; Steel, C. *J. Am. Chem. Soc.* **1978**, *100*, 5147.
55. Encinas, M. V.; Lissi, E. A.; Lemp, E.; Zanoeco, A.; Scaiano, J. C. *J. Am. Chem. Soc.* **1983**, *105*, 1856.
56. Heitner, C. Light-induced yellowing of wood-containing papers. An evolution of the mechanism; In *Photochemistry of lignocellulosic materials. ACS Symposium Series 531*; Heitner, C., Scaiano, J. C., eds. American Chemical Society: Washington, 1993; pp 1-24.
57. Zhu, J. H.; Gray, D. G. *J. Photochem. Photobiol. A:Chem.* **1995**, *87*, 267.
58. Lucarini, M.; Pedrielli, P.; Pedulli, G. F.; Cabiddu, S.; Fattuoni, C. *J. Org. Chem.* **1996**, *61*, 9259.
59. Das, P. K.; Encinas, M. V.; Steenken, S.; Scaiano, J. C. *J. Am. Chem. Soc.* **1981**, *103*, 4162.
60. Avila, D. V.; Ingold, K. U.; Lusztyk, J.; Green, W. H.; Procopio, D. R. *J. Am. Chem. Soc.* **1995**, *117*, 2929.
61. Valgimigli, L.; Banks, J. T.; Ingold, K. U.; Lusztyk, J. *J. Am. Chem. Soc.* **1995**, *117*, 9966.
62. Spange, S.; Maenz, K.; Stadermann, D. *Liebigs Ann. Chem.* **1992**, 1033.
63. Vedernikova, I.; Tollenaraere, J. P.; Haemers, A. *J. Phys. Org. Chem.* **1999**, *12*, 144.
64. Jacques, P. *Chem. Phys. Lett.* **1987**, *42*, 96.
65. Becker, H.-D. *J. Org. Chem.* **1967**, *32*, 2115.
66. Becker, H.-D. *J. Org. Chem.* **1967**, *32*, 2124.

67. Becker, H.-D. *J. Org. Chem.* **1967**, *32*, 2140.
68. Turro, N. J.; Engel, R. *Mol. Photochem.* **1969**, *1*, 143.
69. Turro, N. J.; Engel, R. *Mol. Photochem.* **1969**, *1*, 235.
70. Turro, N. J.; Engel, R. *J. Am. Chem. Soc.* **1969**, *91*, 7113.
71. Turro, N. J.; Lee, T. J. *Mol. Photochem.* **1970**, *2*, 185.
72. Das, P. K.; Encinas, M. V.; Scaiano, J. C. *J. Am. Chem. Soc.* **1981**, *103*, 4154.
73. Bobrowski, K.; Das, P. K. *Chem. Phys. Lett.* **1981**, *80*, 371.
74. Scaiano, J. C.; McGimpsey, W. G.; Leigh, W. J.; Jakobs, S. *J. Org. Chem.* **1987**, *52*, 4540.
75. Evans, C.; Scaiano, J. C.; Ingold, K. U. *J. Am. Chem. Soc.* **1992**, *4*, 4589.
76. Levin, P. P.; Shafirovich, V. Y.; Batova, E. E.; Kuzmin, V. A. *Chem. Phys. Lett.* **1994**, *228*, 357.
77. Wakasa, M.; Hayashi, H. *J. Phys. Chem.* **1995**, *99*, 17074.
78. Yoshihara, T.; Yamaji, M.; Shizuka, H. *Chem. Phys. Lett.* **1996**, *261*, 431.
79. Jovanovic, S. V.; Morris, D. G.; Pliva, C. N.; Scaiano, J. C. *J. Photochem. Photobiol. A:Chem.* **1997**, *107*, 153.
80. de Lucas, N. C.; Netto-Ferreira, J. C. *J. Photochem. Photobiol. A:Chem.* **1998**, *116*, 203.
81. Niizuma, S.; Kawata, H. *Bull. Chem. Soc. Jpn.* **1993**, *66*, 1627.
82. Das, R.; Bhatnagar, R.; Venkataraman, B. *Proc. Ind. Acad. Sci. (Chem. Sci.)* **1994**, *106*, 1681.
83. Lutz, H.; Breheret, E.; Lindqvist, L. *J. Phys. Chem.* **1973**, *77*, 1758.

84. Leigh, W. J.; Jakobs, S. *Tetrahedron* **1987**, *43*, 1393.
85. Leigh, W. J.; Workentin, M. S.; Andrew, D. J. *Photochem. Photobiol. A:Chem.* **1991**, *57*, 97.
86. St.Pierre, M. J. 1995, M.Sc. Thesis, McMaster University. *A nanosecond laser flash photolysis study of remote intramolecular phenolic hydrogen atom abstraction by carbonyl triplets.*
87. Bradaric, C. J.; Leigh, W. J. *Can. J. Chem.* **1997**, *75*, 1393.
88. Carmichael, I.; Hug, G. L. *J. Phys. Chem. Ref. Data* **1986**, *15*, 1.
89. Dobson, G.; Grossweiner, L. I. *Trans. Far. Soc.* **1964**, 708.
90. Land, E. J.; Porter, G. *Trans. Far. Soc.* **1963**, 2016.
91. Espenson, J. H. *Chemical kinetics and reaction mechanisms*. 1995. New York, McGraw-Hill, Inc. Speer, J. B. and Morriss, J. M., Eds.
92. Biczok, L.; Berces, T.; Linschitz, H. *J. Am. Chem. Soc.* **1997**, *119*, 11071.
93. Hansch, C.; Leo, A.; Taft, R. W. *Chem. Rev.* **1991**, *91*, 165.
94. Leigh, W. J.; Arnold, D. R.; Humphreys, R. W. R.; Wong, P. C. *Can. J. Chem.* **1980**, *58*, 2537.
95. Zimmerman, H. E.; Sandel, V. R. *J. Am. Chem. Soc.* **1963**, *85*, 915.
96. Lewis, F. D.; Yang, J.-S. *J. Am. Chem. Soc.* **1997**, *119*, 3834.
97. Zimmerman, H. E. *J. Am. Chem. Soc.* **1995**, *117*, 8988.
98. Zimmerman, H. E. *J. Phys. Chem. A* **1998**, *102*, 5616.
99. Wehry, E. L.; Rogers, L. B. *J. Am. Chem. Soc.* **1965**, *87*, 4234.
100. Wan, P.; Yates, K. *Rev. Chem. Intermed.* **1984**, *5*, 157.

101. McEwen, J.; Yates, K. *J. Phys. Org. Chem.* **1991**, *4*, 193.
102. Baldry, P. J. *J. Chem. Soc., Perkin Trans. II* **1979**, 951.
103. Bonner, T. G.; Phillips, J. *J. Chem. Soc. (B)* **1966**, 650.
104. Palm, V. A.; Haldna, U. L.; Talvik, A. J. Basicity of carbonyl compounds. In *The Chemistry of the Carbonyl Group*; Patai, S., ed. John Wiley: London, 1966; p 421.
105. Filipescu, N.; Chakrabarti, S. K.; Tarassoff, P. G. *J. Phys. Chem.* **1973**, *77*, 2276.
106. Ireland, J. F.; Wyatt, P. A. H. *J. Chem. Soc., Far. Trans. 1* **1972**, *68*, 1053.
107. Rayner, D. M.; Wyatt, P. A. H. *J. Chem. Soc., Far. Trans. 2* **1974**, *70*, 945.
108. Shizuka, H.; Kimura, E. *Can. J. Chem.* **1984**, *62*, 2041.
109. Hoshi, M.; Shizuka, H. *Bull. Chem. Soc. Jpn.* **1986**, *59*, 2711.
110. Favaro, G.; Bufalini, G. *J. Phys. Chem.* **1976**, *80*, 800.
111. Weir, D.; Scaiano, J. C. *Tetrahedron* **1987**, *43*, 1617.
112. Previtali, C. M.; Cosa, J. J.; Lema, R. H. *J. Lumin.* **1986**, *36*, 121.
113. Rayner, D. M.; Tolg, P. K.; Szabo, A. G. *J. Phys. Chem.* **1978**, *82*, 86.
114. Favaro, G. *Chem. Phys. Lett.* **1975**, *31*, 87.
115. Rusakowicz, R.; Byers, G. W.; Leermakers, P. A. *J. Am. Chem. Soc.* **1971**, *93*, 3263.
116. Izutsu, K. *Acid-base dissociation constants in dipolar aprotic solvents. IUPAC Chemical Data Series #35*. Blackwell Scientific Publications: Oxford, 1990; pp 17-35.
117. Taft, R. W.; Gurka, D.; Joris, L.; Schleyer, P. v. R.; Rakshys, J. W. *J. Am. Chem. Soc.* **1969**, *91*, 4801.
118. Joris, L.; Mitsky, J.; Taft, R. W. *J. Am. Chem. Soc.* **1972**, *94*, 3438.

119. Bessau, F.; Lucon, M.; Laurence, C.; Berthelot, M. *J. Chem. Soc. ,Perkin Trans. II* **1998**, 101.
120. Leigh, W. J.; Lathioor, E. C.; St.Pierre, M. J. *J. Am. Chem. Soc.* **1996**, *118*, 12339.
121. Mann, C. K.; Barnes, K. K. *Electrochemical reactions in nonaqueous systems*. Marcel Dekker, Inc.: New York, 1970; pp 201-244.
122. Hapiot, P.; Pinson, J.; Yousfi, N. *New J. Chem.* **1992**, *16*, 877.
123. Workentin, M. S.; Wayner, D. D. M. *Res. Chem. Intermed.* **1993**, *19*, 777.
124. Nicholas, A. M. P.; Arnold, D. R. *Can. J. Chem.* **1982**, *60*, 2165.
125. Bordwell, F. G.; Cheng, J.-P. *J. Am. Chem. Soc.* **1989**, *111*, 1792.
126. Kiyota, T.; Yamaji, M.; Shizuka, H. *J. Phys. Chem.* **1996**, *100*, 672.
127. Trammell, S. A.; Wimbish, J. C.; Odobel, F.; Gallagher, L. A.; Narula, P. M.; Meyer, T. J. *J. Am. Chem. Soc.* **1998**, *120*, 13248.
128. Peluso, A.; Brahim, M.; Carotenuto, M.; Del Re, G. *J. Phys. Chem.* **1998**, *102*, 10333.
129. Biczok, L.; Gupta, N.; Linschitz, H. *J. Am. Chem. Soc.* **1997**, *119*, 12601.
130. Cukier, R. I. *J. Phys. Chem.* **1996**, *100*, 15428.
131. Turro, C.; Chang, C. K.; Leroi, G. E.; Cukier, R. I.; Nocera, D. G. *J. Am. Chem. Soc.* **1992**, *114*, 4013.
132. Gadosy, T. A.; Shukla, D.; Johnston, L. J. *J. Phys. Chem. A* **1999**, *103*, 8834.
133. Loutfy, R. O.; Loutfy, R. O. *J. Phys. Chem.* **1972**, *76*, 1650.
134. Leigh, W. J.; Arnold, D. R. *Can. J. Chem.* **1981**, *59*, 3061.
135. Andrews, L. J.; Deroulede, A.; Linschitz, H. *J. Phys. Chem.* **1978**, *82*, 2304.

136. Huggenberger, C.; Labhart, H. *Helv. Chim. Acta* **1978**, *61*, 250.
137. Fujii, T.; Sano, M.; Mishima, S.; Hiratsuka, H. *Bull. Chem. Soc. Jpn.* **1996**, *69*, 1833.
138. Davis, G. A.; Carapellucci, P. A.; Szoc, K.; Gresser, J. D. *J. Am. Chem. Soc.* **1969**, *91*, 2264.
139. Hubig, S. M.; Rathore, R.; Kochi, J. K. *J. Am. Chem. Soc.* **1999**, *121*, 617.
140. Forster, Th.; Kasper, K. *Z. Electrochem.* **1955**, *59*, 976.
141. Gordon, M.; Ware, W. R. *The Exciplex*; Academic Press: New York, 1975.
142. Hubig, S. M.; Kochi, J. K. *J. Am. Chem. Soc.* **1999**, *121*, 1688.
143. Wagner, P. J.; Klan, P. *J. Am. Chem. Soc.* **1999**, *121*, 9626.
144. Creed, D.; Caldwell, R. A. *Photochem. Photobiol.* **1985**, *41*, 715.
145. Bolton, J. R.; Archer, M. D. Basic electron-transfer theory. In *Electron transfer in inorganic, organic and biological systems*. Bolton, J. R., Mataga, N., McLendon, G. L., eds. American Chemical Society: Washington, 1991; pp 7-23.
146. Hoshino, M.; Shizuka, H. Photoinduced electron transfer reactions of aromatic carbonyl and related compounds. In *Photoinduced electron transfer, Part C*. Fox, M. A., Chanon, M., eds. Elsevier: Amsterdam, 1988; pp 313-371.
147. Shizuka, H.; Yamaji, M. *Proc. Ind. Acad. Sci. (Chem. Sci.)* **1993**, *105*, 747.
148. Kavarnos, G. J.; Turro, N. J. *Chem. Rev.* **1986**, *86*, 401.
149. Kavarnos, G. J. *Fundamentals of photoinduced electron transfer*; VCH Publishers: New York, 1993.
150. Wagner, P. J. *Acc. Chem. Res.* **1971**, *4*, 168.

151. Rao, V. S.; Chandra, A. K. *J. Photochem. Photobiol. A:Chem.* **1996**, *101*, 189.
152. Scheffer, J. R.; Garcia-Garibay, M. A.; Nalamasu, O. *Org. Photochem.* **1987**, *8*, 249.
153. Formosinho, S. J.; Arnaut, L. G. *Adv. Photochem.* **1991**, *16*, 67.
154. Winnik, M. A. *Chem. Rev.* **1981**, *81*, 491.
155. Wagner, P. J.; Zhou, B.; Hasegawa, T.; Ward, D. L. *J. Am. Chem. Soc.* **1991**, *113*, 9640.
156. Wagner, P. J. *Acc. Chem. Res.* **1983**, *16*, 461.
157. Klopffer, W.; Liptay, W. *Z. Naturforsch.* **1970**, *25A*, 1091.
158. Bellamy, L. J. In *The infrared spectra of complex molecules*. Chapman and Hall: London, 1975; pp 107-128.
159. Lamola, A. A. *J. Chem. Phys.* **1967**, *47*, 4810.
160. Beck, G.; Dobrowolski, G.; Kiwi, J.; Schnabel, W. *Macromolecules* **1975**, *8*, 9.
161. Bays, J. P.; Encinas, M. V.; Scaiano, J. C. *Macromolecules* **1980**, *13*, 815.
162. Banks, J. T.; Ingold, K. U.; Luszytk, J. *J. Am. Chem. Soc.* **1996**, *118*, 6790.
163. Wayner, D. D. M.; Luszytk, J.; Page, D.; Ingold, K. U.; Mulder, P.; Laarhoven, L. J. J.; Aldrich, H. S. *J. Am. Chem. Soc.* **1995**, *117*, 8737.
164. March, J. *Advanced Organic Chemistry. Reactions, mechanisms and structure*. John Wiley & Sons: New York, 1992; pp 36-38.
165. Lathioor, E. C., Leigh, W. J., and St.Pierre, M. J. *J. Am. Chem. Soc.* **1999**, *121*, 11984.
166. DePuy, C. H.; Bishop, C. A. *J. Am. Chem. Soc.* **1960**, *82*, 2532.

167. Cockerill, A. F. *Tet. Lett.* **1969**, *56*, 4913.
168. Wallwork, S. C.; Harding, T. T. *Nature* **1953**, *171*, 40.
169. Reimers, J. R.; Hush, N. S.; Sammeth, D. M.; Callis, P. R. *Chem. Phys. Lett.* **1990**, *169*, 622.
170. Zeng, Y.; Zimmt, M. B. *J. Am. Chem. Soc.* **1991**, *113*, 5107.
171. Verhoeven, J. W.; Kroon, J.; Paddon-Row, M. N.; Warman, J. M. Kinetic and spectroscopic investigation of the influence of conformation and orbital symmetry on long-range intramolecular donor-acceptor interaction. In *Supramolecular chemistry*. Balzani, V., DeCola, L., eds. Kluwer Academic Publishers: Dordrecht, 1992; pp 181-200.
172. Jacques, P.; Allonas, X.; von Raumer, M.; Suppan, P.; Haselbach, E. *J. Photochem. Photobiol. A:Chem.* **1997**, *111*, 41.
173. Haselbach, E.; Pilloud, D.; Suppan, P. *J. Chem. Soc., Far. Trans.* **1995**, *91*, 3123.
174. Zsom, R. L. J.; Schroff, L. G.; Bakker, C. J.; Verhoeven, J. W.; De Boer, Th. J.; Wright, J. D.; Kuroda, H. *Tetrahedron* **1978**, *34*, 3225.
175. Staab, H. A.; Rebafka, W. *Chem. Ber.* **1977**, *110*, 3333.
176. Staab, H. A.; Herz, C. P.; Krieger, C.; Rentea, M. *Chem. Ber.* **1977**, *110*, 3351.
177. Staab, H. A.; Herz, C. P.; Krieger, C.; Rentea, M. *Chem. Ber.* **1983**, *116*, 3813.
178. Sakata, Y.; Nakashima, S.; Goto, Y.; Tatemitsu, H.; Misumi, S.; Asahi, T.; Hagihara, M.; Nishikawa, S.; Okada, T.; Mataga, N. *J. Am. Chem. Soc.* **1989**, *111*, 8979.
179. Sakata, Y.; Tsue, H.; Goto, Y.; Misumi, S.; Asahi, T.; Nishikawa, S.; Okada, T.; Mataga, N. *Chem. Lett.* **1991**, 1307.
180. Fiebig, T.; Kuhnle, W.; Staerk, H. *Chem. Phys. Lett.* **1998**, *282*, 7.

181. Helsen, N.; Viaene, L.; Van der Auweraer, M.; De Schryver, F. C. *J. Phys. Chem.* **1994**, *98*, 1532.
182. Nagaoka, S.-I.; Nagashima, U. *Chem. Phys.* **1996**, *206*, 353.
183. Tramer, A.; Brenner, V.; Millie, P.; Piuizzi, F. *J. Phys. Chem.* **1998**, *102*, 2798.
184. Tramer, A.; Brenner, V.; Millie, P.; Piuizzi, F. *J. Phys. Chem.* **1998**, *102*, 2808.
185. Ledger, M. B.; Porter, G. *Trans. Faraday Soc.* **1972**, 539.
186. Canonica, S.; Hellrung, B.; Wirz, J. *J. Phys. Chem. A* **2000**, *104*, 1226.
187. Szyllabel-Godala, A.; Madhavan, S.; Rudzinski, J.; O'Leary, M. H.; Paneth, P. *J. Phys. Org. Chem.* **1996**, *9*, 35.
188. *Handbook of Chemistry and Physics*. Lide, D. R. 72. 1991. Boca Raton, CRC Press.
189. Leigh, W. J.; Arnold, D. R.; Baines, K. M. *Tet. Lett.* **1981**, 909.
190. Fieser, L. F.; Fieser, M. *Reagents for Organic Synthesis*; John Wiley and Sons: New York, 1967.
191. Miyake, A.; Itoh, K.; Tada, N.; Tanabe, M.; Hirata, M.; Oka, Y. *Chem. Pharm. Bull.* **1983**, *31*, 2329.
192. Hartmann, R. W.; Bayer, H.; Grun, G. *J. Med. Chem.* **1994**, *37*, 1275.
193. Bachmann, W. E.; Thomas, D. G. *J. Am. Chem. Soc.* **1942**, *64*, 94.
194. Moreau, C.; Rouessac, F. *Bull. Soc. Chim. Fr.* **1973**, *12*, 3427.
195. Crispin, D. J.; Vanstone, A. E.; Whitehurst, J. S. *J. Chem. Soc. (C)* **1970**, 10.
196. Collins, D. J.; Fallon, G. D.; Skene, C. E. *Aust. J. Chem.* **1992**, *45*, 71.